UNIVERSITA' DELLA CALABRIA

Dipartimento di Ingegneria Civile

Dottorato di Ricerca in

Scienze ed Ingegneria per l'Ambiente, le Costruzioni e l'Energia

Con il contributo di

Programma Operativo Regionale Calabria FSE/FESR 2014 – 2020 (CCI 2014IT16M2OP006)

CICLO

XXXIV

Fire Behaviour of GFRP sandwich panels for the rehabilitation of building floors

Settore Scientifico Disciplinare: ICAR/09

Coordinatore: Ch.mo Prof. Salvatore Critelli

Firma Critelli Salvatore 15.06.2022 14:24:08 GMT+02:00

Supervisore: Eng. João Pedro Lage da Costa Firmo

Firma João Pedro Firmo

Co-Supervisori: Ch.mo Prof. João Pedro Ramôa Ribeiro Correia

Firma João Ramôa Correia

Ch.mo Prof. Luciano Ombres

Firma

Dottorando: Dott. Pietro Mazzuca

Pietro Mazzuca

UNIVERSITA' DELLA CALABRIA

Dipartimento di Ingegneria Civile

Dottorato di Ricerca in

Scienze ed Ingegneria per l'Ambiente, le Costruzioni e l'Energia

Con il contributo di

Programma Operativo Regionale Calabria FSE/FESR 2014 – 2020 (CCI 2014IT16M2OP006)

CICLO

XXXIV

Fire Behaviour of GFRP sandwich panels for the rehabilitation of building floors

Settore Scientifico Disciplinare: ICAR/09

Coordinatore: Ch.mo Prof. Salvatore Critelli

Firma Critelli Salvatore 15.06.2022 14:24:08 GMT+02:00

Supervisore: Eng. João Pedro Lage da Costa Firmo

Firma João Pedro Firmo

Co-Supervisori: Ch.mo Prof. João Pedro Ramôa Ribeiro Correia

Firma João Ramôa Correia

Ch.mo Prof. Luciano Ombres

Firma

Dottorando: Dott. Pietro Mazzuca

Pietro Mazzuca

ABSTRACT

The replacement of degraded floors (namely timber ones) with traditional materials, such as steel and reinforced concrete, introduces significant dead loads in existing constructions, increasing their seismic vulnerability. In this context, glass fibre reinforced polymer (GFRP) sandwich panels present several advantages, namely their high mechanical performance, lightness, durability and increasingly competitive costs. In spite of this great potential, a challenging issue regarding the use of GFRP composite sandwich panels as buildings structural members is related with their thermomechanical performance when subjected to elevated temperature and fire. This issue is yet to be addressed in a comprehensive manner and has hampered their widespread use in buildings, where strict fire performance requirements have to be met.

In this context, this thesis centres on the fire resistance behaviour of sandwich panels composed of GFRP face sheets and longitudinal webs, and two different core materials, namely polyurethane (PUR) foam and polyethylene terephthalate (PET) foam, produced by vacuum infusion. The investigations developed in this thesis aimed at evaluating three main aspects of the fire behaviour of these composite sandwich panels: (i) the characterisation of the mechanical and thermo-physical properties at elevated temperature of their constituent materials; (ii) the influence of different core materials and GFRP configurations on their fire resistance, and (iii) the effectiveness of different passive fire protection systems in enabling their structural use in buildings.

In a first stage, experimental, analytical and numerical studies were performed to evaluate the thermophysical and mechanical properties of the constituent materials of GFRP panels (namely GFRP and polymeric foams, PET and PUR) as a function of temperature. The research about the mechanical behaviour at elevated temperature of the GFRP laminates and polymeric foams comprised small-scale mechanical tests (tension, compression and shear) at elevated temperatures (up to 300 °C). These tests allowed determining the variation with temperature of the mechanical properties (strength and stiffness) of the materials. With respect to the thermophysical properties, an inverse numerical analysis was developed using a one-dimensional (1D) heat transfer model together with experimental thermal data. These temperature-dependent thermophysical properties were then used as input data in finite element (FE) models to simulate the thermal response of foam-filled GFRP sandwich panels under fire. The results obtained confirmed that the compressive and shear properties of both PET and PUR foams undergo significant reductions with temperature, which generally take place when the T_g of the polymeric material is approached and exceeded. Such reductions occur for lower temperature in the PET foam when compared to the PUR foam, and this is mainly due to the lower T_g of the former

material. Similarly to polymeric foams, the mechanical properties of the GFRP laminates presented considerable reductions of their strength and moduli, mainly due to the softening of the organic matrix caused by the glass transition process. For the specific material considered in this study, the tensile properties and compressive modulus were less sensitive to temperature when compared to the shear modulus and compressive strength. Finally, the results obtained from the inverse numerical analysis highlighted that the specific heat and thermal conductivity of GFRP laminated and polymeric foams (PET and PUR) are strongly affected by elevated temperatures.

In a second stage, fire resistance tests were performed on loaded GFRP sandwich panels, either unprotected or protected with different passive systems. In this context, simply supported GFRP panels were simultaneously subjected to a service load and the fire curve established in the ISO 834 standard. The influence of using different core materials and the presence of longitudinal webs was investigated. Additionally, the efficacy of different passive fire protection systems was evaluated, including (i) calcium silicate (CS) boards directly applied on the bottom face sheet of the GFRP panels or (ii) suspended from the bottom face sheet, forming an air cavity. The temperature profiles, the evolution of strains and deflections, the fire resistance and failure modes of the GFRP panels were assessed. Finally, two-dimensional (2D) and three-dimensional (3D) numerical models were also developed aiming at understanding in further depth the fire behaviour of GFRP sandwich panels. In particular, FE models were used to provide a better understanding about relevant kinematic and static issues, including the evolution of deflections and the variation of the stress distributions with increasing temperature/time. In addition, the influence of using different passive fire protection systems as well as different core materials and panel configurations was studied. The results obtained confirmed that the type of core material, as well as the passive fire protection systems and cross-sectional configurations, significantly affect the thermal and mechanical response of the sandwich panels in fire. In general, the calcium silicate boards proved to be effective in delaying the temperature increase in the panels, thus improving their fire endurance. As an example, for the homogeneous-PET core sandwich panel, the time to collapse was increased from 8 min (unprotected) to 48 min (adherent CS boards); the fire endurance of web-core sandwich panels was increased from 28 min (unprotected) to 70 min (adherent CS board) and 96 min (suspended CS board). The FE models developed provided a relatively good agreement with the experimental results in terms of thermal and mechanical responses (*e.g.* evolution of temperature and mid-span deflection with time). The Hill-criterion used to simulate the orthotropic behaviour of the foam was successful in simulating its degradation in close to the interface between the bottom face sheet and the PET foam (as observed in the experiments). The numerical results showed that the progressive heating through-the-thickness of the panels led to a significant stress transfer from their bottom part (more degraded) to the upper part (less degraded).

Keywords: sandwich panels, glass fibre reinforced polymers (GFRP), polymeric foams, elevated temperature, fire behaviour, fire protection systems; experimental tests; numerical studies.

RESUMO

A substituição de pisos degradados (sobretudo de madeira) por soluções tradicionais, como o aço e o betão armado, introduz cargas significativas nas construções existentes, aumentando a sua vulnerabilidade sísmica. Neste contexto, os painéis sanduíche com lâminas de polímeros reforçados com fibra de vidro (GFRP) e núcleo de espuma polimérica apresentam várias vantagens, nomeadamente o seu elevado desempenho mecânico, leveza, durabilidade e custos cada vez mais competitivos. Apesar desse potencial, um dos desafios da utilização destes painéis sanduíche como elementos estruturais em edifícios está relacionado com o seu comportamento termomecânico quando submetidos a temperaturas elevadas ou ao fogo. Este problema, que ainda não foi estudado de forma aprofundada, tem impedido a utilização destes painéis em pisos de edifícios, onde têm de ser cumpridos requisitos de segurança ao fogo bastante exigentes.

Neste contexto, o principal objectivo desta tese consistiu em estudar a resistência ao fogo de painéis sanduíche constituídos por laminados de GFRP e dois materiais de núcleo diferentes, nomeadamente espuma de poliuretano (PUR) e espuma de polietileno tereftalato (PET), produzidos por infusão a vácuo. A investigação desenvolvida teve como objectivo avaliar os seguintes três aspectos principais: (i) a caracterização das propriedades mecânicas e termofísicas a temperatura elevada dos materiais constituintes dos painéis; (ii) a influência de diferentes materiais de núcleo e configurações de laminados de GFRP na sua resistência ao fogo, e (iii) a eficácia de diferentes sistemas de proteção passiva contra incêndio para permitir a sua utilização estrutural em edifícios.

Numa primeira fase, foram realizados estudos experimentais, analíticos e numéricos para avaliar as propriedades termofísicas e mecânicas dos materiais constituintes dos painéis de GFRP (nomeadamente, GFRP e espumas poliméricas, PET e PUR) em função da temperatura. A investigação sobre o comportamento mecânico dos laminados de GFRP e das espumas poliméricas incluiu ensaios mecânicos (tração, compressão e corte) a temperaturas elevadas, até 300 °C. Estes ensaios permitiram determinar a variação com a temperatura das propriedades mecânicas (resistência e rigidez) dos materiais. Em relação às propriedades termofísicas, recorreu-se a análises numéricas inversas utilizando um modelo de transferência de calor unidimensional (1D) e considerando as distribuições de temperatura experimentais. Essas propriedades termofísicas dependentes da temperatura foram utilizadas como dados de *input* em modelos de elementos finitos (EF) para simular a resposta térmica de painéis sanduíche sujeitos ao fogo. Em relação ao comportamento mecânico, os resultados obtidos confirmaram que as propriedades à compressão e ao corte das espumas de PET e PUR apresentam reduções significativas com a temperatura, o que geralmente ocorre quando a

temperatura de transição vítrea (T_g) do material polimérico é atingida e ultrapassada. Tais reduções ocorrem a temperaturas inferiores na espuma de PET quando comparadas às da espuma de PUR, o que se deve principalmente ao facto de a sua T_g ser inferior. Tal como para as espumas poliméricas, as propriedades mecânicas dos laminados de GFRP apresentaram reduções consideráveis de resistência e rigidez, principalmente devido ao amolecimento da matriz polimérica (de natureza orgânica), causado pelo processo de transição vítrea. Para o material GFRP considerado neste estudo, as propriedades de tração e o módulo de elasticidade em compressão apresentaram menor susceptibilidade à temperatura quando comparados ao módulo de distorção e à resistência à compressão. Por fim, os resultados obtidos a partir da análise numérica inversa confirmaram que o calor específico e a condutividade térmica dos laminados de GFRP e das espumas (PET e PUR) são afetados pelo aumento da temperatura.

Numa segunda fase, foram realizados ensaios de resistência ao fogo em painéis sanduíche de GFRP com diferentes configurações e sistemas de protecção. Neste contexto, os painéis de GFRP foram submetidos simultaneamente a uma carga de serviço e à curva de incêndio padrão da norma ISO 834. A influência do uso de diferentes materiais de núcleo e a presença de nervuras longitudinais em GFRP foi investigada. Para além disso, foi avaliada a eficácia de diferentes sistemas de proteção passiva contra incêndio, incluindo placas de silicato de cálcio (SC) (i) aplicadas diretamente na face inferior dos painéis de GFRP ou (ii) suspensas na face inferior, formando uma cavidade de ar. Foram avaliados os perfis de temperatura, a evolução do deslocamento a meio vão, a resistência ao fogo e os modos de rotura dos painéis. Por fim, foram desenvolvidos modelos numéricos bidimensionais (2D) e tridimensionais (3D) com o objetivo de entender com maior profundidade o comportamento ao fogo de painéis sanduíche de GFRP. Em particular, os modelos de EF foram utilizados para obter um melhor entendimento sobre aspectos térmicos e termomecânicos, incluindo a evolução de deslocamentos e deformações, e a variação das distribuições de tensões com o aumento da temperatura/tempo. Além disso, foi estudada a influência do uso de diferentes sistemas de proteção passiva contra incêndio, bem como diferentes materiais de núcleo e arquitecturas de painel. Os resultados obtidos confirmaram que o tipo de material do núcleo, bem como os sistemas de proteção passiva contra o fogo e as configurações da seção transversal afetam significativamente a resposta térmica e mecânica dos painéis ao fogo. De um modo geral, as placas de silicato de cálcio mostraram-se eficazes em retardar o aumento da temperatura nos painéis, melhorando assim a sua resistência ao fogo. Como exemplo, para o painel sanduíche sem nervuras e com núcleo de PET, a resistência ao fogo aumentou de 8 min (sem protecção) para 48 min (protegido com placas de SC aderentes); a resistência ao fogo dos painéis sanduíche com nervuras aumentou de 28 min (sem protecção) para 70 min (protegido com placa de SC aderente) e 96 min (protegido com placa SC suspensa). Os resultados dos modelos de EF desenvolvidos apresentaram boa concordância com os medidos experimentalmente em termos de respostas térmicas e mecânicas. O critério de Hill utilizado para

simular o comportamento ortotrópico da espuma de PET permitiu simular a degradação próximo da interface entre a face inferior e a espuma de PET (de acordo com o que foi observado no estudo experimental). Os resultados numéricos mostraram que o aquecimento progressivo ao longo da espessura dos painéis levou a uma significativa transferência de tensão da parte inferior (mais degradada) para a parte superior (menos degradada).

Palavras-chave: painéis sanduíche, polímeros reforçados com fibra de vidro (GFRP), espumas poliméricas, temperatura elevada, comportamento ao fogo, sistemas de proteção ao fogo; ensaios experimentais; estudos numéricos.

ACKNOWLEDGEMENTS

First of all, I would like to thank my scientific supervisors, Eng. João Firmo and Prof. João Ramôa Correia for their tireless support, guidance, friendship and encouragement during the past years. They provided me with the tools that I needed to choose the right direction and successfully complete this thesis. I'm probably not able to find the right words to express all the gratitude I have for João, he accompanied me since my MSc dissertation, and from that moment he has always been a role model for me. I consider myself privileged to have collaborated with Prof. João Ramôa Correia, not only for his indisputable quality as a professor and researcher but also for his incredible mentality; he taught me the importance of "raising the bar" in everything I do.

I would also like to thank Prof. Luciano Ombres, for his support, encouragement and for always having such faith in me. His huge experience in the construction field is allowing me to improve as a researcher and engineer.

I am very grateful to all the CORE group family, namely Antonio Duarte, Josè Gonilha, Francisco Nunes, Mario Arruda, Mario Garrido, Mario Sà, Adriana Azevedo, Andrè Castelo, David Martins, Eloisa Castilho, Inês Rosa, Lourenço Fernandes, Madalena Ponte, Mateus Hofmann, Md Abu Toyob Shahid and Wallace Maia. I learnt a lot from all of you (not only from a professional point of view) and I will never forget all the time we spent together. I miss you all, but I know that, wherever I am, I can always count on you.

To my colleague (and friend) Mattia Nisticò; I would like to express my gratitude for his support, suggestions, constant discussion and the good moments spent in the office.

I also want to express my deep gratitude to Mr. Fernando Alves. I will never forget all the laughs I had with him when I was working in the lab; his impressive experience was crucial in the development of the experimental campaign. I would also like to thank Eng. Jorge Pontes, for always helping me with the experimental work.

Lastly, I would like to thank my family for all their love and understanding in some periods of absence. To my parents and my brother, thank you for your unconditional love, encouragement, support and for making me who I am today. To my supportive, encouraging, and patient girlfriend Marianna whose faithful support during the past years is so appreciated. Thank you.

To my dear friend Miguel

TABLE OF CONTENTS

LIST OF FIGURES

LIST OF TABLES

NOTATION

Roman Lower Case

c_p	Specific heat
dD/dt	Maximum deformation increase rate
g	Gauge length
h	Specimen height
h_c	Convection coefficient
k'	Parameter empirically derived
m	Weibull exponent
n_{ct}	Temperature conversion factor
n	Parameter empirically derived
t	Time, specimen thickness
t_c	Core thickness
t_{col}	Time to collapse
t_{dl}	Time to exceed maximum deformation
t_{irl}	Time to exceed maximum increase rate
t_w	Web thickness
$tan\ \delta$	Loss factor
x, y, z	Global reference axes of the structural element

Roman Capital

A	Area of the specimen
B	Parameter empirically derived
C	Parameter empirically derived
D	Maximum deformation
E	Elastic modulus
E'	Storage modulus
E''	Loss modulus
E_c	Compressive modulus
E_t	Tensile modulus
G	Shear modulus
K	Stiffness
L	Span

M_{max}	Maximum bending moment
P	Mechanical property; applied load
P_{av}	Average property
P_i	Individual property
P_{fire}	Load applied during fire exposure
P_R	Relaxed property
P_u	Failure load
P_U	Unrelaxed mechanical property
R_{ij}	Yield stress ratios
R_d	Design values of resistance
T	Temperature
T_a	Ambient temperature
T_d	Decomposition temperature
T_e	Experimental temperature
T_g	Glass transition temperature
$T_{g,mech}$	Parameter obtained by fitting a hyperbolic tangent function to the experimental data
T_n	Normalized temperature, numerical temperature
T_o	Initial temperature of the oven, relaxation temperature
V_{max}	Maximum shear force
V_x	Coefficient of variation of the material properties
W	Specimen width
X_k	Material property characteristic value

Greek symbols

α	Sensitivity of a given material property, coefficient of thermal expansion
ΔH	Horizontal shortening
ΔV	Vertical elongation
γ	Distortion
γ_M	Single partial material factor accounting for the uncertainty in a resistance model
γ_m	Partial factor for a material
Γ_h	Convective boundary
Γ_r	Radiative boundary
δ	Deflection
ε	Strain, material emissivity
λ	Thermal conductivity
ν	Poisson ratio

ρ	Density
σ	Stress, Stefan-Boltzmann constant
σ_c	Compressive strength
σ_o	User-defined reference yield stress
σ_t	Tensile strength
τ_o	Yield shear stress
τ_s	Shear stress

Acronyms

1D	One-dimensional
2D	Two-dimensional
3D	Three-dimensional
AMPE	Absolute mean percentage error
ASTM	American Society for Testing and Materials
CFRP	Carbon fibre reinforced polymer
CLT	Classical laminate theory
CNC	Computerized Numerical Control
CS	Calcium silicate
DMA	Dynamic mechanical analysis
DTS	Diagonal Tension Shear
GFRP	Glass fibre reinforced polymer
FCT	Fundação para a Ciência e a Tecnologia (Portuguese National Foundation for Science and Technology)
FE	Finite element
FRP	Fibre reinforced polymer
ISO	International Organization for Standardization
IST	Instituto Superior Técnico
LERM	Laboratório de Estruturas e Resistência de Materiais (Structures and Strength of Materials Laboratory)
LVDT	Linear variable displacement transducer
PET	Polyethylene terephthalate
PIEP	Pólo de Inovação em Engenharia de Polímeros
PIR	Polyisocyanurate
PMI	Polymethacrylimide
PVC	Polyvinylchloride
PUR	Polyurethane
SLS	Serviceability limit states
STA	Simultaneous Thermal Analyser

TGA	Thermogravimetric analysis
TPA	Thermal properties analyser
TPS	Transient plane source
TS	Technical Specification
ULS	Ultimate Limit states
XPS	Polystyrene

Part I. Introduction

CHAPTER 1

INTRODUCTION

1.1 CONTEXT AND MOTIVATION

The degradation of buildings in historic districts is a major problem with social and economic repercussions. The natural degradation of materials leads to the deterioration of building elements, many of them also requiring seismic rehabilitation. The resolution of these problems based on current steel/concrete solutions usually involves high costs and practical constraints, associated to the additional dead load introduced in the existing construction and the need for heavy weight elevation devices.

In this context, sandwich construction presents a great potential to be used in the rehabilitation of degraded building floors, offering high strength- and stiffness-to-weight ratios, good insulation properties and low maintenance requirements, namely when fibre-reinforced polymer (FRP) faces are used together with polymeric foams as core materials [1]. Moreover, this type of highly durable and lightweight structural solutions is particularly advantageous for rehabilitation applications, as it reduces the need of structural strengthening of the remaining building members, which ultimately contributes to a reduction on the demand for natural resources and raw materials. Additionally, FRP sandwich panels exhibit very high thermal resistance and therefore contribute to the energetic efficiency of the constructions where they are installed. Hence, the use of these composite panels for building rehabilitation can contribute for a reduction of the CO_2 emissions and the consumption of natural resources, again improving the sustainability of the construction industry.

In spite of this great potential, a challenging issue regarding the use of FRP sandwich panels in several applications is related with their mechanical performance when subjected to elevated temperature and fire [2]. Because of the organic nature of polymeric materials, the mechanical properties (*i.e.* strength and stiffness) of the polymeric foams and GFRP face sheets suffer steep reductions with increasing temperature, especially when their glass transition temperature (T_g), typically ranging from 65 ºC to 90 ºC, is approached and exceeded. In addition, when exposed to high temperatures (300–500 °C), their organic matrix decomposes, releasing heat, smoke, soot and toxic volatiles [3].

At the structural scale, most previous studies focused on the fire resistance of FRP multi-cellular panels (*i.e.* non-sandwich solutions). In these experiments, the panels were simultaneously loaded in

bending and heated from the bottom to the ISO 834 fire curve [4–7]. In general, the authors found that either passive (*e.g.* adherent or suspended CS boards) or active (*e.g.* water cooling system) fire protection systems were effective in delaying the temperature increase in the panels and, as a consequence, in increasing their fire resistance. Concerning the fire behaviour of foam-filled sandwich panels, experimental results available in the literature are very limited [8–11] and are mostly concerned with the in-plane behaviour (typically of wall members) rather than the out-of-plane response (relevant for building floors). The results obtained in those studies showed that, as for the multi-cellular panels, the use of passive fire protection systems can significantly improve the fire resistance; in addition, the thermomechanical response of the panels was found to be strongly dependant on the type of core material used. Therefore, further investigations are needed to provide a better understanding about the fire behaviour of foam-filled sandwich panels loaded in bending; in fact, the lack of knowledge about this topic is reflected in the future Eurocode for FRP structures [12], where only limited information is provided regarding the fire design and protection of FRP-sandwich elements.

With respect to the numerical simulation of the thermomechanical response of FRP members in fire, only a few studies were found in the literature [9,10,13–15]. Most of the thermal analyses were based on 1D or 2D simplifications, presenting some limitations due to uncertainties related to the thermal boundary conditions and thermophysical properties of the materials considered. The mechanical models were developed to provide strain, stress and deflection estimates in FRP members subjected to fire, both unprotected and protected with different protection systems. However, significant differences between experimental and numerical results are often reported in the literature due to uncertainties regarding the constitutive relations as a function of temperature of the materials (FRPs and polymeric foams). Existing studies about this topic often point out that the numerical simulation of the complex fire behaviour of FRP-sandwich panels remains an open issue; therefore, further numerical studies are needed in order to provide an in-depth understanding about the fire behaviour of these structural elements. A key point in this respect is the lack of data about the temperature-dependent thermophysical and mechanical properties of the constituent materials.

It is important to mention that the experimental and numerical studies conducted in this thesis were developed (and funded) within the framework of the FIRE-FLOOR project (reference PTDC/ECI-EGC/30611/2017, funded by the Portuguese national funding agency for science, research and technology – FCT), and also supported by POR CALABRIA 2014–2020 through an individual doctoral scholarship.

1.2 OBJECTIVES AND METHODOLOGY

The main objectives of the present study were to provide further insights about (i) the effects of elevated temperatures on both mechanical and thermophysical properties of glass-FRP (GFRP)

sandwich panels and their constituent materials, (ii) the influence of using different polymeric foams as core materials - polyurethane (PUR) and polyethylene terephthalate (PET) foams - and panel configurations on the fire behaviour of GFRP sandwich panels, and (iii) the effectiveness of different passive fire protection systems in improving their fire resistance. To this end, comprehensive experimental studies were performed together with the development of supporting numerical modelling tools.

The experimental study included (i) small-scale mechanical characterisation tests at elevated temperatures (tension, compression, shear) on GFRP laminates and two polymeric foams used as core materials (PET and PUR foams); (ii) specific tests to evaluate the thermophysical properties of all materials; and (iii) fire resistance tests on loaded GFRP-sandwich panels insulated with different passive fire protection systems.

In what concern the mechanical characterisation tests, the objective was to determine the variation with temperature of the mechanical properties of both GFRP laminates and polymeric foams, which is a crucial information for the design of sandwich structures exposed to elevated service temperatures or where the fire action has to be considered (*e.g.* building applications). To determine the stiffness and strength properties of the constituent materials of GFRP panels as a function of temperature, small-scale specimens were tested over a temperature range from 20 to 300 °C, involving a total of 150 tests.

Regarding the thermophysical properties, the glass transition and decomposition processes of the materials were studied through dynamic mechanical analysis (DMA) and thermogravimetric (TGA) tests, respectively. In addition, an inverse numerical analysis based on a 1D heat transfer model and experimental data was performed, in order to calibrate the variation with temperature of the specific heat and thermal conductivity of the constituent materials of the sandwich panels (GFRP laminates and both foams).

Concerning the fire behaviour of homogeneous-core (*i.e.* without longitudinal webs) and web-core sandwich panels, fire resistance tests were performed on specimens simultaneously exposed to fire and mechanical loading, both unprotected and protected using different passive fire protection systems. These tests aimed at providing insights about the temperature evolution in the panels, deflection evolution, failure modes, fire resistance and effects of fire protection systems on those properties. The influence of using different core materials (PUR *vs.* PET foam) and the presence of longitudinal GFRP webs was also assessed. The experimental campaign involved a total of 11 fire resistance tests, 5 in homogeneous-core sandwich panels and 6 in web-core sandwich panels; all types of panels used in this campaign were also tested up to failure under ambient temperature conditions in a 4-point bending configuration.

The ultimate objective of the numerical models was the simulation of the fire behaviour of GFRP panels, both unprotected and protected with different insulation systems. The main innovation of the numerical modelling comprised the consideration of (i) the thermophysical and (ii) mechanical properties of all materials as a function of temperature. Thermal models were developed with the objective of predicting the temperature evolution in sandwich panels heated from the bottom to the ISO 834 temperature *vs.* time curve. The temperature fields across the GFRP panels obtained from the thermal model were then used as input data in mechanical models to simulate their behaviour when simultaneously subjected to four-point bending and a pre-defined time-temperature heating curve. The mechanical models comprised the investigation of the out-of-plane deflections and stress fields in the panels during the fire resistance tests.

1.3 MAIN SCIENTIFIC CONTRIBUTIONS

The work presented in this thesis provided a better understanding about (i) the mechanical behaviour (under shear or compressive stresses) at elevated temperature of PUR and PET foams, delivering a significant amount of experimental data that were not available in the literature; (ii) the temperature dependence of the mechanical properties of GFRP laminates (under shear, tensile or compression stresses) produced by vacuum infusion with a balanced fibre architecture, (iii) proposed a methodology for the determination of the thermophysical properties of polymeric foams and GFRP materials as a function of temperature; (iv) delivered comprehensive and significant experimental data about the fire behaviour of GFRP sandwich panels, both in terms of thermal and mechanical responses. In the following paragraphs the main scientific contributions of this thesis are presented.

The study regarding the influence of temperature on the mechanical behaviour of the constituent materials of sandwich panels (Chapter 2 and Chapter 3) confirmed a significant temperature dependence of the mechanical response of both foams and GFRP materials and allowed quantifying it. When the test temperature approached and exceeded the T_g of the materials, considerable reductions in stiffness and strength were observed. The mechanical characterisation tests performed on the GFRP materials highlighted that, for the fibre's fraction and architectures used in the present study, the tensile properties and the compressive modulus can be classified as fibre-dominated properties, whereas the compressive modulus and the shear properties are matrix-dominated. The study about the mechanical response of GFRP and polymeric foam (PUR and PET) at elevated temperatures resulted in the following publications:

- Mazzuca P, Firmo JP, Correia JR, Castilho E. Mechanical behaviour in shear and compression at elevated temperature of polyethylene terephthalate (PET) foam. Journal of Building Engineering 2021;42:102526.

- Mazzuca P, Firmo JP, Correia J, Garrido M. Mechanical behaviour in shear and compression of polyurethane foam at elevated temperature. Journal of Sandwich Structures and Materials 2021, 1-21.
- Mazzuca P, Firmo JP, Castilho E, Correia JR. Influence of elevated temperatures on the mechanical properties of glass fibre reinforced polymer laminates produced by vacuum infusion. Construct Build Mater 2022, 128340.

With respect to the study about the influence of elevated temperatures on the thermophysical properties (thermal conductivity and specific heat) of GFRP and foam materials, several aspects can be highlighted. The results obtained confirmed that the thermophysical properties of both materials undergo significant changes with temperature. The temperature *vs.* time curves determined by the 1D heat transfer model were in relatively good agreement with the experimental thermal data, thus validating the numerical procedure used to determine the variation with temperature of the specific heat and thermal conductivity of the GFRP and both types of foams. The following publication is being prepared and will be submitted for publication:

- Duarte APC, Mazzuca P, Lopo de Carvalho JM, Tiago C, Firmo JP, Correia JR. Temperature-dependent thermophysical properties of polymeric foams. Construction and Building Materials. To be submitted in October 2022.

The investigation about the fire behaviour of GFRP sandwich panels provided further insights regarding the structural behaviour of these composite components during fire exposure. In the first stage, flexural tests at ambient temperature (Chapter 5) were performed to define the fire loads to be applied in the fire resistance tests described in Chapter 6. Then, the fire resistance tests were performed on homogeneous-core and web-core sandwich panels; the results obtained showed the effectiveness of the passive fire protection systems (either suspended or directly applied to the bottom surface) in reducing the temperatures in the panels and, consequently, in improving their fire resistance. The results obtained also allowed to assess the effects of different core materials and GFRP configurations on the fire resistance behaviour of the sandwich panels. This experimental study provided relevance results on this topic, which are currently being prepared and will be submitted for publication:

- Mazzuca P, Firmo JP, Correia JR. Experimental study on the fire resistance behaviour of GFRP composite sandwich panels. Composite Part B: Engineering. To be submitted in November 2022.

Two-dimensional and three-dimensional finite element models were developed to simulate the fire resistance tests performed on homogeneous-core and web-core sandwich panels. The temperature-dependant material properties obtained in the material characterisation tests were used as input data. The thermal models provided relatively accurate temperature predictions, thus further validating the

methodology adopted to determine the variation with temperature of the thermophysical properties presented in Chapter 4. The numerical models also provided a deeper understanding about the mechanical response of the panels, illustrating the influence of the panels' configuration (*i.e.* the presence of webs) and core materials on their fire behaviour, showing significant changes in the internal stresses distributions during the fire exposure. This numerical study resulted in the following publication, which is also being prepared and will be submitted for publication:

- Mazzuca P, Firmo JP, Correia JR. Simulation of fire resistance behaviour of GFRP composite sandwich panels. Composite Structures. To be submitted in December 2022.

1.4 OUTLINE OF THE DOCUMENT

The present document is organized in eight chapters, grouped in the following four parts:

- Part I: Introduction (chapter 1);
- Part II: Characterisation of materials at elevated temperatures (chapters 2, 3 and 4);
- Part III: Fire behaviour of GFRP sandwich panels (chapters 5, 6 and 7);
- Part IV: Conclusions (chapter 8).

The present chapter provides a brief introduction about the thesis subject, describes the objectives and methodology used to purse them and presents the organization of the document.

Chapter 2 and Chapter 3 present experimental and analytical investigations about the mechanical behaviour at elevated temperature of polymeric foams (PUR and PET) and GFRP laminates, respectively. Mechanical tests were carried out on small-scale specimens, under steady-state conditions, for temperatures ranging from 20 ºC to 300 ºC, to determine the degradation of their shear, compressive and tensile properties (only for GFRP) with temperature. The experimental data obtained in terms of strength, stiffness and failure modes is presented, discussed and compared with results available in literature. The experimental studies were complemented with an analytical study that aimed at assessing the accuracy of different models available in the literature in simulating the experimental results in terms of stiffness and strength reductions with increasing temperatures.

Chapter 4 presents experimental and numerical investigations about the thermophysical properties of GFRP and polymeric foam (PUR and PET) materials. The experimental tests were performed on unloaded (i) GFRP laminates and (ii) sandwich specimens subjected from the bottom to the ISO 834 temperature *vs.* time fire curve aiming at assessing the temperature evolution across the specimens' depth. The numerical study aimed at determining the thermophysical properties as a function of temperature of the GFRP and foam materials. The 1D heat transfer model was validated from the comparison between numerical results and experimental data. The results obtained were then used as input data in the thermal models developed in chapter 7.

Chapter 5 presents the work developed regarding the flexural behaviour of the GFRP composite sandwich panels at ambient temperature conditions. The first part of this chapter concerns the panel design, in particular the description of the GFRP's fibre architecture and the panel configurations considered. In the second part of the chapter, the test set-up and instrumentation adopted are described and the experimental results are presented. The flexural tests aimed at determining the influence of using different core materials and GFRP architectures on the mechanical response of the GFRP sandwich panels; the performance of the different types of panels is evaluated in terms of ultimate load, stiffness, and failure modes. In addition, the results obtained were used to define the fire load to be used in the fire resistance tests described in Chapter 6.

Chapter 6 presents the experimental study about the fire resistance behaviour of the GFRP sandwich panels. The specimens were simultaneously loaded in bending and heated from the bottom following the temperature *vs.* time curve defined in the ISO 834 standard. The effect of using different core materials, GFRP configurations and passive fire protection systems is evaluated. The first part of the chapter focuses on the thermal response of the sandwich panels; the results obtained from these tests are plotted in temperature *vs.* time curves. Subsequently, for each type of specimens tested, the mid-span displacements curves, the failure modes and the fire resistance are presented and discussed.

Chapter 7 presents a numerical study that consisted of simulating some of the fire resistance tests reported in Chapter 6. First, a detailed description of the numerical procedure is presented, in particular, the material properties and the boundary conditions considered in the simulation. Next, the numerical results obtained in terms of temperature evolution, stresses and displacements are presented, discussed, and compared (when applicable) with the results obtained in the fire resistance tests.

In chapter 8 the main conclusions of this thesis are presented and recommendations for future research are proposed.

Part II.
Characterisation of constituent materials at elevated temperature

CHAPTER 2

CHARACTERISATION OF PUR AND PET CORE FOAMS AT ELEVATED TEMPERATURE

2.1 INTRODUCTION

Polymeric foams are being increasingly used as core materials of composite sandwich panels for structural applications because of their improved thermal insulation, lightness, high stiffness, and strength [1,2]. However, there is a major gap in the knowledge about their mechanical response at elevated temperature or under fire exposure. Because polymeric foams play a key role in the structural effectiveness of sandwich panels, it is of the utmost importance to characterise their mechanical behaviour at elevated temperatures. In this context, after the state-of-the-art review in section 2.2., the present chapter described an experimental investigation developed about the mechanical characterisation (in shear and compression) at elevated temperatures of the PET and PUR foams used as core materials in the GFRP-sandwich panels studied in the next chapters.

2.2 LITERATURE REVIEW AND SIGNIFICANCE

Despite the important contribution of core materials to the structural response of sandwich systems, the information available in the literature about the influence of elevated temperatures on the mechanical properties of polymeric foams is still very scarce.

Regarding the out of plane shear behaviour at elevated temperatures of these core materials, according to the author's best knowledge, only four studies were performed so far [16–19].

Garrido *et al*. [16] used the Iosipescu test method, according to the ASTM D 5379/D 5379M [20] standard, to study the shear behaviour of PUR and PET core foams (densities of 68 and 94 kg/m^3, respectively) for temperatures ranging from -20 ºC to 120 ºC. In this study, Dynamic Mechanical Analysis (DMA) were also performed on both polymeric foams, allowing to define their T_g*s* as 65 ºC and 90 ºC (respectively for PET and PUR) based on the onset of the storage modulus curves. The results obtained from the shear tests confirmed that PET foam is significantly more affected by temperature than PUR - although at ambient temperature the shear modulus of the former was 3 times higher than that of the PUR foam, at 80 ºC both presented similar (absolute) values, respectively 24% and 66% of those at ambient temperature. This study also allowed to conclude that the Iosipescu test

method is not appropriate to determine the shear strength of these polymeric foams at elevated temperatures – apart from the very small dimension of the specimens used (therefore being less representative of the actual shear response of foam cores used in real full-scale sandwich constructions), due to the very high deformation capacity of these materials (especially at elevated temperatures), it was not possible to reach shear failure in most tests performed at elevated temperatures – for this reason, only the shear modulus could be determined.

Rezaei *et al.* [17] evaluated the shear properties of a PET foam (density of 110 kg/m^3, T_g not reported) up to 100 °C by means of four-point bending tests performed according to ASTM C393 on sandwich specimens with GFRP face sheets. The specimens were pre-conditioned at 50 °C for 16 hours (the effect of this conditioning was not reported). The shear failure of the core material was observed only at room temperature, and hence, for the remaining test temperatures only the values of shear modulus were determined. The authors reported drastic reductions of the shear modulus with increasing temperatures - decreases of 66% and 87% were obtained at 75 °C and 100 °C, respectively.

Benderly and Putter [18] performed four-point bending tests on sandwich specimens made of PMI foam core (density of 205 kg/m^3, T_g not reported) and aluminium face sheets at - 40 ºC, room temperature and 70 ºC. The authors adopted a modified test configuration to that suggested in ASTM C393 [21], with the aim of determining the shear/compression failure envelope of that core material at different temperatures. It is worth mentioning that the foam was dried at 130 °C for 4 hours before and after being bond to the aluminium skins (the influence of this conditioning was not analysed). Although similar shear and compressive strength reductions were obtained at 70 ºC (31% and 35% for shear and compression, respectively) the compression/shear failure criteria for that specific foam was described by an elliptical curve.

Zhang *et al.* [19] investigated the shear behaviour of a cross-linked PVC foam using a modified Arcan rig test setup at temperatures from 25 ºC to 85 ºC. The foam had density of 100 kg/m^3 and T_g of 70 ºC (determined by Saenz [22], from DMA experiments on the same foam and defined based on the onset of the storage modulus curve). Overall, the degradation trend of the shear strength with temperature was similar to that of shear modulus; at 85 ºC, the retained strength and stiffness were almost 50% of their ambient temperature values.

Although the core materials are responsible for most of the shear response of sandwich panels (particularly, those without web-cores), in most cases its flatwise compressive behaviour is also relevant, namely when a panel is loaded in bending; in this case, crushing of the panel can occur at the supports or under the loading points, due to compressive failure of the core. Thus, when a sandwich panel is subjected to elevated (service) temperatures or fire, failure can also be triggered due to reduction of compressive strength of the core material. Despite its scientific and practical relevance, few studies are available in the literature regarding the effects of elevated temperature on

the compressive properties of polymeric foams used as core materials in sandwich construction [23–26].

Thomas *et al*. [23] studied the compressive behaviour at elevated temperature (up to 110 ºC) of three closed-cell PVC foams (densities of 75, 130 and 300 kg/m^3; T_g*s* not reported). The authors found out that the compressive properties of the foams are associated to their relative density - although foams with higher density presented higher compressive strength at all test temperatures, they concluded that the strength degradation with temperature was more significant in foams with higher densities, primarily because of the more dominant behaviour of the solid polymer with increasing density when compared to the influence of the deformation mechanism in the foams' microstructure (*i.e.* related with the nodal connectivity between the foam's cells).

Zhang *et al*. [24] studied the compressive behaviour of a closed-cell cross-linked PVC foam (same foam studied in [19]; density of 100 kg/m^3 and T_g of 70 ºC) at moderately elevated temperatures, from 20 ºC up to 90 ºC. The compressive modulus of the PVC foam exhibited a non-linear reduction with increasing temperatures; moreover, it was also observed that this mechanical property is highly affected even for moderately elevated temperatures – at 90 ºC a reduction of about 50% was obtained, which agreed with the variation of storage modulus with temperature derived from the DMA experiments.

Arezoo *et al*. [25] assessed the effects of elevated temperature on the compressive behaviour of PMI foams. The authors tested foams with four different densities (from 57 to 200 kg/m^3; T_g*s* not reported) at two elevated temperatures (70 ºC and 200 ºC) and also at very low temperatures (up to -69 ºC). All the foams exhibited an elasto-plastic behaviour at ambient temperature and 70 ºC, for which the compressive strength reduction was about 40%; at 200 ºC a rubbery type response was obtained with very low compressive strength retention, only 10% of that at room temperature.

More recently, Siivola *et al*. [26] conducted compressive tests on PMI foam (measured density of 60 kg/m^3, T_g not reported) at different temperatures (30, 60 and 80 ºC) and humidity conditions (dry, ambient and wet). The results obtained showed that increasing the temperature from 30 ºC to 80 ºC caused reductions of both stiffness and strength of 70% to 90% of the ambient temperature values (depending on humidity conditions - higher reductions were obtained with increasing humidity); these changes were attributed to the softening and plasticization of the polymeric material.

The literature review presented above showed that the number of studies about the influence of elevated temperatures on compressive and shear properties of polymeric foam cores is still limited. A key limitation on most of those studies is that the reduction with temperature of the mechanical properties was not correlated with the thermomechanical ones; in fact, in most cases, the T_g was not reported.

Regarding the investigation of the shear properties of polymeric foams at elevated temperatures (the most relevant mechanical properties for sandwich panels in bending), the following limitations were found in the available research: (i) in some studies ([17,18]) the shear properties of the core materials were derived from sandwich specimens subjected to bending - *i.e.* the core was not subjected to a pure shear stress state (but also to bending and flatwise stresses); (ii) the lack of representativeness of foam core specimens regarding real full-scale sandwich constructions, due to their very small dimension ([16,19]); (iii) in other studies, it was not possible to determine the shear strength at elevated temperature, because shear failure was not observed (due to limitations of the test setup [16,17] or the occurrence of different failure modes [17]).

The experiments had two main objectives: (i) to understand and determine the response at elevated temperatures of the PET and PUR foams under compression and shear stresses (including both strength and modulus), thus contributing to the definition of temperature-dependent constitutive relationships and failure criteria (essential information for numerical modelling and fire design of sandwich panels); and (ii) to validate and assess the feasibility of an alternative experimental method – the DTS method (proposed and used in ambient temperature tests by Garrido and Correia [27]) – to characterize the shear behaviour of polymeric foams at elevated temperatures. In order to validate the DTS test setup, the numerical results obtained from a finite element (FE) analysis were used to assess the stress state developed in the specimens.

2.3 EXPERIMENTAL PROGRAMME

2.3.1 Description of the materials

In the present study, two closed-cell PUR foams with measured densities of 40 kg/m^3 and 93 kg/m^3 and a PET foam with measured density of 99 kg/m^3 were used.

The PUR foams were produced through a moulding procedure using blowing agents by the company *ALTO – Perfis Pultrudidos, Lda*, and were supplied in blocks of 200 × 100 × 12 cm^3. With this production method, cells with quasi-homogeneous sizes are obtained and the foams are expected to present quasi-isotropic or slightly orthotropic properties. These foams are comparable to those used in the Dynamic Mechanical Analysis (DMA) carried out by Garrido *et al.* [16], who reported a T_g value of 90 ºC (defined based on the onset of the storage modulus curve).

The thermoplastic closed-cell PET foam used in this work was manufactured by 3A Composites under the commercial designation *Airex T92.100*. The material was produced through a process in which the foam strands are extruded through a breaker plate (with hexagonal holes) and pressed together with a calibration unit; after this stage, the foam is subjected to multiple rearrangements including cutting and welding. The thermomechanical response of a similar PET foam with a measured density of 94 kg/m^3 (produced by *GURIT*) was investigated earlier by Garrido *et al.* [16]

through DMA. These tests allowed defining a reference T_g of 65 ºC, based on the onset of the storage modulus curve decay; such value is assumed representative of the foam tested in this study, as both foams are made from the same bulk material and present very similar densities.

2.3.2 Thermogravimetric analysis (TGA)

2.3.2.1 PUR foam

TGA experiments were performed according to ISO 11357 [28] on PUR foam specimens with density of 93 kg/m^3 extracted from the panels in order to determine the mass variation as a function of temperature. The experimental programme carried out to study the thermophysical response of PUR foam is presented in Table 1.

Table 1 - TGA test programme.

Mass	Purge gas		Heating programme
	Air	Nitrogen	
6 mg	2 specimens	2 specimens	30 to 900 °C at 10 °C/min

The specimens, with mass of ~6 mg, were placed in an alumina pan and tested in a Perkin Elmer Simultaneous Thermal Analyser (STA) 6000 following a predefined heating programme, from 30 ºC to 900 ºC at 10 ºC/min. Two types of purge gas were considered, namely air and nitrogen, and two specimens were tested for each type of atmosphere.

Figure 1 presents representative[1] mass loss curves obtained from the TGA tests performed on the PUR foam specimens in both air and nitrogen atmospheres.

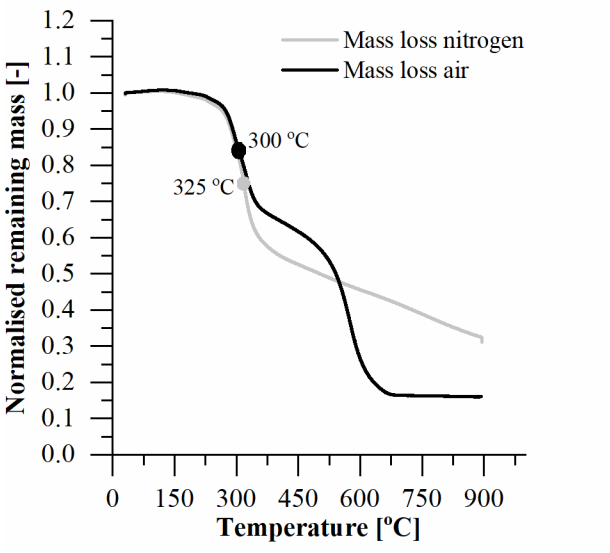

Figure 1 - TGA results in air and nitrogen atmospheres on PUR foam specimens with 93 kg/m^3.

[1] No significant differences were obtained for the replicate specimens.

Concerning the results obtained in air atmosphere, the foam presents two main steep drops in the remaining mass curve at around 300 °C and 550 °C. The full decomposition of the material occurred at 650 °C; for higher temperatures, the presence of char residue was noted and no significant changes were reported in the mass loss curve.

The normalised remaining mass curves of the PUR foam tested in nitrogen atmosphere exhibit a significant drop at around 300 °C, above which the mass gradually decreases up to 900 °C. It is still worth mentioning that no significant mass losses were observed up to 100 °C in both atmospheres, thus showing that the presence of humidity inside the foam was very low. The T_d of the PUR foam, determined based on the middle temperature of the drops in remaining mass curve, was set as 300 °C (*i.e.* at the first steep reduction) and 325 °C for air and nitrogen atmospheres, respectively.

2.3.2.2 PET foam

TGA tests were also performed on PET foam specimens (with initial mass around 6 mg), following the same test programme reported in Table 1, in order to determine the T_d of the material. As for the PUR specimens, the decomposition process in the PET specimens was analysed in both air and nitrogen atmosphere. Two specimens were tested for each condition. Figure 2 shows, for each of these conditions, the normalised mass loss curves of one representative specimen as a function of temperature (differences among replicate specimens were negligible).

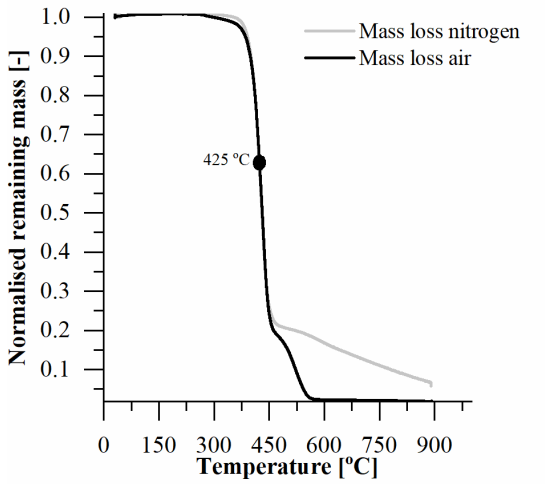

Figure 2 - TGA results in air and nitrogen atmospheres on PET foam specimens.

In both atmospheres, no evidence of mass losses was found up to 200 ºC, indicating a very low moisture content in the PET foam. In air atmosphere, the normalised mass curve presents a big and steep drop from around 350 ºC to 450 ºC (21% of remaining mass), followed by a smaller and less steep drop from 450 C to 570 ºC. For higher temperatures, the residual mass was almost null, thus indicating the complete decomposition of the polymer. In nitrogen atmosphere, the normalised mass loss curve of the specimen was initially quite similar to that in air atmosphere, also exhibiting a major drop (similar mass loss rate) between 350 ºC and 450 ºC, for which the remaining mass was also

approximately 23%. Next, the mass reduction was much slower, with a residual mass of about 5% at 900 ºC. The T_d of the PET foam was defined as 425 ºC for both air and nitrogen atmosphere, based on the middle temperature of the first major reduction observed in the remaining mass curves.

2.3.3 Mechanical characterisation at elevated temperatures

2.3.3.1 Overview of test programme

The shear and compressive tests on PUR and PET foam specimens were carried out using a *Tinius Olsen* thermal chamber (maximum temperature of 300 ºC) coupled to an *Instron* universal testing machine with load capacity of 250 kN (*cf.* Figure 3a). The test temperatures for each load condition and foam specimens are reported in Table 2.

Table 2- Overview of the tests performed on PUR and PET foams.

Foam type	Test temperature	
	Compressive tests	Shear tests
PUR foam 40 kg/m^3	-	20 ºC, 50 ºC, 80 ºC and 110 ºC
PUR foam 93 kg/m^3	20 ºC, 40 ºC, 60 ºC, 100 ºC, 140 ºC, 180 ºC and 200 ºC	20 ºC, 60 ºC, 100 ºC and 140 ºC
PET foam 99 kg/m^3	20 ºC, 40 ºC, 60 ºC, 100 ºC, 140 ºC and 190 ºC	20 ºC, 40 ºC, 60 ºC and 100 ºC

It is worth mentioning that the shear tests were carried out for both PUR foam densities, while the compressive tests were performed only for the PUR foam with 93 kg/m^3. Both types of tests were performed in steady-state conditions; *i.e.* the load was applied up to failure after the specimens had attained a constant temperature condition.

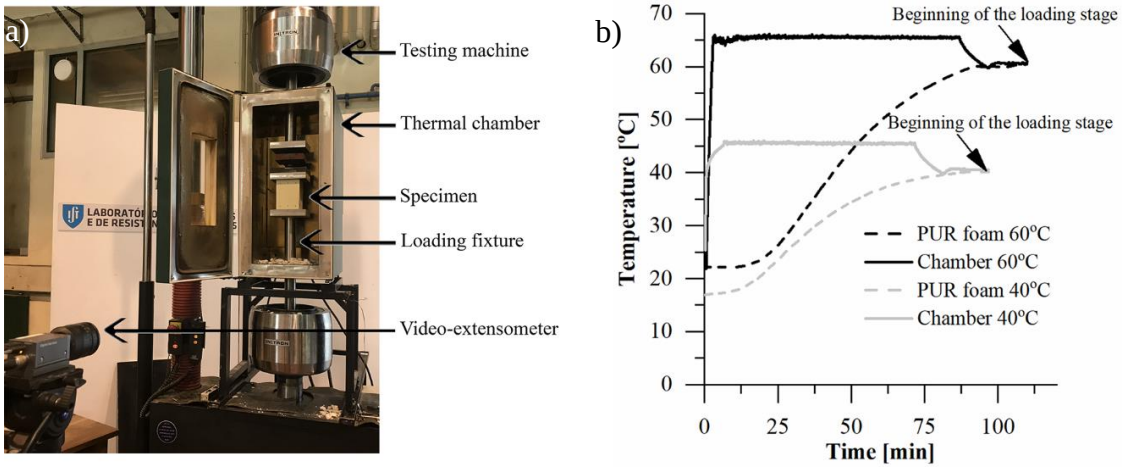

Figure 3 - Mechanical characterisation tests: (a) equipment and (b) heating procedure.

2.3.3.2 Instrumentation and test procedure

The target temperatures mentioned in Table 2 were selected to characterize the reductions of compressive and shear properties down to very low values when compared to those exhibited at ambient temperature. The temperature inside the foam during the tests was measured with a type K thermocouple (0.25 mm of conductor diameter) placed in the centre of a dummy specimen (with the

same dimensions of tested specimens) positioned inside the thermal chamber; an additional thermocouple was also used to control the air temperature inside the thermal chamber.

The specimens were heated up to the target temperature at an average heating rate of the air inside the thermal chamber of 14 ºC/min (0.3 ºC/min in PUR foam and 0.45 ºC/min in PET foam). To reduce the specimen's heating time, the initial temperature of the thermal chamber was set 5 ºC above the specimen's target temperature. Once the temperature inside the foam specimen (from now on referred to as "specimen temperature") approached the target temperature (*i.e.*, 1 ºC lower), the temperature of the thermal chamber was reduced (to the target value) and maintained for a soaking period of 15 minutes, thus guaranteeing a constant temperature in the specimen during the loading stage (procedure described in the next sections). This heating procedure is exemplified in Figure 3b, which shows, for two different target temperatures (40 ºC and 60 ºC), the temperature-time curves of both the specimens and the air inside the thermal chamber. It is worth mentioning that the specimens were left unrestrained during the heating stage (*i.e.* no mechanical restrictions were imposed, so thermal expansion of the specimens was free).

During the loading stage of the tests, the surface deformations of the specimens were measured using a video extensometer (video camera *Sony*, model XCG 5005E, with *Fujinon* lens, model Fujifilm HF50SA-1) placed on a tripod; to this end, target dots were marked on the surface of the specimens (positions described in sections 2.3.4 for the shear tests and 2.3.5 for the compressive tests) allowing to monitor their position and therefore to compute axial and shear strains. The data from the video extensometer were collected at an acquisition rate of 5 Hz.

2.3.4 Shear tests

In order to evaluate the shear response of the foam specimens at elevated temperature, the DTS test method, initially proposed by Garrido and Correia for ambient temperature tests in [27], was adopted in the present study. In this test method, a cubic specimen with chamfered edges is encased in a square loading frame composed of four metal plates connected by metal rods that work as hinges (*cf.* Figure 4). A tensile load is transferred to the specimen through two loading rods placed at the top and bottom corners of the frame that are then connected to the universal testing machine.

The foam specimens were adhesively bonded to the test fixtures by means of an epoxy-based adhesive (*Sikadur 330*) and then were cured for (at least) 7 days in a room with controlled atmosphere (constant temperature of 21 ºC and relative humidity of 56%). After reaching the target temperature, (*cf.* heating protocol in section 2.3.3.2), specimens were loaded up to failure (steady state conditions) under displacement control, at a cross-head displacement speed of 1 mm/min (set in order to guarantee that failure would occur within the first 10 min of loading); for each target temperature, at least three replicate specimens were tested.

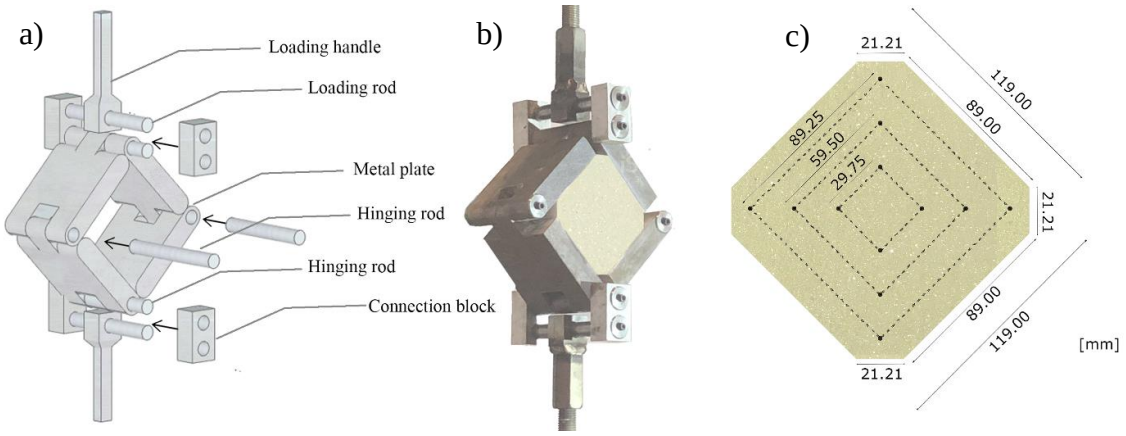

Figure 4 - Diagonal tension shear (DTS) test method: (a) test fixture components, (b) overview of the test setup and (c) specimen geometry.

The imposed deformations and force distributions on the specimens considered to be produced in the DTS method are illustrated in Figure 5. Therefore, the developed shear stress, τ_s, can be evaluated as (according to [27,29]):

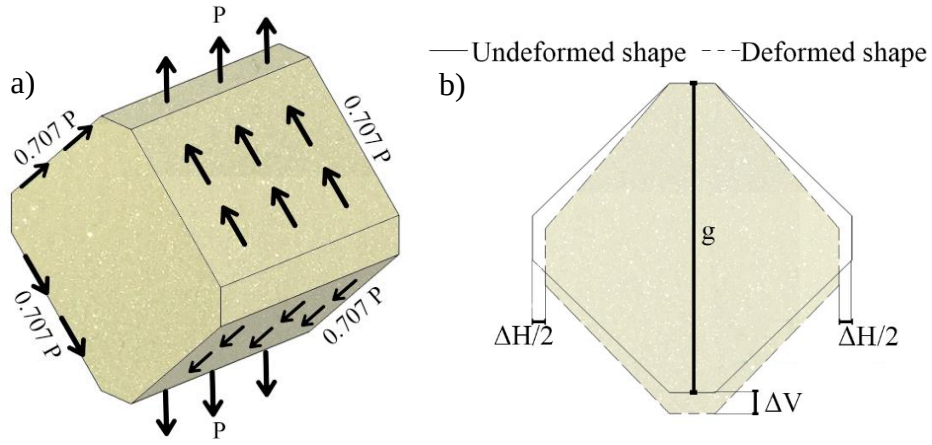

Figure 5 - Diagonal Tension Shear (DTS) test method: (a) force equilibrium and (b) kinematic concepts.

$$\tau_s = \frac{\sqrt{2}}{2}\frac{P}{A} \quad (1)$$

where P is the applied load, and A is the area of the specimen, calculated as:

$$A = \frac{(W + h) \times t}{2} \quad (2)$$

where W, h and t are the width, the height and the thickness of the specimen, respectively. Concerning the shear strain/distortion, γ, it can be obtained through the following expression:

$$\gamma = \frac{\Delta V + \Delta H}{g} \quad (3)$$

where ΔV is the vertical elongation of the specimen, ΔH is the horizontal shortening of the specimen, and g is the gauge length. Both vertical elongation and horizontal shortening were measured with a video extensometer (*cf.* previous section) that tracked the position of 12 target dots marked on the

surface of the specimens, forming 3 square alignments (*cf.* Figure 4c); the strains were computed using the results from the inner alignment as it was concluded that they were located in the area subjected to an approximate pure shear state (*cf.* section 2.7), less affected by stress concentrations developed close to the chamfered edges of the specimens.

2.3.5 Compressive tests

The compressive behaviour along the through-thickness direction of the foam specimens was determined through flatwise compression tests performed according to ASTM C365/365M [30]. The tests were carried out under steady state conditions, at different target temperatures (*cf.* heating protocol in section 2.3.3.2) on cubic foam specimen (with dimensions of 120 × 120 × 120 mm^3). After attaining the target temperature (measured in the centre of the foam, for the entire duration of the test – *cf.* section 2.3.3.2), the specimens were loaded up to failure under displacement control at a speed of 2 mm/min (set in order to cause failure within 3 to 6 min). At least three replicate specimens were tested at each temperature with the exception of the tests performed on the PUR foam at 180 °C and 200 °C, for which it was only possible to perform two tests. The compressive load was applied through two metal plates and a spherical hinge (*cf.* Figure 6) to avoid non-uniform load distribution due to potential geometric imperfections of the specimens. The compressive strains were measured with the aid of a video extensometer that tracked the position of six reference points (three alignments) painted on the surface of the foam - the average strain between these three alignments (gauge length of 90 mm) was considered to estimate the (average) compressive strains shown in section 2.4.2 and 2.5.2.

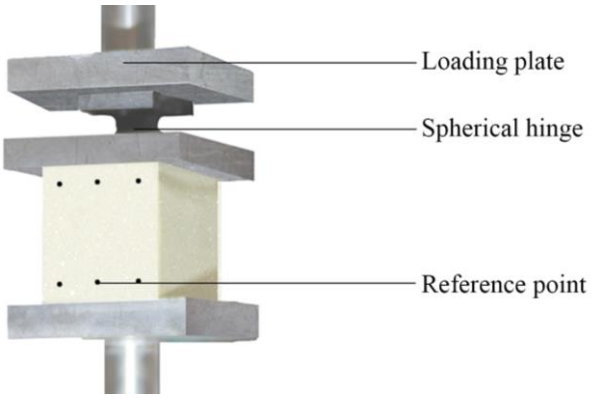

Figure 6 - Components of the compression test.

2.4 PUR FOAMS: RESULTS AND DISCUSSION

2.4.1 Shear behaviour

Figure 7 shows representative shear stress *vs.* distortion curves of the PUR foams obtained; as expected, for all tested temperatures, the strength and stiffness were higher in the foam with higher density. The results presented in this figure highlight the significant influence of elevated temperature

on the mechanical response in shear of PUR foam (for both densities), which caused considerable reductions of stiffness and strength, and also changes in the shape of the constitutive law.

Specimens tested at temperatures ranging from 20 °C to 80 °C presented a quasi-linear elastic behaviour up to failure; at higher temperatures, the level of nonlinearity significantly increased – this should be attributed to the thermophysical changes undergone by the PUR polymer during the glass transition process (more pronounced for the lower density foam), namely its softening and viscosity increase, which also resulted in an increase in the deformation capacity with temperature.

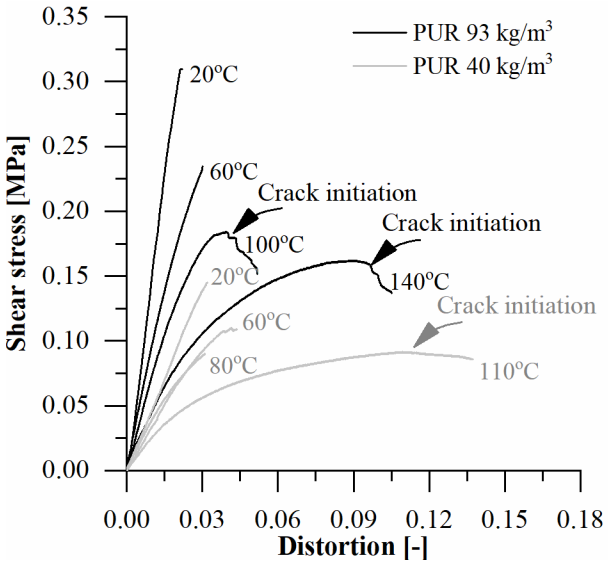

Figure 7 - Shear stress vs. distortion curves of both PUR foams for all temperatures tested.

This change in the material behaviour was also reflected in the failure modes: (i) specimens tested up to 80 °C presented brittle failure, with a sharp crack formed in the centreline of the specimens (*cf.* Figure 8a); while (ii) at 100 °C and above, the failure mode was more ductile, with a progressive development of cracks starting from the lateral edges towards the centre of the specimens, as shown in Figure 8b. It is also worth mentioning that, concerning the higher density foam, in some specimens tested at temperatures above 100 °C, it was not possible to attain the ultimate strain of the material due to the occurrence of debonding between the foam and the metal fixtures; however, this phenomenon occurred during the descending branch of the shear stress *vs.* distortion curves, after the development of the shear cracks mentioned above – therefore, it did not compromise the results obtained in terms of shear modulus and maximum shear stress (*i.e.* shear strength). This result stems from the very low stiffness/strength exhibited by the PUR foam at elevated temperature compared to those of the adhesive and bonded joint. Note that after the cracks initiation (*i.e.* after reaching the shear strength) the shear stress *vs.* distortion curves no longer have an accurate physical meaning, as the actual "shear area" of the specimens is changed.

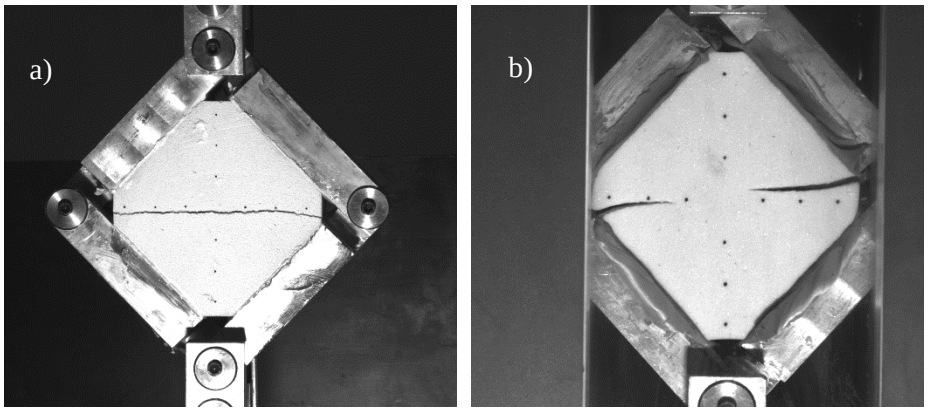

Figure 8 - Failure modes at different temperatures (similar for both PUR foam densities): (a) up to 80 ºC and (b) from 100 ºC to 140 ºC.

The influence of temperature on the shear properties (strength τ_s and modulus G) of the PUR foams with densities of 40 kg/m^3 and 93 kg/m^3 is summarized in Table 3 and Table 4. It is worth mentioning that the shear modulus (G) was calculated as the slope between two points within the linear-elastic range of the shear stress *vs.* distortion curve – for each tested temperature these two points corresponded to 25% and 50% of the respective maximum shear stress. Concerning the foam with lower density (40 kg/m^3), the shear modulus was more affected by elevated temperature than the shear strength: at 110 ºC, the average reductions of shear modulus and strength were respectively 62% and 32%, when compared to the corresponding values at ambient temperature.

Table 3 - Results of the shear tests on the PUR foams with density of 40 kg/m^3 (average ± standard deviation).

PUR 40 kg/m^3				
T [°C]	τ_s [MPa]	τ_s/τ_{20} [-]	G [MPa]	G/G_{20} [-]
20	0.13±0.01	1.00	4.6±0.85	1.00
50	0.11±0.01	0.86	3.4±0.39	0.75
80	0.10±0.01	0.81	3.2±0.16	0.71
110	0.09±0.01	0.68	1.7±0.16	0.38

Table 4 - Results of the shear tests on the PUR foams with density of 93 kg/m^3 (average ± standard deviation).

PUR 93 kg/m^3				
T [°C]	τ_s [MPa]	τ_s/τ_{20} [-]	G [MPa]	G/G_{20} [-]
20	0.31±0.02	1.00	15.1±0.75	1.00
60	0.24±0.01	0.77	9.9±1.13	0.63
100	0.17±0.01	0.60	7.7±0.33	0.51
140	0.15±0.01	0.53	3.70±0.33	0.24

For the PUR foam with higher density (93 kg/m^3), the shear modulus was also more affected by elevated temperature than the shear strength: at 100 ºC, the shear strength and modulus were reduced to 60% and 51% of their ambient temperature values, respectively; for higher temperatures, a more drastic reduction of shear modulus was observed, 75% at 140 ºC; for this temperature range, the reduction of shear strength was less pronounced, with a decrease of 47% at 140 ºC (from 100 ºC to 140 ºC, the shear strength was only further reduced by 7%). This less pronounced reduction of shear

strength at higher temperatures, observed for both foam densities, may be related to the deformation mechanism, more ductile at higher temperatures, which may have promoted a more uniform stress distribution. This aspect is discussed in further depth ahead in this chapter (*cf.* section 2.7).

Figure 9 presents a comparison of the shear properties for the two foams tested – modulus and strength normalized to corresponding ambient temperature values. Concerning the shear modulus, both PUR foams showed similar reductions, despite having different densities. This suggests that density did not significantly influence the reduction of shear modulus with temperature. Regarding shear strength, the foam with higher density exhibited more significant reductions with temperature – similar results had already been reported by Thomas *et al.* [23] and Arezoo *et al.* [25] about the compressive behaviour of PVC foams at elevated temperatures. In this respect, as suggested by [31], foams with different densities are likely to undergo different deformation mechanisms (from stretch dominated to bending dominated) due to changes in thickness and length of the cell wall/strut – this may explains why low density foams exhibit (i) a more ductile behaviour at elevated temperature, and (ii) lower strength reductions with temperature when compared to higher density foams. As shown in Figure 9, for the temperature range tested, the shear properties decreased almost linearly with temperature.

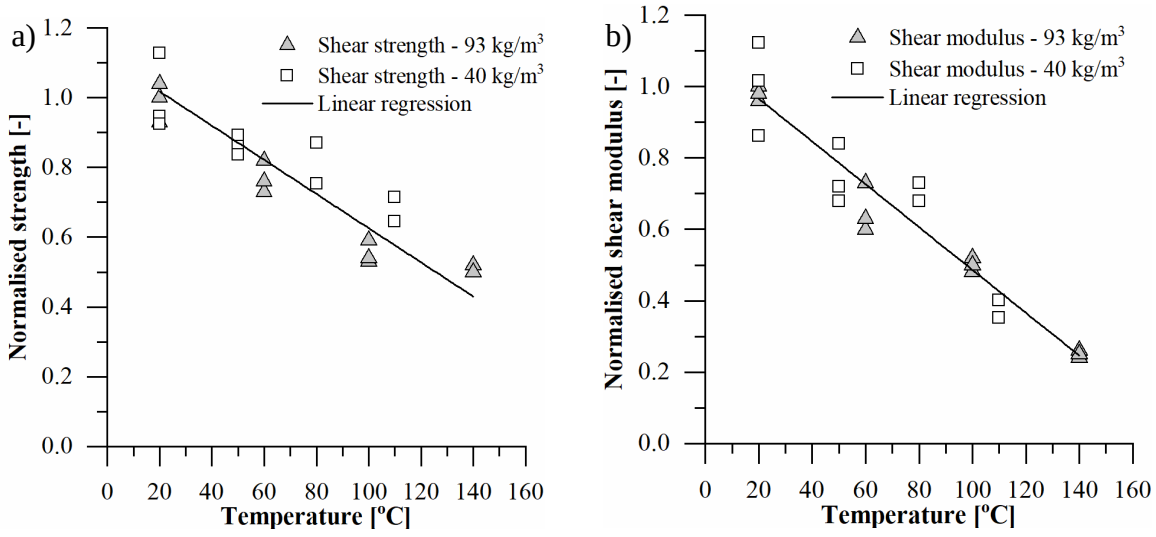

Figure 9 - Normalised (a) shear strength and (b) shear modulus reductions with temperature.

2.4.2 Compressive behaviour

For all temperatures, the PUR foam showed the typical compressive response of polymeric foams, with three different stages [31]: (i) a first linear elastic segment, governed by two mechanisms, namely cell face stretching and cell wall bending (*cf.* Figure 10a-b); followed by (ii) a stress peak and a horizontal plateau, in which the cell struts start collapsing by plastic bending, elastic buckling or brittle fracture, depending on the properties of the cells (*cf.* Figure 10c-e); and (iii) a final steep increase in the compressive stress (less pronounced with increasing temperatures) - after all the cells are collapsed, their walls compact and the material starts behaving increasingly like a solid, in a

phenomenon known as densification. For higher temperatures (*i.e.* tests performed at 180 ºC and 200 ºC), it should be noted that the constitutive relation did not present a visible yield point, probably due to the high viscous flow the foam underwent; a similar behaviour was reported by Arezoo *et al*. [25].

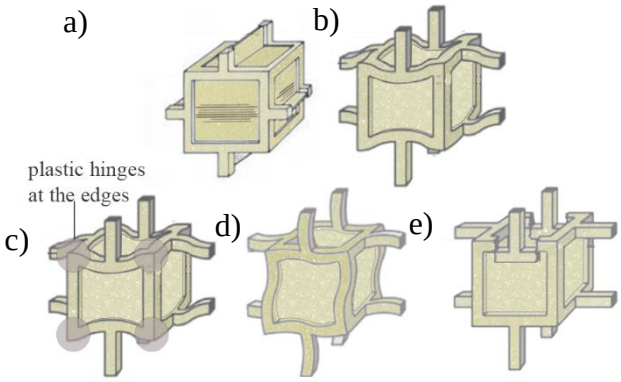

Figure 10 - Typical cell deformation mechanisms: (a) axial stretching, (b) elastic bending, (c) plastic bending, (d) elastic buckling and (e) brittle fracture (adapted from [31]).

Figure 11 also shows that increasing temperature leads to a progressive reduction of both compressive strength and modulus. For all tested temperatures, the compressive modulus was estimated considering the slope (almost linear) of the compressive stress *vs.* strain curves between 25% and 50% of the compressive strength (determined as the stress peak observed before the plateau). As in the shear tests, the non-linearity of the response at the first stage of the compression behaviour became more pronounced with temperature. In addition, a progressive shortening of the plateau was observed with increasing temperatures; a similar behaviour was observed on PMI foam by Thomas *et al.* [23], the authors attributed this effect to the influence of foam softening, which promotes the occurrence of contact between the cell walls at lower stress levels, and thus densification to take place for smaller strains. Figure 11b shows the normalised compressive properties reductions with temperature. Overall, for the temperature range tested, the reduction of the compressive properties with temperature was approximately linear.

It is worth mentioning that, for the range of temperature tested, no signs of thermal decomposition were observed (*e.g.* discoloration). Table 5 summarizes the reduction of compressive strength σ_c and modulus E_c with temperature with respect to room temperature. At 40 ºC the reductions are very low, with retained strength and modulus of 89% and 97%, respectively, compared to ambient temperature. At 100 °C, both properties undergo reductions of almost 50%. When the test temperature increased to 180 ºC, the material still retained some compressive strength (the average reduction was about 18%), whereas the compressive modulus decreased significantly to 5% of the ambient temperature values. For higher temperature, the reduction of the compressive strength presented a further increase, while the compressive modulus did not present significant variations.

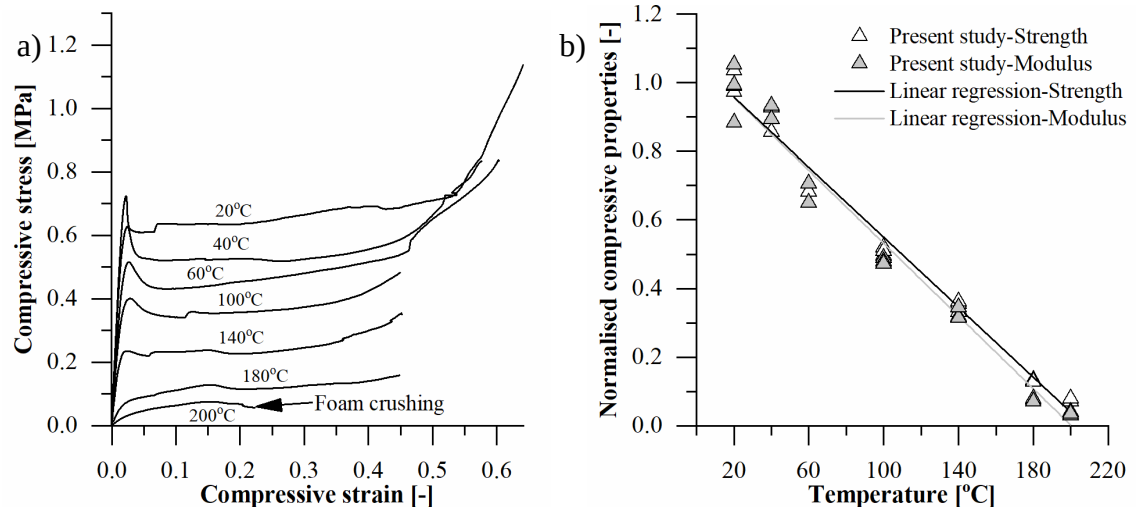

Figure 11 - Results of compressive tests: (a) representative compressive stress vs. strain curves at different temperatures and (b) normalised compressive properties reductions with temperature.

Table 5 - Results of compressive tests on PUR foam (93 kg/m^3) (average ± standard deviation).

T [°C]	σ_c [MPa]	σ/σ_{20} [-]	E_c [MPa]	E_c/E_{c20} [-]
20	0.73±0.02	1.00	42.4±5.08	1.00
40	0.65±0.04	0.89	41.1±4.62	0.97
60	0.51±0.01	0.69	26.8±2.26	0.62
100	0.39±0.02	0.53	22.8±0.39	0.54
140	0.26±0.01	0.35	13.8±0.71	0.32
180	0.13±0.01	0.18	2.3±0.01	0.05
200	0.08±0.01	0.10	1.4±0.05	0.03

2.5 PET FOAM: RESULTS AND DISCUSSION

2.5.1 Shear behaviour

Figure 12 presents representative shear stress *vs.* distortion curves of the PET foam for each test temperature, obtained from the DTS test method.

Similarly to the PUR foam, the PET foam first exhibits a quasi-linear elastic response, which is followed by a markedly non-linear behaviour up to failure with progressive stiffness reduction. At 40 ºC and 60 ºC, the non-linearity of the shear stress *vs.* strain curves becomes more pronounced and starts at lower stress levels; for these temperatures, there is also a progressive increase in the deformation capacity – again, this is associated to the increasing influence of viscous effects in the PET foam at elevated temperature, namely when the material undergoes the glass transition process.

Table 6 lists the shear properties of the PET foam – strength (τ_s) and modulus (G) – as a function of temperature and the ratios between those properties at elevated temperature and at room temperature.

Concerning the shear strength at 20 ºC, the results obtained with the DTS test method agree well with those provided by Fathi *et al.* [32] – this seems to confirm the ability of this test method in determining the shear strength of polymeric foams. Regarding the shear modulus at the same

temperature, the values provided by Fathi *et al.* [32], obtained using four-point bending and single lap shear tests, are slightly lower (~18%) compared to the result obtained in the present study using the DTS method. Such difference can be attributed (at least partly) to the combined stresses developed in the material close to the free edge (*i.e.* single lap) and in the shear failure region (*i.e.* bending test). For this reason, in the present study, the shear modulus was computed using the distortion computed in the central area of the specimen, since this area should present an approximately pure shear stress state, thus being more representative of the actual shear modulus of the core material (as described in detail in section 2.7).

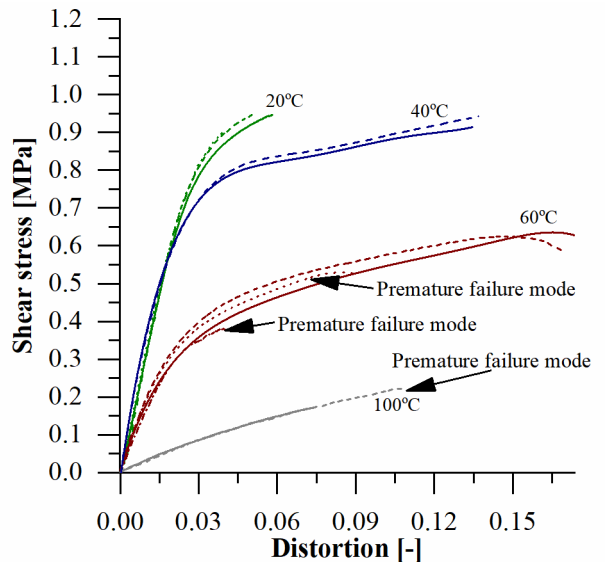

Figure 12 - Shear stress vs. distortion curves of the PET foam for all tested temperature.

At 40 ºC, the shear strength showed negligible reductions, while the shear modulus slightly decreased compared to the results obtained at room temperature (only 6%). When the test temperature approached and exceeded the T_g of the foam, the variation of the shear properties was more pronounced - at 60 ºC the shear strength was reduced to 67% of its room temperature value, whereas the shear modulus was reduced to 48%; at 100 ºC, more severe reductions were observed - the retained shear modulus was only 7% of the ambient temperature values; as described ahead, it was not possible to determine the shear strength at 100 ºC, however, the results showed that the retained shear strength was higher than 19%. As for the PUR foam, the reduction of the shear modulus with temperature is steeper than that of the shear strength.

Table 6 - Shear properties of PET foam as a function of temperature (average ± standard deviation).

T [ºC]	τ_s [MPa]	τ_s/τ_{20} [-]	G [MPa]	G/G_{20} [-]
20	0.93±0.02	1.00	31.97±0.65	1.00
40	0.92±0.02	0.99	30.33±0.14	0.94
60	0.62±0.01	0.67	14.17±0.30	0.48
100	>0.18*	>0.19*	2.6±0.02	0.07

*Note: these values are a lower bound of the shear strength, as only premature failures were obtained at this temperature.

As for the PUR foam, for temperatures ranging from 20 ºC to 60 ºC, the failure mode involved a sharp horizontal crack in the foam specimen (*cf.* Figure 13), representing the typical 45º crack observed in the core of sandwich panels loaded in bending.

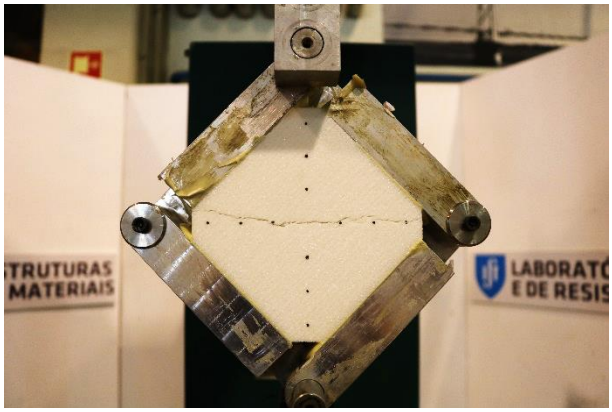

Figure 13 - Typical shear failure observed in PET foam.

However, as highligthed in Figure 12, at 60 ºC and 100 ºC, some specimens presented premature failure at the fixture-foam bonded interface (*cf.* Figure 14), *i.e.*, the bond strength was lower than the shear strength of the foam. This is a limitation of the DTS method when testing foam core materials at elevated tempeature, highlighting the importance of selecting an adhesive that is able to bond the specimen to the fixture, namely at elevated temperature [33]. Regarding these premature failure modes that ocurred in some of the tested specimens, it is worth referring that, with the exception of the results at 100 ºC, the shear properties reported in Table 6 were obtained from tests in which pure shear failure occurred.

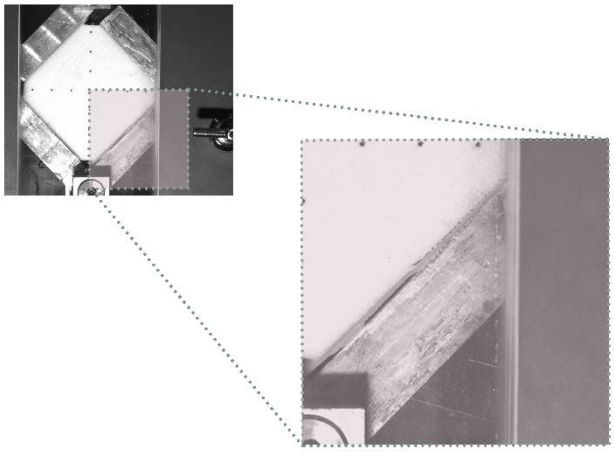

Figure 14 - Failure at the fixture-foam bonded interface in some specimens tested at 60 ºC and 100 ºC.

2.5.2 Compressive behaviour

Figure 15 shows for each target temperature, the compressive stress *vs.* strain curves of one representative PET foam specimen.

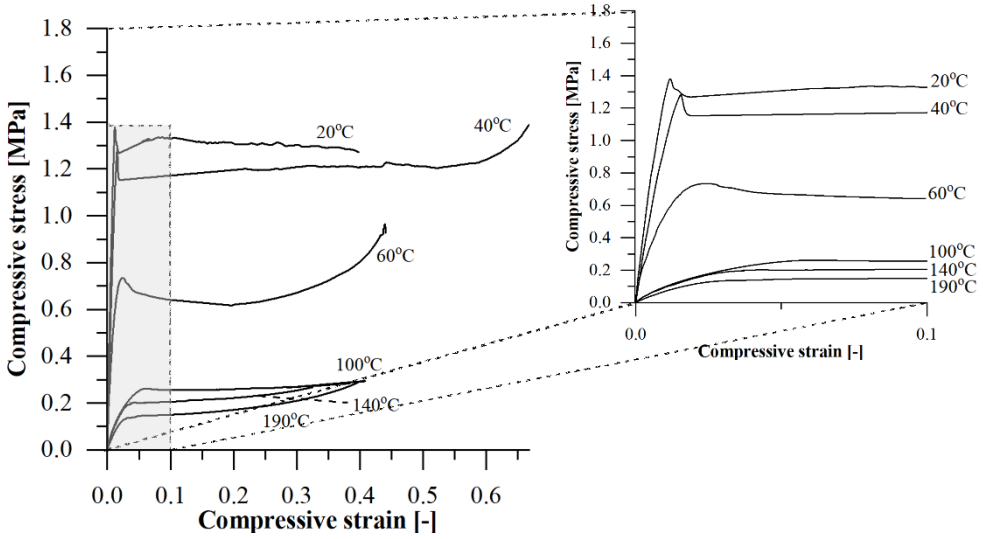

Figure 15 - Compression stress vs. compression strain curves at elevated temperature[2].

For temperatures above 20 ºC, the curves exhibit the typical three-stages of development reported also for PUR foam (at ambient temperature conditions): quasi-linear elastic behaviour at low strains, followed by a horizontal plateau and a final region of densification. It is worth mentioning that at 20 ºC it was not possible to attain the densification stage of the foam - this may be related to the failure mode observed at this temperature (cell crushing close to the loading plate – as described ahead) that hindered an uniform stress distribution in the specimens for strains beyond 0.4. As for the PUR foam, the non-linearity of the compressive response was found to increase considerably with temperature.

It is also worth noting that elevated temperature changed the post-yielding softening: at room temperature, a sharp load drop was observed, which is indicative of highly localised cell deformations [34]; at elevated temperature, the load drops were softer, which seems to indicate that the specimens were deformed more uniformly – this behaviour may be associated to softer deformation modes occurring in the cells at these temperatures (namely, cell wall bending instead of axial shortening). In addition, for increasing temperatures, the densification occurred at smaller strains due to the polymer softening, which was reported to accelerate the cell collapse process ([23,25]).

Table 7 presents the compressive properties – modulus (E_c) and strength (σ_c) - at the various test temperatures and the corresponding ratio with the property at room temperature: at this reference

[2] At very high compression strains, the readings of the video-extensometer were lost, preventing the full quantification of the densification stage.

temperature (20 ºC), the foam exhibited relatively high compressive properties (when compared to PUR foam of similar density) mainly due to their honeycomb-like structure and the elongated cells in the through-thickness direction. The compressive properties obtained from the tests performed at room temperature are in line with the results provided by the manufacturer [35]. When the test temperature increased to 60 ºC, the compressive modulus and strength suffered reductions of about 60% of their ambient temperature values; at 100 ºC, the compressive modulus and the compressive strength were drastically reduced to 7% and 19% of the corresponding values at ambient temperature. For higher temperatures, the variation of the compressive properties was less pronounced: compressive strength reductions of 5% and 4% occurred respectively in the range 100-140 ºC and 140-190 ºC, while the compressive modulus remained almost constant up to 190 ºC – these results seem to indicate that the rate of degradation of the mechanical properties decrease once the polymer undergoes its rubbery regime.

Figure 16a shows the typical failure mode exhibited by the PET foam specimens in the compressive tests performed at room temperature - localised failure occurred in the specimens' surface next to the loading fixture; according to Fathi [24], this behaviour can be attributed to: (i) high out-of-plane stiffness of the foam; (ii) damage of the surface cells during the manufacturing process (*i.e.* in the welding and cutting process). When the test temperature was increased, the foam presented a more ductile failure mechanism, with the formation of several crushed bands at different heights of the specimen (*cf.* Figure 16b).

Table 7 - Compressive properties of PET foam as a function of temperature (average ± standard deviation).

T [°C]	σ_c [MPa]	σ_c/σ_{20} [-]	E_c [MPa]	E_c/E_{c20} [-]
20	1.40±0.01	1.00	103.10±5.41	1.00
40	1.27±0.02	0.90	101.26±2.88	0.98
60	0.86±0.01	0.61	65.18±2.74	0.63
100	0.26±0.01	0.19	7.33±0.07	0.07
140	0.20±0.01	0.14	7.13±0.18	0.07
190	0.14±0.01	0.10	6.13±0.18	0.06

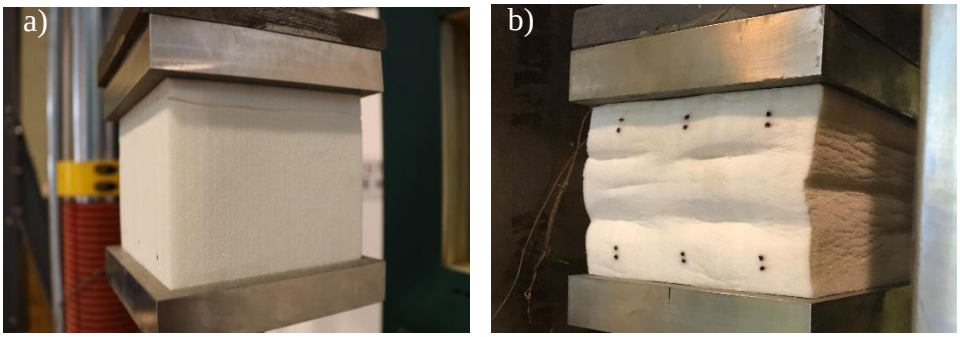

Figure 16 - Typical failure modes obtained in the compression tests at (a) room temperature and (b) elevated temperatures.

2.5.3 Analytical study

In this section, the results described in section 2.5.1 and 2.5.2 and those provided by Rezaei *et al.* [17] are used to assess the ability of empirical models in describing the degradation of the mechanical properties of PET foam at elevated temperature. To this end, four empirical models were considered in this study, namely those developed by Gibson *et al.* [36], Wang *et al.* [37], Correia *et al.* [38] and Mahieux *et al.* [39]. Although these models were developed for FRP materials, in accordance with [16], they are also expected to describe the behaviour of polymeric foams at elevated temperature, since both types of materials undergo the same relaxation processes with temperature.

Gibson *et al*. [36] proposed a model to describe the temperature-dependence of a generic mechanical property, *P*, as a function of temperature, *T*, using the following equation,

$$P(T) = P_u - \frac{P_u - P_r}{2} \times (1 + \tanh[k'(T - T_{g,mech})]) \quad (4)$$

where P_u and P_r are the properties of the material at room temperature and after the glass transition (but before decomposition), respectively. The k' and $T_{g,mech}$ parameters are derived from curve fitting of experimental results.

Wang *et al*. [37] proposed a model to simulate the tensile response of carbon fibre reinforced polymer (CFRP) laminates as a function of temperature. The following equation was proposed,

$$P(T) = P_u \times [A - \frac{(T - B)^n}{C}] \quad (5)$$

in which *A*, *B*, *C*, and *n* are unknown parameters that are numerically fitted based on the experimental data.

To simulate the mechanical response of glass fibre reinforced polymer (GFRP) laminates as a function of temperature, Correia *et al*. [38] proposed the following model, based on Gompertz statistical distribution,

$$P(T) = P_r + (P_u - P_r) \times (1 - e^{Be^{C \times T}}) \quad (6)$$

where *B* and *C* are obtained through the fitting of the equation to a set of experimental results.

Finally, Mahieux *et al*. [39] proposed a model based on Weibull distribution,

$$P(T) = P_r + (P_u - P_r) \times \exp[-\left(\frac{T}{T_0}\right)^m] \quad (7)$$

where T_0 and *m* are defined as the relaxation temperature and the Weibull exponent, being obtained by curve fitting of experimental data.

The four empirical models were calibrated using the results obtained in the present experimental campaign on the PET foam and those provided by Rezaei *et al.* [17]; for each model, the analytical parameters were computed minimising the absolute mean percentage error (AMPE) to the

experimental data. In this study, the unrelaxed property P_r was taken as 1.0 (normalized average property value at 20 ºC), while the relaxed property P_u was considered as the retained material property obtained at the maximum temperature tested (see experimental results described in section 2.5). The latter assumption stems from the DMA results obtained by Garrido *et al.* [16], which shows that the glass transition process for this PET foam is completed at around 100 ºC (*cf.* Figure 1).

Figures 17 and 18 show the modelling (fitted) curves for the shear modulus and compressive properties – strength and modulus – of PET foam as a function of temperature (the shear strength was not considered due to the limited amount of test data available), together with the experimental data; the parameters defining the degradation models and the absolute mean percentage error (AMPE) are listed in Table 8, which also includes a linear regression model based on the average of the normalised shear and compressive strength and modulus.

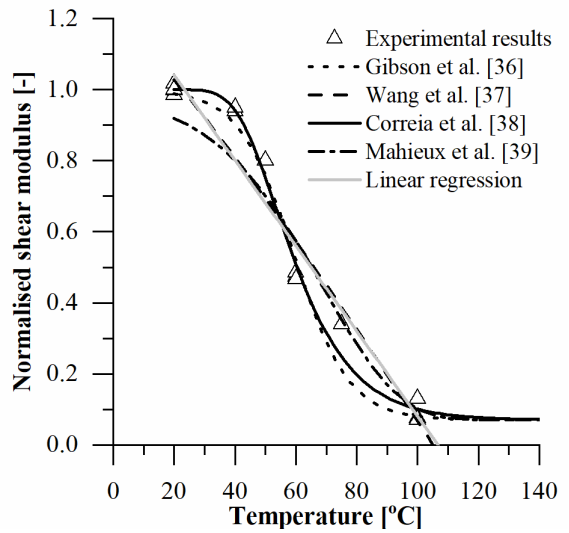

Figure 17 - Variation of shear modulus with temperature.

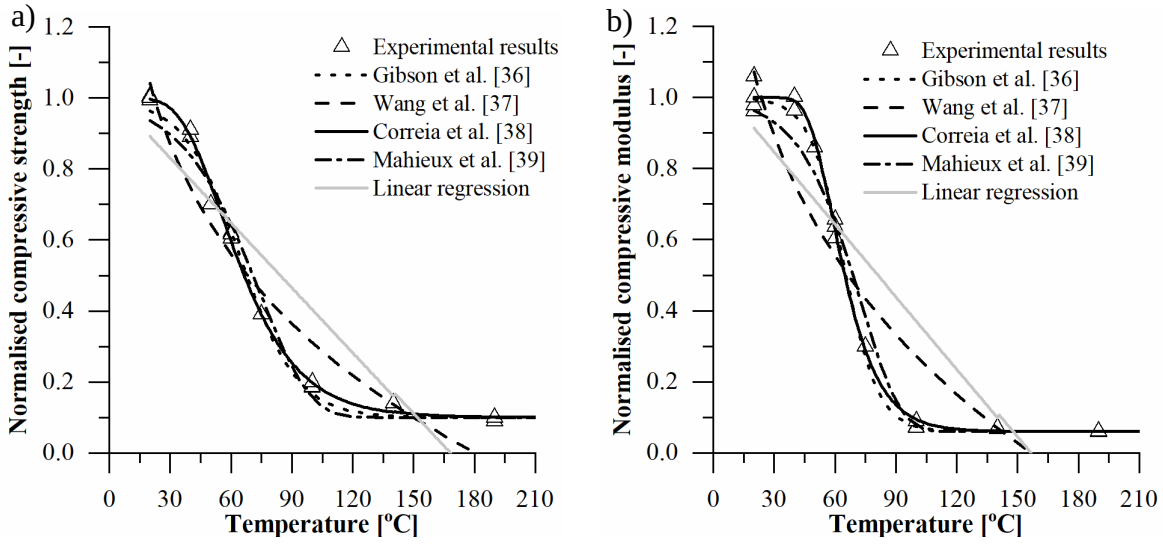

Figure 18 - Variation of (a) compressive strength and (b) modulus with temperature.

As shown in Table 8, there is a satisfactory agreement between the experimental data and all models; the AMPE values varied from 1.8% and 13.8%. The model of Correia *et al*. [38] provided the most accurate estimates of the mechanical properties of PET foam as a function temperature, presenting the lowest values of AMPE.

Table 8 - Defining parameters and absolute mean percentage error (AMPE) for the various models.

Model	Parameter	Shear modulus	Compressive strength	Compressive modulus
Gibson *et al*. [36]	*k'[-]*	0.05	0.03	0.06
	$T_{g,mech}$ *[ºC]*	59.43	64.74	64.33
	AMPE [%]	4.83	3.69	3.07
Wang *et al*. [37]	*A [-]*	1.20	4.02	3.18
	B [-]	0.97	0.55	1.21
	C [-]	172.64	0.50	0.86
	n [-]	1.14	0.13	0.19
	AMPE [%]	7.66	8.61	13.78
Correia *et al*. [38]	*B [-]*	-51.04	-14.69	-113.25
	C [-]	-0.07	-0.04	-0.08
	AMPE [%]	3.52	1.78	2.31
Mahieux *et al*. [39]	*m [-]*	19.00	15.00	19.00
	T_0 *[-]*	344.41	348.37	346.53
	AMPE (%)	8.12	4.88	5.36
Linear regression	*AMPE (%)*	7.31	1.93	7.14
	Slope	1.19	1.27	1.21

2.6 COMPARISON WITH RESULTS FROM THE LITERATURE

In this section, results obtained in the present study in terms of shear and compressive properties (strength and modulus) of PET and PUR foams as a function of temperature are compared with those available in the literature [16,17,19,23–25]. These studies comprised different types of foams (*e.g.* PUR, PMI, PVC and PET) with densities ranging from 30 kg/m^3 to 300 kg/m^3. To enable a sound comparison, only the tests performed in similar test conditions (*i.e.* steady-state) to those used in the present work were considered. Some results were not included in the comparison due to the following reasons: (i) experiments that focused on a relatively narrow temperature range and did not correlate the reductions in mechanical properties with the glass transition process underwent by the materials when heated (*e.g.* tests by Grace *et al.* and Benderley *et al.* [18,40]); and (ii) experiments in which the material was pre-conditioned for a relatively long period of time (24 hours or longer), whose effect in the "initial" mechanical properties was not accounted for (*e.g.* tests by Siivola *et al.* [26]). A major limitation was found in most of the studies involved in the comparison: the lack of information concerning the T_g of the foam material. Results of DMA tests (according to ISO 6721-11) were only provided by Saenz [22] and Garrido *et al.* [16], concerning PUR, PET and PVC foams – the T_g values of those polymeric foams, determined from the onset of the storage modulus curve decay, were defined as follows: 65 ºC (PET), 70 ºC (PVC) and 90 ºC (PUR).

Figure 19 and Figure 20 show the variation with temperature of the normalized compressive and shear properties (with respect to ambient temperature values) of various polymeric core materials, respectively. Overall, it can be seen that increasing temperature causes a progressive reduction in mechanical properties; from a qualitative point of view, all the foams tested seems to follow a similar reduction trend. However, foams with lower T_g (*i.e.* PET) undergo more significant reductions for lower temperatures than foams with higher T_g (*i.e.* PUR), which is logical. These results confirm that the thermophysical behaviour of the foams at elevated temperature plays a crucial role in their mechanical (engineering) properties.

Concerning the PET foam, the results obtained in this study are in line with those reported by Garrido *et al.* [16] and Rezeai *et al.*[17]; the test data show that the compressive modulus presents non-linear reductions with temperature, while the compressive strength decreases linearly up to 100 ºC (*i.e.* before the rubbery regime starts). In what concerns the shear properties, they seem to be only slightly less affected by the temperature increase than the compressive ones; both shear properties – strength and modulus – decrease almost linearly with temperature.

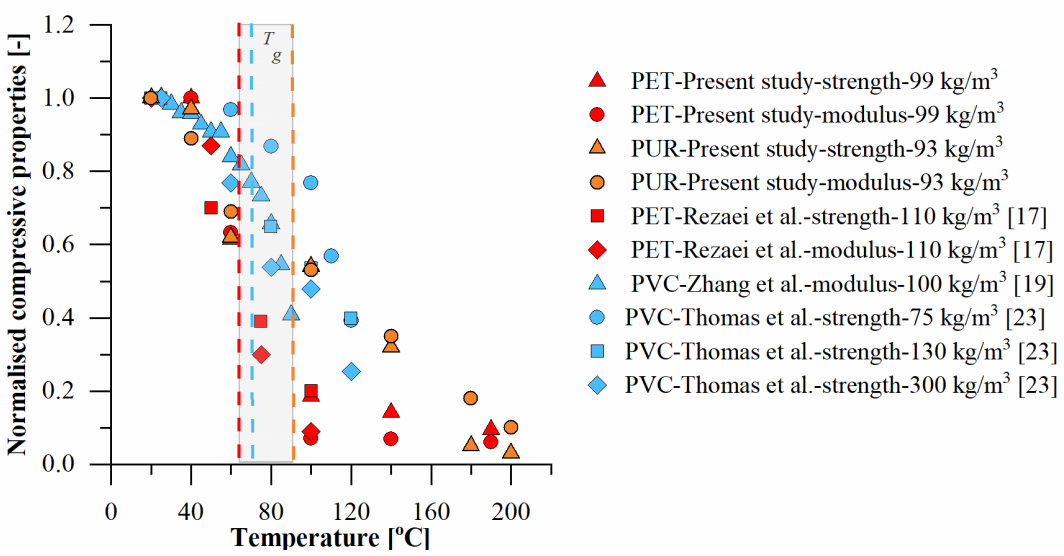

Figure 19 - Comparison of normalised compressive properties vs. temperature available in the literature with the results obtained in the present study.

As shown in Figure 20, all PUR foams showed similar shear modulus reductions, with no evidence of correlation between the density and the reduction of shear modulus with temperature. In addition, the reductions in shear and compressive moduli of the PUR foam with 93 kg/m^3 are similar; thus, it seems that these properties are more dependent on the thermophysical changes experienced by the polymer material due to heating than on possible changes in the deformation mechanism of its closed-cell microstructure. The test data also shows that the shear strength is less affected by temperature than compressive strength, especially for temperatures above 100 ºC. This result may be associated to the different deformation modes developing within the PUR foam cells in the two loading scenarios, namely after glass transition.

Given the lack of test data, especially for higher temperatures, further studies are needed (on foams with different densities and made from different solid polymers) (i) to confirm these trends and hypotheses, and (ii) to correlate the "micro" deformation mechanisms of the cell's structure with the "macro" mechanical properties of the material.

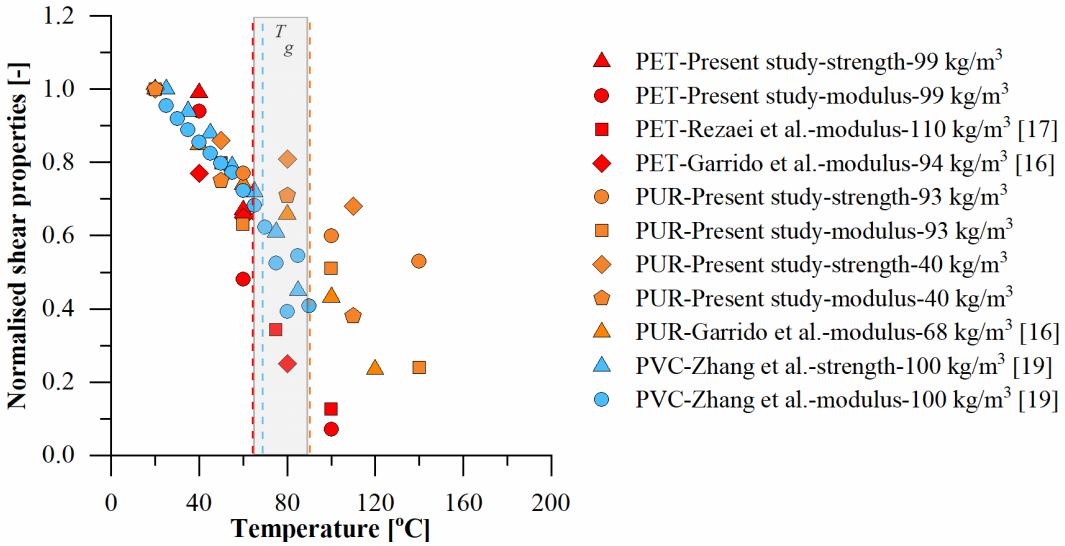

Figure 20 - Comparison of normalised shear properties vs. temperature available in literature with the results obtained in the present study.

2.7 NUMERICAL ASSESSMENT OF THE DTS TEST METHOD

2.7.1 Context and motivation

The development of the DTS method was prompted by the recurring issues reported in traditional single-lap methods (*e.g.* ASTM C273 [41]), where premature failure can occur due to excessive peeling stresses developing at the end of the bonded length of the specimens, especially when relatively thick foam specimens (often used in full-scale structural applications) are tested. Additionally, previous studies about the characterisation of the shear behaviour at elevated temperatures of polymeric foams have also highlighted some of the drawbacks of alternative test methods, namely (i) their lack of representativeness (*e.g.* Iosipescu and modified Arcan rig test methods, used in [16,19]) or (ii) the influence of combined stresses preventing the occurrence of "pure" shear failure (*e.g.* bending tests, used in [17]).

In the above-mentioned context, and in order to provide a further validation of the DTS as a reliable and representative method for the characterisation of highly deformable polymeric foams, including at elevated temperature conditions, a numerical model of the test (including the test fixtures) was developed based on the finite element (FE) method. The main purpose of this study was to assess if an approximately pure shear stress state develops within the specimen, and therefore to confirm if the obtained results (especially the strength values) are representative of the shear properties of the material.

2.7.2 Description of the finite element (FE) model

Two-dimensional (2D) FE models of the DTS tests performed on the PUR foam specimens with density of 93 kg/m^3 at ambient temperature and at 140 ºC (the maximum temperature tested) were developed using the commercial package *Abaqus*. After performing a mesh sensitivity study, the geometry of the foam as well as the metal plates of the test fixtures were discretized using quadrilateral plane stress elements with an approximate size of 1.25 mm. The bond between the foam and the plates was simulated using a tie constraint (*i.e.* assuming a perfect adhesion) - this simplification is acceptable since the epoxy adhesive used in this study is much stiffer than the PUR foam (*e.g.* tensile modulus of 4500 MPa *vs.* shear modulus of 15 MPa, respectively).

Regarding the boundary conditions, as shown in Figure 21, the following displacements were restricted: (i) horizontal displacement (u_x) in the top node; (ii) vertical (u_y) and horizontal displacements in the bottom node (rotations φ were allowed in both nodes). For both temperatures (20 ºC and 140 ºC), the analysis was made by imposing the maximum experimental displacement in the top node; the stress distributions developed in the PUR specimens at these two extreme temperatures were then evaluated.

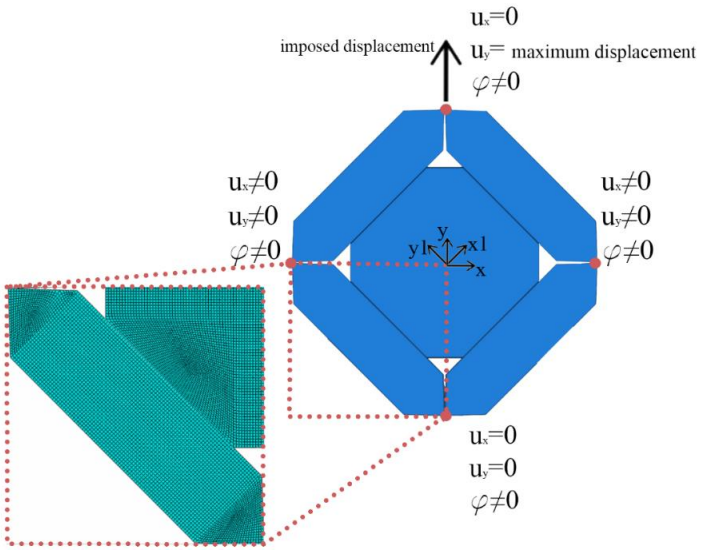

Figure 21 - Boundary conditions in the numerical analysis.

The material properties of the foam presented in section 2.4 were used as input data in the numerical model. Both the PUR foam and the metal plates were modelled as isotropic materials, which is a simplifying assumption in the case of the former. Linear elastic behaviour was assumed for the foam model at room temperature, while elastic-plastic behaviour was assumed at 140 °C. The following PUR material properties were considered in the model: elastic modulus of E = 42 MPa at 20 ºC and E = 13 MPa at 140 ºC; for the plastic stage (only at 140 ºC), a yield strength of 0.25 MPa and null stiffness were considered - these values were taken from the compressive constitutive law determined in the experimental tests at 140 °C (*cf.* Figure 11). For the Poisson's ratio (υ), a typical value for

PUR foams proposed by Gibson and Ashby [31] was assumed, υ = 0.33; according to [16,19], this property does not present relevant changes for the range of temperatures considered in this study, so it was considered temperature independent. Concerning the metal plates, linear elastic and temperature independent properties were considered - E = 210 GPa and υ = 0.30.

2.7.3 Results and discussion

Figure 22 plots the distribution of axial stresses, σ_{xx} and σ_{yy}, obtained from the FE model at 20 ºC. The stress distributions showed in this figure are in agreement with those expected from the deformation imposed to the specimen in the test: along the y direction the specimen is subjected to tension, while in the x direction a compressive stress state is observed; moreover, the maximum tensile stresses occur at the horizontal chamfered edges, which is consistent with the position where cracks developed in the experimental campaign (*cf.* Figure 8). Figure 23 shows the axial stress distributions at 20 ºC and 140 ºC in the directions x_1 (σ_{x1}) and y_1 (σ_{y1}) and the corresponding shear stresses (τ_{x1y1}) for an axis system rotated 45º with respect to the (x,y) one (*cf.* Figure 23); the stresses are shown according to this rotated axes system as it allows understanding if a pure shear stress state is developed within the specimen.

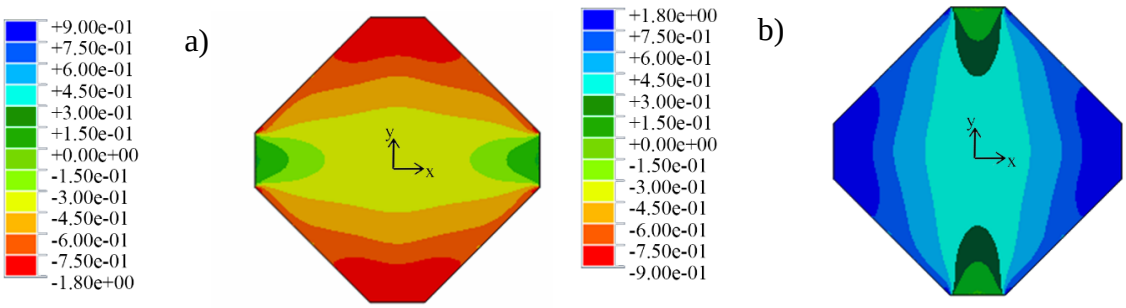

Figure 22 - Axial stress distribution obtained at 20 ºC: (a) σ_{xx}, and (b) σ_{yy} (values in MPa).

The results obtained at 20 ºC show that, although non-negligible stress concentrations are observed close to the chamfered edges (where a geometrical singularity exists), in the central part of the specimen, σ_{x1} and σ_{y1} are negligible and an approximately constant (pure) shear stress field (*i.e.* constant τ_{x1y1}) is developed in that region. At 140 ºC, those stress concentrations are almost null, pointing out that with increasing temperatures the area of the specimen subjected to a pure shear state also increases – this is a consequence of the non-linear response of the foam (here modelled as elasto-plastic) that promotes a more uniform stress distribution.

The shear stress distributions at 20 ºC and 140 ºC along the path defined in Figure 23c are plotted in Figure 24, which also includes the estimation of the (constant) shear stress developed for the maximum experimental displacement obtained using the expression reported in [27]. It can be seen that, for both temperatures, the numerical results showed an approximately pure shear stress distribution in the central area of the specimens, therefore justifying the positioning of the targets

dots (inner alignment; *cf.* section 2.3.4) used with the video-extensometer to calculate the shear strain (and estimate the shear modulus). Regarding the shear stresses, at ambient temperature, the results presented above prompt the following two main comments: (i) in the central area of the specimen the numerical model predictions agree well with the experimental results; nevertheless, in ~90% of the path length the experimental stresses are considerably lower than the numerical ones; (ii) stress peaks are observed close to the free edges, mainly due to combined stresses occurring at those areas stemming from the geometrical and material discontinuities at those locations – this complex stress state, characterized by transverse compression, may help improving the local resistance to shear stress peaks, thus not triggering premature failure modes. Therefore, at ambient temperature, the estimates obtained using the equation proposed by Garrido and Correia [27] are lower bound of the shear strength of the material.

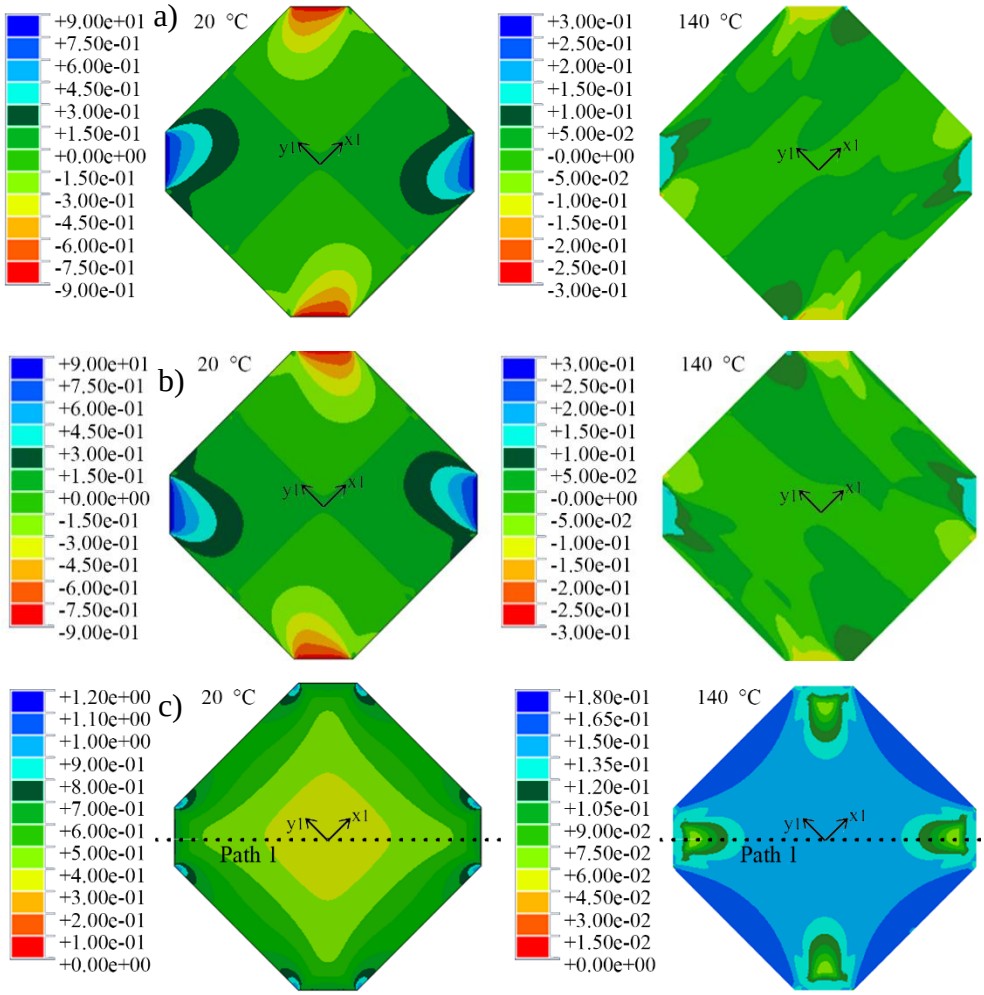

Figure 23 - Stress distributions (a) σ_{x1}, (b) σ_{y1} and (c) τ_{x1y1} (i.e. shear stress) for a coordinate system rotated 45º in relation to x,y – stresses corresponding to the maximum experimental displacement at 20 ºC and 140 ºC.

For higher temperature, because of the non-linear behaviour of the material, the shear stress distribution becomes much more uniform and the stress peaks are clearly mitigated (*cf.* Figure 24) – these results show that at high temperatures the maximum shear stress calculated using equation reported in [27] (which assumes a pure shear stress state) is a quite accurate estimate of the shear

strength of the material. From the experimental observations and the numerical results presented in this section, it can be concluded that the DTS test represents a valuable alternative to traditional test methods for determining the shear properties of highly deformable foam materials, especially when tested at elevated temperatures. The FEM analyses validated the procedure adopted to determine the shear modulus, as this property is determined using measurements obtained from a region of the specimens where an approximate pure shear stress state is developed. Regarding the shear strength, although at ambient temperature stress concentrations developed closed to chamfered edges of the specimens, it was concluded that these singularities did not trigger premature collapses (possibly due to the complex/combined stress state in those zones, as mentioned above), moreover, failure occurred when the shear stress at the centre of the specimens attained approximately the value obtained when a pure shear state is assumed. For higher temperatures, the stress concentrations were minimized, thus further validating the expression reported in [27] to determine the shear strength of the material.

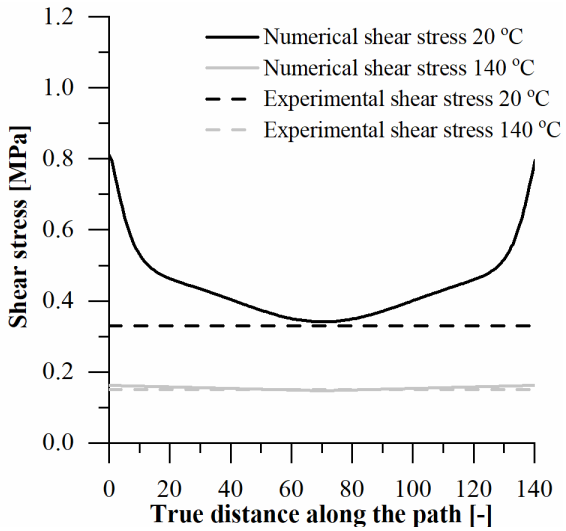

Figure 24 - Shear stress along path 1: numerical values and results derived from the tests.

2.8 CONCLUDING REMARKS

This chapter presented experimental, analytical and numerical investigations about the compressive and shear behaviour of PET and PUR foams at elevated temperature (up to 200 ºC). From the results obtained, the following main conclusions are drawn:

- The compressive and shear responses of PET and PUR foams are strongly affected by elevated temperature: for both loading cases, the non-linearity of the stress *vs.* strain response at ambient temperature becomes more pronounced with increasing temperature – this is mostly due to the softening of the foams, when the constituent polymer undergoes the glass transition process.
- For the range of PUR foam densities tested, density does not seem to influence the variation of shear modulus with temperature; however, in what concerns shear strength, reductions

were more pronounced in the denser foam. For the denser foam, reductions in the compressive modulus were very similar to those of the shear modulus, as both depend mostly on thermophysical changes experienced by the polymer material. On the other hand, reductions in compressive strength were significantly higher than those of shear strength, especially for temperatures above 100 ºC.

- The compressive and shear properties of PET foam are very significantly reduced at elevated temperature, namely when the glass transition temperature (T_g) of the polymer is approached and exceeded. At 100 ºC, the compressive strength and modulus are reduced to about 10% of the ambient temperature values. Concerning the shear properties, at 60 ºC, the shear modulus and shear strength are reduced to 48% and 67% of the corresponding ambient temperature properties; at 100 ºC, the shear modulus presents a retention of only 7%.
- Overall, the degradation of the mechanical properties of PET foam occurs for lower temperatures compared to PUR foams – this agrees with the corresponding DMA data, as the PET foam presents lower T_g than PUR foam.
- All the empirical models assessed in the analytical study were able to describe accurately the reductions of the mechanical properties of PET foam with increasing temperature. The model proposed by Correia *et al.* provided the best estimates, with the AMPE value ranging from 1.8% to 3.5%.
- The numerical (FE) analysis developed to assess the shear stress state developed within the specimen tested with DTS method showed that although stress peaks occur next to the chamfered edges of the specimens, a uniform shear stress distribution is attained in their central part (particularly at elevated temperature), validating the test method and the analytical formulae used to estimate the shear properties.

CHAPTER 3

CHARACTERISATION OF GFRP MATERIAL AT ELEVATED TEMPERATURE

3.1 INTRODUCTION

During the second half of the twentieth century, glass fibre reinforced polymer (GFRP) materials found increasing use in civil engineering applications, either in the rehabilitation of degraded structures or in new construction, owing to their advantages over traditional materials, such as high strength-to-weight ratio, lightness, corrosion resistance and low life cycle costs [42,43]. In spite of such advantages, there are major concerns about the behaviour of GFRP materials when subjected to elevated temperature or fire, which have been hindering their widespread use in several civil engineering applications, namely in buildings, where the fire action has to be considered in design. These concerns stem from the severe reductions of strength- and stiffness-related mechanical properties of GFRP that occur even when the material is heated to moderately elevated temperatures. This is mostly due to the softening of the polymeric matrix during the glass transition process, which takes place when the GFRP material is heated to elevated temperatures, typically within the 50-150 ºC range. In addition, when exposed to 300-500 ºC, the polymeric matrix decomposes, releasing heat, smoke and toxic volatiles [44]. These features of the behaviour of GFRP at elevated temperatures explain the above-mentioned concerns that have been raised about the use of these materials in structures likely to be exposed to fire, in which relatively strict fire reaction and fire resistance related requirements must be met.

The aim of the work presented in this chapter is to further extend the current knowledge about the mechanical properties at elevated temperature of GFRP materials manufactured by vacuum infusion, with a relatively balanced fibre architecture. To this end, dynamic mechanical analysis (DMA) and thermogravimetric analysis (TGA) were first performed in order to determine the glass transition and decomposition temperatures of the GFRP material, respectively. Then, the stiffness and strength properties in tension, compression and shear at elevated temperature were determined by means of mechanical characterisation tests performed under steady state conditions up to 300 ºC. The main objectives of these tests were two-fold: (i) to define temperature-dependent constitutive relationships that can be used in fire analysis and design; and (ii) to evaluate the possible influence of the fibre architecture on the mechanical properties of the GFRP material at elevated temperature, comparing

the results obtained with those reported in the literature, which mostly concern quasi-unidirectional fibre reinforcement. Finally, the results obtained from the mechanical characterisation tests were used to assess the suitability of empirical models available in the literature and of a design-oriented temperature conversion factor to take into account the reduction with temperature of the stiffness- and strength-related properties of the GFRP laminates produced by vacuum infusion.

3.2 LITERATURE REVIEW AND RESEARCH SIGNIFICANCE

The experimental studies available in the literature about the tensile properties of GFRP materials at elevated temperatures [17,38,45–47] have focused especially on the assessment of the tensile strength, and hence, very limited information is available on their tensile modulus reduction with temperature; this stems from the inherent difficulties associated to measure strains at elevated temperatures. A comprehensive study regarding the effect of elevated temperatures up to 220 ºC on the tensile strength of pultruded GFRP laminates (isophthalic polyester resin; T_g of 104 ºC, defined from DMA tests, based on the onset of the storage modulus, E', decay) was conducted by Correia *et al.* [38], who reported tensile strength retentions of 54% at 220 ºC. Bai and Keller [45] performed tensile tests on pultruded GFRP laminates (isophthalic polyester matrix, T_g of 110 ºC, DMA, onset of E') at temperatures up to 220 ºC; these authors obtained valid tensile failure modes only for temperatures up to 100 ºC, for which the tensile strength retention was 81% (gripping failure occurred for higher temperatures). Rezaei *et al*. [17] performed tensile tests up to 175 ºC on vacuum-infused GFRP laminates (epoxy matrix, T_g of 87 ºC, test method not reported); in this study, for temperatures ranging from 125 ºC to 175 ºC, the specimens exhibited premature failures (*i.e*. rupture in the gripping area); for this reason, only the tensile modulus was determined for that temperature range. The authors found out that increasing the temperature from 20 ºC to 100 ºC caused a tensile strength reduction of 40%. As expected, the influence of elevated temperatures on the tensile modulus was less pronounced, with an average reduction of about 30% at 100 ºC, which remained almost constant up to the maximum test temperature (175 ºC). Chowdhury *et al.* [47] studied the influence of elevated temperatures (up to 200 ºC) on the tensile behaviour of unidirectional GFRP laminates produced by hand-layup (epoxy matrix, T_g of 48 ºC, defined from DMA tests, by a 50% reduction of E'). The authors reported significant reductions of the tensile properties for temperatures above T_g: at 90 ºC, the tensile strength and modulus were reduced to 45% and 62% of their room temperature values, respectively. More recently, Jafari *et al.* [46] performed tensile tests at temperatures up to 550 ºC on vacuum-infused GFRP laminates (epoxy matrix, T_g of 87 ºC, test method not reported) with different fibre architectures: (i) unidirectional fibres; (ii) woven bi-directional fibres, and (iii) randomly oriented fibres. Up to 150 ºC, a similar reduction of tensile strength (~25%) was observed for both unidirectional and woven fibre architectures, whereas for the laminate with randomly oriented fibres a much more pronounced tensile strength reduction (~70% at 150 ºC) occurred. At higher

temperatures, as expected, the unidirectional laminate presented the best mechanical performance among the three types of GFRP laminates tested – at 550 ºC, the retained tensile strength was 35%, whereas for the laminate with bi-directional fibres the strength retention was almost negligible (4%). Regarding the GFRP with randomly oriented fibres, its tensile strength was highly matrix-dependent, therefore, being severely affected by temperature: at 300 ºC, the tensile strength reduction was 96%.

Regarding the effect of elevated temperatures on the shear properties of GFRP materials, according to the author's best knowledge, only four studies were carried out until the present date [17,38,45,48]. Rosa *et al.* [48] studied the shear behaviour of pultruded GFRP laminates (isophthalic polyester matrix, T_g of 104 ºC, based on the onset of the storage modulus curve), by means of Iosipescu tests, at temperatures ranging from 20 ºC to 180 ºC. The authors observed significant reductions of the shear properties even at moderately elevated temperatures: at 60 ºC, the shear strength and modulus were reduced to 64% and 69% of the ambient temperature values, respectively. When the test temperature was increased to 180 ºC, the reductions of shear properties were more severe, with residual shear modulus and strength of 22% and 12%, respectively. Correia *et al.* [38] performed 10º off-axis shear tests on pultruded GFRP laminates (isophthalic polyester matrix, T_g of 104 ºC, based on the onset of E') up to 250 ºC. A steep reduction of shear strength was observed when the material underwent the glass transition - when the test temperature was increased to 150 ºC, the average reduction was about 75%. Bai and Keller [45] also studied the shear behaviour of pultruded GFRP laminates (isophthalic polyester matrix, T_g of 110 ºC, DMA, onset of E', the same material tested in tension) when subjected to elevated temperatures (up to 220 ºC) through 10º off-axis shear tests. The shear strength, being a matrix-dependent property, was severely affected by temperature: reductions of about 40% and 87 % were observed at 100 ºC and 220 ºC, respectively. Rezaei *et al.* [17] assessed the shear behaviour of vacuum-infused GFRP laminates through V-notch rail shear tests, for temperatures ranging from 20 ºC to 100 ºC. The authors reported drastic reductions of the shear properties for temperatures approaching and exceeding the T_g (87 ºC, test method not reported); at 100 ºC, both strength and shear modulus were less than 10% of the values obtained at room temperature.

Few studies have also been published about the compressive properties of GFRP materials at elevated temperature [17,38,45,49,50]; moreover, most of these works did not report the influence of elevated temperature on the compressive modulus of the material (due to the aforementioned difficulty in measuring strains at elevated temperature). Correia *et al.* [38] studied the effect of temperature on the compressive response of I-section pultruded GFRP profiles (T_g of 104 ºC, same material described above for tension and shear) up to 250 ºC. The results confirmed the high susceptibility to temperature of the GFRP profiles when loaded in compression: at 200 ºC, the retained compressive strength (a matrix-dominated property) was only 8% of the ambient temperature value. Bai and Keller [45] studied the influence of temperature on the compressive strength of pultruded GFRP

tubes (T_g of 110 ºC, the same material described above) over a temperature range from 20 ºC to 220 ºC. When the test temperature increased from 60 ºC to 140 ºC, the strength reduction was about 50%, and at 220 ºC the residual compressive strength was only 9% of that at ambient temperature. Rezaei *et al.* [17] performed compressive tests, according to ASTM D3410/D3410 [51], on vacuum infused GFRP laminates (T_g of 87 ºC, test method not reported, same material described above) for temperatures ranging from 25 ºC to 100 ºC. It is worth mentioning that a valid compressive failure of the laminates was only obtained at ambient temperature, thus not allowing the definition of the compressive strength reduction for the remaining temperatures. Overall, the reduction of the compressive modulus with temperature was relatively limited: at 100 ºC, the compressive modulus was reduced to 74% of its ambient temperature values. Wong *et al.* [50] evaluated the compressive behaviour of C-section pultruded GFRP profiles (comprising an isophthalic polyester matrix, T_g not reported[3]) over a temperature range from 20 ºC to 250 ºC. As expected, a steep reduction of compressive strength was observed when the test temperature approached the (assumed) T_g of the material; in fact, when the temperature was increased from 20 ºC to 120 ºC, the authors found an average reduction of 84%. Peng *et al.* [49] performed compressive tests on pultruded GFRP tubes (epoxy matrix, T_g of 65 ºC, based on the onset of E') for temperatures ranging from -40 ºC to 90 ºC. As in the previous studies, the GFRP material was severely affected by the temperature increase, presenting a compressive strength reduction of 70% at 90 ºC.

The literature review presented above clearly points out the influence of elevated temperature on the mechanical properties of GFRP materials; however, it also shows that further knowledge is needed about their mechanical behaviour at elevated temperature, especially in what concerns stiffness-related properties. In fact, to the best of the author's knowledge, only three studies reported information about the variation of stiffness-related properties with temperature [17,47,48]. Furthermore, most of the previous experimental investigations have focused on quasi-unidirectional composites produced by pultrusion; much less data is available about GFRP materials with more balanced fibre architectures that are more often used in a wide variety of civil engineering applications, such as face sheets of sandwich panels used in bridge decks and building floors, roofs and facades. It is still worth highlighting that the reduction with temperature of the mechanical properties of FRP materials depends on several factors, including the type of resin, the type and architecture of the fibre reinforcement, and the manufacturing process. Therefore, it is of utmost importance to obtain further experimental data about the mechanical properties at elevated temperatures of such different GFRP materials produced with methods other than pultrusion, such as vacuum infusion. Moreover, such data is necessary to define and calibrate degradation models and temperature conversion factors for the analysis and design of GFRP structures subjected to elevated

[3] Based on DMA experiments performed in similar material, the T_g was assumed to be ~100 ºC (considering the onset of the storage modulus curve) – this result is relevant in section 3.6.2 of this chapter.

temperatures in service conditions or to the accidental fire action. The study presented in this chapter aims at filling these research needs, by (i) providing both strength- and stiffness-related properties for different load conditions up to 300 ºC of GFRP laminates with relatively balanced fibre architecture, produced by vacuum infusion, and (ii) assessing the corresponding degradation models and temperature conversion factors.

3.3 EXPERIMENTAL PROGRAMME

3.3.1 Materials

The GFRP laminates used in the experimental study consisted of unidirectional (*UNI E500*, areal weight of 530 g/m^3) and biaxial (*EBX 400*, +/-45º fibres with a total areal weight of 400 g/m^3) E-glass stitched fibres embedded in a urethane acrylate thermoset resin, produced by *Scott Bader*, with the commercial designation *Crestapol 1261*. Two different fibre architectures were considered for the production of the GFRP laminates: (i) 5.8 mm thick laminates with a $[0/0/0/90/45/-45/0]_s$ fibre layup, and (ii) 3.8 mm thick laminates with a $[0/90/45/-45/0]_s$ fibre layup. The 5.8 mm thick laminates present more fibres aligned with the 0º direction and were designed to be representative of GFRP face sheets used in homogeneous-core and web-core sandwich panels and, therefore, likely to be subjected mostly to tension or compression stresses in the fibre (0º) direction (with the 0º direction corresponding to the longitudinal direction of the panel); whereas the 3.8 mm thick laminates, with less fibres along the 0º direction, were design to be representative of the vertical webs of the web-core sandwich panels (mostly subjected to shear), therefore presenting a more balanced fibre distribution in the different directions. Both types of GFRP laminates present an average inorganic content of 68%, determined from burn-off-tests.

The GFRP specimens described in the next sections were cut from large laminates (overall dimension of 1500 × 1500 mm^2, produced by vacuum infusion) by means of a computer numerical control (CNC) machine, which guaranteed high accuracy in terms of specimens' geometry and their alignment with respect to the directions of the fibre reinforcement.

3.3.2 Thermophysical and thermomechanical experiments

The thermophysical properties and thermomechanical behaviour of the GFRP laminates were investigated through TGA and DMA experiments. In addition to the definition of the decomposition temperature, T_d, and the glass transition temperature, T_g, the results obtained in these tests provided useful information to better understand the variation with temperature of the mechanical properties of the material.

3.3.2.1 DMA tests

DMA tests were performed according to ASTM E1640 [52] on GFRP specimens with dimensions of 35 × 12 × 3.8 mm, tested in a dual-cantilever configuration (35 mm of length aligned with the 0º fibres). Tests were conducted from 20 ºC up to 150 ºC (heating rate of 2 ºC/min) in air atmosphere (oxidative environment), at an oscillatory frequency of 1 Hz and a strain amplitude of 0.3‰, using a Q800 dynamic mechanical analyser from TA Instruments. Two replicate specimens were tested given the low variability of the results obtained (differences in T_g values lower than 0.5 ºC).

Figure 25 depicts representative curves obtained from DMA tests on the 3.8 mm thick GFRP laminates. As expected, the storage modulus (E') curve presents a sigmoidal shape, while the loss modulus (E'') and the loss factor (tan δ) curves present the typical peaks that are observed when FRP materials undergo glass transition. The glass transition temperature (T_g) estimated from the onset of the storage modulus curve (log scale) decay is 102 ºC. The T_g estimates obtained from the peaks of the loss modulus and loss factor curves are respectively 110 ºC and 118 ºC.

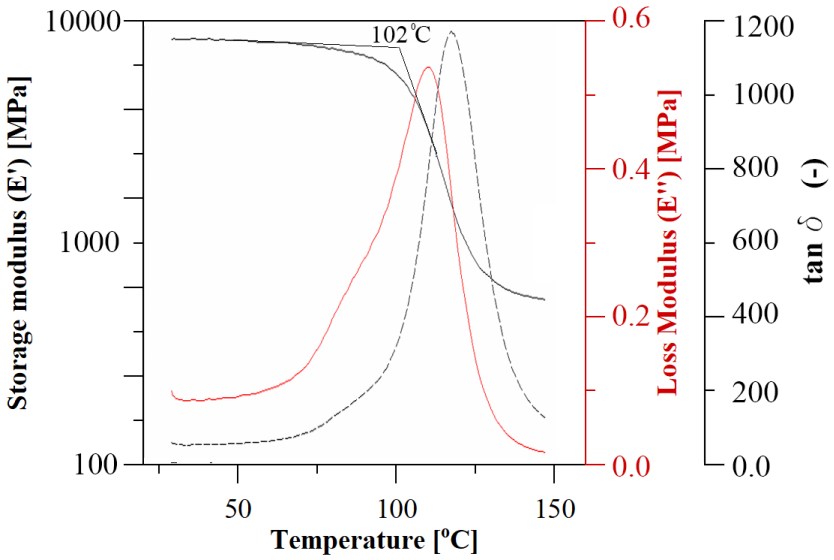

Figure 25 - DMA result for a representative GFRP laminate (3.8 mm thick).

3.3.2.2 TGA tests

The mass variation with temperature of the GFRP material was assessed according to ISO 11357 [28]. Specimens with initial mass of ~6 mg were extracted from a 3.8 mm thick laminate and heated from 30 ºC to 900 ºC, at a heating rate of 10 ºC/min, under two different purge gases, air (oxidative) and nitrogen (inert). Two specimens were tested in each atmosphere. Figure 26 shows the remaining mass *vs.* temperature curves of representative specimens for both atmospheres.

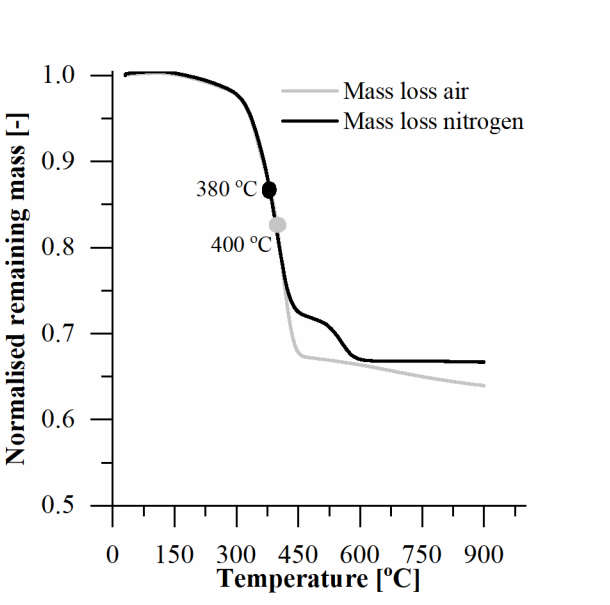

Figure 26 - TGA result for the GFRP material tested in air and nitrogen atmospheres.

The normalised remaining mass curves of the specimens tested in air atmosphere present a significant drop at temperatures ranging from 300 ºC to 450 ºC. For higher temperatures, a lower (and almost constant) reduction rate of the remaining mass was observed up to 900 ºC. In nitrogen atmosphere, the remaining mass curve exhibited two drops: (i) a significant steep drop at around 300 ºC, and (ii) a small and less steep drop from 450 ºC to 600 ºC, after which no significant mass variation was observed.

The decomposition temperatures of the GFRP material, determined based on the middle temperature of the major drops observed in the remaining mass *vs.* temperature curves, were set as 400 ºC and 380 ºC for air and nitrogen atmospheres, respectively.

3.4 MECHANICAL CHARACTERISATION OF GFRP LAMINATES AT ELEVATED TEMPERATURES

3.4.1 Overview of test programme

With the objective of investigating the mechanical behaviour of GFRP laminates at elevated temperatures, tensile, compressive and shear tests were performed using a *Tinius Olsen* thermal chamber coupled to a universal testing machine (same as those described in section 2.3.3), *cf.* Figure 27. The details of the experimental programme are presented in Table 9, which includes the test temperatures for each laminate (3.8 or 5.8 mm thick) and type of test.

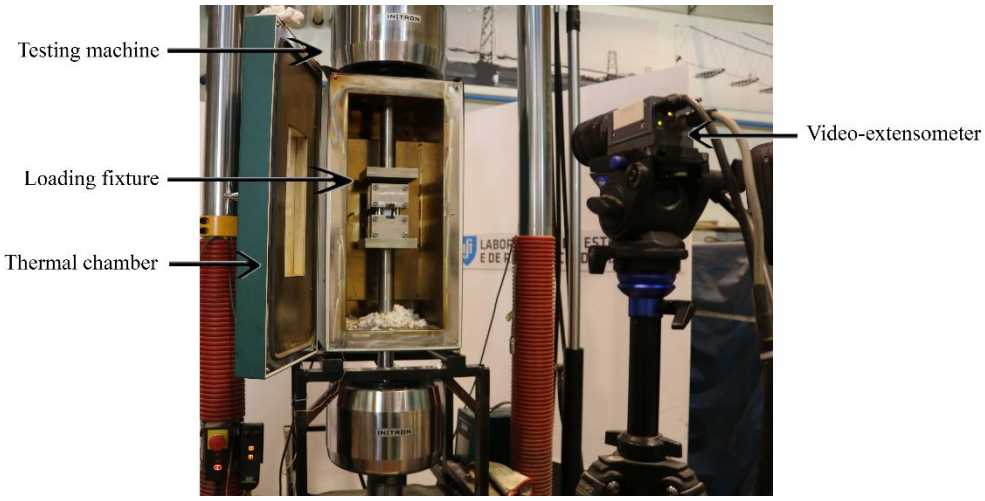

Figure 27 - Overview of the test setup adopted in the material characterisation tests at elevated temperatures (this picture shows the fixture used in the compressive tests).

Table 9 - Test programme: temperatures for each laminate thickness and type of test.

GFRP laminate thickness	Test temperatures		
	Shear tests	Compressive tests	Tensile tests
3.8 mm	20 ºC, 50 ºC, 100 ºC, 150 ºC and 200 ºC	-	-
5.6 mm	-	20 ºC, 50 ºC, 100 ºC, 150 ºC, 200ºC and 250 ºC	20 ºC, 50 ºC, 100 ºC, 150 ºC, 200 ºC and 300 ºC

3.4.2 Instrumentation and test procedure

The temperature of the GFRP specimens during the tests was monitored using a type K thermocouple (0.25 mm of conductor diameter) installed in the centre (*i.e.* at half-thickness) of a dummy specimen with the same geometry of the one tested up to failure; an additional thermocouple was placed inside the thermal chamber to measure the air temperature during the tests. All tests were performed under steady-state conditions: firstly, the specimens were heated up to the target temperature at an average heating rate of the air inside the thermal chamber of 14 ºC/min (0.80 ºC/min in GFRP specimens); then, when the dummy specimen attained the target temperature, a monotonic load was applied until failure, under displacement control, at a predefined speed (defined below for each type of test), while the temperature of the specimens was kept constant. Figure 28 shows, for two temperatures (150 ºC and 200 ºC, as an example), the temperature *vs.* time curves in the air inside the furnace and in the dummy specimens. With the purpose of reducing the heating time, the initial furnace temperature was set 5 ºC above the target temperature of the specimen. When the temperature in the dummy was close to the target (*i.e.*, 1 ºC lower), the furnace temperature was reduced to the target value and then held constant for 15 minutes before testing (enough to ensure a uniform temperature distribution throughout the specimens' thickness).

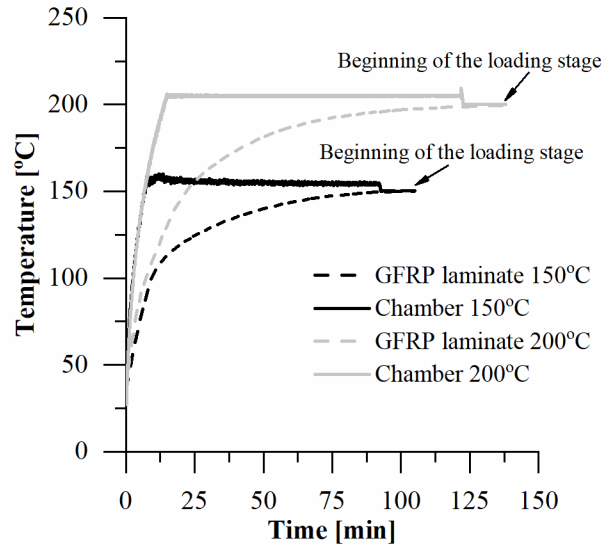

Figure 28 - Representative temperature vs. time curves in the air of the thermal chamber and in the dummy specimens for 150 ºC and 200 ºC.

3.4.3 Tensile tests

The longitudinal tensile properties of the GFRP laminates (*i.e.* aligned with the 0º fibre reinforcement) were determined according to the recommendations of ASTM D3039/D3039M [53] standard, in rectangular specimens with dimensions of 25 × 1000 × 5.6, mm (width × length × thickness), *cf.* Figure 29a. The length of the specimens was defined to allow the clamps of the testing machine to remain at room temperature, thus preventing GFRP premature failures in the grips. The specimens were tested under steady state conditions, *i.e.*, they were first heated up to the target temperature (20 ºC, 50 ºC, 100 ºC, 150 ºC, 200 ºC or 300 ºC), and then a tensile load was applied up to failure, under displacement control, at a speed of 2 mm/min (set to reach failure within 1 to 10 min). At least three specimens were tested for each target temperature.

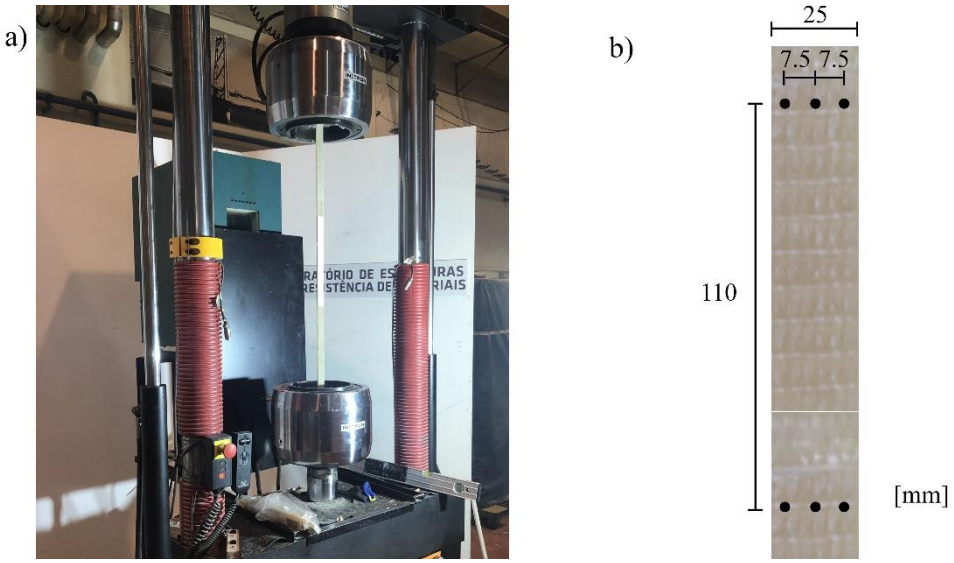

Figure 29 - Tensile test: (a) test setup and (b) target dots positioning.

The tensile strains were measured with a video extensometer (video camera Sony, model XCG 5005E, with Fujinon lens, model Fujifilm HF50SA-1), which monitored the position of target dots distanced of 110 mm along three longitudinal alignments (*cf.* Figure 29b). The average strain of these alignments was used to define the tensile stress *vs.* strain curves shown in section 3.5.1. The tensile modulus was calculated from the slope (obtained by linear regression) of the tensile stress *vs.* strain curves between strains of 1.0‰ and 3.0‰.

3.4.4 Compressive tests

The variation with temperature of the longitudinal compressive properties of the GFRP material (*i.e.* strength and modulus aligned with the 0º fibres) was determined by means of tests carried out according to the ASTM D6641/D6641 [54] standard at the following temperatures: 20 ºC, 50 ºC, 100 ºC, 150 ºC, 200 ºC and 250 ºC (for the last temperature only the elastic modulus was determined)[4]. The compressive strength was determined in specimens with rectangular cross section (25 mm × 5.6 mm) and 140 mm of length, while the elastic modulus was determined using specimens with the same cross section, but with 300 mm of length – this extended length was needed in order to install a clip-on extensometer for measuring the axial strains (Epsilon, Model 7642, gauge length of 50 mm) - Figure 30 illustrates the test setup adopted in these tests. It is worth referring that to prevent any possible buckling phenomenon on the longer (slenderer) specimens, these tests were performed only up to 50% of the maximum load (at each temperature), obtained from tests carried out up to failure on shorter (stockier) specimens.

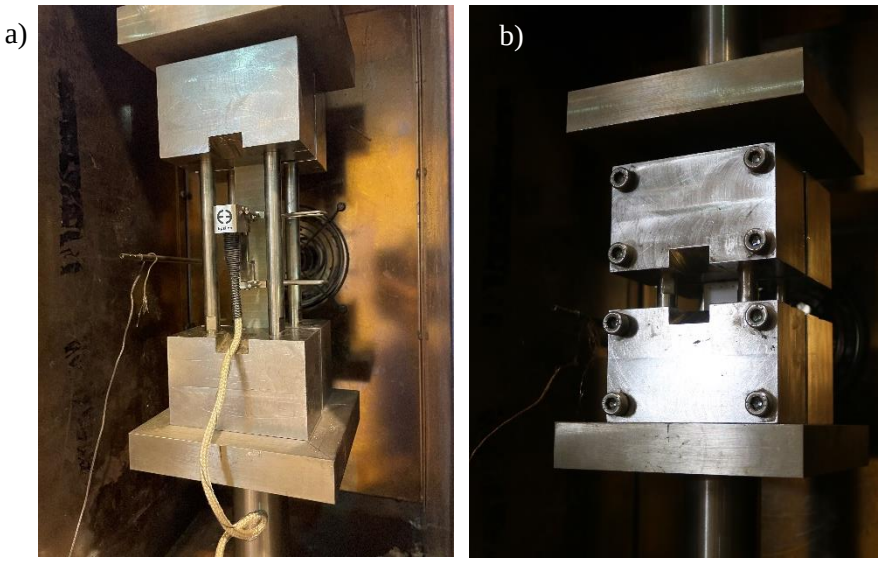

Figure 30 - Compression test setup: (a) longer specimens (300 mm) to determine compressive modulus, and (b) specimen with standard geometry to determine compressive strength.

The compressive modulus was estimated from the slope (obtained by linear regression) of the compression stress *vs*. strain curves between 25% and 50% of the maximum compressive stress, for

[4] At 200 ºC, the retained compressive strength was already very low.

which the overall response was linear for all test temperatures. The compressive tests were performed under displacement control, at a speed of 0.5 mm/min; for each target temperature and type of test, at least three replicate specimens were tested.

3.4.5 Shear tests

The in-plane shear response of the GFRP material was studied by means of Iosipescu shear tests, performed according to the recommendations of ASTM D5379/D5379M [20] standard, at five different temperatures: 20 ºC, 50 ºC, 100 ºC, 150 ºC and 200 ºC. The tests were conducted under steady-state conditions on V-notched GFRP specimens with dimensions of 75 × 20 × 3.8, mm (width × height × thickness, with the 0º fibres aligned with the 75 mm dimension, *cf.* Figure 32), comprising a notch depth of 5.5 mm. After reaching thermal equilibrium, a compressive load was applied, under displacement control, at a speed of 0.5 mm/min, which led to failure of the specimens within 1 to 10 min. The test setup adopted for the shear test is shown in Figure 31.

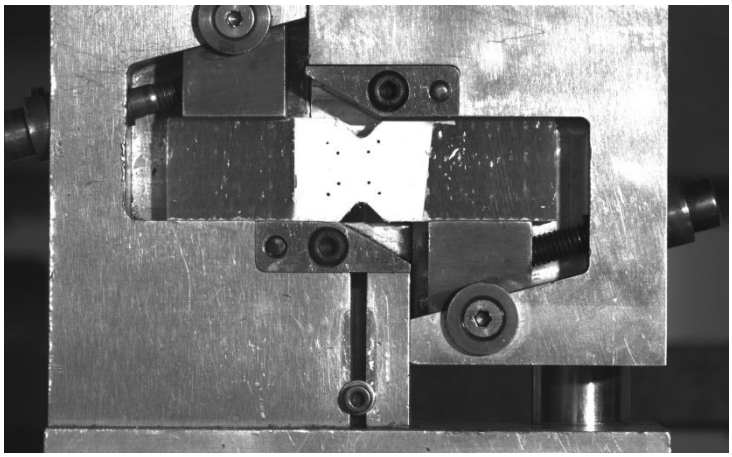

Figure 31 - Iosipescu test setup.

The shear strains, γ, were computed using the video extensometer readings, that tracked the distortions of a square alignment (with dimensions of 10 × 10 mm^2) painted around the notched area of the specimens (*cf.* Figure 32a). The distortion angle was taken as $\gamma = \alpha + \beta$, where $\alpha = \overline{aa'}/\overline{ac}$ and $\beta = \overline{dd'}/\overline{cd}$, as shown in Figure 32b.

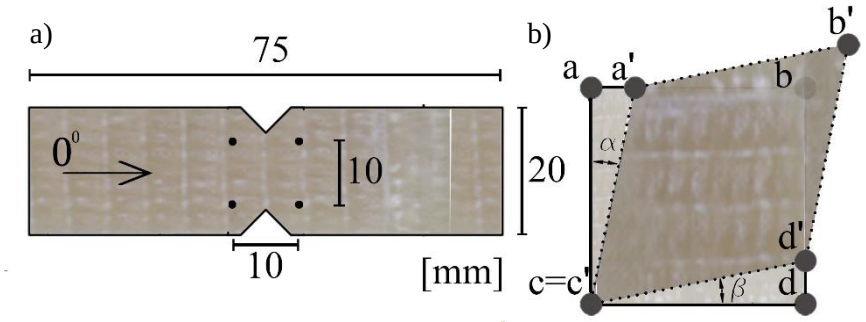

Figure 32 - Iosipescu shear test: (a) target dots position and (b) shear deformation tracked by the video extensometer.

The in-plane shear modulus (G) was calculated from the chord modulus over a 4‰ amplitude, considering the lower strain point ranging between 1.5‰ and 2.5‰, as recommended in the ASTM D5379/D5379M [20] standard. For each target temperature, at least three specimens were tested.

3.5 RESULTS AND DISCUSSION

3.5.1 Tensile behaviour

Figure 33 plots the tensile stress *vs*. strain curves for representative specimens tested at temperatures up to 200 ºC; it is worth referring that due to the resin decomposition process and the inherent colour change of the material, it was not possible to measure strains at 300 ºC, as the video-extensometer was no longer able to track the position of the target dots marked on the material's surface. At 150 ºC, that colour change also prevented the video-extensometer from measuring the failure strain – as marked in Figure 33, the tracking of the target dots was lost before failure. Notwithstanding these difficulties of measuring strains at the highest test temperatures, the results of Figure 33 show an overall reduction of both tensile strength and elastic modulus with increasing temperature, especially when the test temperature exceeded the T_g of the material. For temperatures ranging from 20 ºC to 100 ºC, the tensile stress *vs.* tensile strain curves reflected a linear elastic response up to failure; while for higher temperatures a certain degree of nonlinearity was observed in the brink of failure (again, this behaviour is related to the softening of the resin).

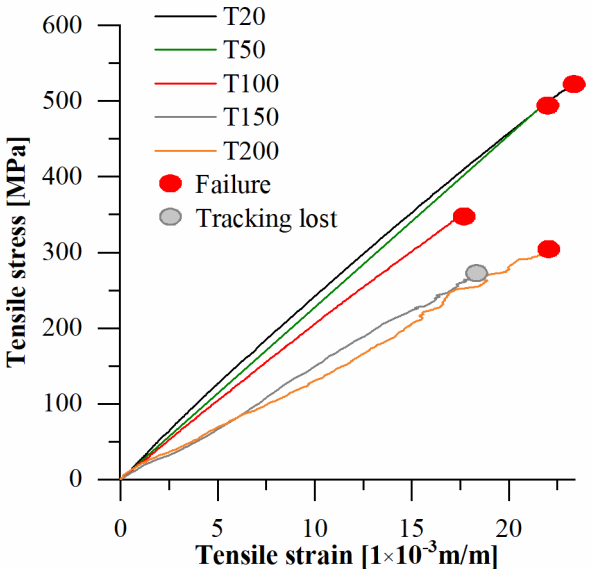

Figure 33 - Representative tensile strength vs. strain curves at each target temperature.

Table 10 lists the tensile properties (strength and modulus) obtained at each target temperature, together with the corresponding normalized values (ratio to the values obtained at ambient temperature). As shown in Table 10, the material exhibited negligible strength and modulus reductions at 50 ºC. When the temperature increased to 100 ºC, both tensile properties were reduced to about 80% of their ambient temperature values, showing that although these properties are both

expected to be mostly fibre-dominated, non-negligible reductions can be observed at temperatures approaching T_g. From 100 ºC to 150 ºC, the tensile properties were further reduced – the retained tensile strength was 64%, whereas the tensile modulus retained about 55% of its room temperature value. The steep reduction in tensile strength observed for the 100-150 ºC range should be related to the softening of the matrix that caused the degradation of the fibre-matrix interaction, thus decreasing the effectiveness of the stress transfer between adjacent fibres [46]. For temperatures significantly above T_g, the load-carrying capacity of the specimens is mostly dependant on the response of the fibres (whose mechanical properties are significantly less affected by temperature); for this reason, both tensile strength and modulus remained almost constant for temperatures above 150 ºC (for which the glass transition process of the polymeric matrix is mostly completed, *cf.* Figure 25). These results are discussed in further depth ahead.

Table 10 - Tensile properties of GFRP laminate at elevated temperatures (average ± standard deviation).

T [°C]	σ [MPa]	σ/σ_{20} [-]	E_t [GPa]	E_t/E_{t20} [-]
20	512.5±11.2	1.00±0.02	25.7±0.9	1.00±0.03
50	489.1±12.3	0.95±0.02	25.7±0.6	0.99±0.02
100	410.1±13.5	0.80±0.03	20.7±0.2	0.81±0.01
150	328.5±9.7	0.64±0.02	14.2±0.5	0.55±0.02
200	307.3±7.9	0.60±0.01	13.4±0.6	0.52±0.03
300	275.6±5.9	0.54±0.01	-	-

Concerning the failure modes, all specimens exhibited valid tensile ruptures within the central zone (*i.e.* in the heated length). Figure 34 illustrates the effects of exposure to elevated temperatures on the failure modes of the specimens: for temperatures up to 100 ºC, the tensile rupture of the fibres occurred in a well-defined section of the specimens (*cf.* Figure 35a), while for temperatures ranging from 150 ºC to 300 ºC, a more progressive failure mode was observed, involving delamination and tensile rupture of the fibres along the heated length of the specimens (*cf.* Figure 35b); for this temperature range, the colour change of the specimens was clearly visible (*cf.* Figure 34).

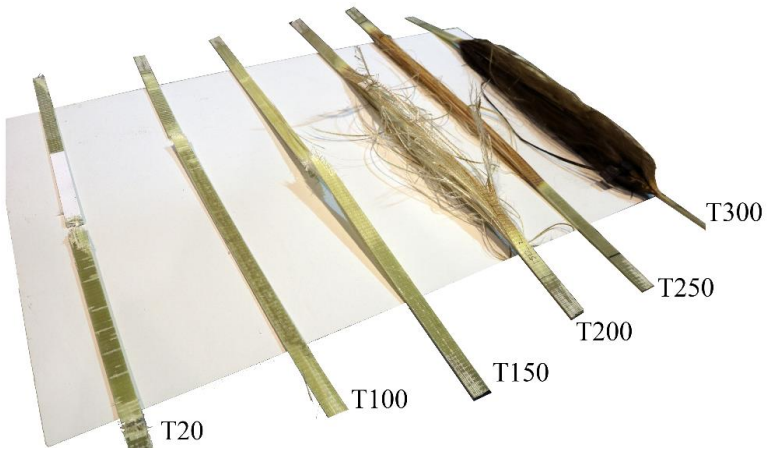

Figure 34 - Failure modes observed in the tensile tests at different temperatures.

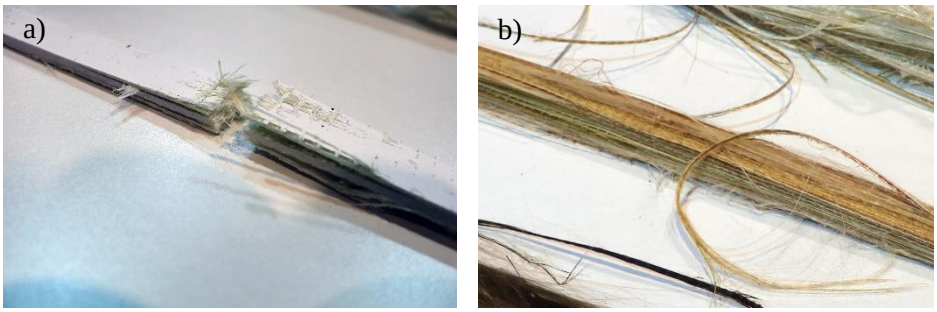

Figure 35 - Details of the failure modes observed in the tensile tests: (a) up to 100 ºC, and (b) from 150 ºC to 300 ºC.

Figure 36 compares the variation with temperature of the normalized tensile strength and modulus measured in the present study with experimental data available in the literature (from tensile tests performed under steady state conditions on different GFRP materials [17,38,45–47,55]).

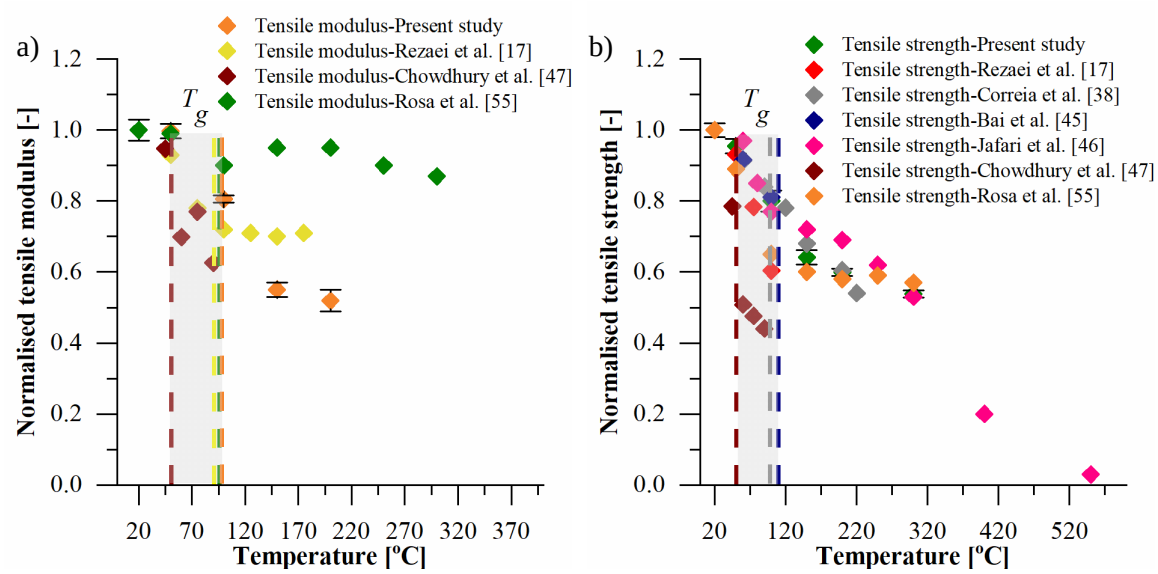

Figure 36 - Normalised tensile properties vs. temperature: (a) tensile modulus and (b) tensile strength.

Concerning the tensile strength, the reductions obtained in the present study present an overall good agreement with those reported in the literature (except those by Chowdhury *et al.* [47]), showing significant reductions when the materials undergo the glass transition process (the $T_g s$ of the materials shown in Figure 36b ranged from 48 ºC to 110 ºC). Regarding the tensile modulus, although all results in Figure 36a) follow a similar qualitative trend, the experimental data obtained in the current study present a higher reduction with temperature than those reported by Rezaei *et al.* [17], Chowdhury *et al.* [47] and Rosa *et al.* [55], who performed tensile tests on quasi-unidirectional laminates (Rezaei *et al.* [17] and Chowdhury *et al.* [47]) and unidirectional bars (Rosa *et al.* [55]). In fact, in the previous studies reported in the literature, the tensile strength was more affected by temperature than the tensile modulus. However, in the present study, after 150 ºC, the degradation of the tensile modulus was more pronounced than that of the tensile strength. This difference with respect to results from the literature should be related to the different fibre layup adopted in the materials; for temperatures significantly higher than T_g (*e.g.* 150 ºC in the present study), the tensile

modulus is expected to be almost entirely dependent on the longitudinal fibres; consequently, the contribution of the 45º oriented plies of the GFRP material tested in the present study (*cf.* layup sequence in section 3.3.1) is expected to be highly affected, as the mechanical mobilization of these plies relies on the load-transfer capacity between fibres granted by the polymeric matrix, which in turn is severely reduced by the resin softening. This may explain why the tensile properties of laminates with more balanced fibre architectures are significantly more affected by temperature than unidirectional GFRPs. In addition, it can be seen that the reduction of the tensile strength obtained in the present study occurs for higher temperatures compared to those reported by Rezaei *et al.* [17] and Chowdhury *et al.* [47]: such difference should be related to the lower T_g of the materials tested in those studies.

3.5.2 Compressive behaviour

Figure 37 presents the compressive stress *vs.* strain curves obtained in the tests performed in longer specimens, up to around 50% of the failure load at each temperature (*cf.* section 3.4.4). For all tested temperatures, the curves reflect an approximately linear response, with a progressive reduction of modulus with increasing temperature; it can be seen that the stress *vs.* strain curves present an initial non-linear branch due to adjustments in the test fixture. After this initial stage, the GFRP laminates exhibited linear behaviour - therefore these perturbations did not compromise the results obtained in term of compressive modulus (this parameter was computed between 25% and 50% of the maximum compressive stress).

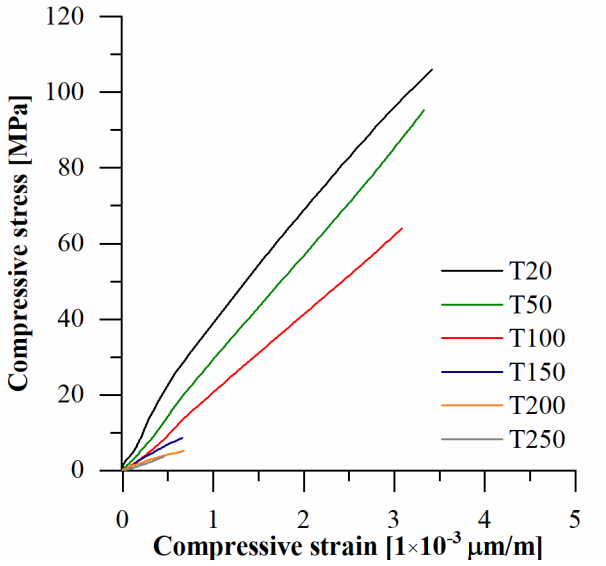

Figure 37 - Representative compressive stress vs compressive strain curves obtained in the elastic modulus tests (curves shown only up to around 50% of the compressive strength at each temperature).

The compressive properties at each target temperature – strength (σ_c) and modulus (E_c) – and the corresponding ratio with respect to the room temperature values are presented in Table 11. The values listed in this table show that a drastic strength reduction occurred when the test temperature

approached the T_g of the material: at 100 ºC, the compressive strength was reduced to 39% of its room temperature value, whereas the corresponding reduction of the compressive modulus was less marked, with an average modulus retention of 67%. When the test temperature was increased, the compressive strength remarkably decreased, with reductions of 93% and 96% at 150 ºC and 200 ºC, respectively. Overall, the compressive modulus was significantly less affected by exposure to elevated temperatures than the compressive strength: at 150 ºC, the compressive modulus decreased to 43% of its ambient temperature values; for higher temperatures, no significant further reductions were observed (from 150 ºC to 250 ºC the average reduction was about 12%) – these results show that the compressive modulus of the GFRP material tested in the present study is more fibre-dominated (*i.e.* presents lower sensitivity to matrix softening) than the compressive strength, which is clearly matrix-dominated.

Table 11 - Compressive properties of GFRP laminate for each target temperature (average ± standard deviation).

T [°C]	σ_c [MPa]	σ_c/σ_{20} [-]	E_c [GPa]	E_c/E_{c20} [-]
20	228.9±13.9	1.00±0.06	29.6±1.24	1.00±0.04
50	196.7±5.6	0.86±0.03	27.6±1.37	0.93±0.04
100	89.3±3.8	0.39±0.02	19.9±1.05	0.67±0.04
150	15.4±0.1	0.07±0.01	12.7±0.93	0.43±0.03
200	8.9±1.5	0.04±0.01	9.8±1.78	0.33±0.05
250	-	-	9.2±0.29	0.31±0.01

Representative failure modes observed in the compressive tests performed on shorter specimens tested up to failure are shown Figure 38. In the specimens tested from 20 ºC to 100 ºC, through-thickness delamination occurred, while for higher temperatures the specimens presented fibre kinking failure due to resin softening. In addition, at 200 ºC, the specimens exhibited a change in the surface colour – the dark tone visible in this figure is related to the decomposition of the resin at such temperature.

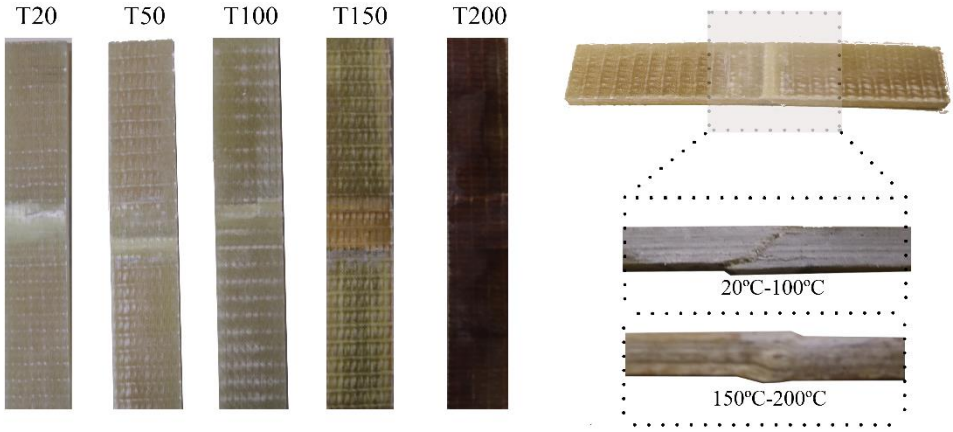

Figure 38 - Failure modes observed in the compressive failure tests.

In Figure 39, the changes in compressive strength and modulus with temperature obtained in this study are compared with the results reported in the literature [17,38,45,49,50]. In spite of the inherent

differences between the FRP materials tested in the various studies, the following two main conclusions can be drawn: (i) regarding the compressive strength, all materials followed a similar reduction trend, indicating that this property is mostly dependent on the thermomechanical response of the matrix, rather than on the fibres; (ii) concerning the compressive modulus, its reduction with temperature seems to be much less pronounced than that of the compressive strength; however, since very limited data are available regarding the compressive modulus of GFRP at elevated temperatures, further studies are needed to confirm that it can indeed be considered as a fibre-dominated property.

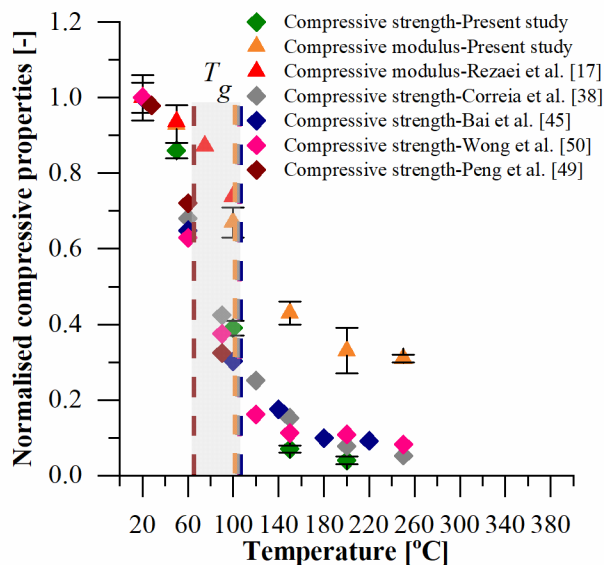

Figure 39 - Normalised compressive properties vs. temperature.

3.5.3 Shear behaviour

Figure 40 shows representative shear stress *vs.* distortion curves for GFRP specimens tested at temperatures ranging from 20 ºC to 200 ºC. All curves present an approximately linear development during the first stage of the tests (*i.e.* for relatively low stress levels). During this linear stage of the response, the slope of the curves (*i.e.* the shear modulus) presented considerable reduction for temperatures above 50 ºC. For higher stress levels, the curves become nonlinear with progressive stiffness reduction up to the maximum shear stress. Regarding the maximum shear stress values, it is worth highlighting that valid shear failure modes were observed only for 20 ºC (as discussed below), whereas for higher temperatures the specimens failed prematurely due to local crushing; consequently, it was only possible to obtain lower bounds of the shear strength at elevated temperatures – for this reason, the curves for temperatures equal to and above 50 ºC plotted in Figure 40 are shown up to the initiation of that crushing phenomenon. In spite of these premature failures at elevated temperatures, it was possible to observe that, as expected, the GFRP material exhibited a progressive reduction of the shear modulus for temperatures above 50 ºC; in addition, a more marked

degree of nonlinearity was observed for the highest temperatures; this effect should be related to the softening of the polymeric matrix during its glass transition process.

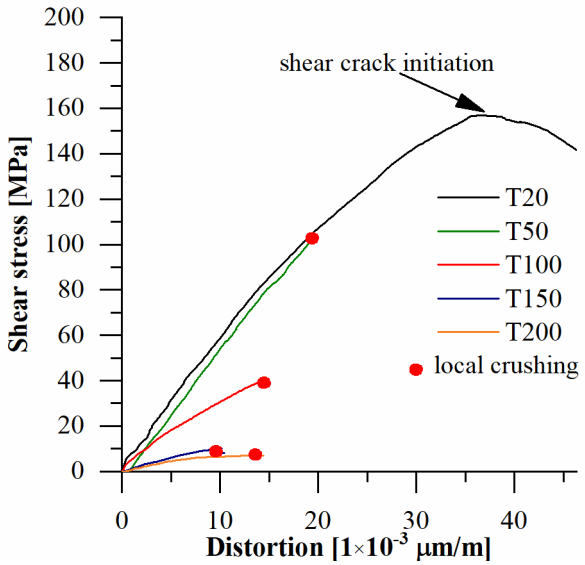

Figure 40 - Shear stress vs. distortion curves.

Table 12 summarizes the variation with temperature of the shear modulus (G); the corresponding normalized values with respect to the properties measured at room temperature (G/G_{20}) are also included.

Table 12 - Maximum shear modulus of GFRP laminates as a function of temperature (average ± standard deviation).

T [ºC]	G [GPa]	G/G_{20} [-]
20	6.5±0.2	1.00±0.03
50	6.0±0.4	0.93±0.04
100	2.5±0.3	0.39±0.02
150	1.4±0.1	0.22±0.03
200	0.8±0.1	0.12±0.04

Table 12 confirms that the GFRP laminate experienced a noticeable degradation of the shear modulus, especially for temperatures around its T_g (102 ºC, *cf.* DMA results in section Figure 25) - at 100 ºC, the shear modulus presented an average reduction of 61% (when compared to the corresponding value at ambient temperature); for higher temperatures, further reductions were observed – the remaining shear modulus was only 22% and 12% at 150 ºC and 200 ºC, respectively.

Figure 41 shows the two failure modes mentioned above. At room temperature, the specimens presented a sharp vertical crack at the notched area, with rupture of both matrix and fibres (*cf.* Figure 41a). In specimens tested at higher temperatures, a premature failure mode was observed, with local crushing occurring at the edge of the notched area (*cf.* Figure 41b) – this type of failure was triggered by the stress concentration induced in this area by the loading blocks; this result suggests that, for the fibre architecture adopted in these specimens, the compressive strength (discussed in section 3.5.2) seems to have been more affected by elevated temperature than the shear strength (as

mentioned, in these experiments, only a lower bound of the actual shear strength could be determined at elevated temperatures).

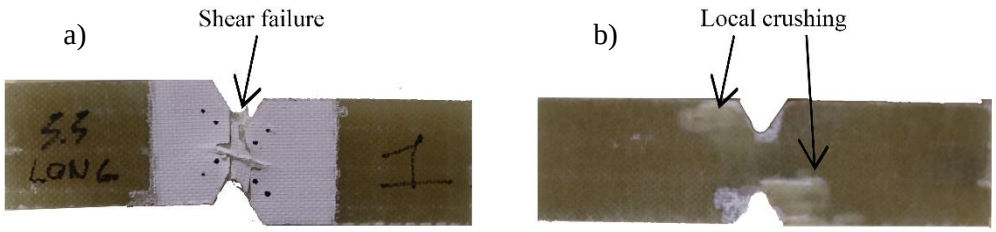

Figure 41 - Failure modes observed in shear tests: (a) at room temperature and (b) at elevated temperatures, from 50 ºC to 200 ºC.

Figure 42 compares the variation of the normalized shear modulus obtained in the present study with the average results reported by Rosa *et al*. [48] and Rezaei *et al*. [17] for GFRP materials produced by pultrusion and vacuum infusion, respectively. Despite having different fibre architectures, the results obtained in the present study are in line with those reported by Rosa *et al*. [48], with significant shear modulus reduction for temperatures ranging from 50 ºC to 150 ºC. Figure 42 also shows that the reduction of the shear modulus with temperature obtained by Rezaei *et al*. [17] seems to occur for lower temperatures, which is in agreement with the slightly lower T_g of the material tested by those authors (87 ºC, test method not reported). These results suggest that the variation with temperature of the shear modulus is mainly governed by the thermomechanical changes of the polymeric matrix, rather than those of the fibres (which are affected for much higher temperatures); in other words, these results confirm that the shear modulus is a matrix-dominated property.

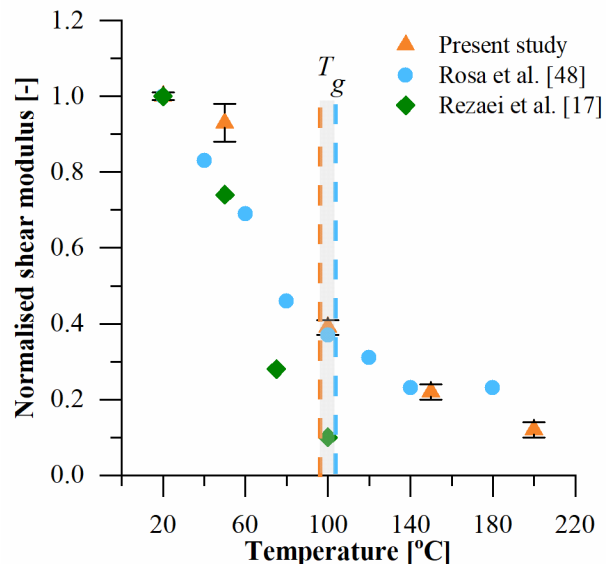

Figure 42 - Normalised shear modulus vs. temperature.

3.6 ANALYTICAL STUDY

In this section, the accuracy of four analytical models proposed in the literature to predict the experimental results obtained in the present study is assessed (*cf.* section 5.1). In addition, in section 3.6.2, a design-oriented temperature conversion factor that was included in the European Technical

Specification prEN 19101: 2021, "*Design of Fibre-Polymer Composite Structures*" for both fibre- and matrix-dominated properties is compared with the reductions obtained in the present investigation.

3.6.1 Empirical degradation models

Various empirical models based on curve fitting procedures to experimental data have been proposed in the literature to describe the evolution with temperature of the mechanical properties of FRP materials, namely those developed by Gibson *et al.* [36], Correia *et al.* [38], Wang *et al.* [37] and Mahieux *et al.* [39]. The interested reader should refer to section 2.5.3 for more detailed information on the these empirical models

With the objective of simulating the reductions with temperature of the mechanical properties of the GFRP material tested in this study, the above-mentioned empirical models were fitted to the experimental data presented in section 3.5. For all models, the parameter P_u was taken as 1 (average normalized value at ambient temperature), whereas the parameter P_r, for each property, was taken as the normalized average value obtained at the maximum temperature tested. Regarding the fitting parameters of the different models, they were obtained by a standard procedure that minimizes the absolute mean percentage error (AMPE) between the test data and the theoretical values of the models. Figure 43 to Figure 45 plot the empirical modelling curves together with the normalized experimental values from the tensile, compressive and shear tests obtained in the present study; the defining parameters and the absolute mean percentage error (AMPE) values associated to each empirical model are summarized in Table 13.

Table 13 - Defining parameters and absolute mean percentage errors (AMPE) of the different empirical models.

Model	Parameter	Tensile strength	Tensile modulus	Compressive strength	Compressive modulus	Shear modulus
Gibson *et al.* [36]	*k' [-]*	0.02	0.03	0.02	0.02	0.03
	$T_{g,mech}$ *[ºC]*	110.11	108.71	90.58	105.56	87.43
	AMPE [%]	2.51	2.01	3.69	4.43	4.73
Wang *et al.* [37]	*A [-]*	1.05	1.06	1.38	1.01	1.40
	B [-]	1.77	0.96	1.33	0.55	0.57
	C [-]	665.32	1446.56	19.93	291.50	19.37
	n [-]	1.11	1.29	0.64	1.04	0.62
	AMPE [%]	14.33	6.20	9.41	13.59	9.18
Correia *et al.* [38]	*B [-]*	-9.19	-74.53	-9.27	-10.70	-14.78
	C [-]	-0.02	-0.05	-0.03	-0.03	-0.04
	AMPE [%]	2.12	1.82	3.22	4.13	3.38
Mahieux *et al.* [39]	m *[-]*	9.00	13.00	11.00	9.00	15.00
	T_0 *[ºC]*	402.47	399.53	381.37	397.53	374.45
	AMPE [%]	2.71	2.63	5.12	4.28	6.02

With the exception of the model proposed by Wang *et al*. [37], all modelling curves presented similar development and very good agreement with all mechanical properties determined in this study, as demonstrated by the low values of AMPE obtained, which varied between 1.8% (tensile modulus

predictions by Correia *et al*. [38]) and 6.0% (shear modulus predictions by Mahieux *et al*. [39]). Regarding the results of the model by Wang *et al*., the shape of the modelling curves was not able to accurately reproduce the reduction with temperature of the experimental results, especially the compressive modulus (*cf.* Figure44b, AMPE of 13.6%) and the tensile strength (*cf.* Figure43a, AMPE of 14.3%) for the highest temperatures tested – these results show that the model of Wang *et al*., initially developed for metallic materials, does not seem appropriate to describe the reduction with temperature of the mechanical properties of the GFRP laminates used in the present study.

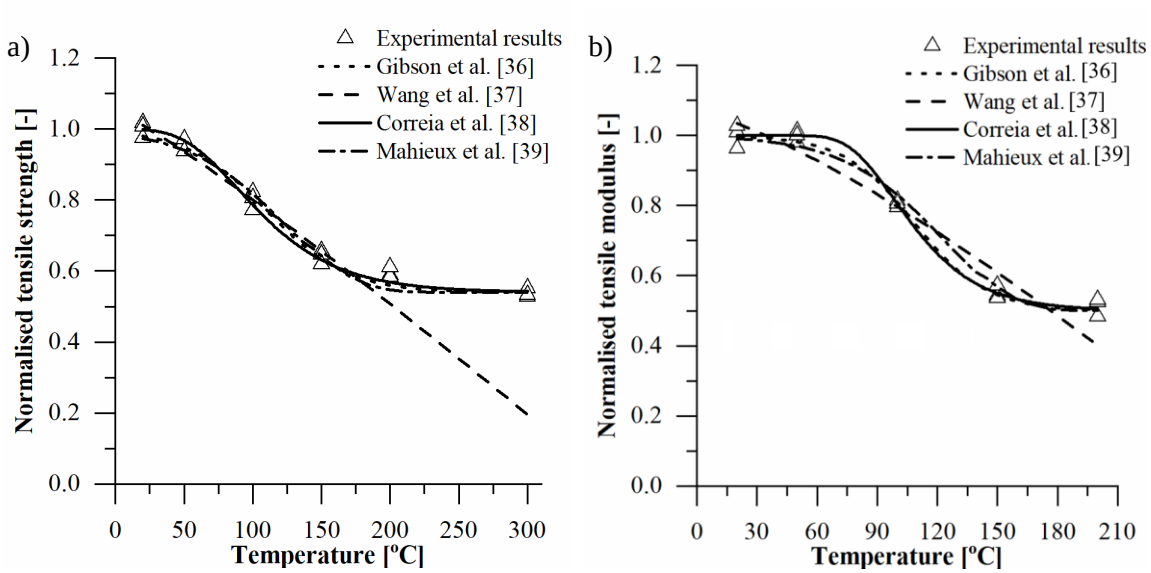

Figure 43 - Variation of tensile properties with temperature: (a) strength and (b) modulus.

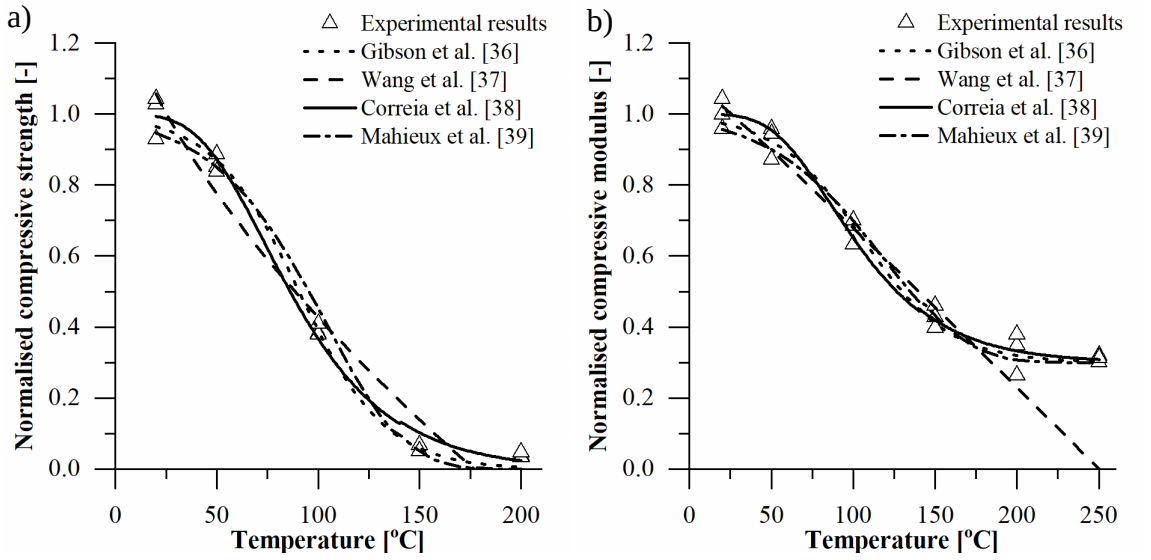

Figure 44 - Variation of compressive properties with temperature: (a) strength and (b) modulus.

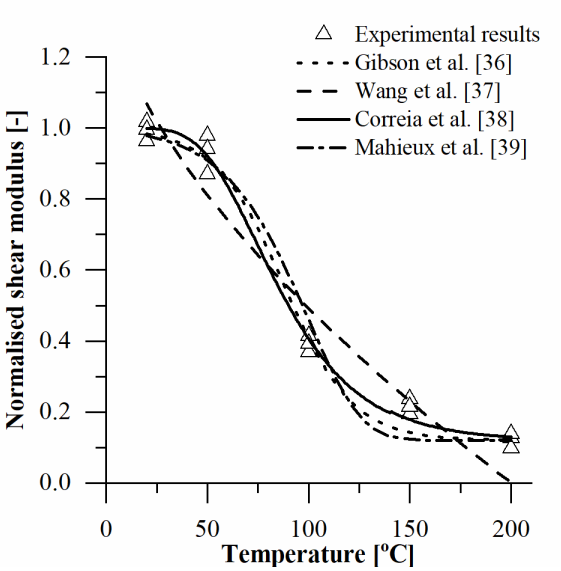

Figure 45 - Variation of shear modulus with temperature.

3.6.2 Assessment of design-oriented temperature conversion factor

The results described in section 3.5 were also compared with a design-oriented model proposed in the European Technical Specification (TS) prEN 19101: 2021, "*Design of Fibre-Polymer Composite Structures*" [12] to take into account (in design) the effects of elevated temperature in the mechanical properties of FRP materials. The main goal was to assess the adequacy of these provisions for the GFRP material tested in this study.

The following general equation is proposed in the above-mentioned document for the temperature conversion factor (n_{ct}) of FRP materials,

$$n_{ct} = min\{1.0 - \alpha \cdot T_n; 1.0\} \tag{8}$$

where α is a parameter that depends on the sensitivity of a given material property to matrix softening (*i.e.*, if it is either matrix- or fibre-dominated) and T_n is the normalized temperature (ranging between 0 and 1), defined as follows,

$$T_n = \frac{T_s - 20}{T_g - 20} \tag{9}$$

in which T_s is the maximum service temperature (*i.e.* temperature in the material, which is limited to a maximum value of T_g– 20 ºC) and T_g is the glass transition temperature, defined based on the onset value of the storage modulus decay (plotted in logarithmic scale) obtained by DMA tests. The values proposed in the TS for the α parameter are 0.25 for fibre-dominated properties (tensile strength and modulus and compressive modulus in direction(s) with high ratio of fibre reinforcement) and 0.80 for matrix-dominated properties (shear properties and compressive strength). These α values were defined [12] based on a comprehensive survey of test data from the literature, so that n_{ct} provides: (i) conservative estimates for more than 90% of the experimental data collected; and (ii) maximum

relative differences to test data of 15% (for the values that are overestimated). It is worth mentioning that the calibration of a temperature conversion factor based on a formal reliability study was not deemed possible in the development of prEN 19101: 2021 due to the insufficient amount of experimental data to support such approach; additional details about the definition of the above-mentioned design-oriented conversion factor can be found in Correia *et al*. [56].

Table 14 shows the comparison between the values of the temperature conversion factor for fibre- and matrix-dominated properties, n_{ct}, with the corresponding experimental properties obtained in the present study (both average P_{av} and individual P_i values), as well as the ratio between the normalized average properties and the conversion factor (P_{av}/η_{ct}). It is worth noting that to comply with the recommendations provided in the TS (upper limit of T_g – 20 ºC), only the test data obtained at 50 ºC were considered.

Table 14 - Conversion factor vs. experimental normalized properties.

Mechanical property	Type of properties	T [ºC]	P_i [-]	P_{av} [-]	n_{ct} [-]	P_{av}/η_{ct} [-]
Tensile strength	Fibre-dominated	50	0.97	0.95	0.92	1.03
			0.93			
			0.95			
Tensile modulus			1.00	0.99		1.08
			0.99			
			0.99			
Compressive modulus			0.96	0.93		1.01
			0.88			
			0.95			
Compressive strength	Matrix-dominated		0.88	0.86	0.71	1.21
			0.85			
			0.84			
Shear modulus			0.91	0.93		1.31
			0.92			
			0.97			

As shown in Table 14, the conversion factor provides conservative estimates for all individual (except one) and average test data obtained in this study. Regarding the compressive modulus, the conversion factor slightly overestimates one individual data obtained in the present study, but considering the average values obtained at each test temperature, the above-mentioned requirements are both fulfilled. However, it is worth mentioning that, to the best of the author's knowledge, apart from the present investigation, only one study is available in the literature about the effects of elevated temperatures on this mechanical property. Further experimental studies about the mechanical properties of FRP materials at elevated temperatures are clearly needed, as they would allow further validating and/or improving the conversion factor that has been proposed in the European Technical Specification prEN 19101: 2021.

3.7 CONCLUDING REMARKS

This chapter presented a comprehensive experimental and analytical study about the effects of elevated temperatures on the mechanical behaviour of GFRP composite materials produced by vacuum infusion, considerably extending the experimental data available in the literature. From the results obtained, the following main conclusions can be drawn:

- Overall, the experimental results obtained in this study confirm that the mechanical properties of the GFRP materials are strongly reduced by the exposure to elevated temperatures due to the softening of the polymeric matrix, especially when the T_g is approached and exceeded.

- The shear modulus and the compressive strength suffer considerable reductions with temperature. At 200 ºC, both properties retained less than 15% of the values observed at room temperature. These results confirm that these material properties are strongly dependent on the thermomechanical response of the matrix, *i.e.* they can be considered matrix-dominated.

- Although presenting important reductions, the tensile properties and the compressive modulus at 200 ºC still retained 50% and 33% of their ambient temperature values, respectively. Thus, these mechanical properties seem to be less sensitive to the matrix softening phenomenon; therefore, they can be considered fibre-dominated.

- Regarding the analytical study, with the exception of the model proposed by Wang et al. [37], all empirical modelling curves presented very good agreement with all mechanical properties obtained in the experimental campaign.

- The design-oriented temperature conversion factor proposed in the European Technical Specification (TS) prEN 19101: 2021 for both fibre and matrix-dominated properties provided reasonably conservative estimates for most individual test data and for all average test data obtained in this study, which confirms its suitability to be used for design purposes. Additional experimental results are needed in order to further validate this temperature conversion factor and to allow its calibration based on formal reliability studies.

CHAPTER 4

THERMOPHYSICAL PROPERTIES OF CONSTITUENT MATERIALS AT ELEVATED TEMPERATURE

4.1 INTRODUCTION

As discussed in Chapter 2 and Chapter 3, when exposed to moderately elevated temperatures (60–200 °C), the mechanical properties of the constituent materials of GFRP sandwich panels undergo significant reductions [2,43,57,58]. Additionally, when GFRP sandwich panels are exposed to high temperatures (300–500 °C), both GFRP and polymeric foams decompose, releasing heat, smoke and toxic gases.

The characterisation of the thermophysical properties of the constituent materials of GFRP sandwich panels as a function of temperature is essential for the accurate prediction of their thermal response under exposure to fire. However, the information available in this respect is scarce. A key limitation of the numerical simulations of the fire behaviour of sandwich panels is that the thermal models developed so far are not able to accurately predict the temperature evolution across the depth of the panels (as discussed further ahead in chapter 7), mainly due to simplifying assumptions about the variation with temperature of the thermophysical properties. It is worth noting that the results obtained from the thermal models can be used as input data in mechanical models, which, in turn, can be used as practical design tools for estimating the fire resistance of GFRP sandwich panels.

Despite the relevance of the topic, very limited information is available in the literature about the influence of high temperature on the thermophysical properties (especially on the thermal conductivity and specific heat) of the typical constituent materials of GFRP sandwich panels used for civil engineering applications, *i.e.* polymeric foams and GFRP material.

Several studies [16,59–61] evaluated the mass changes with temperature of polymeric foams by means of thermogravimetric (TGA) tests performed according to ISO 11357 standard [28]. Concerning the remaining mass *vs.* temperature curves of the foams tested in air atmosphere, they typically present two main drops: the first drop occurs for temperature ranging from 180 ^{o}C to 350 ^{o}C and it involves the decomposition of the foam (which melts and releases gases), while the second (usually observed at around 300-450 ^{o}C) involves the decomposition of the residual molten material

into gases. The results obtained in nitrogen atmosphere depict only one significant drop, which occurs at around 300-450 °C, above which the mass gradually decreases up to 900 °C.

Unlike the mass changes with temperature, for which several investigations have been performed and a comprehensive understanding was acquired, very limited information is reported in the literature concerning the influence of temperature on both thermal conductivity and specific heat of polymeric foams [62–66]. Indeed, direct measurements are challenging to perform, especially for temperatures above the T_g of the solid polymer, because the high deformability of the material with increasing temperature does not allow a proper contact between the sensor of the equipment (*e.g.* hot plate method) and the tested material surface.

Regarding the thermal conductivity, it can be observed that such property is governed by different types of heat transfer [67]: (i) conduction through the solid polymer; (ii) conduction through the gas; (iii) convection within the cells, and (iv) radiation through the cell walls and across the voids. Note that the contribution of convection is relevant only for foams with cells size greater than 10 mm [31]; for this reason, in most commercial foams this factor is negligible. In general, when the density of the foam is reduced, the contribution from the conduction through the solid decreases; and, as a consequence, the contribution of radiation increases due to the more significant transparency of the cell walls to radiation [31]. Additionally, the thermal conductivity decreases as the cell size increases due to the greater number of internal reflections from cell walls. As regards the specific heat, its variation with temperature may be assumed similar to that of the solid from which it is made, since the contribution of the gas is almost negligible [31].

Proença *et al*. [62] studied the thermophysical properties of a PUR foam (density of 40 kg/m^3) up to 200 ^{o}C by means of a transient plane source (TPS) method with a Hot Disk TPS 2500S equipment following the ASTM C177-85 standard. The authors found out that the temperature increase leads to higher values of the thermal conductivity. The latter was increased about 1.1 and 2.6 times at 60 ^{o}C and 200 ^{o}C, respectively, when compared to the ambient temperature value. Concerning the specific heat, a non-monotonic variation with temperature was observed: at 150 ^{o}C and 200 ^{o}C the measured values were 1.2 and 0.8 times that at room temperature, respectively.

Valencia [63] performed TPS tests on a PUR foam (density of 22 kg/m^3) up to 180 ^{o}C and determined that the thermal conductivity is severely affected by temperature increase – *e.g.*, the values measured at 180 ^{o}C were 1.9 times higher than at room temperature. According to the authors, this result might be due to the increase with temperature of the thermal conductivity of the foam's constituent materials (*e.g.* solid and gas). The authors also found that, differently from what had been previously reported [62], the foam exhibited a monotonic increase of the specific heat with temperature: at

100 °C and 180 °C the measured values were approximately 1.1 and 1.3 times those at room temperature.

Wang and Foster [68] considered the formulation developed by Glicksman [67] to model the effective thermal conductivity of a polyisocyanurate (PIR) foam (density of 40 kg/m^3) as a function of temperature. The temperature dependent thermal conductivity model was based on the following contributions: (i) conduction through the solid; (ii) conduction through the gas, and (iii) radiation through the cell walls and across the pores. The contribution of convection was considered negligible due to the small pore size of the PIR foam. The authors found that the thermal conductivity of the PIR foam exponentially increased with temperature – at 1000 °C, the values were 25 times those at ambient temperature. The thermal conductivity model was then validated through the numerical simulation of previous fire tests performed on sandwich panels. The results obtained showed that the predicted temperatures were in good agreement with the measured ones. The highest deviations were observed for T > 500 °C, due to the significant contribution of radiation through the cell walls.

Vahedi *et al.* [69] studied the influence of the temperature on the thermophysical properties of balsa wood (density of 285 kg/m^3), also used in GFRP sandwich structural elements. The authors used an inverse heat transfer analysis based on experimental data and a 1D numerical heat transfer model to determine the thermal conductivity and specific heat, in both longitudinal and transverse directions, as a function of temperature. The estimated thermophysical properties were validated using a FE thermal model, which aimed at predicting the thermal response of a sandwich panel comprising GFRP face sheets and balsa core subjected to the ISO 834 fire curve. The equivalent properties were then calibrated by comparing the results obtained from the FE model with experimental data. Results showed that temperature importantly affects the thermophysical properties of balsa wood.

The inverse analysis proposed by Vahedi *et al.* [69] was also adopted by Dias *et al.* [66] to evaluate the variation with temperature of the thermophysical properties of PET and PUR foams (density ranging from 40 kg/m^3 to 100 kg/m^3), typically used as core materials in sandwich panels. In general, the thermal conductivity of all materials tested increased with temperature. The thermal conductivity of PET and PUR foams exhibited an approximately linear increase up to 140 °C; when the temperature was increased from 30 °C to 140 °C, the thermal conductivity of the PET and PUR foams was respectively 2 and 1.6 times that measured at room temperature. Furthermore, results obtained showed that the specific heat was also affected by elevated temperature: at 130 °C, the specific heat of the PET and PUR foams increased 23% and 34% (compared to the ambient temperature values), respectively.

A significant amount of data about the variation with temperature of density, thermal conductivity and specific heat of GFRP materials are reported in the literature, most of which concerns composites

produced by pultrusion [70–73]. However, the information available, which is valid for specific types of GFRP materials (for a given fibre content and architecture, thickness and manufacturing process), does not provide a comprehensive understanding about the variation with temperature of the specific heat and thermal conductivity of custom GFRP composite materials [72,74,75]. In fact, there are some noticeable differences in the results available in the literature, which mostly stems from differences in (i) the approaches used to determine the thermophysical properties of the materials; (ii) the type of material tested and (iii) the physical phenomena considered (*e.g.* dehydration of the matrix, delamination of the composite, gas generation). In general, similarly to what is observed in polymeric foams, GFRP composites do not present significant mass changes for temperatures below the T_d of the material [70]. When the decomposition of the polymeric matrix starts, a significant drop can be observed in the remaining mass *vs.* temperature curve. It is worth mentioning that the magnitude of this reduction is function of both the organic fraction of the material and heating rate. Concerning the effective specific heat of GFRP composites, it also increases significantly when the polymeric matrix undergoes its endothermic decomposition process [73]. This result is explained by the fact that additional heat is needed in order to break the bonds within the matrix molecular structure. Finally, the thermal conductivity *vs.* temperature curve of the GFRP material presents an (i) initial increase due to the intrinsic behaviour of the matrix, followed by (ii) quite significant reductions during the decomposition process, mainly due to the formation of pores (and delamination), and (iii) a final slight rise due to the fibre volume fraction increase [71].

The literature review presented above shows that the influence of the temperature on the thermal properties of both GFRP composite materials and polymeric foams has not yet been investigated in sufficient depth; hence, further studies are necessary to fill this gap. To this end, this chapter presents numerical and experimental investigations about the thermal behaviour of GFRP laminates produced by vacuum infusion and foam filled sandwich panels aiming to validate a strategy for the determination of their temperature-dependent thermophysical properties or of their constituent materials. In this context, a numerical inverse analysis was performed, comprising (i) experimental fire tests on sandwich specimens and GFRP laminates; and a (ii) numerical approach which includes an optimization routine and a 1D finite element (FE) model for thermal simulation. The optimization routine developed to determine the thermophysical properties of both GFRP and foam materials was established to obtain a good agreement between the predicted temperatures and the measured ones. It is worth mentioning that the obtained equivalent thermophysical properties can be used as input data in the thermomechanical simulation of GFRP foam-filled sandwich panels under fire, allowing to optimize the geometry of the sandwich panels and fire protection schemes, as well as to develop fire design rules.

4.2 EXPERIMENTAL STUDY

4.2.1 Materials

In this study, two 120 mm thick rigid polymeric foams were tested: (i) a PUR foam with measured density of 93 kg/m^3 and (ii) a PET foam with measured density of 99 kg/m^3. In what concern the GFRP laminates (thickness of 12 mm and $[0/0/0/90/45/-45/0/0/-45/45/90/0/0/0]_s$ fibre layup), they were made of E-glass stitched fibres embedded in a urethane acrylate resin (*Crestapol 1261*). The GFRP material was produced by vacuum infusion at the Pólo de Inovação em Engenharia de Polímeros (PIEP) research institute. Two specimens were tested for each material. It is worth mentioning that these are the same materials that were used in the experiments described in chapters 2, 3, 5 and 6.

The through-the-thickness thermophysical properties of both PUR and PET foams at room temperature were determined using a thermal properties analyser (TPA) ISOMET model 2114, coupled to an IPS 1100 surface probe following the recommendations of ASTM-D-5334 [76] and ASTM D-5930 [77]. The tests were performed on two blocks of material with dimensions of 150 × 600 × 100 mm^3 (width × length × thickness), and two measurements for each foam were taken. The ISOMET device uses the transient plane source (TPS) method to determine the thermal properties of the material. In this context, heat flow impulses are transmitted by means of a resistor heater inserted into the probe, which is in direct contact with the foam (*cf.* Figure 46). It is worth mentioning that the foams were placed on top of 30 mm thick polystyrene (XPS) boards; this procedure was chosen to minimise the heat changes between the specimens and the exterior environment.

Figure 46 - TPS tests on PET foam specimens.

The average values of the specific heat, c_p, and thermal conductivity, λ, at room temperature obtained from the tests performed on both PUR and PET foams are listed in Table 15.

The specific heat (c_p=788 J/m^{3o}C) and the thermal conductivity (λ=0.31 W/m^{o}C) at room temperature of the GFRP material were taken from Proença *et al.* [11], who performed experiments

on similar GFRP laminates produced by vacuum infusion and following the same procedure used in the present study.

Table 15 - Average values of specific heat and thermal conductivity at room temperature of PUR and PET foams.

Foam type	Specific heat [J/m^3°C]	Thermal conductivity [W/m°C]
PUR	111333	0.0388
PET	117500	0.0397

4.2.2 Specimens' description and preparation

A custom setup was assembled for these tests, in which GFRP laminates with dimensions of 330 × 625 × 12 mm^3 (width × length × thickness) and sandwich specimens with dimensions of 330 × 625 × 130 mm^3 (width × length × thickness) were subjected to the time-temperature curve defined in the ISO 834 standard [78] from the bottom surface, while the top surface was subjected to ambient temperature.

The sandwich specimens consisted of two steel face sheets with thickness of 5 mm, adhesively bonded to a 120 mm thick polymeric foam core (to be assessed in each test) using a 0.5 mm layer of polyurethane adhesive (*Sikaforce 7710*), as shown in Figure 47. It is worth mentioning that steel face sheets were used in these sandwich panels in order the reduce the number of unknowns for the thermophysical properties of the foams by the numerical procedure described in section 4.3, since steel is a material whose thermophysical properties variation with temperature are well known and reported in the literature [79]. Finally, it should be mentioned that before testing the specimens were stored for at least 7 days in a room with controlled atmosphere (constant temperature of 21 °C and relative humidity of 56%) to guarantee the full curing of the adhesive.

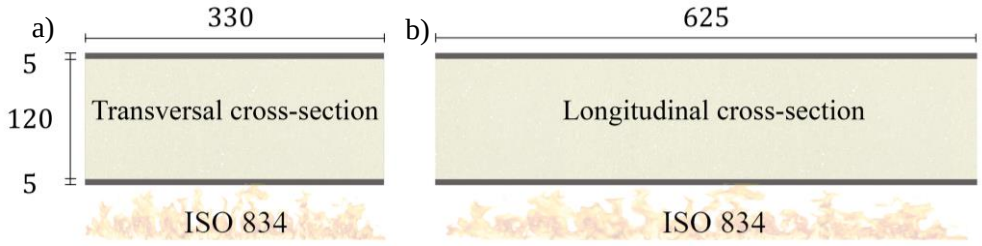

Figure 47 - Geometry of the sandwich panels: (a) transverse and (b) longitudinal cross-section.

Four steel rods were also welded at the four edges of the panel to fix the face sheets in place for all the duration of the fire exposure (*cf.* Figure 48).

Figure 48 - Overview of the steel-foam sandwich specimens before the thermal exposure.

Moreover, aiming at preventing the lateral surfaces of the sandwich specimens from being subjected to heat, these were insulated by (i) covering the foam with aluminium tape and (ii) placing adjacent mineral wool blankets, as shown in Figure 49.

Figure 49 - Test setup: (a) aluminium tape and (b) mineral wool protection along the side walls of the foam.

4.2.3 Instrumentation and procedure

With respect to the instrumentation, the thermal response of the sandwich specimens and GFRP laminate was monitored by means of type K thermocouples (0.25 mm of conductor diameter). The sandwich specimens were instrumented with 12 thermocouples whose nomenclature and position are detailed in Figure 50.

As shown in Figure 50, six thermocouples (for each section, A-A' and B-B') were installed across the height of the foam at a distance of 140 mm from the lateral sides. It is worth mentioning that the thermocouples were inserted in holes drilled horizontally through the core using a drill driver coupled to a 2 mm thick stainless-steel rod. The thermocouples were embedded in a PUR adhesive and then introduced at the predefined locations - this procedure was chosen to keep the thermocouples in place during the fire exposure. In addition, 2 thermocouples were also welded on the bottom and top steel plates.

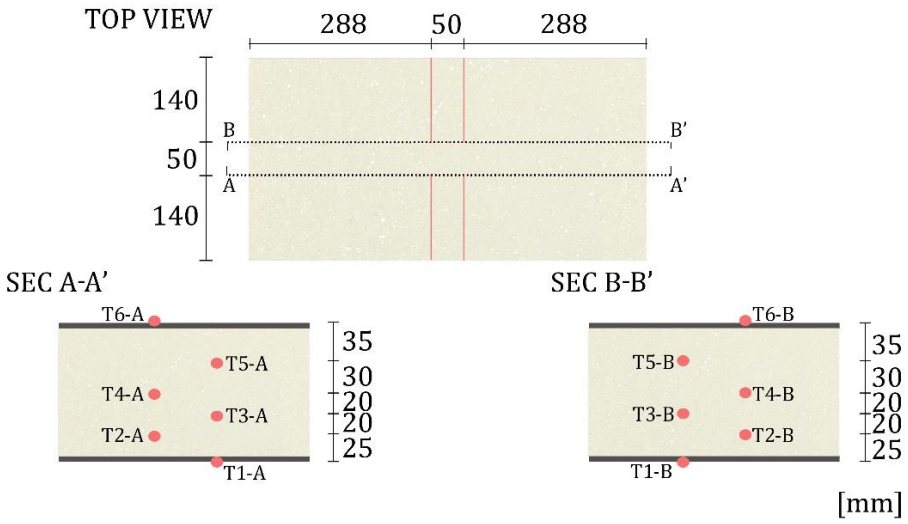

Figure 50 - Thermocouple position across the depth of the core.

As shown in Figure 51, 5 thermocouples were also placed in the GFRP laminate during the manufacturing process (*i.e.* between glass fibre sheets), allowing to monitor with good accuracy the evolution of temperature across the cross-section. The number and position of the thermocouples are presented in Figure 52.

Figure 51 - Thermocouple positioning during the manufacturing process of the GFRP laminate.

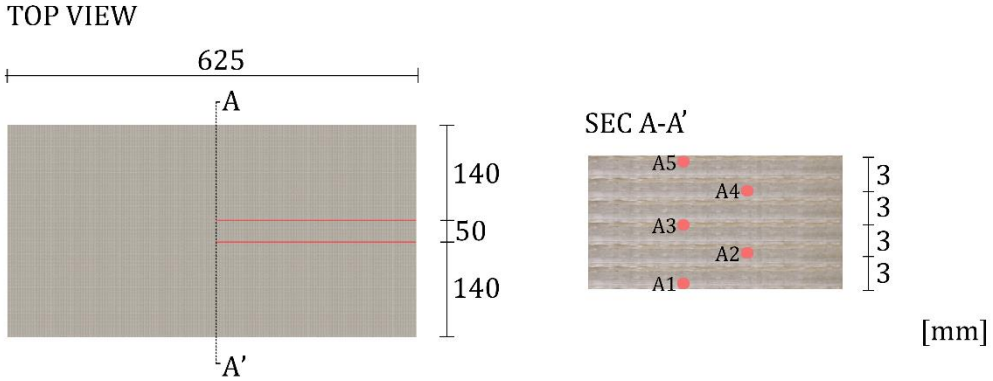

Figure 52 - Thermocouple position across the depth of the GFRP laminate.

During the fire tests, the evolution of temperatures was recorded using a HBM data-logger at an acquisition rate of 2 Hz.

The fire tests were carried out using an intermediate-scale oven, with external dimensions of 1200 × 1350 × 2100 mm^3 (wide × long × high) and a top opening area of 950 × 800 mm^2 (*cf.* Figure 53). In this regard, it is worth mentioning that furnace top covers consisting of a set of metallic frames filled with mineral wool were positioned on the top of the furnace walls (*cf.* Figure 54a). This was necessary due to the large dimensions of the opening area of the furnace compared to the dimensions of the specimens. By using these insulation modules, it was possible to obtain a top opening area of of 300 × 600 mm^2 (slightly lower than the area of the specimens), as shown in Figure 54.

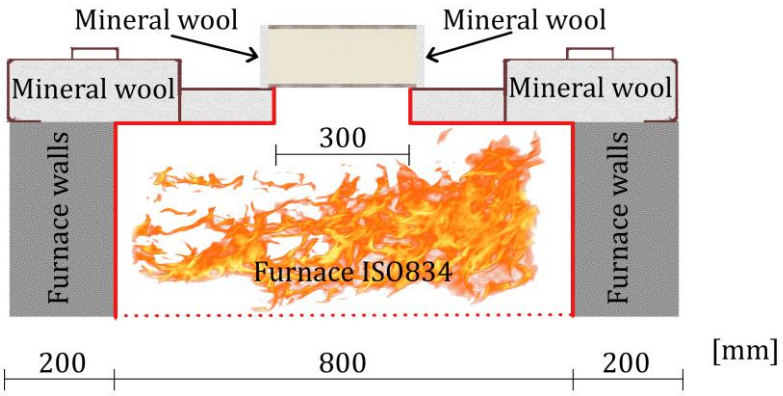

Figure 53 - Transversal schematic view of the test setup.

Once the specimen was placed on top of the furnace (*cf.* Figure 54b), the oven was turned on, and the bottom surface of the specimens was subject to the time-temperature curve defined in the ISO 834 standard [78] up to the full decomposition of the polymeric foam or until 60 minutes of fire exposure.

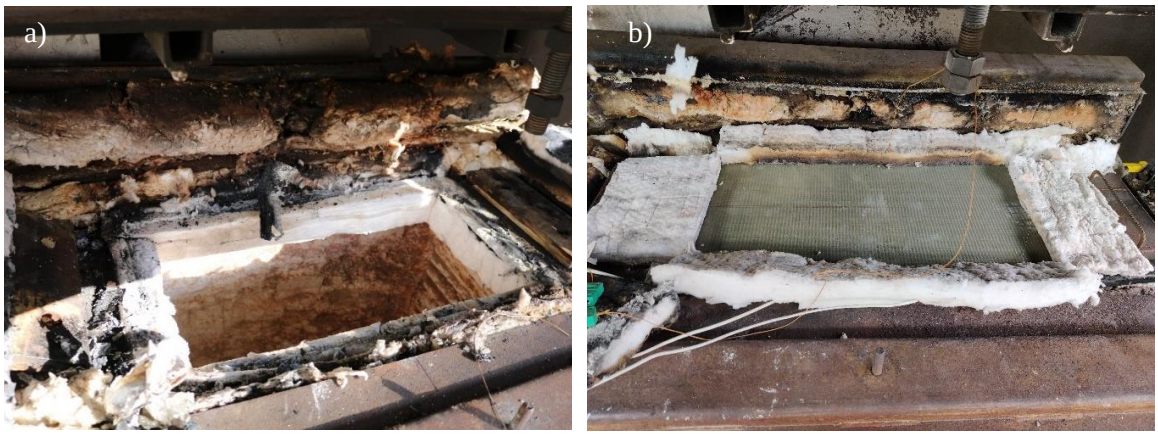

Figure 54 - Test setup: (a) top opening of furnace before specimens' positioning (b) top view of a test on the GFRP laminate.

4.3 NUMERICAL PROCEDURE

In this section, the numerical procedure used to obtain the temperature-dependent thermophysical properties of both GFRP and foam materials is described in detail. Firstly, the global implementation of the inverse analysis used to determine the thermophysical properties of the materials as a function

of temperature is presented. Then, the 1D FE model developed and used within the numerical procedure is described. Figure 55 presents the flowchart of the global implementation of the inverse analysis used. The methodology includes two main parts: a 1D FE thermal model, described in section 4.4, and an optimization routine ('*fminsearchbnd'* [80]), both implemented in *Matlab* - it is worth mentioning that this implementation benefited from the collaboration of two researchers of the *FireFloor* project, Prof. Carlos Tiago and Dr. António Duarte.

As shown in Figure 55, firstly the 1D FE thermal model is ran using an initial set of values defined for the thermophysical properties. To this end, the specific heat and thermal conductivity of both foam and GFRP materials were initially assumed constant and equal to those determined at room temperature (*cf.* section 4.2.1). It is worth mentioning that to avoid results without any physical meaning, the boundaries for the variation of the properties were also defined by means of the '*fminsearchbnd'* optimization function. Additionally, the values of temperatures for which the thermophysical properties are being determined (initially set as 20ºC, 200ºC, 400ºC and 800 ºC) can also be varied. Hence, the variables of the problems are four arrays: (i) thermal conductivity for a set of temperatures; (ii) the corresponding set of temperatures; (iii) specific heat for a set of temperatures (can be different from those for the thermal conductivity) and (iv) the corresponding set of temperatures. After the run of the 1D FE thermal model, temperature-time curves for each node are obtained and compared with their experimental counterparts (temperature-time curves at the thermocouples position). To avoid the need to match the FE mesh and the position of the thermocouples, a linear interpolation function available in *Matlab* ('interp1()') is used. For each instant (i) and height (h) of thermocouples, the normalized difference (*diff*) between numerical (T_N) and experimental (T_E) temperatures is calculated. This consists of the objective function to be minimized,

$$diff = \sqrt{\frac{\sum_i \sum_h (T_{N,ih} - T_{E,ih})^2}{\sum_i \sum_h (T_{E,ih})^2}} \qquad (10)$$

The obtained value of *diff* (implemented by an "if" instruction) for each iteration of the algorithm is compared with a threshold value – this is the verification of the stopping criterion (*cf.* Figure 55). If *diff* < threshold value (set as 3 %), the algorithm stops and the obtained thermophysical properties are assumed to have been determined. Otherwise, new values for the thermophysical properties and corresponding temperatures are proposed by the ('*fminsearchbnd'*) optimization routine and the process restarts with a new run of the 1D FE thermal model using such properties.

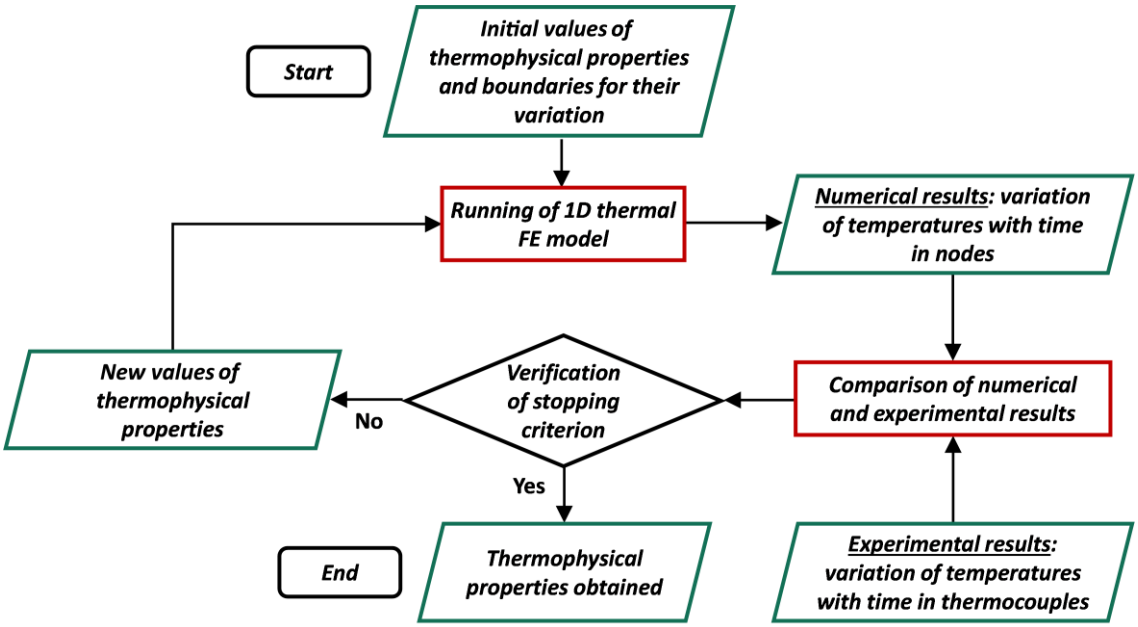

55 - Flowchart of the global implementation of the inverse analysis to determine the thermophysical properties.

4.4 1D FINITE ELEMENT MODEL

4.4.1 Governing equations, spatial and time discretizations and method of analysis

Since the heat transfer across the sandwich and GFRP specimens tested can be assumed as unidirectional, a 1D FE model was developed in *Matlab* to simulate their thermal response when subjected to the predefined heating curve. The unidirectional heat transfer governing equation in the domain (Ω) is given by the following expression:

$$\frac{\partial}{\partial x}\left(\lambda\frac{\partial T}{\partial x}\right)+G=\rho c_p\frac{\partial T}{\partial t} \tag{11}$$

where λ, ρ and c_p are, respectively, the thermal conductivity, density and specific heat of the material, G is the internal heat generated per unit volume and time (in this study, it was assumed that G = 0 W/m^3) and T and t are the temperature and time variables, respectively.

Regarding the boundary conditions at the top and bottom surfaces of the specimens, convection and radiation heat changes were considered. The convective heat flow (q_h) on the convective boundary (Γ_h) is given by,

$$q_h=-h_c(T_a-T) \tag{12}$$

in which h_c is the convection coefficient, and T_a and T are, respectively the ambient and material (surface) temperatures. The radiative heat flow (q_r) on the radiative boundary (Γ_r) reads,

$$q_r=-\varepsilon\sigma(T_a^4-T^4) \tag{13}$$

where ε is the emissivity of the material and σ = 5.67 × 10^{-8} W/(m^2K^4) is the Stefan-Boltzmann constant. Finally, the initial condition of the problem is,

$$T_0 = \bar{T}_0 \quad in \ \ \Omega \quad at \ \ t = t_0 \tag{14}$$

where $\bar{T}_0$ contains the known initial temperatures and t_o is the reference time.

The weak form of the heat transfer problem is considered, which can be written as,

$$\int_{\Omega} \delta T \left[\frac{\partial}{\partial x}\left(\lambda \frac{\partial T}{\partial x}\right) + \rho c_p \frac{\partial T}{\partial t}\right] d\Omega - \int_{\Gamma_h} \delta T \left(h_c(T_a - T)\right) d\Gamma_h - \int_{\Gamma_r} \delta T \left(\varepsilon\sigma(T_a^4 - T^4)\right) d\Gamma_r = 0 \tag{15}$$

As usual in these problems, the domain, Ω, is divided into finite elements. For each element, the variation of temperature is approximated by,

$$T^{(e)}(x_e) = \sum_{i=1}^{n} \psi_i (x_e) T_i \tag{16}$$

In this work, second-order finite elements were used. Hence, the three usual second-order polynomials were adopted as shape functions. To integrate these functions, the Gauss-Legendre quadrature was adopted. The backward Euler method was used for the temporal discretization with a fixed time step (1 sec). In order to obtain the numerical results, the Newton-Raphson incremental/iterative method was implemented. Additional information about the numerical methodology used in this study is provided in a recent work developed within the framework of the Fire Floor project [81].

4.4.2 Geometry and mesh

With respect to the foam-filled sandwich specimens, the domain was separated into three parts: top and bottom steel parts and polymeric foam part, to mimic the actual geometry of the specimens. Each steel part had a height (corresponding to the thickness of the steel plate) of 5 mm, while the foam part had a height (corresponding to the thickness of the foam core) of 120 mm. Along the height of each steel part, 8 FEs (with 2 nodes each) were used, whereas along the height of the foam part, 48 FEs were considered. Hence, each model has a total of 64 FEs and a total of 129 nodes. The numerical results concerning the mesh sensitivity analysis performed are shown ahead. Concerning the GFRP laminates, a total height of 12 mm was considered (as the tested specimen), which comprised a total of 24 FEs and a total of 49 nodes – as for the sandwich specimens, this discretization was selected after an initial mesh sensitivity analysis.

4.4.3 Materials

Regarding the thermophysical properties of steel, namely density (ρ), thermal conductivity (λ) and specific heat (c_p), they were implemented in the model as a function of temperature in accordance with Eurocode 3 [82] (*cf.* Figure 11a). Furthermore, the emissivity of steel was taken as ε_{steel} = 0.70 (temperature independent) also in accordance with Eurocode 3 [82], whereas the emissivity of the GFRP material (ε_{GFRP}) was set as constant and equal to 0.75 according to Bai *et al.* [72].

The density of GFRP and of both foams as a function of temperature was implemented in the models taking into account the results of the TGA tests performed in this work (*cf.* Figure 56b), and already described in chapters 2 and 3, respectively. Since the thermal conductivity and specific heat of the GFRP and foam materials as a function of temperature were the properties to be calibrated, these were initially taken constant with temperature, as the values measured in the experiments performed at room temperature (Table 15).

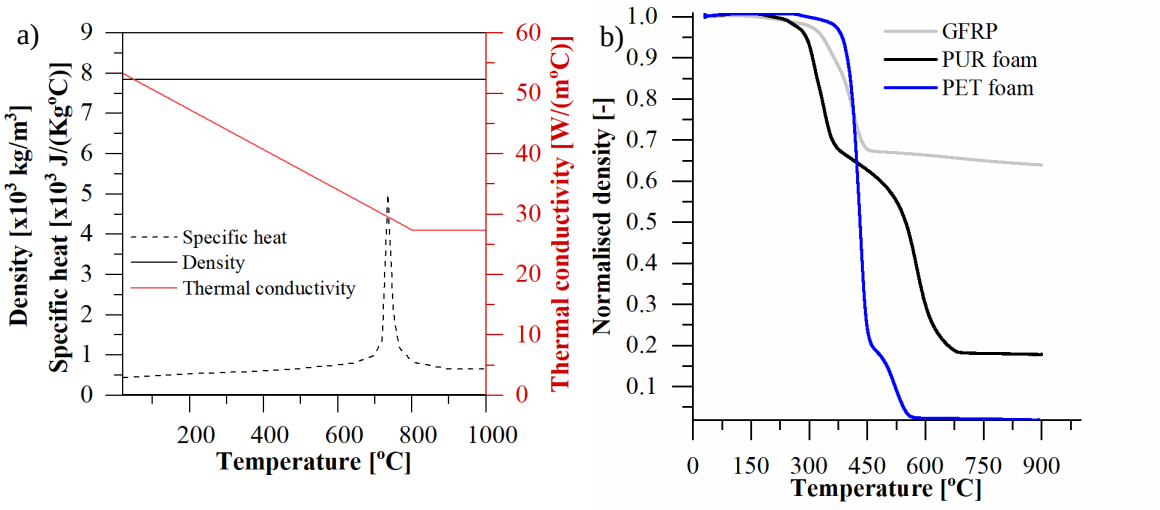

Figure 56 - Variation with temperature (a) of the thermophysical properties of steel and (b) of the densities of the foams and GFRP (determined from TGA tests, cf chapter 2 and 3).

4.4.4 Boundary conditions and loading

In order to replicate the heating conditions of the fire tests and provide accurate estimates of the temperature evolution in the specimens, the temperature of the air underneath the bottom surface of the GFRP laminate and bottom steel face sheet (T_a) was increased according to the ISO 834 standard fire curve [83] as follows

$$T_a = \bar{T}_0 + 345 log_{10}(8t + 1) \qquad (17)$$

where $\bar{T}_0$ is the initial furnace temperature and t is the time in min. For both GFRP and steel face sheet directly exposed to fire, a temperature independent convection coefficient h_c = 25 W/(m² °C) was considered [79]. The convection coefficient for the "cold" steel plate was assumed constant and equal to h_c = 25 W/(m² °C), while the convection coefficient for the top surface of the GFRP laminate

("cold") was set as constant and equal to h_c = 10 W/(m^2 ºC). All the remaining nodes of the thermal models were set to the average of the initial temperatures registered by the thermocouples at the beginning of the fire test.

4.4.5 Verification of the numerical model

In this section the results obtained using the 1D FE thermal model are compared (and validated) with those obtained by means of a similar 1D model developed in the *ABAQUS Standard* software. In this context, a model of a sandwich panel with steel face sheets (thickness of 5 mm) and PUR foam core (thickness of 120 mm) was developed in both FE codes. In *ABAQUS*, for both steel and foam 3-node heat transfer link elements (DC1D3) were adopted. The number of FEs in each steel plate and PUR foam was 8 and 48, respectively (similarly to what was adopted in the 1D FE implemented in *Matlab*). The properties considered for the steel are those presented in Figure 56a. For the foam, the variation of density with temperature was based on the TGA results (Figure 56b), while both the thermal conductivity and specific heat were considered temperature independent for this example. As mentioned in the previous section, the convection coefficient was taken as h_c = 25 W/m^{2}K (temperature independent) and the emissivity of steel was taken as ε_{steel} = 0.70. The temperature increase was imposed by the application of the ISO 834 fire curve with both convection and radiation heat transfer modes at the bottommost node; the initial temperature of all nodes was set to 20 ºC. Finally, the simulation time was 600 sec, considering a time step of 1 sec.

Figure 57a shows temperature-time curves at different depths of sandwich specimen obtained from the 1D FE models developed with the *Matlab* code and with *Abaqus*. Three depths were chosen for illustration purposes (0 mm – bottom face sheet exposed to fire and 10 mm and 20 mm – PUR foam core). As can be observed, there is an almost perfect overlap between the temperature-time curves obtained with both FE models, with a maximum relative difference of 1.6% being registered. Hence, it can be considered that the FE model developed in *Matlab* was validated. Finally, this section is also devoted to show the influence of the discretization degree of both steel and foam on the numerical results (using the 1D thermal FE model developed in *Matlab*). For this, besides the mesh previously described (8 FEs in each steel plate and 48 FEs in the foam core) two additional discretizations were studied: one with half of the number of FEs (4 FEs in each steel plate and 24 FEs in the foam core) and one with twice the number of FEs (16 FEs in each steel plate and 96 FEs in the foam core).

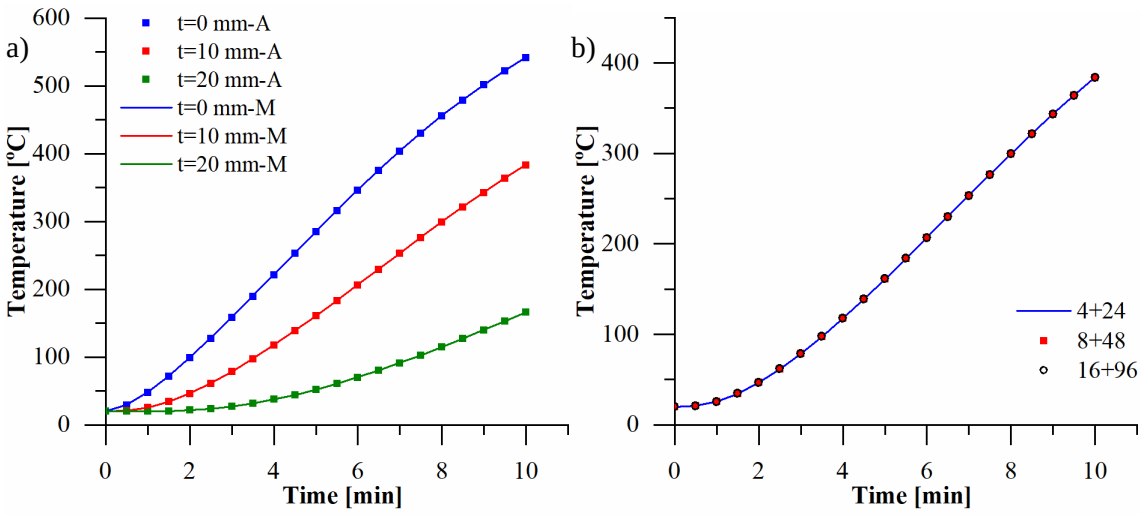

Figure 57 - (a) Temperature-time curves of a steel-PUR foam sandwich panel for several heights obtained with Matlab (M) and with Abaqus (A) and (b) influence of the discretization on the numerical results.

For exemplificative purposes, Figure 57b shows the temperature-time curves of the node with a height of 10 mm for the all the discretizations considered. As can be seen, all curves are apparently coincident: the maximum relative difference between the coarse mesh (4+24 FE) and the reference mesh is about 0.30%, while the maximum relative difference between the finer mesh (16+96 FE) and the reference mesh is around 0.01%. With respect to the simulation time, the increase in time was proportional to the increase in nodes, as expected. Hence, when the number of elements doubled (which approximately corresponds to doubling the number of nodes) the simulation time also double. Therefore, it can be concluded that the mesh with 8 FEs in each steel plate and 48 FEs in the foam core is appropriate to model this problem, being a balanced solution with a good compromise between efficiency and accuracy.

4.5 NUMERICAL RESULTS AND DISCUSSION

In this section, the use of the numerical procedure for the estimation of the thermophysical properties of GFRP and both foam materials is shown in detail. Firstly, Figure 58 and Figure 59 shows the comparison between numerical and experimental temperature-time curves of the foam-filled sandwich panels and GFRP laminate, when the thermal conductivity and specific heat of the materials were considered temperature-independent and equal to those determined experimentally (at room temperature); *cf.* Table 15. It is worth mentioning that the experimental curves presented in each figure result from the average of two specimens.

As can be seen, there is a poor agreement between numerical and experimental curves, which means that indeed considering the thermal conductivity and specific heat of GFRP and both foam materials constant with temperature is a very rough assumption, not allowing to obtain accurate temperature predictions.

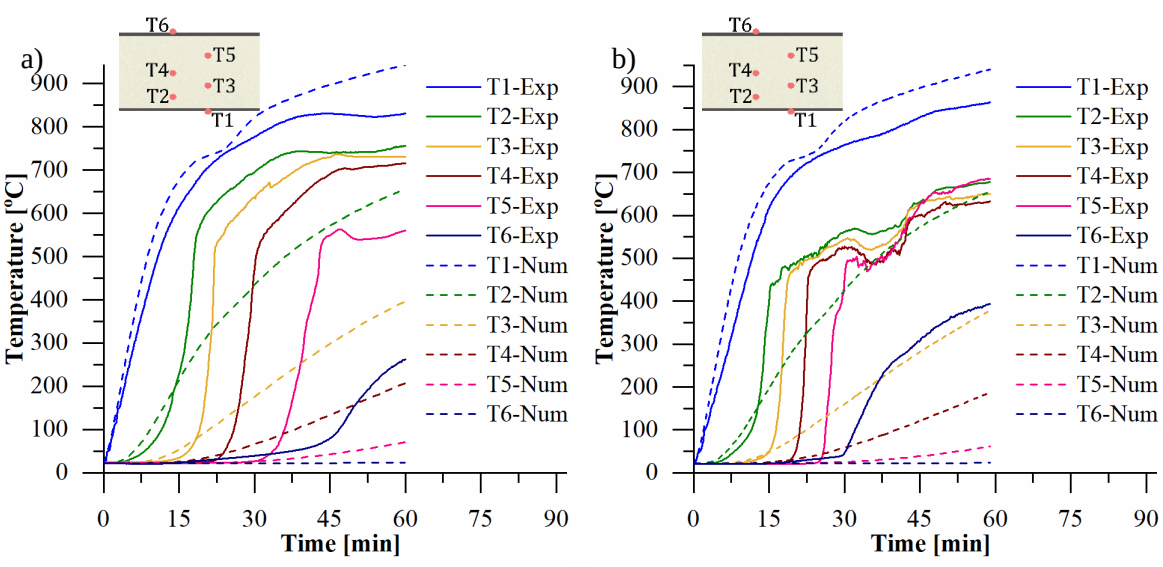

Figure 58 - Comparison between numerical (Num) and experimental (Exp) temperature-time curves before the calibration of the thermophysical properties, assuming temperature-independent properties for: (a) PUR and (b) PET foams.

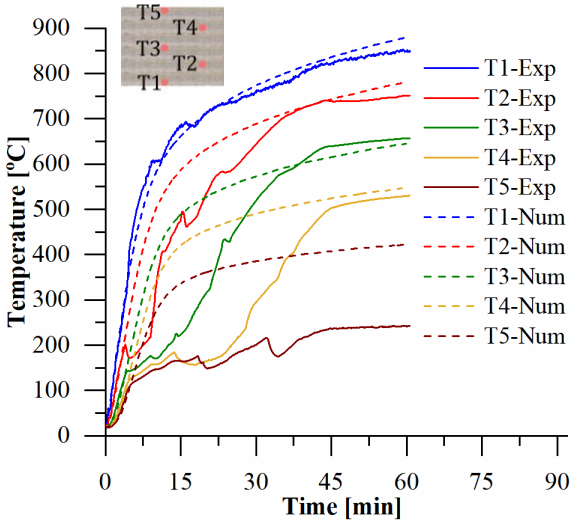

Figure 59 - Comparison between numerical (Num) and experimental (Exp) temperature-time curves for the GFRP laminate before the calibration of the thermophysical properties.

Concerning the foam-filled sandwich specimens, it can be seen that for temperatures above 500 °C the temperatures monitored by the thermocouples positioned at the foams start to become more similar among each other (t > 40 min – PUR foam, and t > 20 min – PET foam), although presenting some scatter. This is probably due to the severe thermal degradation of the foams, which caused the thermocouples to move from their initial position; for PUR foam, this phenomenon occurs for a longer duration of fire exposure than for PET foam. The TGA results (Figure 56b) corroborate this: for T > 500 ºC, the PUR foam still retains 50% of its initial mass, whereas the PET foam only retains about 15%.

Figure 60 and Figure 61 compare experimental temperature-time curves of the sandwich specimens with PUR and PET foams and of the GFRP laminates with those obtained by using modified/calibrated thermophysical properties.

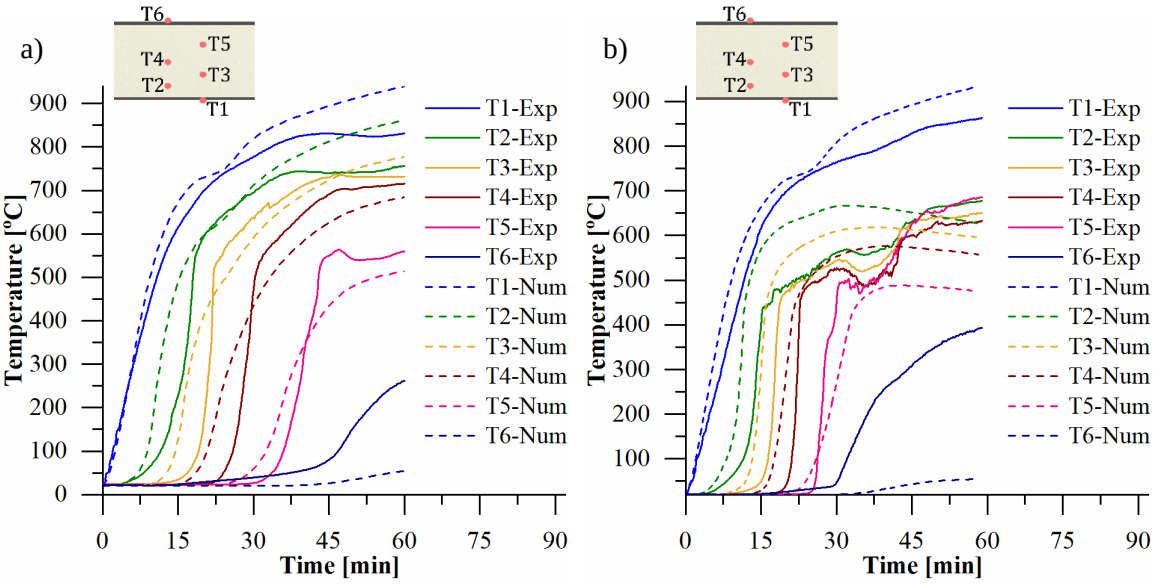

Figure 60 - Comparison between numerical (Num) and experimental (Exp) temperature-time curves after the calibration of the thermophysical properties: (a) PUR and (b) PET foams.

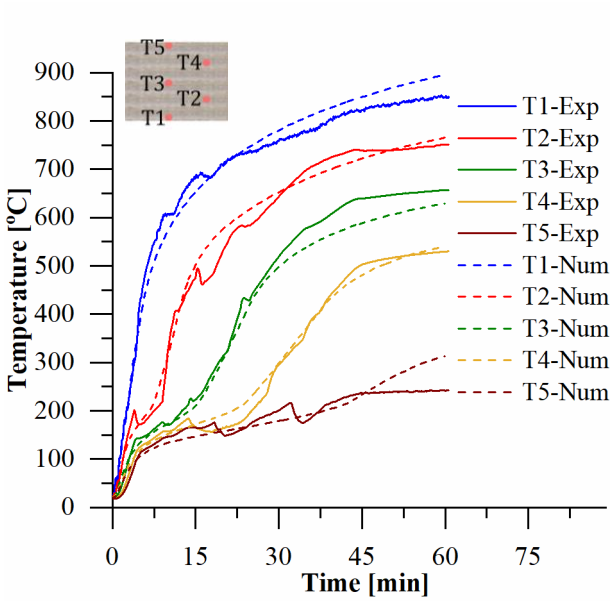

Figure 61 - Comparison between numerical (Num) and experimental (Exp) temperature-time curves for the GFRP laminate after the calibration of the thermophysical properties.

As can be seen, after the calibration process, there is an overall improvement of the agreement between numerical and experimental temperature-time curves for each thermocouple.

With respect to the foam-filled sandwich specimens, it can be seen that the sharp increase of temperature with time occurs earlier in the numerical models than in the experiments, but generally the qualitative behaviour is now very similar. In addition, it can be seen that the difference between temperatures in the foam at different depths for longer periods of fire exposure is higher in the

numerical models than in the experiments, which seems to corroborate the hypothesis of movement of the thermocouples in the foams after their considerable thermal degradation. As an example, in the case of the panel with the PET foam, for t = 60 min, the difference between temperatures at T2 and T5 obtained in the numerical model is of circa 250 ºC (considering both panels), whereas in the experiments such difference is null.

Considering the comparison between the experimental and numerical temperatures, a better agreement was obtained in case of the GFRP laminate, most likely because the inorganic content is higher and this also contributes to keep the thermocouples in a constant position throughout the tests. Overall, both experimental and numerical temperature *vs.* time curves presented a steady increase, with marked non-linearities at around 200 ºC, which are probably related to the beginning of the decomposition process of the polymeric matrix.

The equivalent thermal conductivity and specific heat as a function of temperature obtained for both foams and GFRP materials are shown in Figure 62.

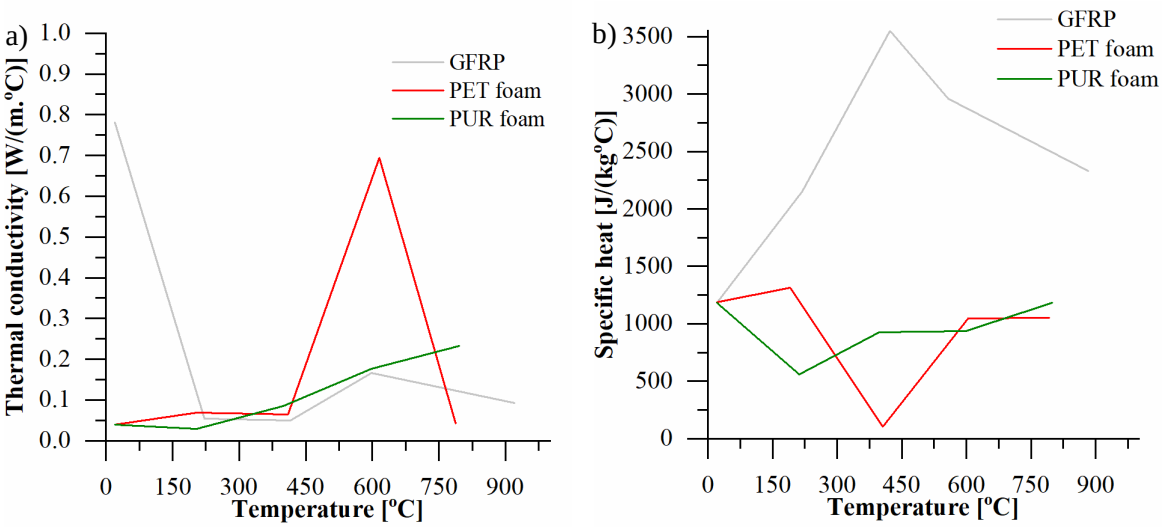

Figure 62 - Calibrated values for the thermophysical properties of GFRP and PUR and PET foams: (a) thermal conductivity and (b) specific heat.

It is still worth mentioning that the numerical procedure presented and discussed above does not take into account explicitly the complex phenomena occurring in the materials through their thermal decomposition; for this reason, the results obtained should only be used as input data in FE thermal models aiming at simulating the evolution of the temperature field. However, from the results obtained, it can be seen that the equivalent thermophysical properties of the GFRP material seem to reflect in a simplified way the thermal decomposition of the material. In fact, Figure 62 b) shows that the specific heat of the GFRP laminate increased significantly at around 400 ºC, reflecting the endothermic nature of its decomposition process. Concerning the thermal conductivity, it initially presented a significant reduction, reflecting the beginning of the decomposition process underwent

by the polymeric matrix, followed by an increasing branch up to 600 ºC, which should be associated to the increase of the fibre volume fraction (consequence of the resin decomposition).

4.6 CONCLUDING REMARKS

This chapter presented and discussed results obtained from experimental and numerical studies about the determination of the temperature-dependent thermophysical properties (specific heat and thermal conductivity) of a GFRP composite produced by vacuum infusion and two polymeric foam materials (PET and PUR) that were absent in the literature. In fact, these properties are needed to simulate the thermal response of sandwich panels exposed to fire (as shown in chapter 7). To this end, a simplified numerical procedure was developed to calibrate the thermophysical properties of PET and PUR foams and of the GFRP laminate. From the results obtained, the following main conclusions may be drawn:

- Results from the fire test showed that the temperature increased at a different rate across the depth of the GFRP laminate and of both polymeric foams. The temperature *vs.* time curves of both PET and PUR foams portrayed a relatively small increase of temperature at the initial stage of the tests, followed by an abrupt temperature increase, and then a temperature plateau until the end of the test. The temperature across the height of the GFRP laminate exhibited an almost steady increase until the end of the tests, with a non-linear behaviour at around 200 ºC.
- The results obtained from the numerical simulations of the fire tests highlighted the remarkable influence of the specific heat and thermal conductivity on the thermal behaviour of both GFRP and polymeric foams under fire. When using temperature-independent thermophysical properties, the FE model was not able to reproduce the temperature *vs.* time curves determined experimentally.
- Despite all the complexity involved in the problem, the numerical results obtained considering the equivalent thermophysical properties presented a general good agreement with experimental results; this validated the procedure adopted to calibrate the thermophysical properties of the materials as a function of temperature.

Part III: Fire behaviour of GFRP sandwich panel

CHAPTER 5

FLEXURAL BEHAVIOUR AT AMBIENT TEMPERATURE OF GFRP SANDWICH PANELS

5.1 INTRODUCTION

This chapter presents an experimental investigation about the flexural behaviour of GFRP composite sandwich panels at ambient temperature conditions. The test programme included a set of flexural tests that aimed at assessing the influence of using different core materials and panel architectures on the stiffness, load-bearing capacity, and failure modes of composite sandwich panels. In the context of the present thesis, the experimental data obtained in the flexural tests described in this chapter were used to define the fire loads to be applied in the fire resistance tests described in chapter 6. For that purpose, the span of the sandwich panels tested at ambient temperature was defined based on the geometrical constraints of the set-up used in the fire resistance tests; notwithstanding these constraints, the cross-sectional dimensions of the panels were defined according to the range of values typically found in building floor applications (where spans are significant longer than that used in the fire tests).

5.2 MANUFACTURING PROCESS AND MATERIALS

The sandwich panels were produced by vacuum infusion at the *Pólo de Inovação em Engenharia de Polímeros* (PIEP) research institute, especially for this study, and according to a set of specifications described/justified in the next paragraphs. Both glass fibre reinforcement layers and core materials were positioned in a dry mould and sealed inside a vacuum bag, as illustrated in Figure 63.

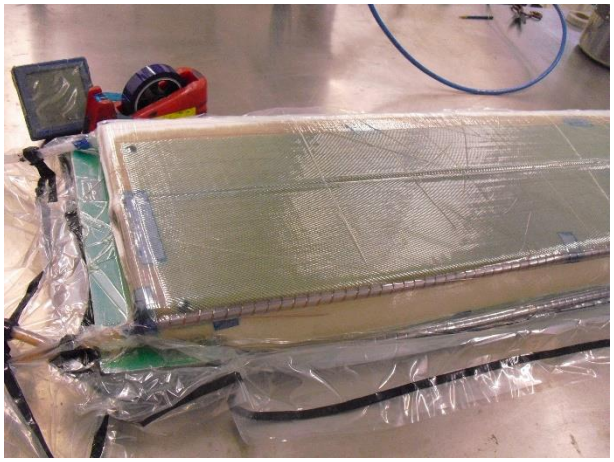

Figure 63 - Production of the GFRP sandwich panel.

Once the entrapped air was removed, the resin was driven within the sandwich panels by means of vacuum pressure. It is worth mentioning that the resin in excess was sucked into the vacuum line; this procedure aimed at minimizing the voids content, increasing the fibre-to-resin ratio, and consequently the strength-to-weight ratio. Before the definition of the cross-section, a survey of materials to be incorporated in the sandwich panels was performed. Concerning the core material, its main purpose is to increase the flexural stiffness and strength of the panel and to stabilise its faces and webs against wrinkling and buckling phenomena; at the same time, the core material must present sufficient shear stiffness and strength. Following these principles, the PUR and polyethylene terephthalate (PET) foams used in the material characterisation tests were incorporated in the sandwich panels studied herein. It is worth mentioning that these foams present an approximate density of 100 kg/m^3, which comply with the minimum density of 40 kg/m^3 set for structural applications in the European Technical Specification (TS) prEN 19101: 2021.

Concerning the face sheets of the panels, GFRP composite laminates were chosen due to their advantages over traditional materials, such as high strength-to-weight ratio, durability and lightness. The same fibre architectures considered for the GFRP laminates used in the mechanical characterisation tests (*cf.* Chapter 3) were also used for the face sheets of the sandwich panels. The fibre layup sequence was designed using a web-app developed by Nunes *et al*. [91], which allowed to determine the laminate properties using the rule of mixtures and the Classical Laminate Theory (CLT). Both GFRP face sheets and webs present a balanced fibre distribution in the different directions (*cf.* next section). This solution aimed at obtaining laminates with relatively high elastic modulus in the longitudinal and transverse directions, as well as an adequate in-plane shear modulus.

5.2.1 GFRP sandwich panel architecture

The present study investigated the flexural behaviour of different types of GFRP composite sandwich panels, focusing on the evaluation of different variables, such as the use of different core materials and various GFRP web configurations, including homogeneous-core and web-core panels. In this context, to enable a sound comparison, the cross-sectional dimensions of the homogeneous-core sandwich panels were assumed identical to those of the web-core sandwich panels; consequently, the latter were overdesigned for flexural/shear capacity.

Figure 64 shows the cross-section of the sandwich panels with homogeneous core considered in this study as the “reference solution”. This type of sandwich panel comprised a 120 mm thick core material and two 5.6 mm thick GFRP face sheets. PET and PUR foams were incorporated in the sandwich panels with the purpose of studying in further depth the influence of using different core materials on the flexural behaviour of the sandwich panels.

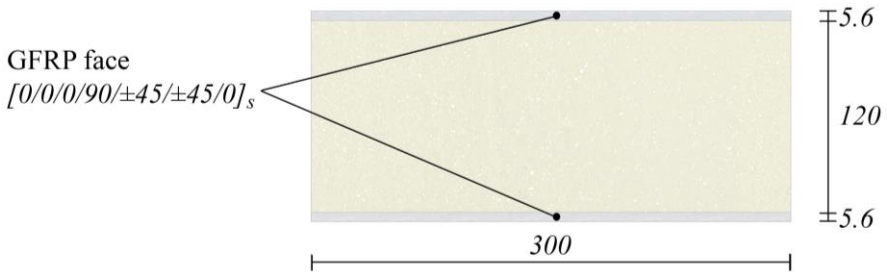

Figure 64 - Homogeneous-core sandwich panel cross-section (dimensions in mm).

As reported in the literature [89,92,93], by adding GFRP webs in the longitudinal direction of the panels it is possible to increase substantially their mechanical performance, namely in terms of shear stiffness and strength, which may represent a key limitation in the structural design of homogeneous-core sandwich panels. To this end, two types of web-core sandwich panels were considered in this study, comprising (i) two GFRP webs along the lateral edges of the panel (*cf.* Figure 65a) or (ii) within the core at the centre of the panel (*cf.* Figure 65b).

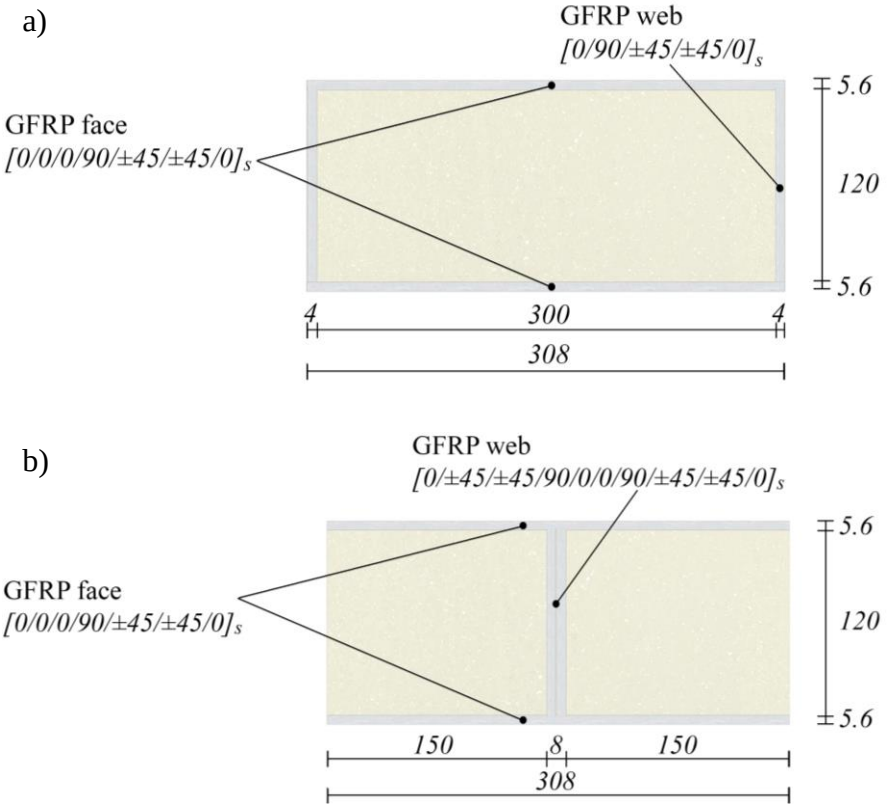

Figure 65 - Web-core sandwich panels cross-section: GFRP webs (a) along the panel edges and (b) within the core (dimensions in mm).

It is worth mentioning that since the contribution of the core to the bending stiffness and strength of web-core panels is low, the influence of using different core materials on their flexural behaviour was not assessed - only PET foam core was used in panels with different web configurations.

5.2.2 Design verifications

Although the span of the sandwich panels tested in this work was limited by the geometrical constraints of the test set-up used in the fire resistance tests (*cf.* chapter 6), the panels were designed considering a span of 4 m, which is typical of building floor applications. Note that a simplified approach has been followed in the design procedure, in which the sandwich panels were considered as simply supported one-way slabs subjected to uniformly distributed loads.

The preliminary design of the sandwich panels was made according to the recommendation of the European Technical Specification (TS) prEN 19101: 2021, "*Design of Fibre-Polymer Composite Structures*". The design approach included in the above-mentioned specification is in line with the Eurocodes, following the general provisions outlined in EN 1990: 2002, which are based on the verification of ultimate limit states (ULS) and serviceability limit states (SLS).

As mentioned above, the design methodology of the Eurocode standards was coupled to the specific provisions included in prEN 191010: 2021, which defines partial factors for material properties, partial factors for resistance models and design formulae for specific failure modes of composite sandwich panels. In accordance with the TS, the design value of resistance (R_d) for a specific design situation should be obtained from,

$$R_d = \frac{1}{\gamma_m \gamma_{Rd}} R\{\eta_{c,i} \cdot X_{k,i}\} \quad (18)$$

where $X_{k,i}$ is a characteristic value of a material property, γ_m is a partial factor for the representative material property, γ_{Rd} is the partial factor that accounts for the uncertainty in the resistance model, $\eta_{c,i}$ is the conversion factor accounting for effects of temperature and moisture, *i* is for the ith material property. The values of the material partial factor γ_m are listed in Table 16 as a function of the coefficient of variation of the material property, V_x; in addition, reference values of the partial factors for the resistance models for different failure modes of sandwich panels are given in Table 17. Concerning the conversion factor η_c, in this study it was taken as 1.0, since the effects of moisture and temperature were not considered (an indoor application was assumed). To fulfil the safety requirements, the design values of the effects of the actions must be lower than the design values of resistance calculated using equation 18.

Table 16 - Material partial factor γ_m as a function of V_x (adapted from [12]).

V_x	0.05	0.10	0.15	0.20	0.25	0.30	0.35	0.40	0.45
γ_m	1.07	1.15	1.23	1.32	1.41	1.51	1.61	1.71	1.82

Table 17 - Partial factors for the resistance model (adapted from [12]).

Composite material failure	Core material failure	Global buckling	Local buckling	Face sheet/web wrinkling	Core indentation	Core punching failure
1.40	1.50	1.40	1.30	1.50	1.50	1.50

In accordance with the TS, various potential failure modes of sandwich panels used for structural applications may be relevant, depending on the panel architecture, type of loading, properties of the constituent materials and panel dimensions. Table 18 presents the typical failure modes likely to occur in composite sandwich panels subjected to out-of-plane loading (relevant for floor applications).

Table 18 - Typical failure modes for composite sandwich panels (adapted from [12]).

Sandwich component	Failure mode	Homogeneous-core sandwich	Web-core sandwich
Face sheet	Tensile failure	×	×
	Crushing	×	×
	Wrinkling	×	×
Core	Shear failure	×	×
	Indentation	×	×
	In-plane tensile or compressive failure	×	×
Web	Shear failure		×
	Wrinkling due to shear		×
	Wrinkling due to in-plane bending		×
	Wrinkling due to transverse compression		×
	Crushing due to transverse compression		×
	Bending failure		×

5.3 EXPERIMENTAL PROGRAMME ON MEDIUM-SCALE SANDWICH PANELS

5.3.1 Specimen geometry and test series

The GFRP sandwich panels tested in this study have rectangular cross-section of 300 mm (width) × 131.2 mm (thickness) and total length of 1500 mm.

The mechanical properties of the constituent materials of the sandwich panels (namely GFRP laminates and polymeric foam cores) were determined by small-scale coupon mechanical characterisation tests and are listed in Table 19 and Table 20.

Table 19 - Mechanical properties of GFRP laminates (average ± standard deviation).

GFRP Laminate	Direction	Tension (ASTM D3039)		Compression (ASTM D6641)		Shear (ASTM D5379)	
		σ_t [MPa]	E_t [GPa]	σ_c [MPa]	E_c [GPa]	τ_s [MPa]	G [GPa]
Faces	Longitudinal	512.5±11.1	25.7±0.8	228.9±13.9	29.6±1.2	-	-
Web	Transverse	-	-	228.5±10.8	20.6±2.6	161.2±2.4	6.5±0.2

Table 20 - Shear and compressive properties of PUR and PET foams (average ± standard deviation).

Core foam	Compression (ASTM C365)		Shear (ASTM E519)	
	σ_c [MPa]	E_c [GPa]	τ_s [MPa]	G [GPa]
PET	1.40 ± 0.01	103.10 ± 5.41	0.93 ± 0.02	31.97 ± 0.65
PUR	0.73 ± 0.02	42.41 ± 5.08	0.31 ± 0.02	15.15 ± 0.75

The experimental campaign comprised 7 flexural tests on sandwich panels with different panel architectures (*cf.* Figure 64 and Figure 65): (i) two homogeneous-PET core sandwich panels, (ii) one homogeneous-PUR core sandwich panel; (iii) two sandwich panels filled with PET foam and reinforced with webs at the lateral edges of the panel; and (iv) two sandwich panels filled with PET foam and reinforced with a central web. Table 21 summarizes the characteristics of all the sandwich panels tested.

Table 21 - Characteristics of the GFRP sandwich panels.

Specimen ID	Core material	Reinforcement
PET-U-1	PET	-
PET-U-2	PET	-
PUR-U-1	PUR	-
PET-LW-1	PET	Lateral webs
PET-LW-2	PET	Lateral webs
PET-CW-1	PET	Central web
PET-CW-2	PET	Central web

It is worth noting that each specimen is labelled according to the following nomenclature: (i) core material, PET or PUR; (ii) type of reinforcement, unreinforced (U) and reinforced with webs at the edges of the panel (LW) or within the core (CW); and (iii) specimen number. For instance, the GFRP sandwich panel comprising PET foam core without longitudinal reinforcement (*i.e.* unreinforced) is identified as *PET-U-1*.

5.3.2 Test set up, instrumentation and test procedure

The flexural tests were performed following the recommendations of ASTM C393/393 M standard [21]. The sandwich panels were tested in four-point bending, in a simply supported span of 1400 mm. Two concentrated loads were applied at thirds of the span by means of a steel transmission beam, which transferred the load to two sets of steel rollers-and-plates (contact area of 100 mm × 300 mm); *cf.* Figure 66. The sliding and pinned supports were materialized by steel bearings with 300 mm long and 100 mm wide top steel plates (thickness of 10 mm). Note that to avoid localised stress concentrations next to the load application points, a 3 mm thick rubber pad was positioned between the loading plates and the top face sheet. Additional layers of rubber pad were placed between the bottom face sheet and the supports to guarantee full contact between those surfaces during the tests.

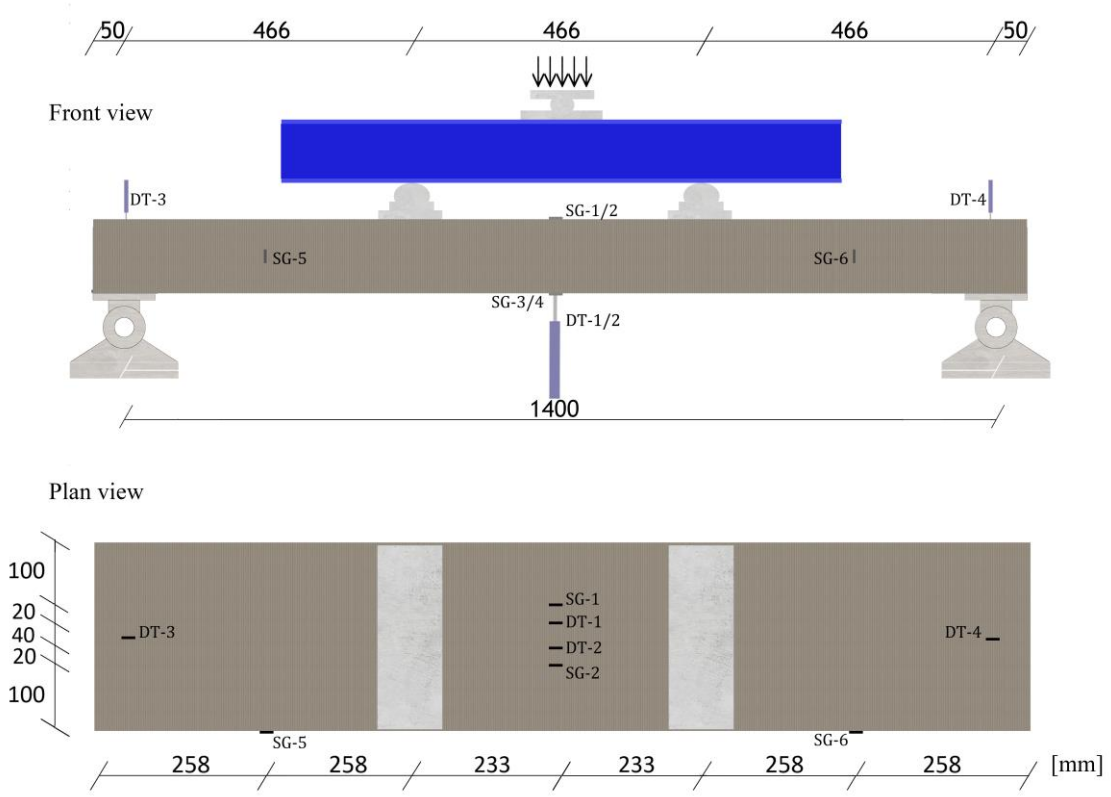

Figure 66 - Test set-up of flexural tests.

The sandwich panels were loaded monotonically up to failure by means of a hydraulic jack coupled to a *Novatech* load-cell with capacity of 300 kN. In terms of instrumentation, four *TML* electrical resistance strain gauges (two for each side) were installed on the GFRP face sheets at 10 cm from the panel edges (SG-1 to SG-4), aiming at measuring the tensile and compressive strains in the bottom and top GFRP face sheets at the mid-span section, respectively. Additional strain gauges (SG-5 and SG-6) were also installed on the webs of the reinforced specimens PET-LW (position depicted in Figure 66) with the objective of measuring the lateral webs axial strains during the tests. The mid-span displacements were measured using two displacement transducers with a measurement range of 100 mm and precision of 0.01 mm, while the vertical displacements of the top face sheet at the support sections were measured using two displacement transducers with a measurement range of 50 mm and precision of 0.005 mm. The data provided by the load-cell, strain gauges and displacement transducers were recorded using an *HBM* data logger at an acquisition rate of 1 Hz. The flexural tests were conducted up to the specimens' failure under load control at an average speed of 0.25 kN/s.

5.4 RESULTS AND DISCUSSION

5.4.1 Homogeneous-core sandwich panels

Figure 67 depicts the load *vs.* mid-span displacements curves of representative homogeneous-core sandwich panels. Note that the mid-span displacement was calculated using the following equation,

$$\delta = \delta_{1/2} - \delta_{3/4} \quad (19)$$

where $\delta_{1/2}$ is the average displacement obtained from the displacement transducers positioned at the mid-span section (DT-1 and DT-2) and $\delta_{3/4}$ is the average displacement of the displacement transducers positioned at the support sections (DT-3 and DT-4). For all the specimens tested, the displacement transducers placed at the mid-span section measured very similar values throughout the test, confirming the symmetry of the test set-up and of the panels' response. Table 22 presents a summary of the results obtained with reference to the following parameters: stiffness (*K*, as defined by the slope of the load *vs.* mid-span displacement curves), failure load (P_u), maximum shear force (V_{max}), maximum bending moment (M_{max}), maximum shear stress in the core (τ_{max}), maximum axial stress in the GFRP face sheet (σ_{max}), maximum mid-span displacement ($d_{1/2,max}$), and maximum strain in top ($\varepsilon_{top,max}$) and bottom ($\varepsilon_{bot,max}$) face sheets.

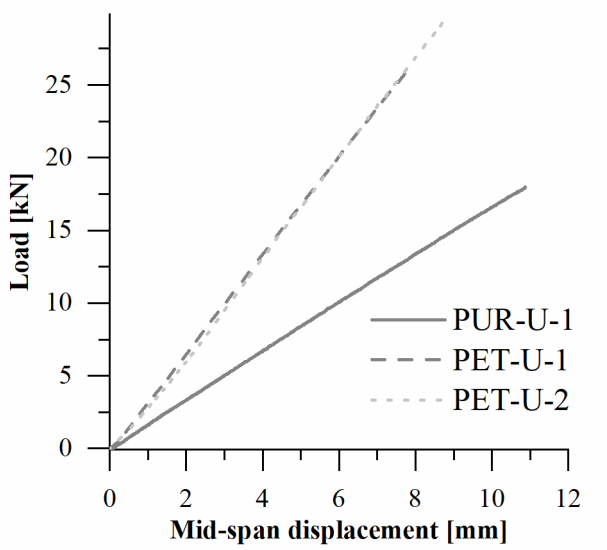

Figure 67 - Representative load vs. mid-span displacement curves of homogeneous core sandwich panels.

Both specimens exhibited linear elastic behaviour until failure, which occurred in a brittle manner due to (i) shear failure of the core and (ii) debonding of the GFRP-core interface (*cf.* Figure 68) - these results agree with the linear behaviour of the shear stress *vs*. distortion curves of both PET and PUR foams, as presented in chapter 2. It is worth mentioning that it was not possible to identify which of the two failure modes mentioned above occurred first (triggering the occurrence of the other).

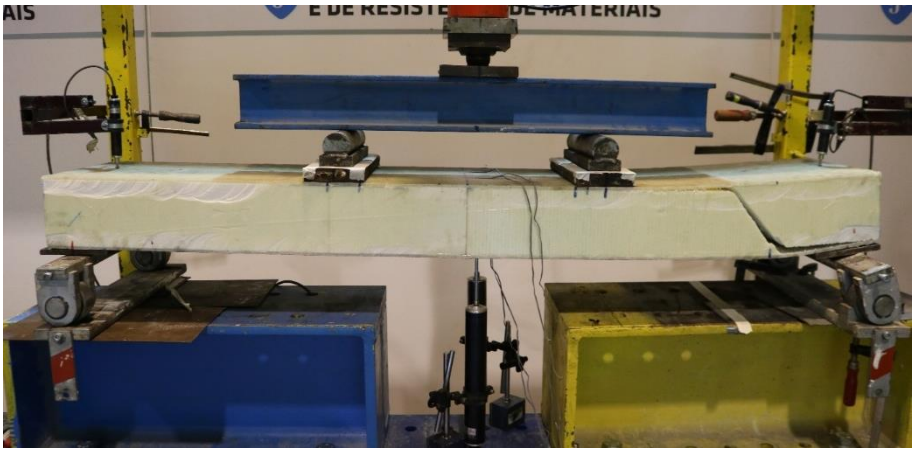

Figure 68 - Typical failure mode for the unreinforced sandwich panel (example of the failure mode observed in specimen PET-U-1).

As shown in Table 22, the PET panels were stiffer than the PUR one; this result stems from the higher mechanical properties of the PET foam, namely its higher shear modulus, compared to the PUR foam (32.0±0.65 *vs.* 15.2±0.75 MPa).

Table 22 - Summary of results obtained in the flexural tests of homogeneous core sandwich panel.

Parameter	PET-U-1	PET-U-2	Average PET-U	PUR-1
P_u [kN]	26.16	29.87	28.01	17.98
K [kN/mm]	3.39	3.29	3.34	1.70
V_{max} [kN]	13.08	14.94	14.01	8.99
M_{max} [kNm]	6.04	6.90	6.47	4.15
τ_{max} [MPa]	0.36	0.41	0.39	0.25
σ_{max} [MPa]	29.90	34.14	32.02	20.54
$d_{1/2,max}$ [mm]	7.85	8.89	8.37	10.88
$\varepsilon_{top,max}$ [µm/m]	-748.98	-1068.43	908.70	-788.79
$\varepsilon_{bot,max}$ [µm/m]	925.17	1095.61	1010.39	703.00

As shown in Table 22, the panel PET-U-1 failed at an applied load of ~26 kN, whereas the ultimate load of panel PET-U-2 was 30 kN (about 14% higher). In the homogeneous-core sandwich panels, the shear stress is assumed to be entirely supported by the core material. The average maximum shear stress of the PET foam computed from the flexural tests was ~0.39 MPa. This value is much lower than the shear strength obtained through the DTS test method (0.91±0.02 MPa). The reason for this quite significant difference is not fully clear, but it may be explained by the fact that shear failure initiated after premature debonding of the GFRP-core interface. This unexpected result was also reported by Garrido [94] (although lower relative differences were reported in that study); that author

also referred that the shear strength of the PET foam in homogeneous-core sandwich panels may be affected by size effects. Unfortunately, it was not possible to perform further experiments to understand this aspect in further depth. In this context, further investigations are needed to determine if the collapse was triggered by the shear failure of the core or by delamination at the GFRP-core interface, a failure mode that should always be prevented.

Regarding the flexural response of panel PUR-U-1, the ultimate load (~ 18 kN) was 36% lower than the average failure load of the PET sandwich panels (~ 28 kN). Such difference is naturally ascribed to the higher shear strength of the PET foam compared to the PUR foam (0.90 *vs.* 0.31 MPa). These results point out the importance of adequately choosing the core material of the sandwich panel, as the bending response is strongly affected by its (shear) behaviour. Unlike the PET panels, the maximum shear stress obtained from the flexural tests (~0.25 MPa) is in relatively good agreement with the shear strength (0.31±0.02 MPa) determined through the small-coupon material characterisation tests (*cf.* Chapter 2), yet it is still lower.

The representative load *vs*. axial stress curves for each type of homogeneous core sandwich panel are presented in Figure 69. For all tested specimens, the curves exhibited a linear behaviour until failure, which is consistent with what was observed in the material characterisation tests for a similar stress magnitude. In general, the axial strains measured by strain gauges bonded in the same cross-sections (top and bottom face sheets) were very similar throughout the tests, indicating that the elastic moduli in tension and compression were relatively similar, as expected.

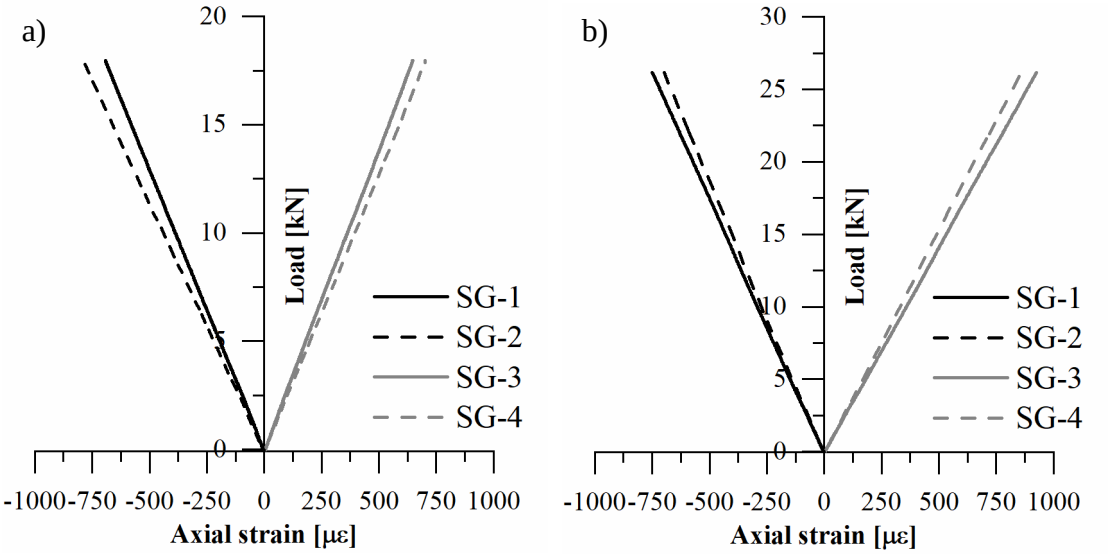

Figure 69 - Load vs. axial strain curves of specimens: (a) PUR-U-1 and (b) PET-U-1.

5.4.2 Web-core sandwich panels

Figure 70 shows representative load *vs*. mid-span displacements curves for each type of web-core sandwich panel tested. Table 23 present a summary of the results obtained, including (in addition to

the parameters defined in Table 22) the maximum transverse axial strain in the web measured by strain gauges SG-5 ($\varepsilon_{web.left}$) and SG-6 ($\varepsilon_{web.left}$), the maximum shear force in the web ($V_{max,web} = V_{max}(\frac{S_{s,w}}{S_s})$), the maximum shear force in the core ($V_{max,core} = V_{max}(\frac{S_{s,c}}{S_s})$), where S_s is the shear stiffness of the panel, $S_{s,w}$ is the shear stiffness of the web and $S_{s,c}$ is the shear stiffness of the core. Regardless of the position of the longitudinal reinforcing web, the web-core panels exhibited a similar behaviour, with all specimens presenting a linear elastic behaviour until ~110 kN (ultimate load of specimen PET-LW-1). For higher load levels, the flexural response of specimen PET-CW-1 became slightly non-linear, with small load drops observed at around 130 kN and 150 kN; such drops corresponded to shear fractures in the PET foam core. As shown in Figure 70, the load carrying capacity of the panel was not affected by the above-mentioned core fractures, since the shear stress in the reinforced panel was mostly carried out by the longitudinal web.

As shown in Table 23, the web-core sandwich panels presented very similar flexural stiffnesses and, as expected, these were significantly higher than those of the homogeneous PET sandwich panels (approximately twice). The similarity in the response of specimens PET-LW and PET-CW was expected since their webs have similar fibre architecture and approximately the same shear area.

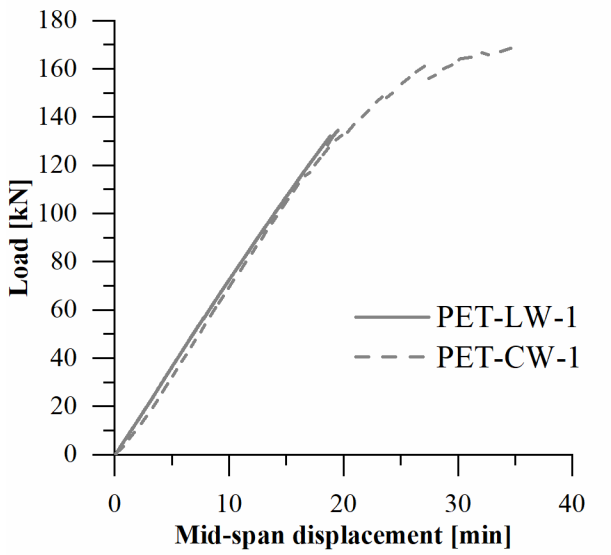

Figure 70 - Representative load vs. mid-span displacement curves of web-core sandwich panels

Concerning the load-bearing capacity, the web-core sandwich panels presented much higher ultimate loads compared to the homogeneous-core sandwich panels, mainly due to the higher shear capacity provided by the webs. The average ultimate load of the PET-LW specimens (122.9 kN) was about 4.3 times higher than that of the PET-U specimens. The load-bearing capacity of the sandwich panels was further increased when the web was positioned within the centre of the core: the ultimate load of specimen PET-CW-1 was about 6.0 and 1.4 times higher than those of specimens PET-U and PET-LW, respectively. These results highlight the effectiveness of the longitudinal web in increasing the flexural strength and stiffness of the sandwich panel. It is still worth mentioning that the lower

bearing capacity of the PET-LW panels when compared to the PET-CW may be explained by the presence of a geometrical defect in the former panels, which also explains their different failure modes. As described in more detail ahead, at the edge of the top face sheet (under the load application point), where a stress concentration develops (due to the applied load), a defect was observed, which caused the premature failure of the PET-LW panels. In the PET-CW panel, such premature failure mode did not occur, as the (central) web did not present this defect (as described next, it presented another geometrical irregularity).

The failure mode of specimens PET-LW involved the crushing of the top face sheet and transverse compressive failure of the web under an edge of a load application steel plate (*cf.* Figure 71) - a similar failure mode was reported by Fam *et al*. [89] and Zhang *et al*. [92], who tested GFRP sandwich panels with a similar panel architecture.

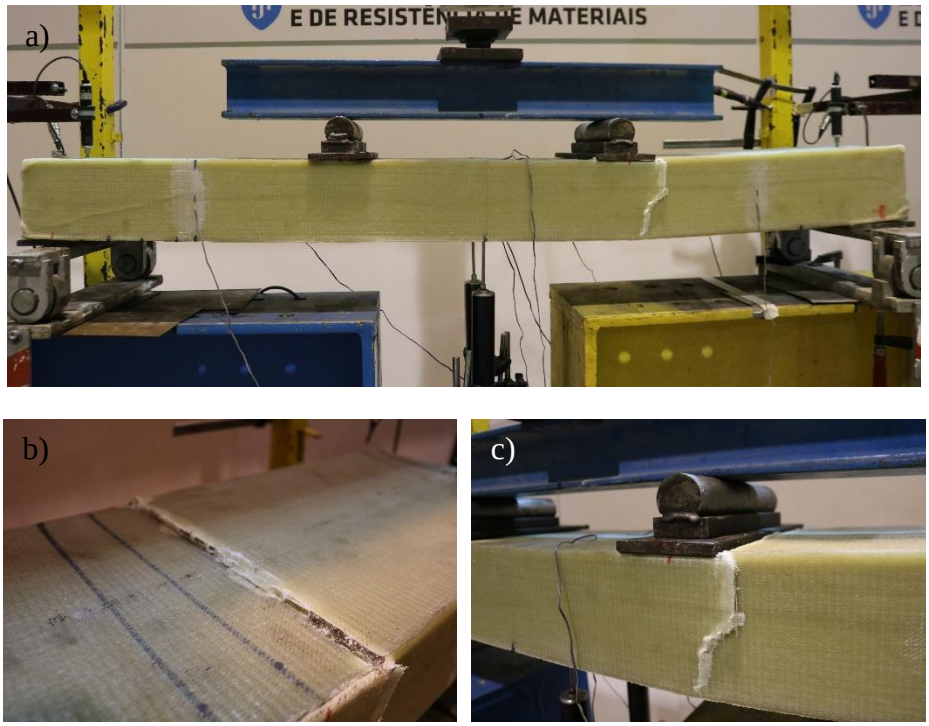

Figure 71 - Typical failure of PET-LW specimens: (a) general view of PET-LW-1 specimen, (b) compressive failure of the top face sheet and (c) compressive failure of the GFRP web.

In this regard, it is worth mentioning that a wrinkle and a marked increase in the thickness of the top face sheet (*cf.* Figure 72) were observed next to the web and this was attributed to limitations of the manufacturing process; this defect is likely to have caused a local weakness in a stress concentration section, which led to localized premature crushing.

In accordance with the TS, the transverse compressive stress in the web $\sigma_{y,w}$ is given by the following equation,

$$\sigma_{y,w} = \frac{P_{ed}}{l_{eff} \times t_w} = 156.25\ MPa \qquad (20)$$

where P_{ed} is the applied transverse concentrate load, l_{eff} is the effective width (~11 cm) and t_w is the web thickness. The transverse compressive stress is considerably lower than the corresponding strength obtained through the material characterisation tests (228.5±10.8 MPa)

Concerning the shear response of the GFRP webs, the average maximum shear stress obtained was 51.4 MPa. This value is far below the shear strength of the GFRP laminate (161.2±2.4 MPa) determined by means of the Iosipescu test method (*cf.* Chapter 3), which is consistent with the non-occurrence of shear failure.

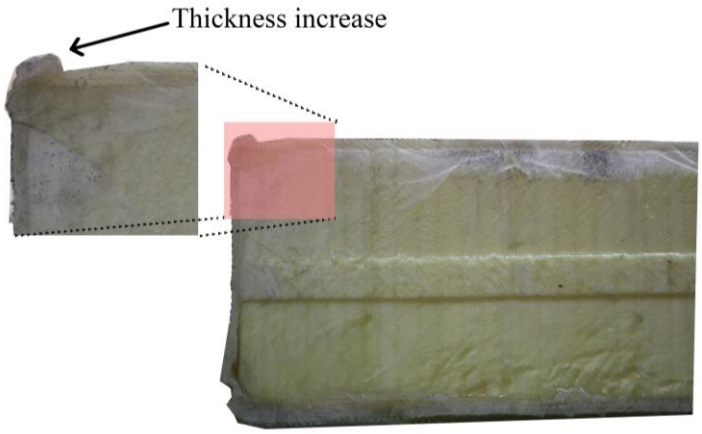

Figure 72 – Detail of the wrinkle and local thickness increase of the top face sheet next to the lateral web (specimen PET-LW-1).

Concerning the failure mode of specimen PET-CW-1, it was triggered by the shear failure of the core followed by delamination failure at the interface. A possible explanation for this failure mode could be that once the shear fracture of the foam occurred, the shear stresses at the GFRP/core interface progressively increased until exceeding its bond strength; and, consequently, delamination between the GFRP and the polymeric foam occurred (*cf.* Figure 73).

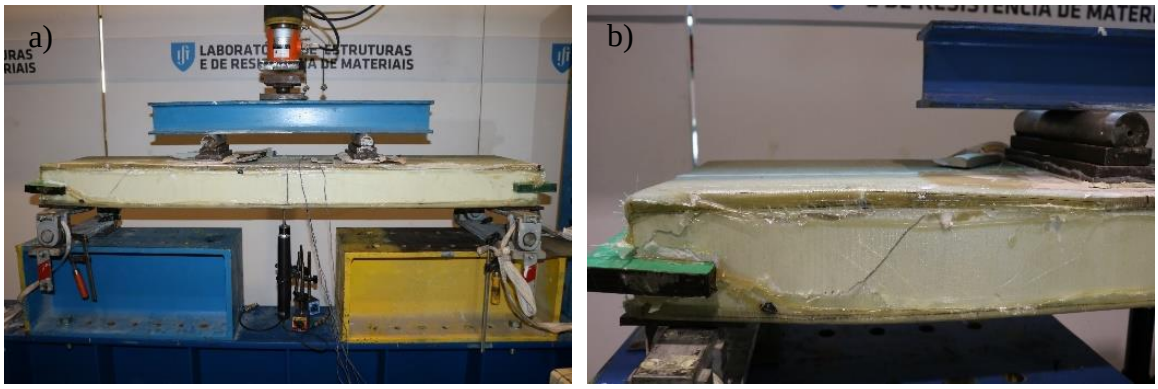

Figure 73 - Failure modes of specimen PET-CW-1: (a) general view and (b) shear fracture in PET foam

As mentioned above, the load *vs.* mid-span displacement curve of specimen PET-CW-1 exhibited two small drops, which occurred due to shear cracks in the PET core. However, the maximum shear force in the core was about 13.4 kN, corresponding to a maximum shear stress of 0.37 MPa, with the latter value being significantly lower than the shear strength of the PET foam determined in the shear

tests presented in chapter 2; again, this may also be attributed to the potential influence of size effects. Concerning the maximum shear force in the web, this value was about 70.7 kN, causing a maximum shear stress of 70.9 MPa in the GFRP, which compares with a shear strength of 161.2 MPa.

Panels with this type of architecture (*i.e.*, longitudinal reinforcement at the centre of the specimen) present some practical disadvantages, namely the relatively high difficulties associated with their manufacturing process, which involve a significant amount of additional effort when compared to specimens with lateral webs. These difficulties are then reflected in the final product, which is likely to present some defects, such as those reported in Figure 74 (*i.e.*, uneven surface).

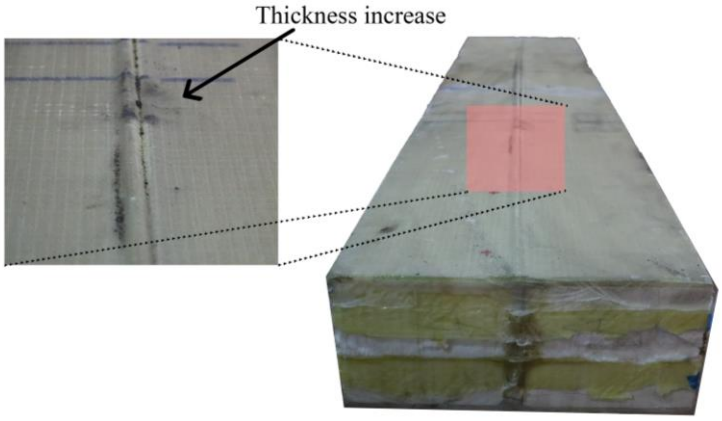

Figure 74 - Detail of the change in the thickness of the top face sheet next to the central web (specimen PET-CW-2).

In this regard, it is worth mentioning that specimen PET-CW-2 started distorting at a certain stage of the tests, and hence it was not loaded until failure; consequently, lower bounds of the flexural properties were reported in Table 23. This result was mainly due to a non-uniform load-distribution caused by the above-mentioned defects.

Regarding the load *vs.* axial strain curves of the web-core sandwich panels (*cf.* Figure 75), qualitatively, they all exhibited similar overall responses (linear up to failure). Despite the relatively high load levels attained, in general, the maximum axial strains measured at the end of the tests were lower than the ultimate strains of the materials determined by means of small-scale mechanical characterisation tests (*cf.* chapter 3). For all the PET-LW specimens tested, the maximum axial strain measured in the GFRP web by SG-5 was higher than that measured by SG-6, indicating that there was some lack of symmetry in load application and/or panel geometry, which involved higher axial stresses in the right side of the panel.

Table 23 - Summary of results obtained in the flexural test of web-core sandwich panels.

	PET-LW-1	PET-LW-2	Average PET-LW	PUR-CW-1	PUR-CW-2*
P_u [kN]	134.49	111.21	122.85	168.69	117.82
K [kN/mm]	7.13	7.09	7.11	7.30	7.22
$V_{max,web}$ [kN]	56.56	47.00	61.38	70.65	49.55
$V_{max,core}$ [kN]	10.69	8.88	9.78	13.35	9.36
M_{max} [kNm]	31.07	25.82	28.45	38.97	27.22
$\tau_{max,web}$ [MPa]	56.52	46.81	51.41	70.85	49.62
$\tau_{max,core}$ [MPa]	0.30	0.28	0.28	0.37	0.26
σ_{max} [MPa]	138.73	115.28	127.05	174.01	121.54
$d_{1/2,max}$ [mm]	19.52	15.89	17.70	34.92	19.57
$\varepsilon_{top,max}$ [μm/m]	-3212.90	-3570.32	-3391.45	-5708.71	-2740.06
$\varepsilon_{bot,max}$ [μm/m]	4470.20	2814.21	3642.12	5261.63	4389.31
$\varepsilon_{rib,left}$ [μm/m]	158.86	341.23	250.04	-	-
$\varepsilon_{rib,right}$ [μm/m]	648.58	547.32	597.95		

*Note: these values represent a lower bound, as the specimen was not loaded until failure.

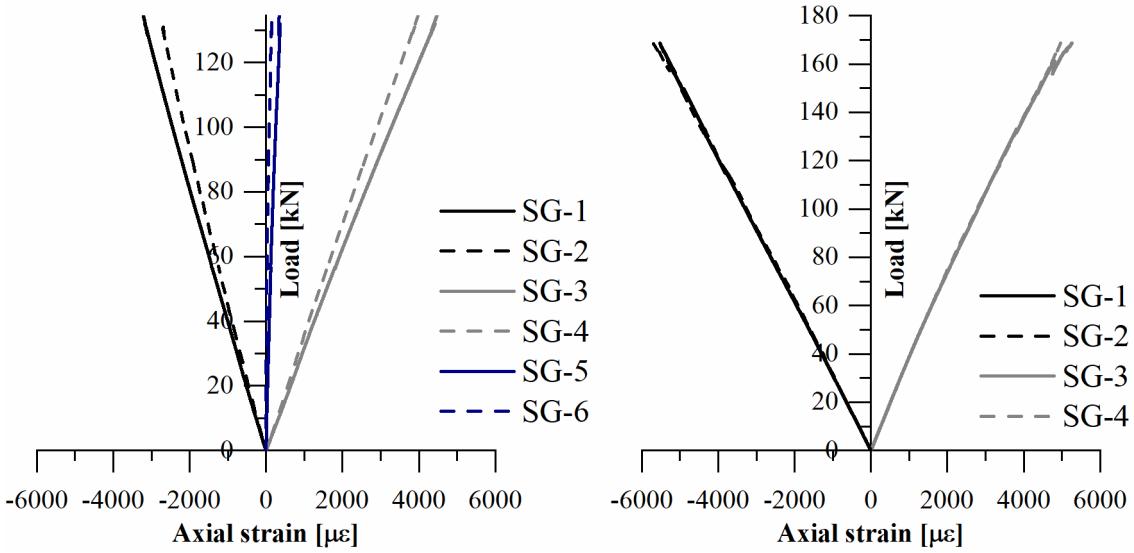

Figure 75 - Load vs. strain curves of specimens: (a) PET-LW-1 and (b) PET-CW-1.

5.5 CONCLUDING REMARKS

The flexural response at ambient temperature of composite sandwich panels comprising different core materials - PUR and PET foams - and panel architectures – homogeneous-core and web-core with different positions of the webs - was assessed by means of four-point bending tests performed on medium-scale specimens. Based on the results obtained several conclusions can be drawn:

- Apart from specimen PET-CW-1, which exhibited a slight stiffness reduction prior to collapse, all specimens presented a linear response until failure, regardless of the type of core materials and panel architectures. Concerning the web-core sandwich panels, the position of the longitudinal web did not have any influence on the stiffness of the load *vs.* mid-span displacement response. Overall, as expected, these panels were much stiffer than the homogeneous-core sandwich panels (from 2.2 to 4.3 times stiffer); this result confirms the important contribution of the longitudinal web reinforcement in increasing the shear stiffness and strength of sandwich panels.
- In general, various failure modes were observed, depending on the architecture of the sandwich panels. The homogenous-core sandwich panels failed in a brittle manner due to (i) shear failure of the foam cores and (ii) delamination failure at the core-GFRP interface. The failure of specimen PET-LW occurred by crushing of the top face sheet, followed by transverse compressive failure of the webs, whereas the collapse of specimen PET-CW seems to have been caused by the excessive shear stresses at the GFRP-core interface, which led to delamination failure between the foam and the GFRP top face sheet.
- The PET-U specimens failed due to shear failure of the core, for an average maximum shear stress of 0.4 MPa. This value is significantly lower than the shear strength of the PET foam; a possible explanation for this lower shear strength could be related to (i) material defects within the foam; (ii) size effects and/or (iii) weak bond between the GFRP and the core leading to debonding of the face-core interface. The PET-LW specimens failed due to crushing of the top face sheet and transverse compressive failure of the web; as for the unreinforced specimen, the maximum stresses estimated in the flexural tests of the panels (longitudinal compressive stress at the top face sheet and transverse compressive stress at the web) were lower than the corresponding material strength measured from coupon tests, indicating that failure may have been triggered due to the combination of stresses occurring at the edge of the panel under the loading point, also stemming from material discontinuities / defects at that location (where stress concentrations develop).

- In terms of load-bearing capacity, the homogeneous PET sandwich panels exhibited higher ultimate loads compared to the PUR specimen (about 1.5 times); this naturally stems from the higher shear strength of the PET foam compared to the PUR foam. As expected, the longitudinal web reinforcement significantly increased the load-bearing capacity of the web-core sandwich panels compared to the homogeneous-core specimens (from 4.3 to 9.3 times). This result is explained by the fact that the GFRP webs were able to significantly increase the shear strength of the panels, thus providing a relevant contribution to their load-bearing capacity.

CHAPTER 6

FIRE RESISTANCE TESTS OF GFRP COMPOSITE SANDWICH PANELS

6.1 INTRODUCTION

Composite sandwich panels are being increasingly used in civil engineering applications, either in the rehabilitation of existing constructions or in new construction, due to their lightness, quick and easy installation, good thermal properties, and reduced maintenance costs. However, there is a major concern about the use of composite sandwich panels in structural applications: the behaviour at elevated temperatures of their constituent materials, namely GFRP face sheets and polymeric foam cores. In fact, when exposed to high temperatures (300–500 °C), the organic matrix of GFRP composites and polymeric foams decompose, releasing heat, smoke, soot and toxic volatiles. In addition, as discussed in chapters 2 and 3, considerable reductions in the mechanical properties of both GFRP composites and polymeric foams have been reported, even at moderately elevated temperatures (*e.g.* 50-150 ºC), due to their softening during the glass transition process. For this reason, legitimate concerns have been raised about the performance of GFRP composite sandwich panels in fire, which still hinder their application whenever relatively strict fire reaction and fire resistance requirements must be met, especially in buildings.

Correia *et al*. [6] performed fire resistance tests on pultruded GFRP tubular beams with cross section of 100 × 100 mm, 8 mm thick walls and a clear span of 1.4 m. The GFRP beams were simultaneously loaded in bending for a service load condition (L/400, L being the span) and heated from the bottom according to the temperature *vs*. time curve defined in the ISO 834 standard. In this study, the authors addressed the influence of using different fire protection systems on the fire performance of the GFRP tubular beams. From the results obtained, it was concluded that the different passive fire protection systems tested were effective in improving the fire resistance behaviour of the GFRP beams: the unprotected beams collapsed after 38 min, whereas the protected ones attained fire endurances between 65 and 120 min. Concerning the failure modes, the collapse involved either axial compressive failure of the top flange or shear and transverse compression of the upper part of the webs; tensile failure of the bottom flange never occurred.

Keller *et al.* [15] performed similar fire resistance tests on multicellular panels made of E-glass fibres and non-retarded isophthalic polyester resin. The 195 mm thick specimens (with flange thickness ranging from 15.2 mm to 17.4 mm and web thickness of 11 mm) were simultaneously exposed to the ISO 834 fire curve and loaded to L/300 in a four-point bending configuration, in a simply supported span of 2.75 m. In this study, the authors assessed the influence of using an active fire protection system (water-cooling) on the fire resistance performance. As for the work by Correia *et al*. [6], the water cooling system was effective in improving the fire endurance of the panel: the unprotected specimen failed after 57 min, while the protected specimen kept its structural stability even after 120 min of fire exposure. Bai *et al.* [7] evaluated the fire behaviour of GFRP columns (same cross-section used in Keller *et al.* [15]) subjected to an axial load of 145 kN (corresponding to a uniform axial stress level of 5 MPa) and exposed to the ISO 834 fire curve. The specimens were either unprotected or protected with a water-cooling system. Similarly to what was found by Correia *et al*. [6] and Keller *et al.* [15], the specimen protected with active passive protection system attained relatively high fire resistance, sustaining the applied load for more than 120 min.

In what concerns the fire behaviour of foam filled sandwich panels, much less information is available; in addition, most previous studies addressed their fire behaviour under in-plane loading (which is relevant for wall applications) [8–10,95], rather than under out-of-plane loading (relevant for building floor or bridge deck applications).

Horold *et al*. [8] performed a preliminary study about the fire resistance behaviour of sandwich panels under in-plane loading. The fire resistance tests were performed on sandwich panels with dimensions of 500 × 500 × 24 mm, which were simultaneously loaded in compression and exposed to heat on one side (the temperature *vs*. time curve was not reported). In this work, the authors studied the influence of using different core materials (PVC foam, PIR foam and balsa wood) and flame retardants in the carbon fibre reinforced polymer (CFRP) face sheets. This study allowed to conclude that applying fire retardants on both fabrics and matrix substantially increased the time to failure of the specimens by almost 2 times. In addition, it was concluded that the fire resistance of the sandwich panels was strongly dependent on the type of core material used, with balsa wood providing the best performance among the materials tested in this study.

To the best of the author's knowledge, the single study about the fire behaviour of foam-filled composite sandwich panels under out-of-plane-loading was conducted by Proença *et al*. [11]. The authors performed four fire resistance tests on GFRP sandwich panels comprising a homogeneous core made of PUR foam (cross section of 134 × 250 mm and length of 1500 mm), both unprotected and protected with calcium silicate (CS) boards. The sandwich panels were simultaneously subjected to the ISO 834 fire curve and to a sustained load applied in a four-point bending configuration, causing a mid-span deflection of L/250. The sandwich panels without fire protection collapsed after only 10 min, whereas those protected with CS boards exhibited fire resistance of 45 min (CS boards

as screen protection) and 60 min (CS boards forming an air cavity). This study also allowed to conclude that the reduction of the shear interaction at the interface between the bottom GFRP face sheet and the PUR foam core with increasing temperature/time may cause a change of structural behaviour during the tests, from beam-type to arch-type.

As mentioned above, a very limited number of studies addressed the fire behaviour of GFRP sandwich panels, in fact, their fire resistance behaviour has not yet been investigated in sufficient depth. Most studies focused on the fire resistance behaviour under in-plane loading; for out-of-plane loading, no previous study has addressed the fire resistance of web-core sandwich panels. In this context, this chapter presents an experimental investigation about the fire resistance behaviour of GFRP sandwich panels with different panel configurations loaded in bending. The experimental campaign included eleven fire resistance tests on medium-scale GFRP sandwich panels with a total length of 1500 mm and cross-section of 300 × 131 mm (the same as those tested at room temperature, *cf.* chapter 5). Several parameters were studied including: (i) panel configurations (homogeneous-core and web-core panels), (ii) core materials (PUR and PET foams) and passive fire protection systems (CS boards, either adherent to the bottom face sheet or suspended from it and forming an air cavity). The main goals were to investigate the evolution of the temperatures with time at different locations/materials of the panels, the evolution of the deflections with temperature/time, their fire resistance, the failure modes and the effectiveness of the different fire protection systems.

6.2 EXPERIMENTAL INVESTIGATIONS

6.2.1 Test series

The fire behaviour of intermediate-scale GFRP sandwich panels was assessed by means of four-point bending tests performed in a vertical oven according to the recommendations of the EN 1363-1 standard [83]. As mentioned, the geometry of the sandwich panels used in the fire resistance tests was the same as those used in the flexural tests performed at ambient temperature (*cf.* Figure 64 and Figure 65). In this context, the panels had rectangular cross-section (300 × 131 mm) and a clear span of 1400 mm.

For the fire resistance tests, eleven panels were tested: (i) 7 unprotected panels, (ii) 3 panels protected with CS boards bonded to the bottom (exposed) face sheet, and (iii) 1 panel protected with CS boards suspended from the bottom face sheet, forming an air cavity. Details of the test programme are summarized in Table 24. The nomenclature presented in the table refers to the following parameters: (i) type of core material - PUR or PET; (ii) type of web reinforcement - unreinforced (U), *i.e.* homogeneous core, or reinforced with lateral (LW) and central webs (CW), *i.e.* web-core; (iii) type of fire protection system, adherent (CS) or suspended (AC) CS boards; and number of the specimen tested (1 or 2, applicable only to part of the test series).

Table 24 - Test series of the fire resistance tests.

Specimen ID	Core material	Reinforcement	Fire protection system
PET-U-U-1	PET	Homogeneous-core	-
PET-U-U-2	PET	Homogeneous-core	-
PUR-U-U-1	PUR	Homogeneous-core	-
PET-U-CS-1	PET	Homogeneous-core	25 mm adherent CS boards
PUR-U-CS-1	PUR	Homogeneous-core	25 mm adherent CS boards
PET-LW-U-1	PET	Web-core - lateral webs	-
PET-LW-U-2	PET	Web-core - lateral webs	-
PET-LW-CS-1	PET	Web-core - lateral webs	25 mm adherent CS boards
PET-LW-AC-1	PET	Web-core - lateral webs	25 mm suspended CS boards
PET-CW-1	PET	Web-core - central web	-
PET-CW-2	PET	Web-core - central web	-

6.2.2 Specimen preparation

Before testing, the lateral edges of all panels were covered with aluminium tape (*cf.* Figure 76a); this procedure was adopted to reduce the heat transfer by radiation along those edges that might occur during the tests. Additionally, intumescent strips were positioned on the bottom corners of the panels along the longitudinal direction, to minimize the heat flow through the lateral sides, which were expected to remain adiabatic (*cf.* Figure 76b).

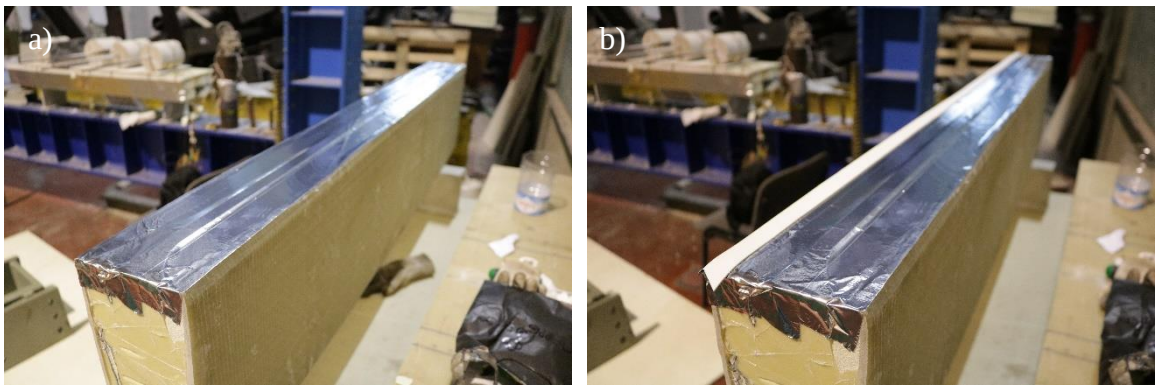

Figure 76 - Specimen preparation: (a) aluminium tape and (b) intumescent tape next to the bottom corner of the panels.

For the panels with passive fire protection adherent to the exposed face, two CS boards with dimensions of 1100 × 310 × 12.5 mm (model H, produced by Promatec, density of 870 kg/m^3 and thermal conductivity at room temperature of 0.09 W/m°C) were directly applied to the bottom face sheet using a fire-resistant acetic sealant, which was cured for (at least) 1 day in the laboratory environment. In addition, temperature resistant wires were used to fix (*i.e.* wrapping) the fire protection system to the specimen (*cf.* Figure 77); this solution was set in order to avoid the loss of the protection system in case of debonding of the acetic sealant due to the exposure to elevated temperatures. Note that the two CS boards were fixed to each other using both (i) fire-resistant acetic sealant and (ii) metal screws distributed along the length of the boards.

Figure 77 - GFRP sandwich panel protected with adherent CS boards.

As for the sandwich panel protected with suspended CS boards, it is worth referring that this solution aims at simulating the thermal exposure commonly found in building floors with suspended ceilings, in which the air cavity is used for building services (*e.g.* piping systems). As shown in Figure 78, two CS boards with dimensions of 1260 × 450 × 12.5 mm were positioned on top of the furnace walls at a vertical distance of 160 mm from the bottom face sheet of the panel, supported on two C-shaped steel profiles and insulated (from them) by means of mineral wool blankets. The main objective of using these steel profiles was to avoid the rupture of the CS boards during the fire test.

Figure 78 - GFRP sandwich panel protected with suspended CS boards.

6.2.3 Test set-up, instrumentation and testing protocol

All sandwich panels were simply supported and subjected to a constant load applied in four-point bending (at thirds of the span) in a span of 1.40 m. Concerning the thermal boundary conditions, the bottom face sheet was directly exposed to fire over a length of 1.10 m (*cf.* Figure 79), whereas the remaining bottom length and lateral surface were kept insulated throughout the fire tests (more details about the lateral insulation are provided ahead). The top surface of the panels was subjected to ambient temperature.

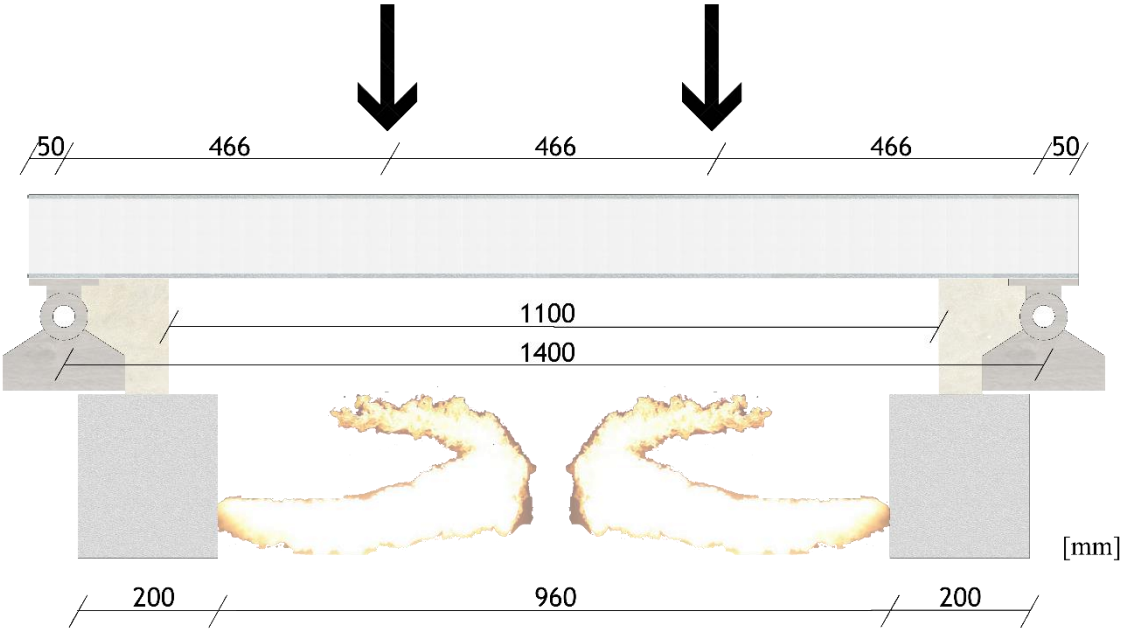

Figure 79 - Test set-up of the fire resistance tests.

The load was applied on the top face sheet of the specimens by means of a load transmission steel beam (with weight of ~100 kgf), in which concrete blocks (known weight) were suspended using pulley blocks. Two rectangular steel plates (with dimensions of 300 × 150 × 25 mm) were used to transfer two concentrated loads from the transmission steel beam to the top face sheet of the specimens. It is worth noting that a hydraulic jack was used to slowly lower the transmission beam into position, thus avoiding dynamic effects in load application. Figure 80 shows details of the test set-up used for the fire resistance tests.

Figure 80 - Details of the fire resistance test set-up.

As shown in Figure 80, an intermediate-scale gas burned furnace was used to apply the ISO 834 standard fire curve. The furnace has external dimensions of 1.35 × 1.20 × 2.10 m (length × width × height) and a top opening area of 0.95 × 0.80 m. To guarantee a proper lateral insulation of the panels,

two insulation modules comprising a metallic structure lined with mineral wool were placed adjacently to the test specimens (*cf.* Figure 81a). In addition, two mineral wool blankets (one for each side) were positioned next to the supports to prevent them from being exposed to heat during the tests (*cf.* Figure 81b).

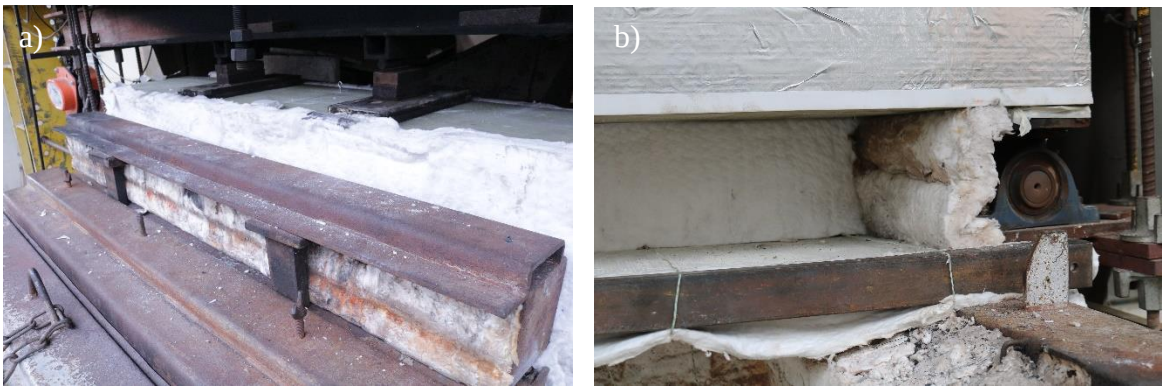

Figure 81 - Thermal insulation of the fire resistance test: (a) insulation modules and (b) mineral wool.

To evaluate the thermal response of the panels, type-K thermocouples (conductor diameter of 0.25 mm) were placed in both GFRP face sheets and core material during the manufacturing process (*cf.* Figure 82). This procedure ensured that the position of the thermocouples remained constant during the fire tests; in previous experimental studies (*e.g.* [62]), specimens had to be drilled and thermocouples were introduced in those holes and fixed with resin – with that procedure it was not possible to guarantee the exact positioning of the thermocouples throughout the fire tests).

Figure 82 - Thermocouples positioning during the manufacturing process.

For all panels tested, thermocouples were positioned across the depth of the panel in three relevant sections: (i) mid-span (section AA'); (ii) end of the fire span (section BB', from now on called "intersection section"), and (iii) one of the supports (section CC'); a schematic view of the distribution of the thermocouples is shown in Figure 83.

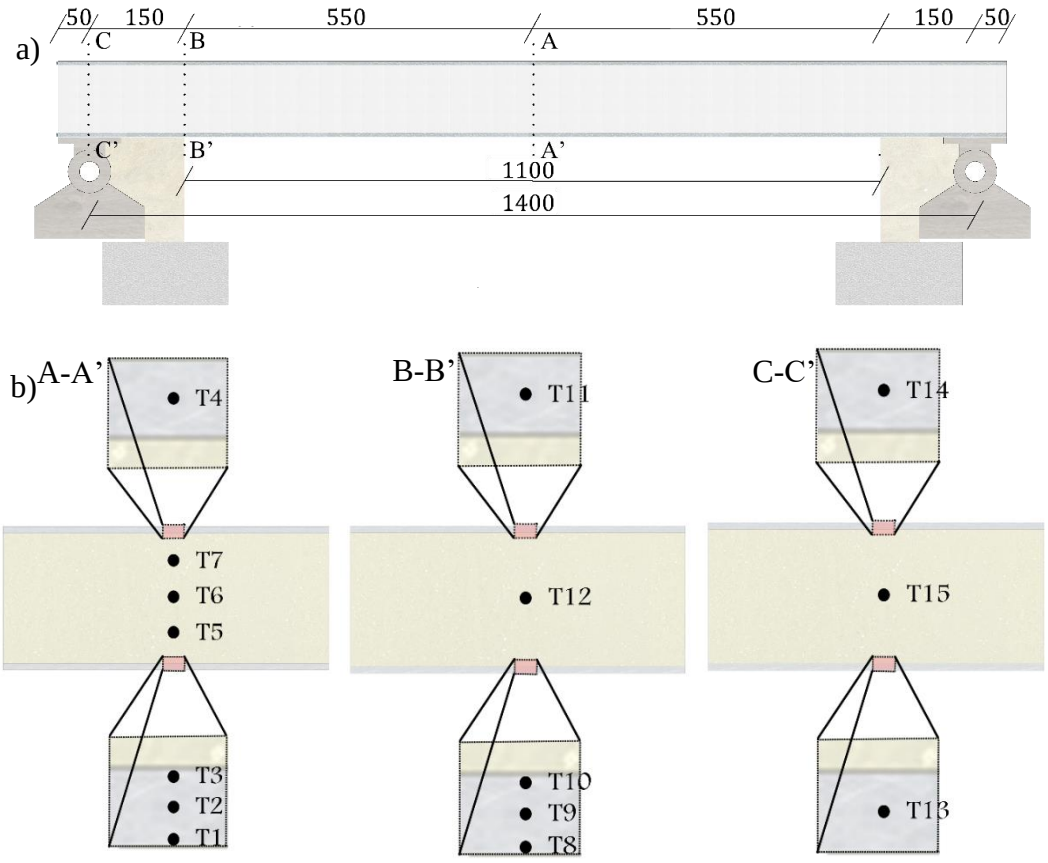

Figure 83 - Thermocouples distribution at different sections of the sandwich panel: (a) longitudinal and (b) transverse view.

As shown in Figure 83, all homogeneous-core sandwich panels contained the following seven thermocouples at mid-span section (AA'): three thermocouples in the bottom GFRP face sheet (distances to the hot face of about 0.5 mm – T1, 2.8 mm – T2 and 5.6 mm – T3), three thermocouples in the core (distances to the hot face of about 35.6 mm – T5, 65.6 mm – T6 and 95.6 mm – T7) and one thermocouple at the mid-depth of the top GFRP face sheet (distance to the hot face of ~128.4 mm – T4). Concerning the temperature measurements at the intersection section (BB'), three thermocouples were installed in the bottom face sheet (distances to the hot face of 0.5 mm - T8, 2.8 mm – T9 and 5.6 mm – T10), one thermocouple was applied at the centre of the foam core (distance to the hot face of 65.6 mm – T12) and one thermocouple was placed in the top face sheet (distance to the hot face of about 128.4 mm – T11). Finally, over one of the support sections, a set of 3 thermocouples was used to measure the temperatures in the centre (*i.e.* in half of its thickness) of the bottom face sheet (T13), foam core (T15) and top face sheet (T14). In PET-LW sandwich panels, as shown in Figure 84, five thermocouples were also placed across the GFRP web at depths of 5.6, 35.6, 65.6, 95.6 and 125.6 mm from the exposed the face, aiming at measuring the temperature profiles at mid-span (T8 to T12), intersection (T18 to T22) and support (T26) sections. With respect to the sandwich panel with the central web (specimen PET-CW), three thermocouples were placed across the GFRP web at depths of 35.6, 65.6 and 95.6 mm, to monitor the evolution of the temperature at the mid-span (T4 to T6), intersection (T18) and support (T25) sections; *cf.* Figure 85.

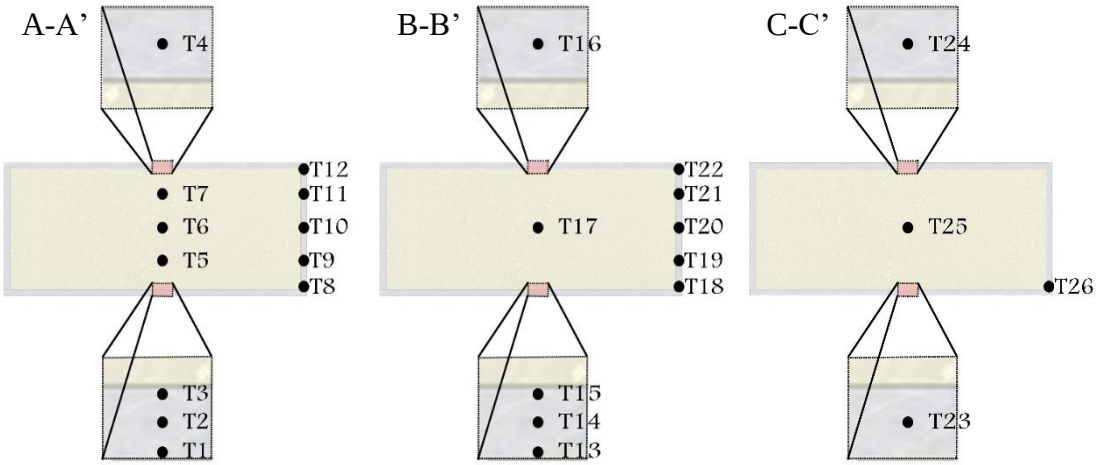

Figure 84 - Sandwich panel with lateral webs: thermocouples position at different panel's sections.

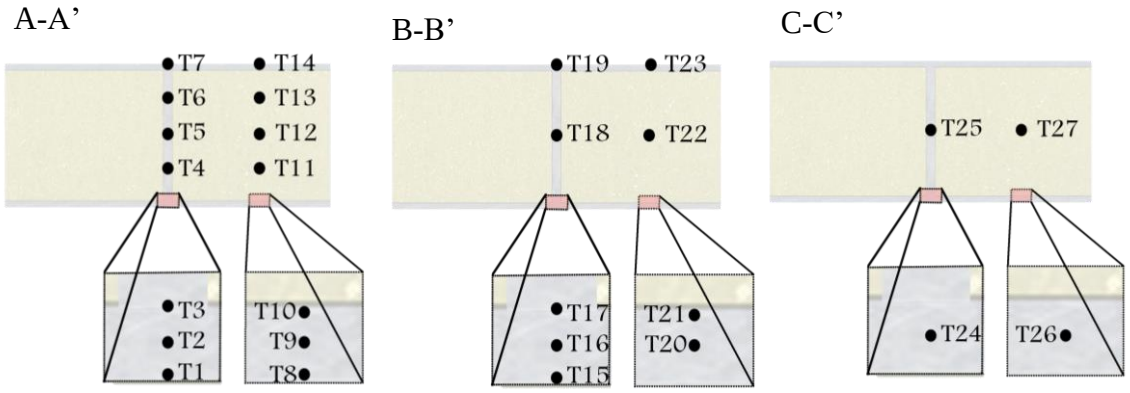

Figure 85 - Sandwich panel with central web: thermocouples position at different panel's sections.

In terms of mechanical response, the mid-span vertical deflection of the top face sheet of the panels was measured by means of a wire displacement transducer (model TML CDP-500, with a 500 mm stroke and precision of 0.01 mm) and a displacement transducer (model TML100, 100 mm of stroke and precision of 0.01 mm); in addition, two displacement transducers (model TML50, with a stroke of 50 mm and precision of 0.01 mm) were used to measure the vertical deflection of the top face sheet at the supports, *cf.* Figure 86. The displacements and the temperatures inside the panel were registered for the entire duration of the tests, by means of *HBM* data loggers at an acquisition rate of 2 Hz.

In accordance with the recommendations given in ISO 834 standard [78], the fire resistance tests were carried out at an initial temperature of the air varying from 16 °C to 25 °C. Firstly, the specimens were mechanically loaded for approximately 15 min - this period was set to guarantee the stabilization of deflections. Then, the thermal load (*i.e.* the heating curve according to ISO 834) was applied until failure. It is worth mentioning that the fire load was defined to cause a mid-span deflection of 5.6 mm (1/250 of the span, observed in the tests performed at room temperature, *cf.* Chapter 5). This deflection aims at being representative of that associated to the fire load combination.

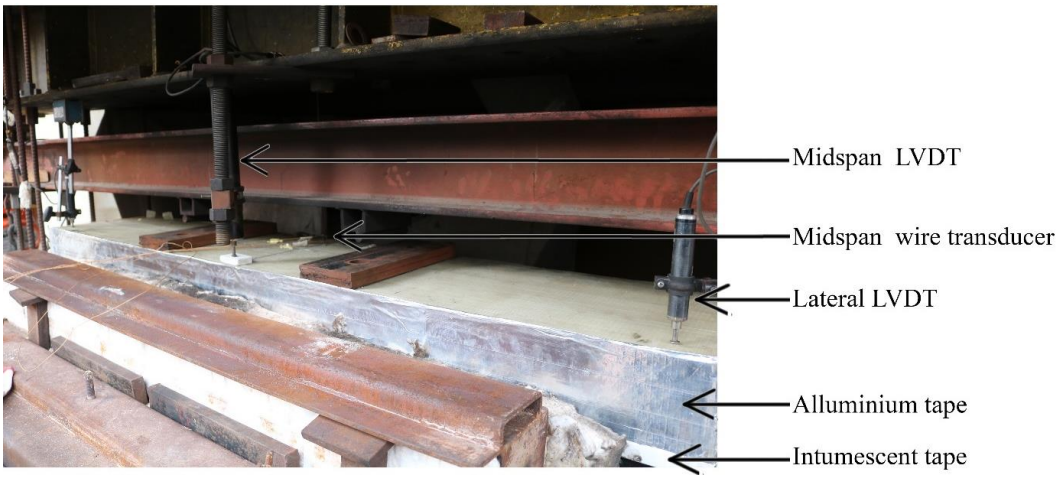

Figure 86 - Lateral/top view of the fire resistance test setup and instrumentation.

Table 25 lists the failure load measured at room temperature, P_{fin}, the load applied in the fire resistance tests, P_{fire}, and the corresponding ratio. Furthermore, Table 26 and Table 27 present, for each specimen, the initial stresses (*i.e.* before applying the thermal load), the material strength at ambient temperature and the corresponding stress-strength ratios. The following material properties (at ambient temperature conditions) and initial stresses are listed in Table 26 and Table 27: tensile stress in the bottom face sheet ($\sigma_{t,fire}$); GFRP tensile strength (σ_t); compressive stress in the top face sheet ($\sigma_{c,fire}$); GFRP compressive strength (σ_c); shear stress in the core ($\tau_{c,fire}$); core shear strength (τ_c); shear stress in the web ($\tau_{web,fire}$) and GFRP web shear strength (τ_{web}).

Table 25 - Failure load at ambient temperature, load applied in the fire tests and corresponding ratios.

Specimen ID	P_{fin} [kN]	P_{fire} [kN]	P_{fire} / P_{fin} [-]
PET-U-U-1	26	18	0.7
PET-U-U-2			
PET-U-CS-1			
PUR-U-U-1	18	9	0.5
PUR-U-CS-1			
PET-R-U-1	134	38	0.3
PET-R-U-2			
PET-R-CS-1			
PET-R-AC-1			
PET-CR-1	172	38	0.2
PET-CR-2			

Table 26 - Overview of the stress fields in the homogeneous core panels before the fire exposure.

Specimen ID	$\sigma_{t,fire}$ [MPa]	σ_t [MPa]	$\sigma_{t,fire}/\sigma_t$ [%]	$\sigma_{c,fire}$ [MPa]	σ_c [MPa]	$\sigma_{c,fire}/\sigma_c$ [%]	$\tau_{c,fire}$ [MPa]	τ_c [MPa]	$\tau_{c,fire}/\tau_c$ [%]
PET-U-U-1	20.5	512.4	4.0	20.5	228.9	8.9	0.25	0.9	27.7
PET-U-U-2									
PET-U-CS-1									
PUR-U-U-1	10.2		2.0	10.2		4.4	0.13	0.3	43.4
PUR-U-CS-1									

Table 27 - Overview of the stress fields in the web-core panels before the fire exposure.

Specimen ID	$\sigma_{t,fire}$ [MPa]	σ_t [MPa]	$\sigma_{t,fire}/\sigma_t$ [%]	$\sigma_{c,fire}$ [MPa]	σ_c [MPa]	$\sigma_{c,fire}/\sigma_c$ [%]	$\tau_{web,fire}$ [MPa]	τ_{web} [MPa]	$\tau_{web,fire}/\tau_{web}$ [%]
PET-LW-U-1	43.7	512.4	8.52	43.7	228.9	19.0	16.7	163.2	10.2
PET-LW-U-2									
PET-LW-CS-1									
PET-LW-AC-1									
PET-CW-1									
PET-CW-2									

6.3 RESULTS AND DISCUSSION

6.3.1 Thermal response

As described in section 6.2.3, all the sandwich beams were heated on their bottom face sheet following the time-temperature curve defined in ISO 834 standard. Figure 87 plots the ISO 834 fire curve together with the experimental temperatures measured by the built-in thermocouple of the oven during the various tests.

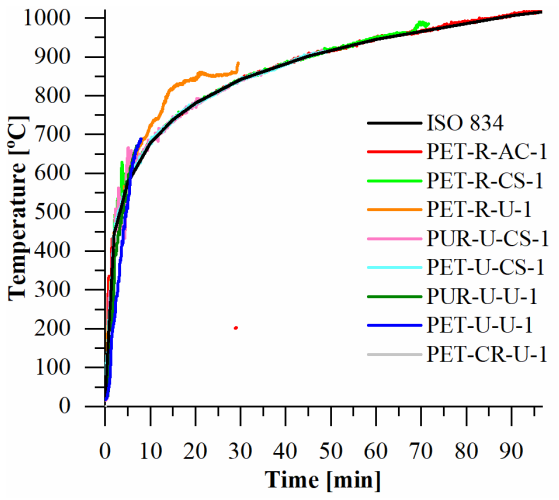

Figure 87 - ISO 834 and oven temperatures measured in the fire resistance tests.

Overall, in all tests, the experimental fire curves were consistent with the ISO 834 reference curve, although presenting some scatter during the early stage of the tests; in any case, experimental temperatures remained always within the range of relative difference allowable in the standard (± 100 °C).

Figure 88 shows the temperature profiles measured at the mid-span section of specimens PET-U-U-1 and PUR-U-U-1. Concerning the evolution of the temperature at the bottom face sheet (T1 to T3),

for both panels, it can be observed that the temperature increased at a different rate across the depth of the laminate. As expected, the thermocouple placed at a depth of about 0.5 mm (T1) measured the highest temperature, attaining the T_g after about ~2 min and the T_d after ~5 min (only in specimen PET-U-U-1). The temperatures at the centre of the bottom face sheet (T2) and at the interface between the bottom face sheet and the core (T3) increased at a much slower rate, reflecting the low thermal conductivity of the GFRP material, exceeding the T_g after less than ~3 min, but remaining always below the T_d of the material.

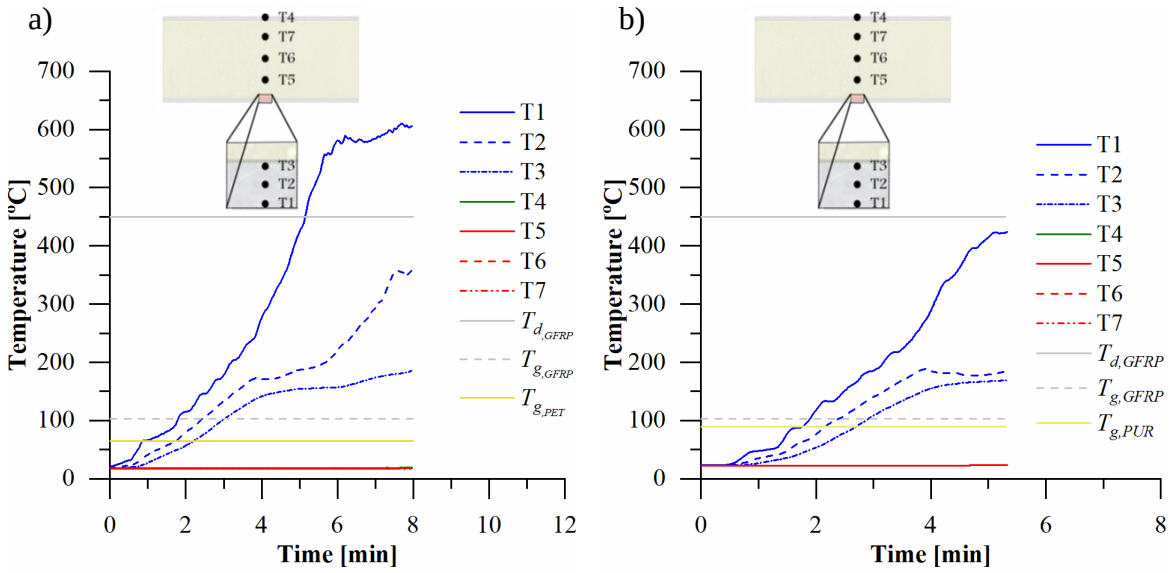

Figure 88 - Temperature vs. time curves measured at the mid-span section of specimens: (a) PET-U-U-1 and (b) PUR-U-U-1.

Concerning the temperatures in the bottom face sheet at the intersection section (T8 to T10), as shown in Figure 89, they present a very similar qualitative pattern with decreasing temperatures throughout the depth. As expected, mainly due to the specific thermal boundary conditions, they were considerably lower than those measured at the mid-span - the maximum temperature attained was lower than 65 °C for specimen PET-U-U-1 and 100 °C for specimen PUR-U-U-1 (in both cases below the T_g of the GFRP material).

Figure 88 and Figure 89 also show that the temperatures measured in the PET and PUR core foams at the mid-span (T5 to T7) and intersection (T12) sections remained always lower than 20 °C (well below the T_g of the foams). This result is mainly due to the very good thermal insulation properties of the polymeric foams (at ambient temperature) together with the relatively short duration of fire exposure (due to the panels' collapse, as detailed in the next sections). For the entire duration of the test, the temperature in the top face sheet at the mid-span (T4), interface (T11) and support (T14) sections was approximately constant, remaining well below the T_g of the GFRP material - this result is mainly due to the insulation provided by the underlying volume of foam (before its thermal decomposition).

Finally, the maximum temperature increase measured next to the support (T13) did not exceed 0.25 °C during the whole duration of the test – for this reason, these readings are not shown.

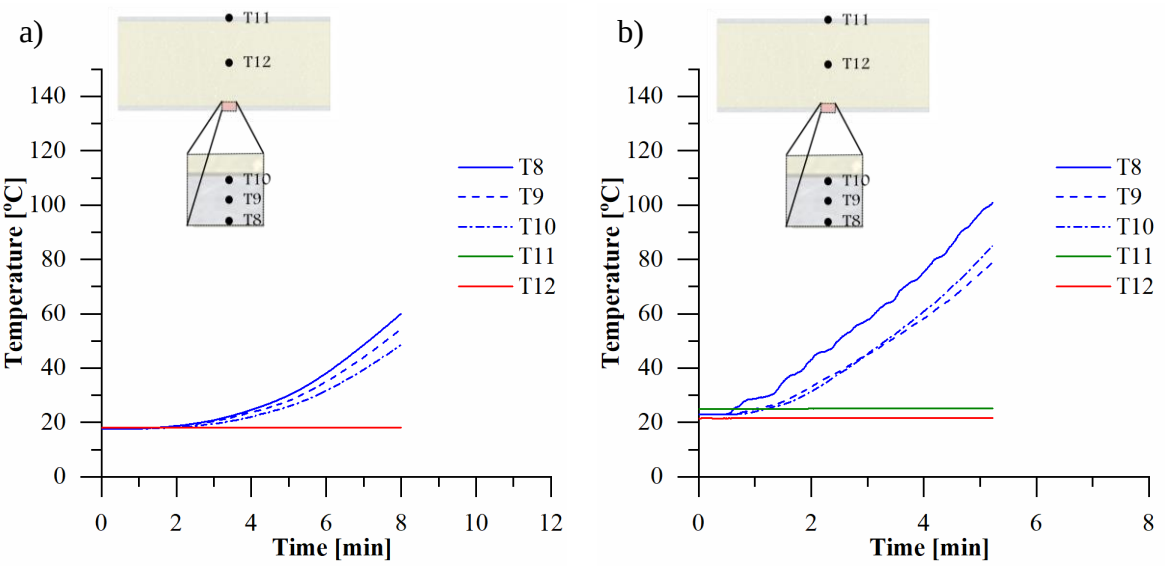

Figure 89 - Temperature vs. time curves measured at the intersection section of specimens: (a) PET-U-U-1 and (b) PUR-U-U-1.

Figure 90 plots the temperature profiles measured at the mid-span section of both PET and PUR homogeneous-core panels protected with two 12.5 mm thick CS boards (total thickness of passive protection of 25 mm) adherent to the bottom face sheet (directly exposed to fire).

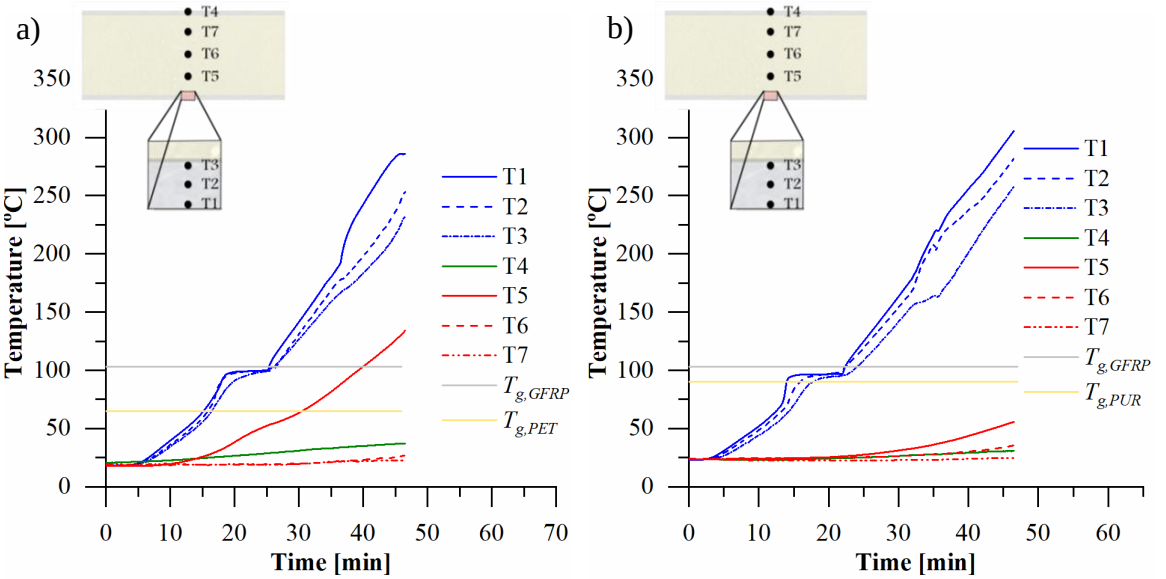

Figure 90 - Temperature vs. time curves measured at the mid-span section of specimens: (a) PET-U-CS-1 and (b) PUR-U-CS-1.

In the two protected GFRP sandwich panels, the bottom face sheet temperatures followed a very similar pattern: as expected, the temperatures at the bottom face sheet (T1 to T3) were much lower (maximum temperature attained of about 300 °C) compared to those measured in the unprotected specimens, thus confirming the effectiveness of the passive fire protection system in reducing the temperature progression in the panel. It is worth noting that the T_d of the GFRP was never attained

in the bottom face sheet, whereas the T_g was exceeded after ~25 min. At the mid-span section, the temperature profiles of the bottom face sheet increased at a similar rate, presenting marked nonlinearities when reaching ~100 ºC; this result stems from the water vaporization occurring in the CS boards at that temperature.

From Figure 90, it is also relevant to note that the thermal response of the PET and PUR foams was significantly different (unlike those measured in the bottom face sheet), which should be naturally due to differences in their thermophysical properties: when compared to the PET specimen, for similar durations of fire exposure, the maximum temperature measured at the bottom part of the core (T5) of panel PUR-U-CS-1 was significantly lower (65 ºC *vs.* 140 ºC). After 10 min of fire exposure, the progression of the temperature in the bottom part of the core of specimen PET-U-CS-1 (T5, distance to the hot face of 3.5 cm) presented an almost steady increase, exceeding the T_g of the PET foam (65 ºC) after 30 min and reaching the maximum temperature of about 140 ºC at the end of the test (but still well below the decomposition temperature of the foam – 425 ºC). For this temperature range, both foams were still able to provide a relatively good thermal insulation: for this reason, very limited temperature increases were observed at distances from the exposed face of 6.5 and 9.5 cm (T6-T7-T12-T15); accordingly, temperature in the top face sheet remained roughly unchanged up to the end of the tests.

A similar qualitative behaviour, but with a time delay, was observed at the intersection section (T8 to T10), as depicted in Figure 91 – here, the maximum temperature attained was lower than that observed at the mid-span section (*cf.* Figure 90) - again, this should be attributed to the thermal boundary conditions of the test set-up.

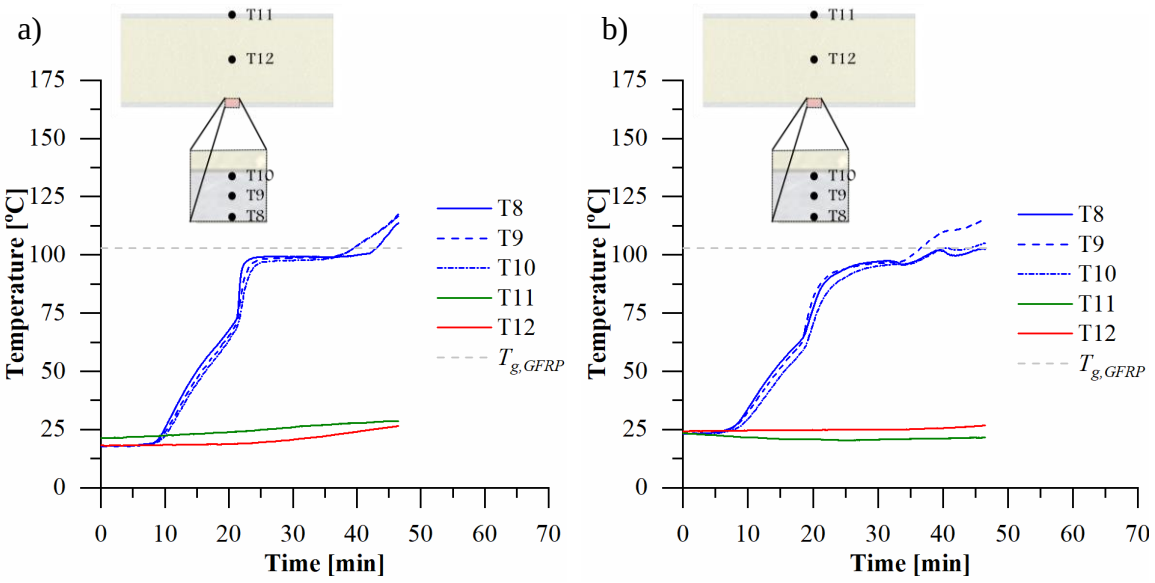

Figure 91 - Temperature vs. time curves measured at the intersection section of specimens: (a) PET-U-CS-1 and (b) PUR-U-CS-1

Similarly to what was observed in specimen PET-U-U-1, the temperatures at the support section remained approximately constant with the fire duration exposure.

Figure 92 shows the temperature progression *vs*. time curves measured at the mid-span section of a representative web-core sandwich panel comprising PET foam (specimen PET-LW-U-1).

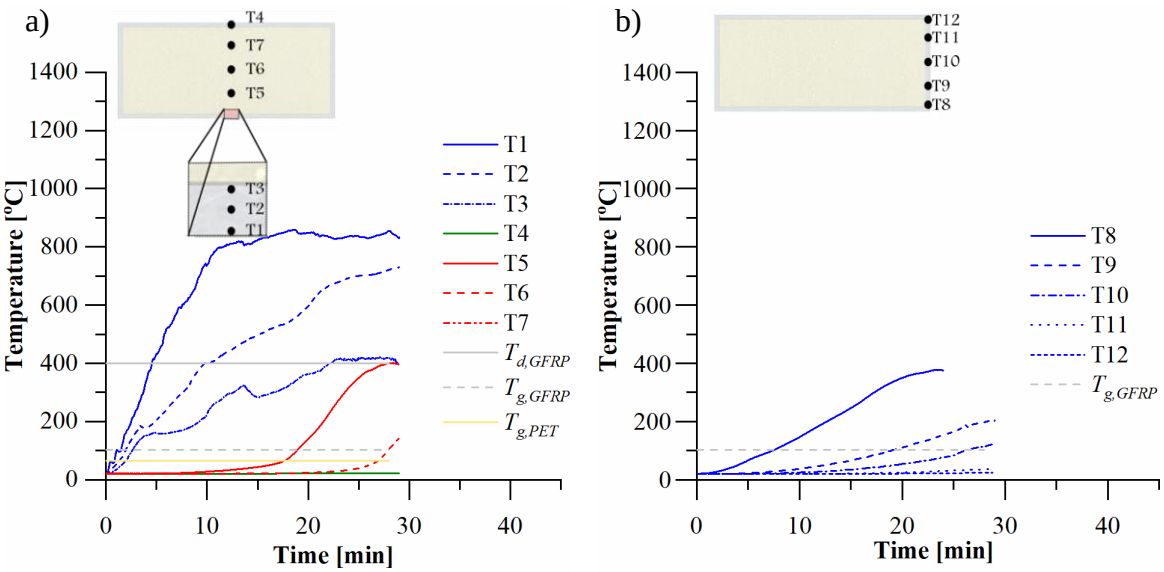

Figure 92 - Temperature vs. time curves measured at the mid-span section of specimen PET-LW-U-1.

Concerning the thermal behaviour at the mid-span section, it can be observed that the temperature at the bottom face sheet (T1) presented a steady increase up to 800 ºC (~10 min of fire exposure), which was then followed by a plateau until failure. After 10 min of fire exposure, the temperatures at the centre of the GFRP laminate (T2) and at the GFRP-core interface (T3) were also considerably higher than the T_g of the GFRP, attaining respectively 400 ºC and 300 ºC.

The temperature at the bottom part of the core (T5) presented the following behaviour: (i) up to 10 min of fire exposure, it remained almost constant; (ii) from 10 min to 18 min, it increased at a relatively slow rate; (iii) from 18 min to 26 min, it presented an abrupt temperature increase due to the thermal degradation of the foam core, and (iv) at the end of the test, it exhibited a small plateau, which can be associated to the full decomposition of the material. After the decomposition of the core, according to Proença *et al.* [11], the foam core transforms into a cavity, filled with residues of the foam, combustion gases and air; the formation of this cavity can lead to a reduction of the heat transfer between the bottom and top face sheets. Concerning the temperature progression at the centre of the core (T6), the maximum temperature attained at the end of the test was 150 ºC: for this temperature range, the core undergoes severe reductions of its mechanical properties, but is still able to provide thermal insulation (*cf.* Chapter 4). In what concerns the GFRP webs, after 30 min of fire exposure, the temperatures in their lower half (T8-T9-T10) were above the T_g of the GFRP material – this involved a reduction of their mechanical properties and hence a loss of effectiveness of the (shear) reinforcement they provide to the panel. Note that after 25 min of fire exposure, the readings of the thermocouple positioned at the bottom part of the webs at the mid-span section (T8) were lost.

Figure 93 shows the temperatures at the intersection section. They presented very similar magnitudes to those measured at the mid-span section, thus being in contrast with the thermal response observed at the same section of the homogeneous core panels. A possible explanation for this unexpected result may be that the insulation system placed next to the support (*cf.* Figure 81b) lost its effectiveness after the beginning of the fire exposure; this could also explain the marked non-linearities found in the temperature *vs*. time curves at the positions of thermocouples T13-T14-T18 after ~7 min.

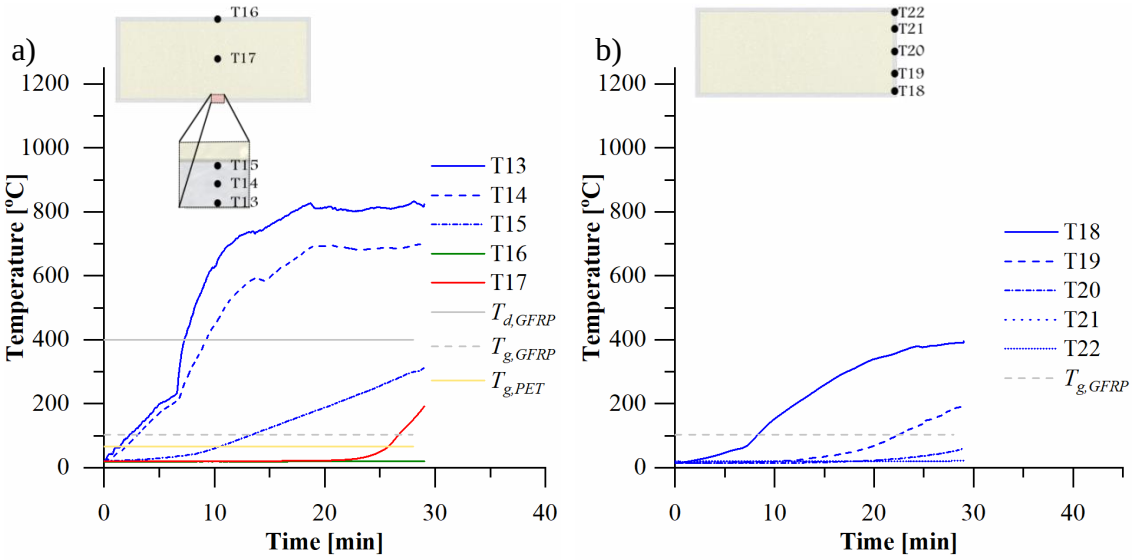

Figure 93 - Temperature vs. time curves measured at the intersection section of specimen PET-LW-U-1.

At the support section, temperatures across the depth of the panel did not present any relevant variation during the test (less than 1 °C), remaining well below the T_g of both GFRP and PET foam – for this reason they are not shown.

Figure 94 plots the temperature *vs*. time curves at the mid-span section of specimen PET-LW-CS-1.

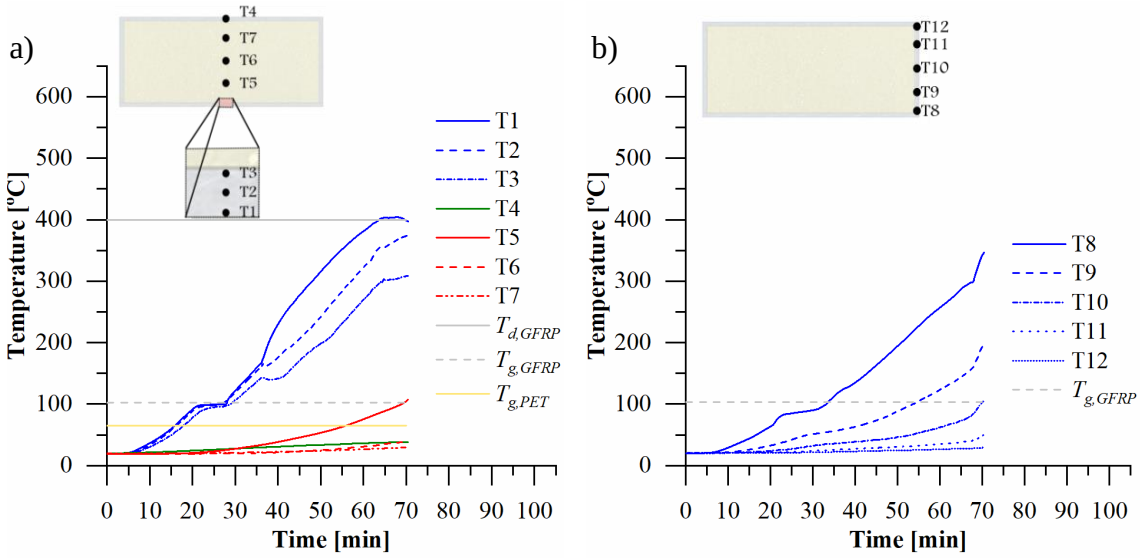

Figure 94 - Temperature vs. time curves measured at the mid-span section of specimen PET-LW-CS-1.

In the tests performed on specimen PET-LW-CS-1, the temperature *vs*. time curves at the bottom GFRP face sheet presented non-linearities due to water evaporation in the CS board. In Figure 94a,

it is also possible to observe that the maximum temperature attained by the core at the position of thermocouple T5 (distance from the hot face of 3.5 cm) was approximately 100 °C, suggesting that most of the core volume was able to provide thermal protection for all the duration of the test. Regarding the temperatures at the lower half of the webs (thermocouples T8 to T10), they presented an almost steady increase until the end of the test (*cf.* Figure 94b), exceeding the T_g of the material after 30 to 70 min of fire exposure.

Figure 95 shows that the passive fire protection were effective in reducing the temperatures across the depth of sandwich panel PET-LW-CS-1 (at the mid-span section) when compared to those observed in specimen PET-LW-U-1.

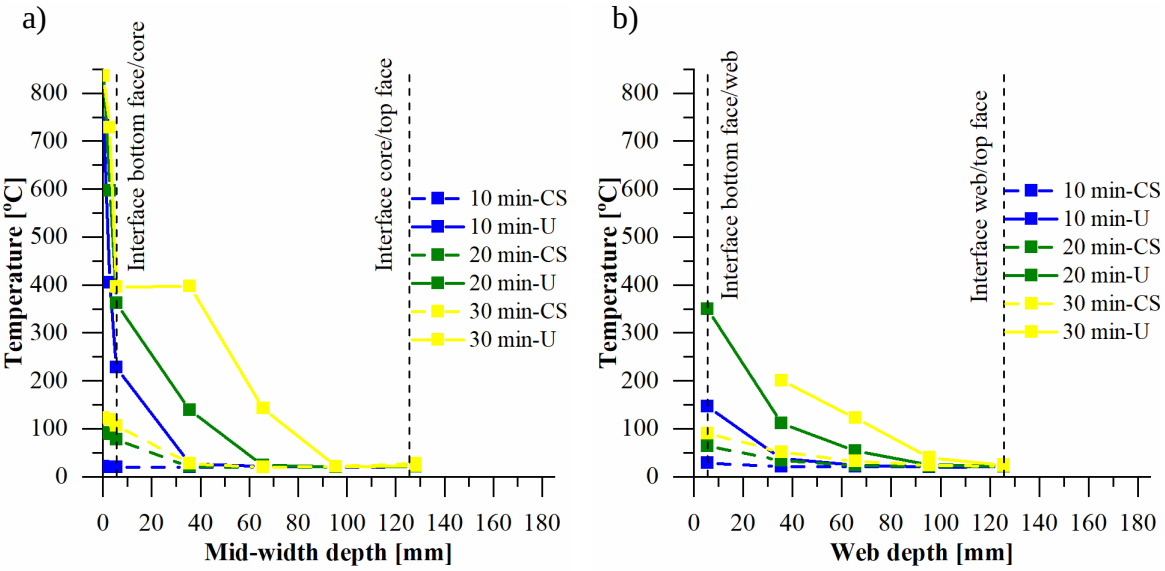

Figure 95 - Comparison between the temperature profile across the unprotected (U, i.e. PET-LW-U-1) and protected (CS i.e. PET-LW-CS-1) panel depths: (a) mid-width and (b) lateral web.

After 27 min (time of collapse of specimen PET-LW-U-1), the maximum temperature measured at the bottom GFRP face sheet of panel PET-LW-CS-1 was approximately 100 °C, well below its T_d and slightly below its T_g. At the end of the test, the maximum temperature attained at the bottom GFRP face sheet was around 400 °C, much lower than that measured in specimen PET-LW-U-1 for a shorter time of fire exposure.

For the intersection section of specimen PET-LW-CS-1, Figure 96 shows that the temperature *vs.* time curves followed a (qualitatively) similar pattern to those observed at the mid-span section, although the maximum temperature attained were lower in the former section.

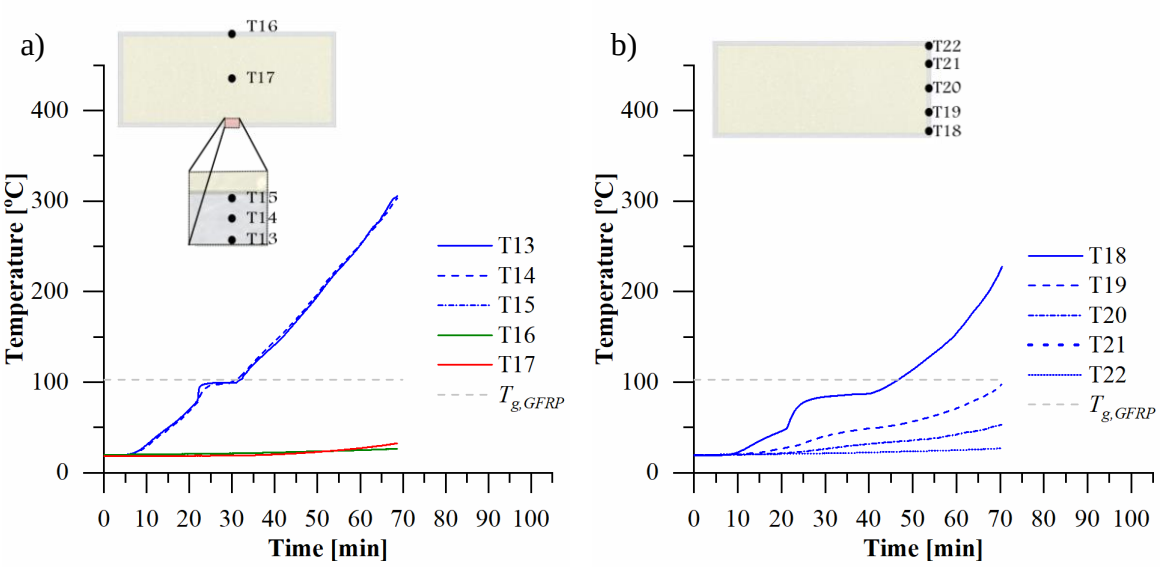

Figure 96 - Temperatures vs. time curves measured at the intersection section of specimen PET-LW-CS-1.

Figure 97 shows the thermal response of specimen PET-LW-AC-1 measured at the mid-span section.

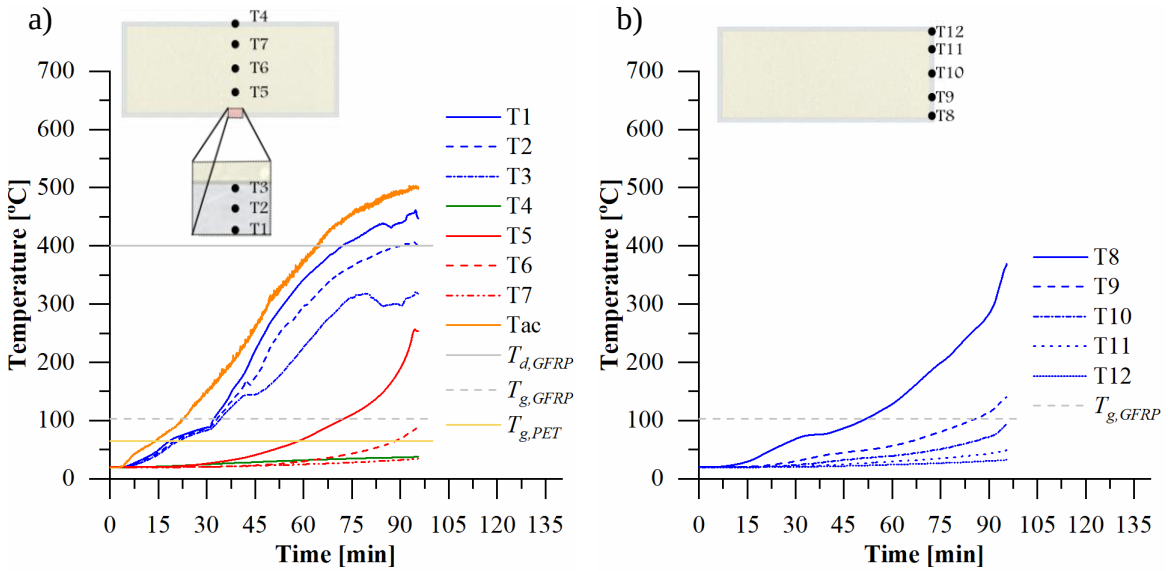

Figure 97 - Temperature profiles measured at the mid-span section of specimen PET-LW-AC-1.

As expected, the use of suspended CS boards as a passive fire protection greatly reduced the temperatures evolution, compared to the unprotected panel. As shown in Figure 97, the temperature measured in the air cavity (T_{ac}) increased almost linearly during most of the test duration, reaching a maximum temperature of about 500 ºC after 95 min of fire exposure. Similarly to what was observed for the specimens protected with an adherent CS boards, the temperatures at the bottom GFRP face sheet exhibited marked non-linearities after 30 min (at around 100 ºC); for longer durations of fire exposure, the temperatures increased at a higher rate, reaching a maximum temperature of 400 ºC (T2) at the end of the test. Regarding the temperatures in the core, the thermal behaviour was very similar to that observed in specimen PET-LW-CS-1, with temperatures remaining always lower than the T_d of the material (425 ºC). In general, the thermocouples placed in the core at depths from the

exposed face of 3.5 and 6.5 cm (T5 and T6) presented significant temperature increase, whereas that installed at the top part of the core (T7) presented minor temperature variation during the entire duration of the test. It is worth noting that the temperature at the top face sheet and across the support section remained roughly constant during the test. In what concerns the webs, for similar duration of fire exposure, the air cavity provided significant temperature reductions throughout its depth compared to both specimens PET-LW-U-1 and PET-LW-CS-1: at the end of the test, the maximum temperature measured at the bottom of the web (T8) was about 400 °C, similar to that observed in specimen PET-LW-CS-1, but for a longer duration of fire exposure (*cf.* Figure 97).

Figure 98 plots the temperatures measured at the intersection section as a function of the time of fire exposure in specimen PET-LW-AC-1. The evolution of the temperature at this section, although presenting lower magnitude, was qualitatively similar to that registered at the mid-span section. It is worth mentioning that thermocouple T15 was damaged during the manufacturing process of this panel; for this reason, it was not possible to assess the evolution of the temperature at the interface between the bottom GFRP face sheet and the core at the intersection section.

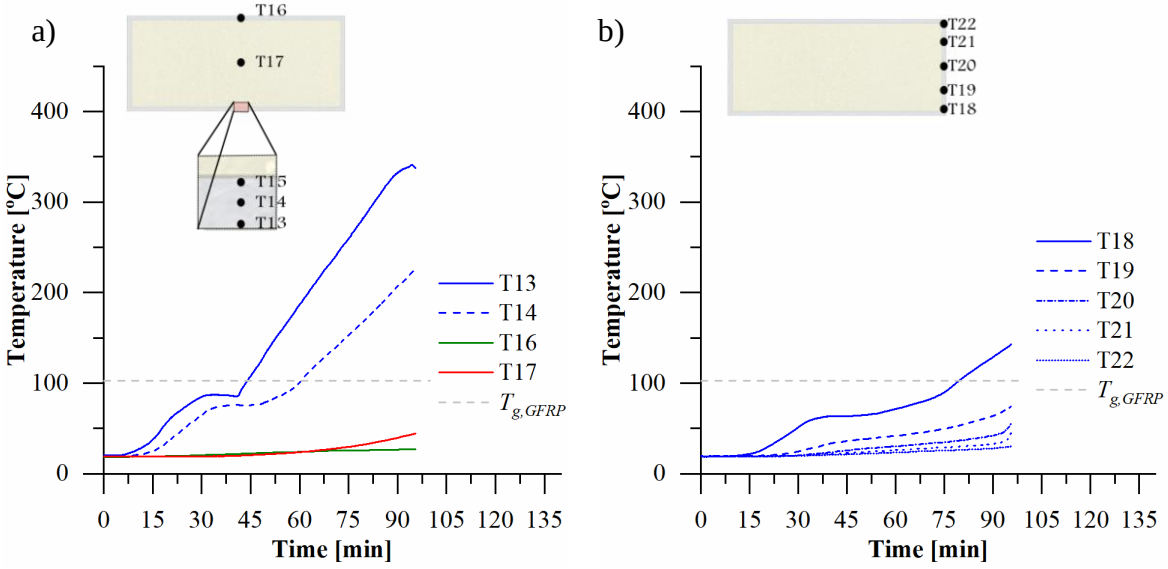

Figure 98 - Temperatures measured at the intersection section of specimen PET-LW-AC-1.

Figure 99 shows the temperature profiles measured in specimen PET-CW-U-1 at the mid-span and intersection sections.

Note that in the case of this panel, comprising a web at the centre of the cross-section, the thermocouples were placed in two different locations: (i) at the mid-width, along the web alignment (T1 to T7), and (ii) at a distance of 9 cm from such central web (T8 to T14). As expected, the temperatures measured in the bottom face sheet at distances from the exposed face of 0.25 mm (T1 and T8) and 2.8 mm (T2 and T9) followed a very similar pattern, with the T_g of the material being exceeded after ~4 min in thermocouples T1 and T8. It can also be seen that the temperature profile measured in the web at a distance from the hot face of 5.6 mm (T3), although presenting the same

qualitative pattern to that measured at the position of thermocouple T10, exhibited higher values. Concerning the temperatures in the web and core at a distance from the exposed face of 35.6 mm (T4 *vs.* T11), they presented a relatively small temperature increase until 20 min of fire exposure; then, the core (T11) exhibited an abrupt increase of temperature, which should be associated to the decomposition of the foam core located underneath such depth (at T10 the core reached the material T_d), and a final plateau when the foam turns into char residue.

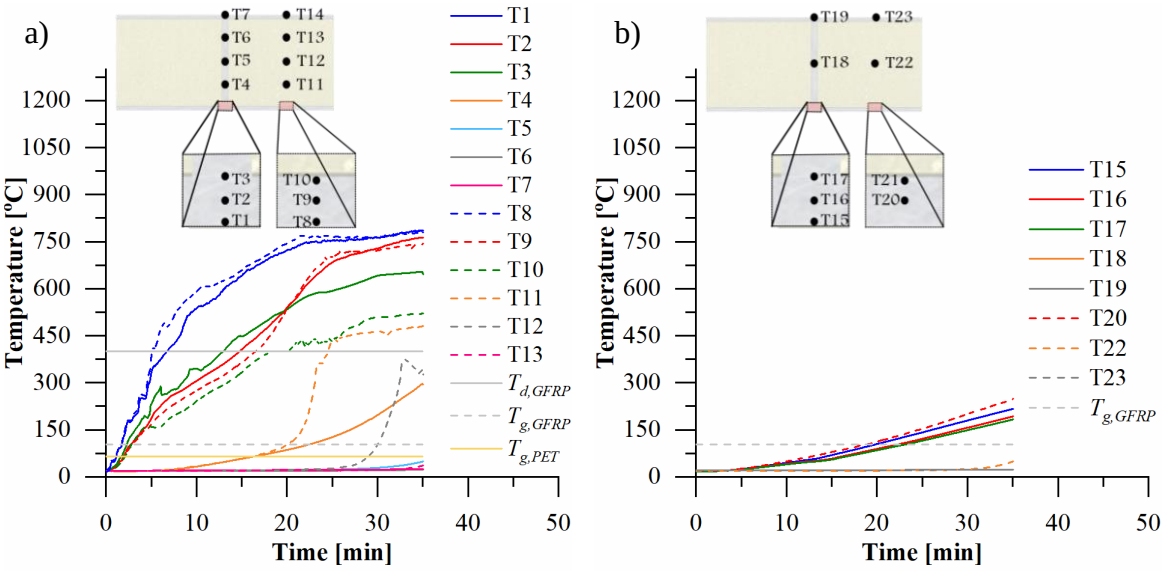

Figure 99 - Temperatures profiles for specimen PET-CW-U-1 measured at the: (a) mid-span and (b) intersection sections[5].

Figure 100 shows the temperature profiles in both the webs and foam of specimens PET-LW-U-1 and PET-CW-U-1 for different periods of fire exposure. It can be seen that, for the same duration of fire exposure, the temperatures across the core's depth of specimen PET-LW-U-1 are roughly similar to those of specimen PET-CW-U-1, although some differences are observed at a depth of 35.6 mm. This different thermal response of the core at that depth may be due to a non-fully effective lateral insulation of the specimen, that may have promoted the heat flow through the side of the panel; a similar result was found by Morgado [96] for multi-cellular GFRP panel with square tubular cross section. In this context, since the core of specimen PET-LW-U-1 was laterally covered by the webs, the inner volume of core was more insulated from the lateral heat flow, thus exhibiting lower temperatures compared to those of the web-core panel with the web positioned at the centre of the cross-section.

In what concerns the thermal response of the web of specimen PET-CW-U-1, when compared to specimen PET-LW-U-1, the temperatures were significantly lower, especially those at depths of 65.6 mm and 95.6 mm. Again, this result could be associated to the lateral heat transfer discussed above: it is possible that the outer surface of the webs of specimen PET-LW-U-1 were subjected to

[5] Note that a problem was encountered with thermocouple T21, not allowing the measurement of the temperature at the interface between the bottom GFRP face sheet and the core.

some heat along the lateral edges, whereas the web of specimen PET-CW-U-1 remained protected from lateral heat flow by the non-degraded volume of foam core.

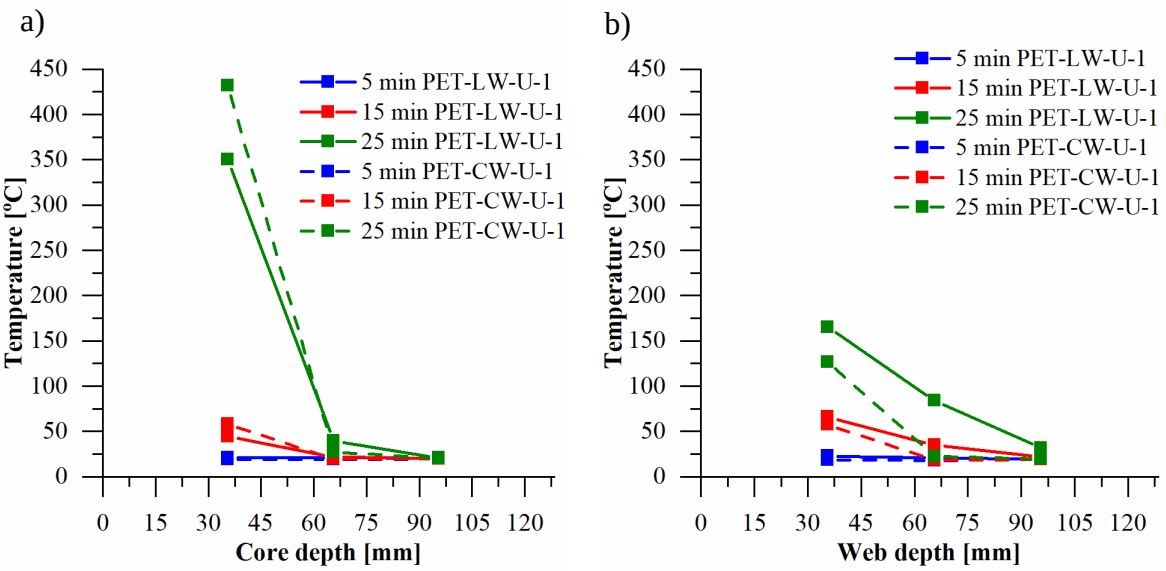

Figure 100 - Temperature profiles across the depth of the web-core panels for different periods of fire exposure: (a) core and (b) webs.

Figure 102 to Figure 105 show the temperature profiles for different durations of fire exposure (up to failure) at the mid-span section of representative homogeneous and web-core sandwich panels, either unprotected or protected with passive fire protection systems. For the web-core panels, the temperature profiles were measured across the depth of the panel in four relevant sections (*cf.* Figure 101): (i) mid-width, section A-A'; (ii) lateral web, section B-B'; (iii) central web, section C-C' and (iv) at a distance of 90 mm from the mid-width, section D-D'.

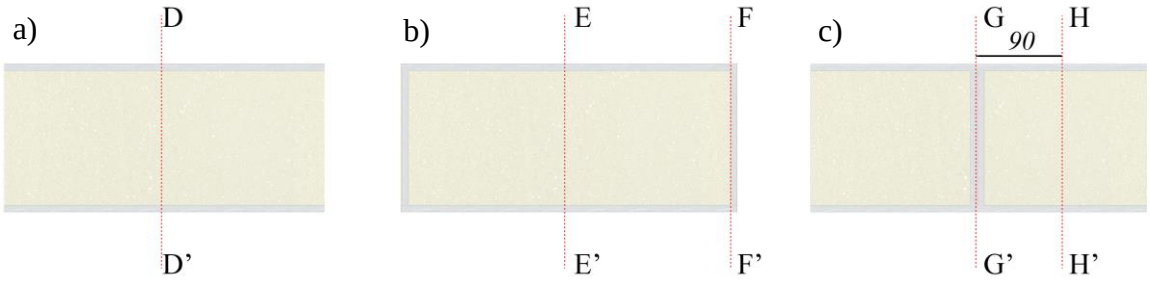

Figure 101 - Different sections for the web-core sandwich panels: (a) specimen PET-U; (b) specimen PET-LW and (c) specimen PET-CW.

For specimens PET-U-U-1 and PET-U-CS-1, Figure 102 shows that the bottom GFRP face sheet presented the highest temperature gradient across the depth of the mid-span section, while the top upper half of PET foam presented almost null thermal gradient, confirming its effectiveness in forming a thermal barrier before decomposition. As expected, the CS boards were effective in reducing the temperature evolution (or delaying the temperature increase) in the bottom face sheet.

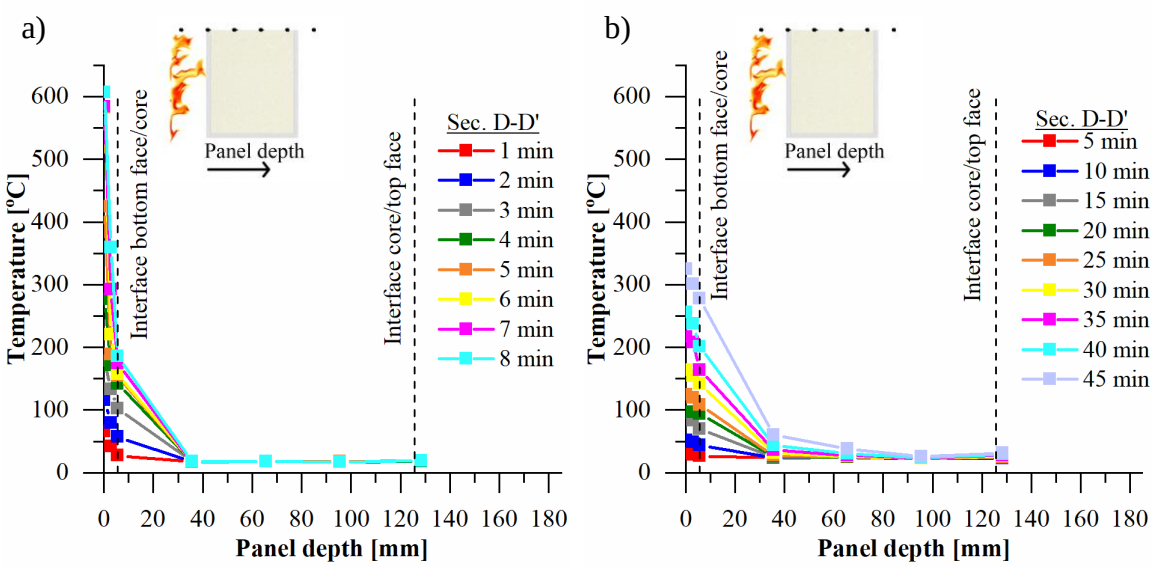

Figure 102 - Temperature profiles at the mid-span section for different periods of fire exposure: (a) PET-U-U-1 and (b) PET-U-CS-1.

For specimen PET-LW-U-1 and PET-CW-U-1, Figure 103 and Figure 104 show that, similarly to the unreinforced panels, the bottom GFRP face sheet presented the highest temperatures across the depth of the cross-section. Additionally, the lower part of the core also presented relatively high temperatures, especially if compared to panels PET-U-U-1 and PET-U-CS-1; this result is mainly due to (i) the much higher time of fire exposure compared to specimen PET-U-U-1, and (ii) the absence of fire protection system compared to specimen PET-U-CS-1. Figure 103b and Figure 104a shows the temperature profile across the web depth; as expected, temperatures decrease along the depth; in addition, almost null thermal gradients were observed in the top half of the web.

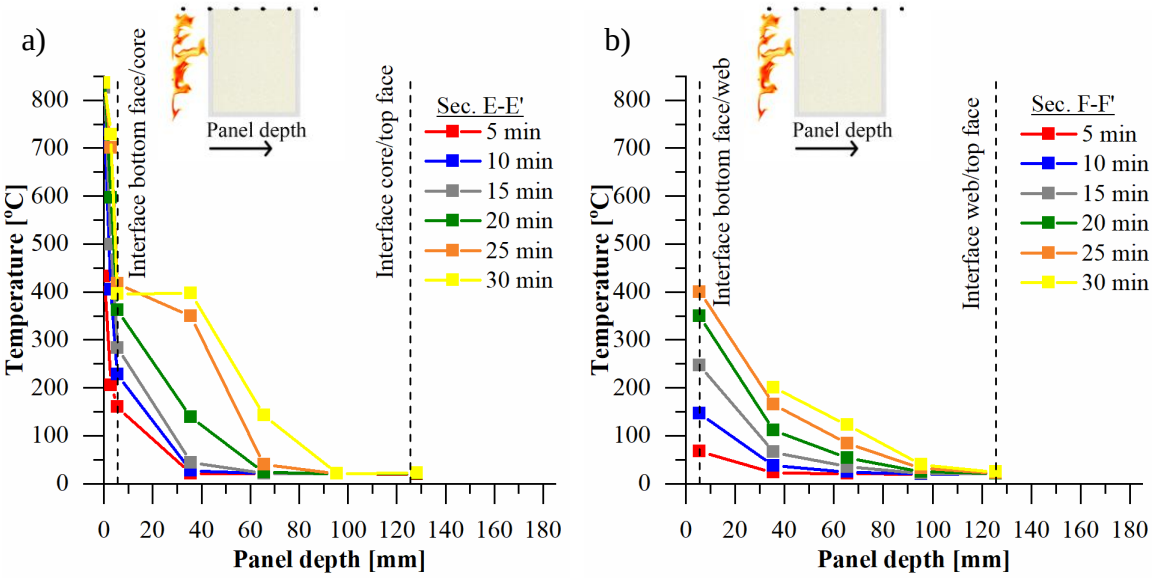

Figure 103 - Temperature profiles at the mid-span section of specimen PET-LW-U-1 for different periods of fire exposure: (a) section E-E' and (b) section F-F'.

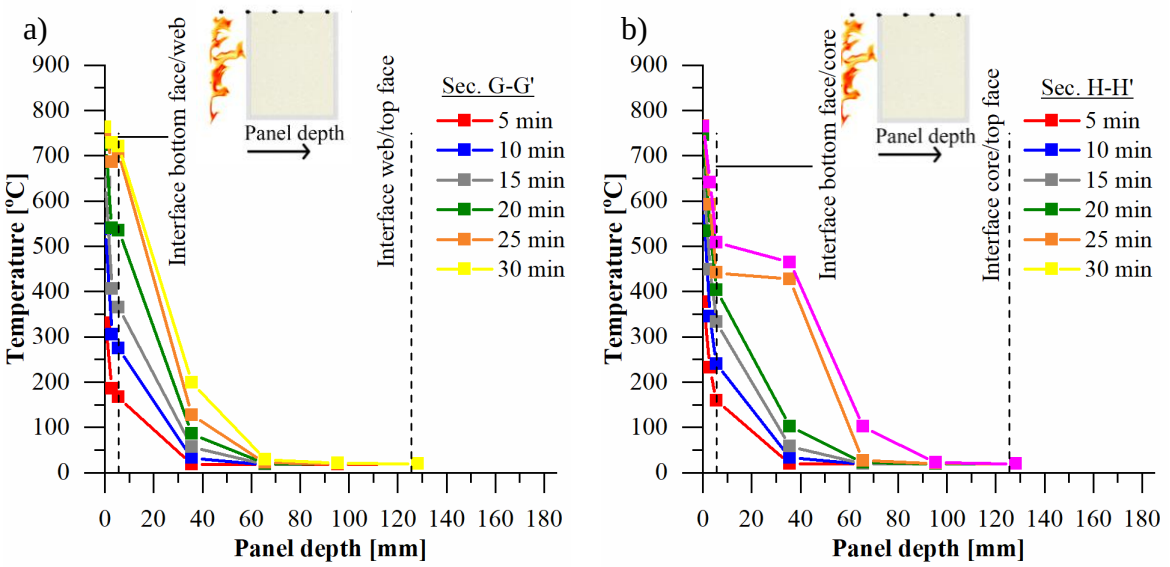

Figure 104 - Temperature profiles at the mid-span section of specimen PET-CW-U-1 for different periods of fire exposure: (a) section G-G' and (b) section H-H'.

For the two web-core sandwich panels protected with a passive fire protection system, Figure 105 and Figure 106 show that, although being exposed to fire for a much longer period of time compared to specimen PET-LW-U-1, the maximum temperatures attained across the depth of the web at failure were similar to those of the unprotected specimen, thus confirming the effectiveness of using passive fire protection in lowering the temperatures inside the panel. With the exception of the temperature measured in specimen PET-LW-CS-1 at a distance of 35 mm from the exposed face, the temperatures across the mid-width are lower than those measured at the web; this result could be due to some heat flowing through the outer surface of the webs.

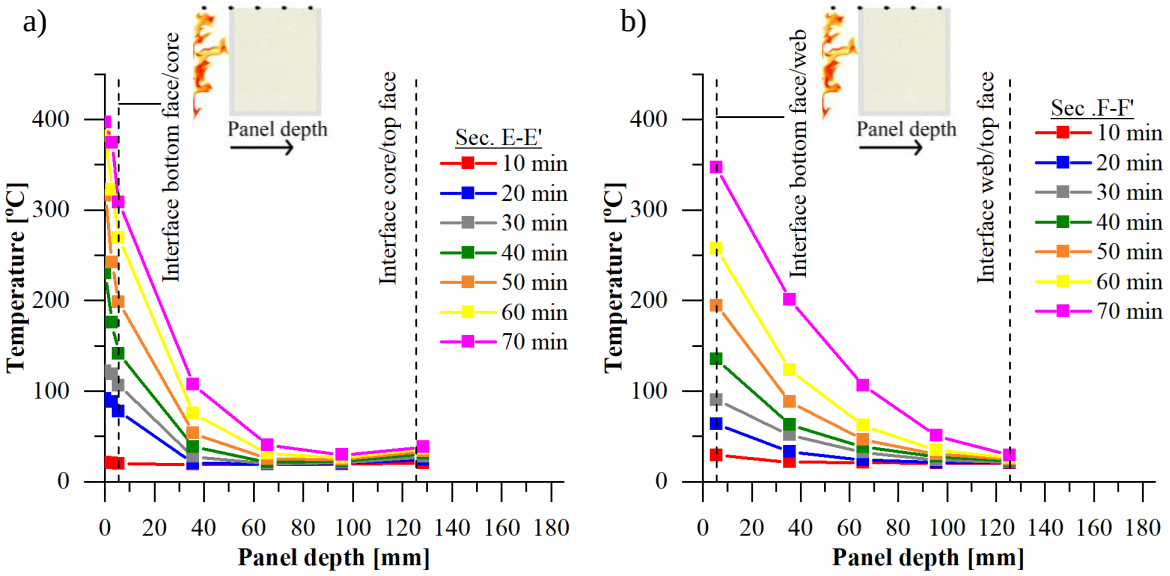

Figure 105 - Temperature profiles at the mid-span section of specimen PET-LW-CS-1 for different periods of fire exposure: (a) section E-E' and (b) section F-F'.

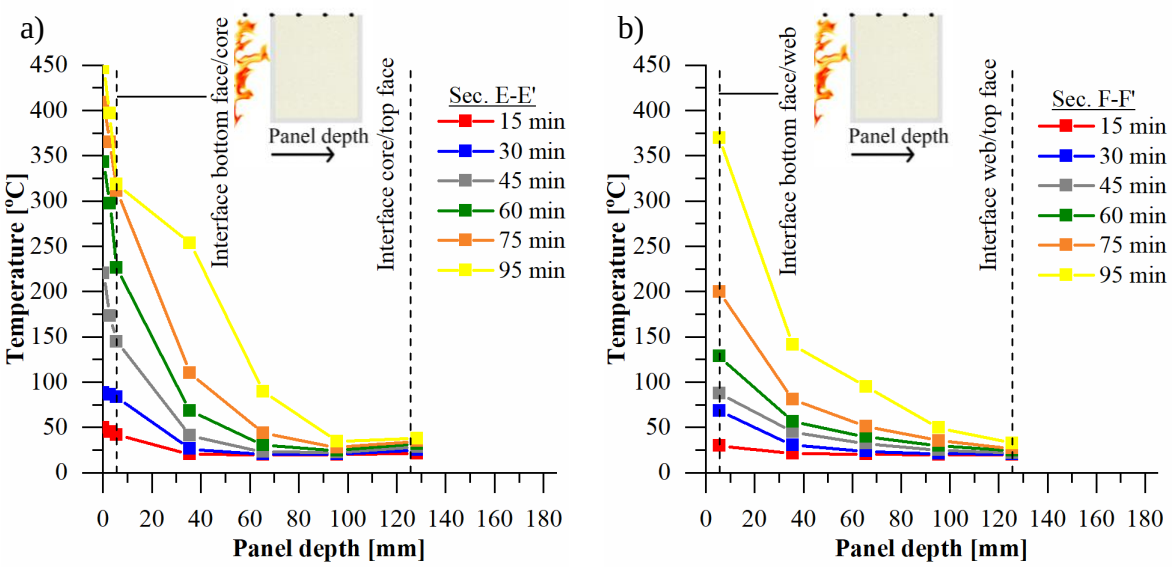

Figure 106 - Temperature profiles at the mid-span section of specimen PET-LW-AC-1 for different periods of fire exposure: (a) section E-E' and (b) section F-F'.

6.3.2 Mechanical response

Figure 107a presents the variation of the mid-span displacement of the homogenous-core panels (comprising either PET or PUR core foam) with the time of fire exposure. In general, all the unprotected panels presented a similar mechanical response, exhibiting deformation increase since the initial stage of the test, with a final steep increase of mid-span displacement - this initial behaviour is due to the thermal bowing caused by the thermal gradient installed in the cross-section depth and the reduction of tensile modulus experienced by the bottom GFRP face sheet at high temperature - the very low temperatures attained by the core caused negligible stiffness reductions. In this context, it can also be seen that the mid-span displacement of PET-U specimens increased at a higher rate compared to that of specimen PUR-U; this result could be related to the higher magnitude of the axial stresses applied in the bottom face sheet of the former panel.

Despite some relative differences up to 6 min of fire exposure, the mechanical behaviour of specimen PET-U-U-1 is qualitatively similar to that of specimen PET-U-U-2. These differences may stem from the different heating at the early stage of the tests; in fact at that stage, the ISO 834 presents a steep temperature increase, and the furnace temperature presents some deviations from the nominal time-temperature curve (but still within the admissible range defined in the ISO 834 standard).

Concerning the homogenous panels protected with CS boards adherent to the bottom face sheet (Figure 107b), as expected, the mid-span displacement rate was much lower than that observed in the corresponding unprotected panels, mainly due to the thermal insulation provided by the passive fire protection system, which reduced/delayed the temperature increase across the panel's depth. Both PUR-U-CS-1 and PET-U-CS-1 presented a similar mechanical response up to ~20 min of fire exposure. After this instant, the mid-span displacement increase rate of specimen PET-U-CS-1

started to be higher than that exhibited by the PUR-U-CS-1 panel, which may be explained by (i) the higher temperatures in the foam core of the former panel, and (ii) the fact that the shear modulus reduction with temperature of the PET foam is higher than that of the PUR foam, due to its lower T_g. However, after ~35 min of fire exposure, the PUR-U-CS-1 panel started presenting a significant increase of deflections. In this context, it is worth mentioning that the initial stress ratio (fire shear stress/shear strength before the thermal loading) in the homogeneous-PUR core panel is higher compared to that of specimen PET-U-CS-1. Additionally, as shown in Figure 107, the final increase of mid-span displacement of specimen PET-U-CS-1 was much faster compared to that observed in specimen PUR-U-CS-1. A possible explanation to this different behaviour may be related to the different failure mode of the specimens, as described in detail in the next section.

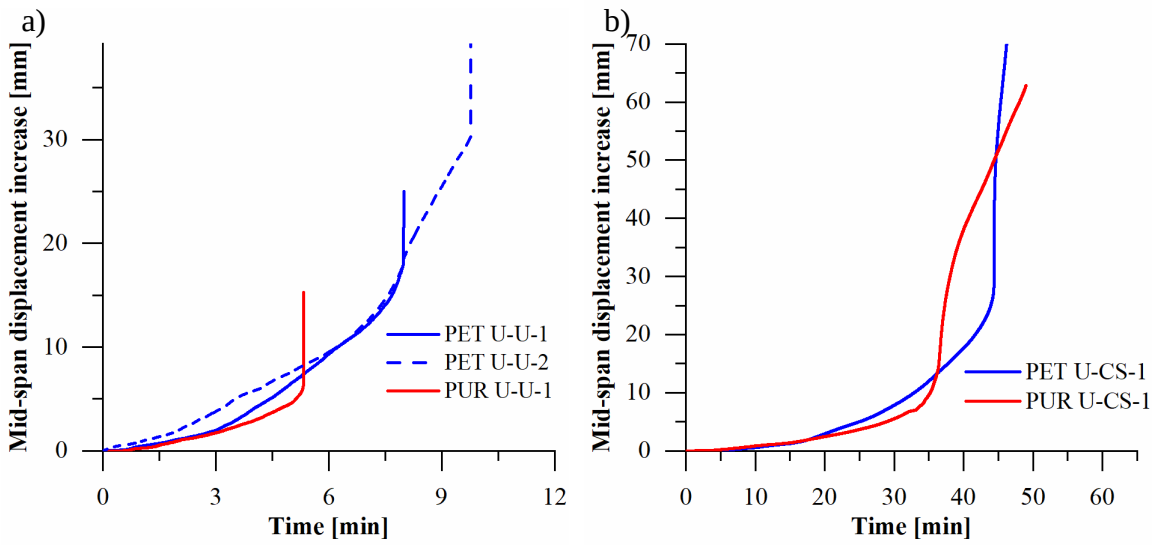

Figure 107 - Mid-span displacement increase vs. time curves of homogeneous sandwich panels: (a) unprotected and (b) protected specimens.

Figure 108 shows the mid-span displacement *vs*. time curves of the web-core sandwich panels, either unprotected or protected with passive fire protection systems. In general, the mid-span displacement increase of the unprotected web-core panels was qualitatively similar to that of the unprotected homogeneous panels (for similar duration of fire exposure); however, the former exhibited a significant improvement in terms of fire endurance, which is consistent with the higher stiffness provided by the presence of the longitudinal webs.

As expected, the web-core panels with passive fire protection systems presented a slower mid-span displacement increase (compared to the unprotected panels), thus confirming the effectiveness of the CS boards, used either as screen protection (in specimen PET-LW-CS-1) or as a suspended ceiling (in specimen PET-LW-AC-1) in delaying the thermal degradation. In particular, it is shown that the AC system was the most effective in improving the fire endurance of the GFRP panels; this result stems from the better insulation performance of the AC protection, compared to the adherent one. The results obtained in the present study are in line with those reported by Proença *et al*. [11] for

homogeneous- PUR core sandwich panels. As shown in Figure 108, all sandwich panels comprising composite webs at the panels' edges exhibited a sudden increase of mid-span displacement at the end of the test, which could be related to the loss of stiffness experienced by the webs at high temperature; in fact, when the T_g of the material is approached and exceeded, the webs are no longer able to transfer shear stresses across the panel's depth.

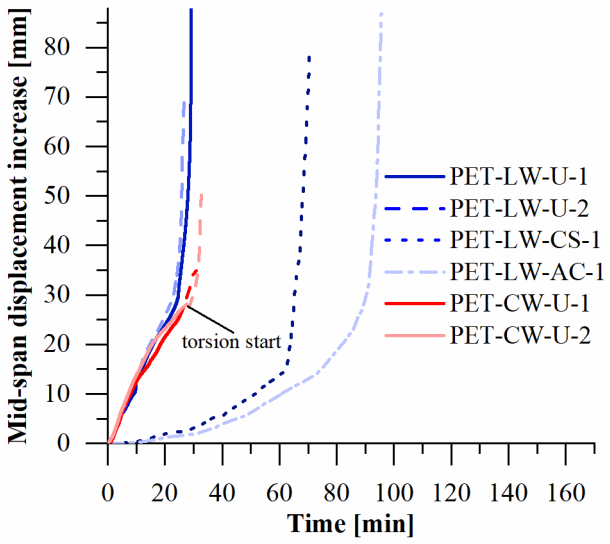

Figure 108 - Mid-span displacement increase vs time curves of web-core sandwich panels either unprotected or protected with passive fire protection systems.

Figure 108 also shows the mid-span deflection as a function of time measured in specimens PET-CW-U-1 and PET-CW-U-2, with webs at the centre of the panels. Comparing the mechanical response of the panels reinforced with webs positioned at the panels' edges or at their centre, roughly similar mechanical responses were observed until 30 min of fire exposure. However, after ~30 min of fire exposure, specimens PET-CW-U-1 and PET-CW-U-2 started to present torsional deformations and at a certain point they became unstable, and so their tests had to be prematurely interrupted.

6.3.3 Post-fire assessment

Figure 109 to Figure 118 show the thermal degradation experienced by the GFRP sandwich panels after the fire resistance tests. It is worth mentioning that the procedure to remove the specimens from the furnace took some minutes; for this reason, the figures shown below are not fully representative of the actual state of the panels immediately after failure.

As shown in Figure 109a, the collapse of specimen PET-U-U-1 seems to have been triggered at the top face sheet (between the loading points), which exhibited compressive failure, involving the crushing of the GFRP laminate (*cf.* Figure 109b). When the panel failed (in a brittle manner), the temperature at the centre of the bottom face sheet reached 350 °C (well above the T_g of the material, while the temperature at the GFRP bottom face sheet-core interface was about 175 °C. In this context, the degradation of this interface may have led to a change of the panel's structural behaviour from

beam type to arch-type, where the top and the bottom faces behaved respectively as a strut and a tie, with the non-degraded part of the core contributing to transfer the load from the top part of the panel to the support through an "arch effect". Despite the very high temperature reached by the bottom face sheet, no signs of tensile failure of the fibres were observed; the bottom face sheet presented only some signs of thermal decomposition (charring) of the polymeric matrix, which is consistent with the measured temperatures (roughly 600 ºC, above the T_d of the material). Note that the significant signs of thermal degradation observed at the top face sheet and at the core (*cf.* Figure 109a) occurred after the panel's collapse; indeed, at the end of the fire exposure, the thermocouples placed at the mid-span measured temperatures of about (i) 175 ºC at the interface between the bottom face sheet and the core and (ii) 20 ºC at a distance from the hot face of 35.6 mm (*cf.* Figure 88).

Figure 109 - Failure of specimen PET-U-U-1: (a) general view and (b) crushing of the GFRP laminate.

Figure 110 shows the homogenous-core panel comprising PUR foam (specimen PUR-U-U-1) after being exposed to fire for ~6 min.

Figure 110 - Failure of specimen PUR-U-U-1: (a) shear failure of the core and (b) debonding at the bottom face sheet/core interface.

The collapse of the panel seems to have been caused by two main failure mechanisms: (i) shear failure of the core, which exhibited a crack at approximately 45 º along the shear span of the panel (*cf.* Figure 110a); and (ii) delamination or failure at the interface between the core and the GFRP bottom face sheet (*cf.* Figure 110b), which was associated to the thermal degradation of that interface. Unfortunately, mainly due to the limitation of the test setup, which did not allow to observe the panel during the fire exposure (only the top part of the specimen was visible), it was not possible to identify

the primary failure mechanism. It is worth noting that unlike specimen PET-U-U-1, specimen PUR-U-U-1 probably kept its beam-type response until the end of the test: in the latter specimen a lower temperature was attained at the interface between the core and the GFRP bottom face sheet (150 ℃ *vs.* 175 ℃). Finally, the bottom face sheet presented significant thermal degradation (maximum temperature attained of 600 ℃, above the T_d of the GFRP material), but, as in specimen PET-U-U-1, no signs of tensile failure were observed.

Figure 111 shows the homogenous-core panel comprising PUR foam protected with CS board adherent to the exposed face (PUR-U-CS-1) after the fire resistance test.

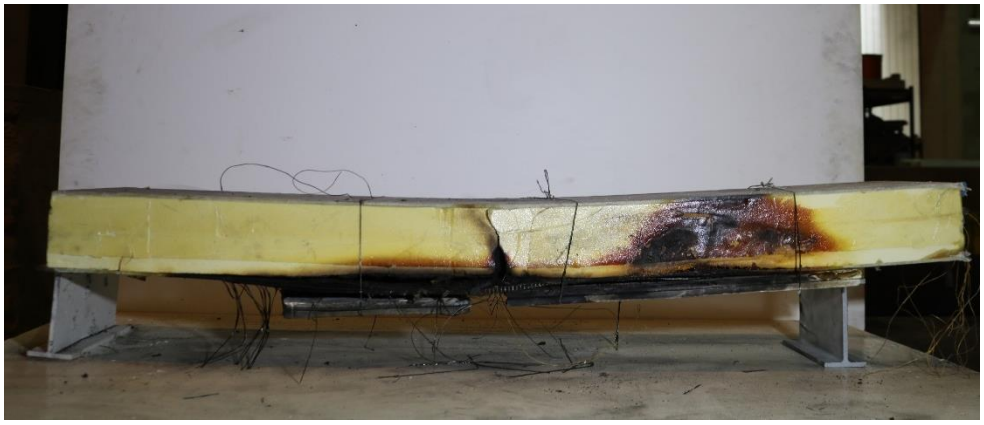

Figure 111 - Failure of specimen PUR-U-CS-1.

As shown in Figure 112, the collapse of the panel seems to have been caused by various failure mechanisms, involving (i) bending failure of the core (between the loading points) and (ii) GFRP-core delamination failure.

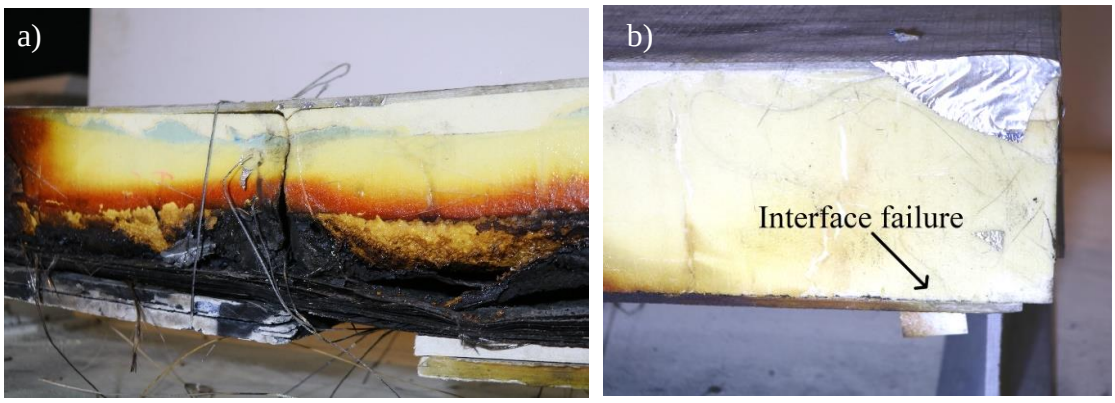

Figure 112 - Failure mode details of panel PUR-U-CS-1: (a) bending failure of the core and (b) debonding at the GFRP-core interface.

Again, it was not possible to identify which failure mechanism occurred first. In this case, at failure, the temperatures at the GFRP-core bottom interface and at a distance from the hot face of 35.6 mm reached respectively 300 ℃ and 190 ℃ (*cf.* Figure 90); for this reason, it is reasonable to assume that due to its thermal degradation the core was no longer able to transfer shear stresses across the panel's depth and an arch system may have developed, as also described for specimen PET-U-U-1.

It is also relevant to note that unlike the unprotected panels, the bottom face sheet of specimen PUR-U-CS-1 never attained the T_d of the material: the combustion of the GFRP bottom face sheet occurred only after the collapse.

In what concern the homogenous-PET panel protected with CS boards adherent to the exposed face (PET-U-CS-1), the failure mode (*cf.* Figure 113) was different to that observed in specimen PUR-U-CS-1. During the post-fire assessment, neither shear/bending failure of the core nor bond failure at the GFRP-core interface were observed. As explained next, a different local failure mechanism under the loaded sections probably occurred.

Figure 113 - Post-fire assessment of specimen PET-U-CS-1.

Figure 114 illustrates the specimen after the collapse (still loaded): the figure shows that the panel appears to be significantly bent, apparently due to the local failure of the core under the loading points due to crushing and/or shear, with no visible crushing of the top face sheet. It is worth mentioning that since the top face sheet remained almost undamaged (the maximum temperature attained was 25 °C), the panel recovered most deformations after unloading.

Figure 114 - Specimen PET-U-CS-1 aspect after collapsing.

The typical failure mode observed in web-core panels, either unprotected or protected with passive fire protection systems, is illustrated in Figure 115.

Figure 115 - Failure of specimen PET-LW-CS-1.

The loss of structural effectiveness of the panels seems to have been triggered by (i) the compressive failure of the top face sheet under the loading point, together with (ii) the transverse compressive failure of the webs (*cf.* Figure 116a) - a similar failure mode was observed at room temperature (*cf.* Chapter 5). In addition, a winkling failure due to in-plane shear or compression was also observed at the bottom part of the webs (between the support and the intersection section, *cf.* Figure 116b.

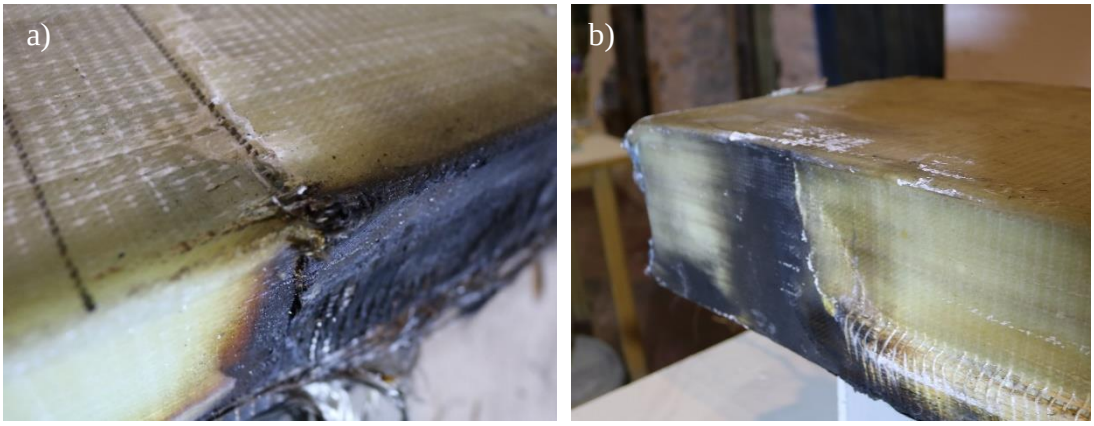

Figure 116 - Failure mode details of panel PET-LW-CS-1: (a) compressive failure of top face sheet/web under the loading point and (b) wrinkling at the bottom part of the web.

As mentioned above, it was not clear which of these failure mechanisms triggered the collapse of the panel PET-LW-CS-1. It is also relevant to note that, similarly to the homogeneous-core panels, the tensile failure of the bottom face sheet never occurred. As expected, in the web-core panels protected with calcium silicate, either bonded to the bottom face sheet or forming an air cavity, the loss of structural effectiveness (*i.e.* reduction of the webs residual section) was delayed, compared to specimen PET-LW-U-1. For all the panels tested, at the collapse instant, the bottom part of the webs reached temperatures well above the T_g of the material (roughly 400 °C); and, therefore, their contribution to the stiffness of the panel was significantly reduced - details of the residual cross-section at the mid-span section are depicted in Figure 117.

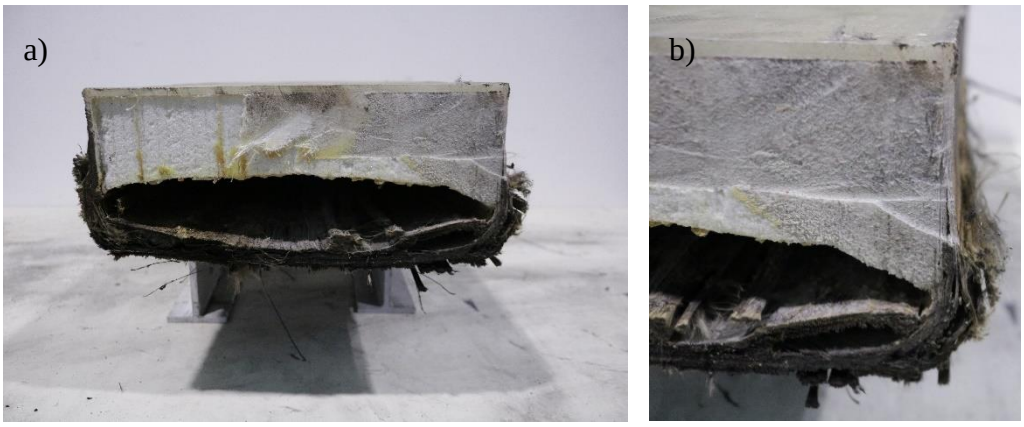

Figure 117 – Mid-span cross-section of specimen PET-LW-U-1 after the fire resistance tests.

As mentioned in section 6.3.2, for safety reasons, the fire resistance tests of specimens PET-CW-U-1 and PET-CW-U-2 were stopped before reaching the collapse of the specimens. During the post-fire assessment, significant thermal degradation of both core and bottom face sheet were detected; however, no signs of failure, neither of the core nor of the GFRP, were observed (*cf.* Figure 118).

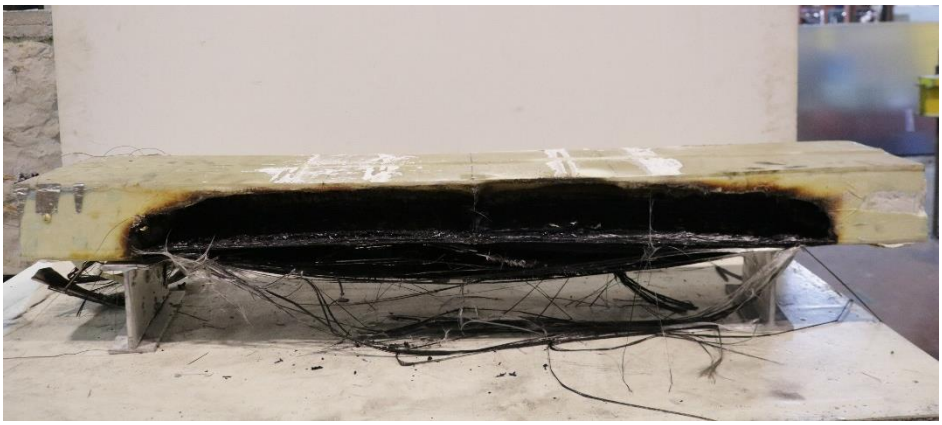

Figure 118 - Post-fire assessment of specimen PET-CW-U-1.

6.3.4 Fire resistance

The fire resistance of a structural member is its ability (i) to maintain an adequate load-bearing performance without collapsing or exceeding certain deformation criteria and, when applicable, (ii) to meet adequate insulation and integrity requirements, maintaining its separating function.

In accordance with the current European standard EN 1363-1 [83], to define the load-bearing performance, besides the structural collapse, the two following deformation criteria should be considered: (i) the maximum deformation, *D*, and (ii) the maximum deformation increase rate, *dD*/*dt*, defined as follows:

$$D = \frac{L^2}{400d} \tag{21}$$

$$\frac{dD}{dt} = \frac{L^2}{9000d} \tag{22}$$

where L and d are respectively the panel's span and height (expressed in mm). For the sandwich panels studied in this work, the deformation limits (calculated using the equations reported above) were set as D =37.5 mm and dD/dt=1.65 mm/min. It is worth mentioning that, according to the recommendation of EN 1363-1 [83], the deformation increase rate is not applicable within the first 10 min of the fire resistance tests.

Table 28 indicates the time to collapse t_{col}, and the time to exceed the maximum deformation t_{dl} and the maximum increase rate t_{irl}, together with the fire resistance class achieved by all specimens tested. Table 28 shows that the time to collapse of the sandwich panels ranged from 5 to 96 min depending on the type of panel geometry and fire protection system.

Table 28 - Fire resistance tests summary

Specimen ID	t_{col} [min]	t_{dl} [min]	t_{irl} [min]	Fire resistance class
PET-U-U-1	8	n.a[6]	n.a	
PET-U-U-2	9	n.a	n.a	
PET-U-CS-1	48	46	46	REI 45
PUR-U-U-1	5	n.a	n.a	
PUR-U-CS-1	46	40	35	REI 30
PET-LW-U-1	29	23	25	REI 15
PET-LW-U-2	27	25	25	REI 15
PET-LW-CS-1	70	67	62	REI 60
PET-LW-AC-1	96	92	91	REI 90

As shown in Figure 119a, the time to collapse of the unprotected homogeneous-core panels was very low (from 5 to 10 min), being far beyond the minimum load-bearing (R) requirement defined in most design codes – this shows that it is not possible to use this type of homogeneous-core sandwich panels without fire protection in buildings. For all the panels tested, the temperature measured at the top face sheet was always below 30 °C, thus meeting the insulation (I) requirement, which is concerned with the maximum temperature of the unexposed face (no more than 140 °C). Finally, all the panels fulfilled the integrity (E) requirements; in fact, no spread of flames and/or smoke through the unexposed face was observed.

As discussed in the previous sections, the fire performance of the homogenous-core panels was remarkably improved when using CS boards as screen protection: specimen PET-U-CS-1 exceeded both deformation limits after 46 min, while specimen PUR-U-CS-1 exceed the maximum deformation and deformation increase rate limits after 40 min and 35 min, respectively (*cf.* Figure 119b). The fire resistance class, defined following the criteria of EN 1363-1, was set as REI 45 for specimen PET-U-CS-1 and REI 30 for specimen PUR-U-CS-1. These fire resistance classes do not comply with the corresponding requirements set in several building codes, which define a minimum REI of 60 min for multi-familiar residential buildings with height from 9 m to 28 m [97,98].

[6] In some case, the maximum deformation and the maximum deformation increase rate criteria were not attained; n.a.- not attained

However, it would be possible to use such panels in smaller buildings, with heights up to 9 m, *i.e.* with up to 2 to 3 storeys.

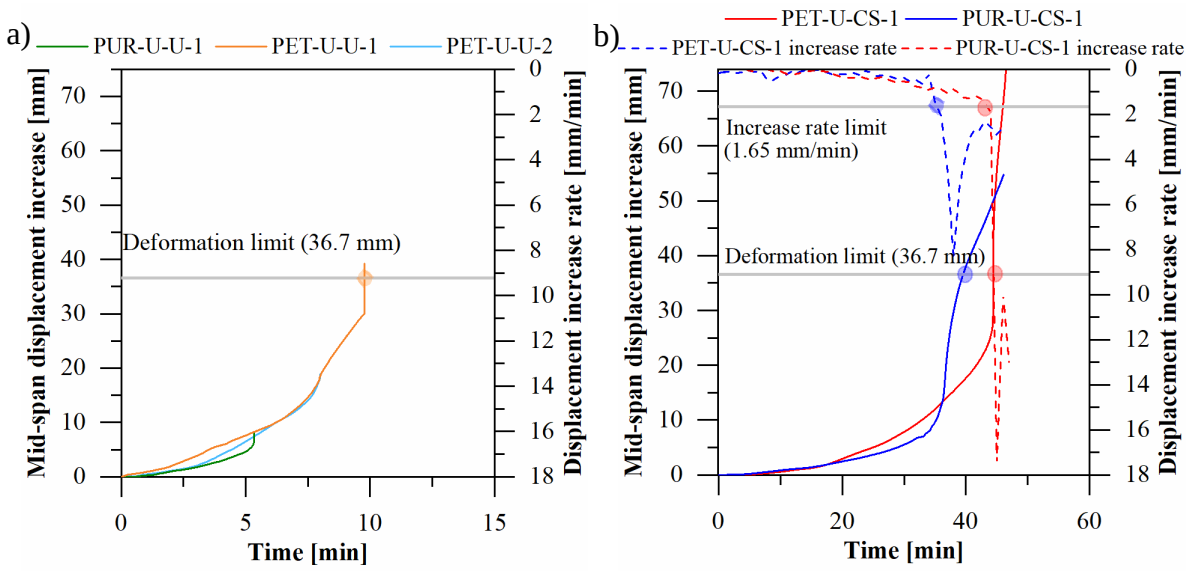

Figure 119 - Deformation limits for the load-bearing capacity of homogeneous core panels: (a) unprotected and (b) protected panels.

In what concern specimens PET-LW-U-1 and PET-LW-U-2, the results obtained point out that reinforcing the panel with longitudinal webs provides a significant increase of fire endurance compared to homogenous-core panels. Both specimens PET-LW-U-1 and PET-LW-U-2 exceeded the deformation limits after about 25 min of fire exposure (R15), thus not achieving the fire resistance class REI 60 (*cf.* Figure 120a).

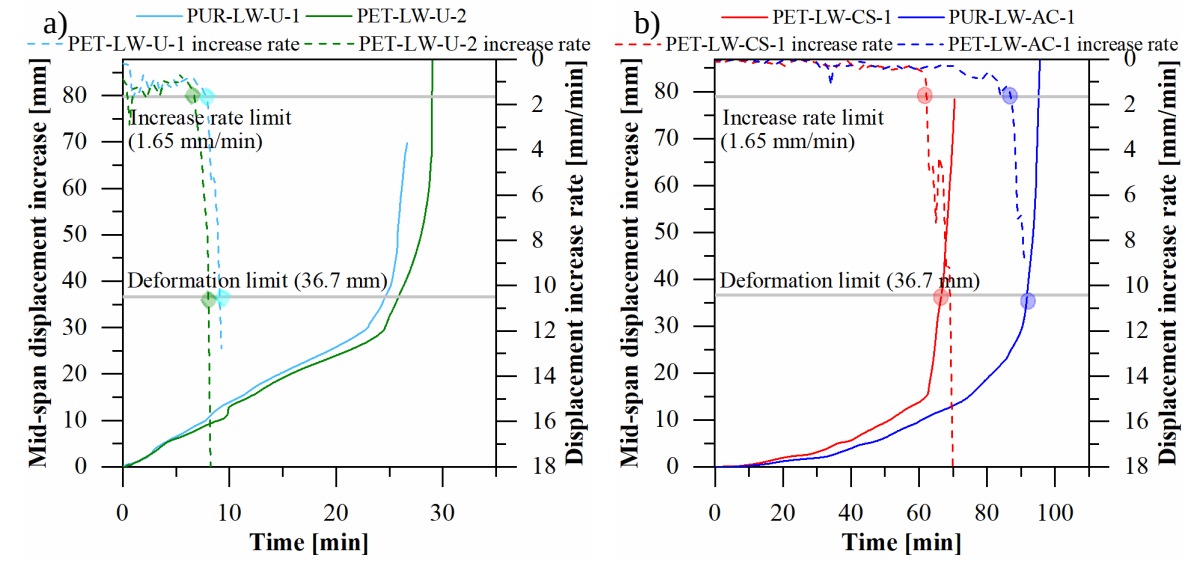

Figure 120 - Deformation limits for the load-bearing capacity of web-core panels: (a) unprotected and (b) protected panels.

As for the homogeneous-core panels, the use of CS boards, either suspended or adherent to the bottom surface, provided a noticeable increase of the fire resistance, compared to the unprotected panels: the fire resistance class increased from REI 15 to REI 60 and REI 90 min in specimens PET-

LW-CS-1 and PET-LW-AC-1 (*cf.* Figure 120b), respectively; thus guaranteeing compliance with the building fire resistance requirements applicable for a large portion of buildings. Based on the results obtained, the passive fire protection system with CS boards suspended and forming an air cavity was the most effective in increasing the fire performance of the panel, achieving the highest fire resistance class (REI 90). Therefore, the use of suspended CS boards is also suggested to be used for homogeneous panels in an attempt to meet the minimum fire resistance requirements.

6.4 CONCLUDING REMARKS

This chapter presented the results of a comprehensive experimental study about the fire resistance behaviour of GFRP sandwich panels, where the influence of various parameters, such as different panel's geometry (homogeneous-core *vs.* web-core panels), core materials (PET and PUR foams) and passive fire protection systems was assessed. Based on the results obtained, the following conclusions can be drawn:

- The temperature gradient across the depth of the sandwich panels was not constant; as expected, the bottom GFRP face sheet, directly exposed to fire, always presented the highest values, while the top face sheet exhibited almost no temperature increase mainly due to excellent insulation properties of the underlying volume of core material. It is worth mentioning that only a relatively low thickness of the bottom part of the foams decomposed during the tests. For all the panels tested, the insulation and integrity requirements set in the European regulation were satisfied.
- The homogenous-core panels presented very poor fire resistance performance (lower than 15 min), not achieving the minimum load-bearing requirements set in building codes. Significant improvements were achieved by using CS boards as a screening protection: when protected with passive fire protection systems, both PUR and PET homogeneous panels achieved fire resistance classes REI 30 and REI 45, respectively. However, none of these protected panels was able to fulfil the fire resistance threshold of 60 min, usually required by residential buildings with more than 9 m of height.
- By adding lateral webs, the fire endurance of the sandwich panels significantly increased (compared to the homogeneous-core ones) and this was attributed to the higher shear stiffness (and strength) provided by the GFRP webs. The unprotected web-core specimens collapsed after 28 min (REI 15), while the panels protected either with adherent or suspended CS boards collapsed after respectively 75 min (REI 60) and 96 min (REI 90), thus meeting the above-mentioned fire resistance requirement.

- For all the web-core sandwich panels tested, the failure mode was consistent, involving longitudinal compressive failure of the top face sheet and transverse compressive failure of the webs. In what concern the homogeneous-core panels, at least one of the following failure modes were observed: shear or bending failure of the core, delamination between the bottom GFRP face sheet and the core and compressive failure of the top face sheet.

CHAPTER 7

NUMERICAL SIMULATION OF THE FIRE BEHAVIOUR OF GFRP SANDWICH PANELS

7.1 INTRODUCTION

Modelling the thermal response of GFRP members in fire requires the consideration of the material temperature-dependent thermophysical properties (density, specific heat capacity and thermal conductivity) and appropriate boundary conditions, including heat conduction, convection, and radiation. A limited number of studies were developed in the past decade to model the thermal response of GFRP materials and components (*e.g*., [99–101]).

A numerical study focusing on the thermal behaviour of pultruded GFRP profiles was carried out by Morgado *et al*. [100]. Two-dimensional (2D) and three-dimensional (3D) models were developed to simulate the thermal response of GFRP tubular profiles exposed to the ISO 834 fire curve, considering the thermophysical properties as a function of temperature of the GFRP material, defined as suggested by Bai *et al*. [72]. In this study, the authors considered the heat transfer due to conduction, radiation and convection. The results obtained highlighted the importance of considering the contribution of convection and internal radiation within the cavity of tubular sections to the heat-transfer problem, as the accuracy of the results was seen to depend on the consideration of those phenomena, especially the latter. Despite the complexity involved and the several assumptions considered, the predicted temperatures presented a good agreement with the experimental data, thus confirming the suitability of the methodology used to provide accurate temperature predictions. The FE models also confirmed the effectiveness of CS boards (adherent to the bottom face sheet) and of an internal water-cooling system in reducing the temperature in the tubular profile.

The modelling of the mechanical response of GFRP structural members in fire has mostly been studied for marine and aerospace applications (*e.g.*, [9,10,14]); for civil engineering applications, previous research is very limited (*e.g*., [15,102–104]).

Luo *et al.* [9] developed a 3D numerical model to study the thermomechanical behaviour of GFRP homogeneous balsa core sandwich panels simultaneously subjected to in-plane compressive loading and one-side heat exposure. In this study, the GFRP material was modelled using a temperature-dependent orthotropic linear elastic model, while the mechanical properties of the balsa core were

assumed temperature-independent. In addition, a cohesive model with traction-separation capabilities was used to predict the delamination failure between the face sheet and the core. The numerical results obtained were then compared with experimental data. Overall, the FE models were able to provide good results, both in terms of temperature evolution and time-to-failure. Furthermore, the cohesive model considered in the simulation was able to predict the delamination failure at the interface between the GFRP laminate and the balsa core observed in the experiments.

A numerical study addressing the fire behaviour of GFRP homogeneous balsa core sandwich panels under in-plane loading was conducted by Feih *et al.* [10]. First, a one-dimensional (1D) thermal analysis was performed using the thermal model developed by Henderson *et al.* [105], which considers the heat transfer due to conduction and mass transport of decomposed gases in the through-thickness direction. Then a mechanical model was developed considering the laminate theory and temperature-dependent material properties. The temperature profiles measured in the experiments were then compared to those provided by the thermal model, which proved to be accurate. In what concerns the mechanical model, a good agreement was obtained in terms of time-to-failure (determined by comparing the compressive strength of the GFRP face sheet with the compressive stress); from the results obtained, the authors found out that the time-to-failure increases with the GFRP face sheet thickness.

Yu and Zhou [14] presented similar numerical procedures to those adopted by Luo *et al.* [9] and Feih *et al.* [10] aiming at evaluating the fire behaviour of GFRP sandwich panels with balsa core exposed to fire in one side and subjected to in-plane compressive loading. For both thermal and mechanical analysis, the authors considered temperature-dependent material properties. In this study, the (compressive) kinking of the GFRP face sheet (directly exposed to heat) was considered as the main failure mechanism; in this context, the time-to-failure was predicted by comparing the compressive stress with the compressive strength of the material. In addition, aiming at simulating the effect of delamination, a cohesive model with a traction-separation capabilities was used to simulate the interaction between the core and the face sheets. The numerical results obtained were then compared with the test data. In general, a good agreement was obtained in terms of deflection and structural response, while the prediction of the temperatures presented some differences compared to the experimental results, probably due to uncertainties regarding the temperature-dependent thermophysical properties of the materials. Finally, the authors found that the mechanical behaviour of GFRP sandwich panels under in-plane loading is mostly governed by their resistance to buckling.

Keller *et al*. [15] developed a 3D model using the software *ANSYS* to simulate the mechanical behaviour of pultruded GFRP multi-cellular sandwich panels (without foam in-fill) exposed to the ISO 834 fire curve on the bottom face sheet. The numerical study evaluated the thermomechanical response of sandwich panels either unprotected or protected with an internal water-cooling system. It is worth mentioning that all materials were modelled using temperature-dependent mechanical and

thermophysical properties. Concerning the protected panel, the results obtained from the mechanical simulations were in line with those observed in the experiments, presenting some differences, which were attributed to the simplifying assumptions made, including the variations with temperature of the axial modulus of the GFRP materials (assumed identical in both tension and compression). Regarding the unprotected specimen, the FE models overestimated the mid-span deflection increase. According to the authors, this result should be related to some limitations of the thermal model (namely of the boundary conditions in the cavities of the cross-section), which was not able to capture accurately the temperature increase at the top face sheet.

The literature review reported above shows that the number of numerical studies about the thermal and mechanical responses of GFRP sandwich panels under fire are still very limited. In addition, according to the best of the author's knowledge, no comprehensive studies were reported about the numerical simulation of the fire behaviour of foam-filled sandwich panels subjected to bending. A key limitation that was found in the literature is the uncertainty about the temperature-dependent material (thermal and mechanical) properties; in fact, the lack of such input data prevents the numerical simulation of the thermal and mechanical responses of sandwich panels subjected to fire with good accuracy.

This chapter presents a numerical study that aimed at providing a better understanding about the thermomechanical response of GFRP sandwich panels, by means of both thermal and mechanical simulations. The main objectives were two-fold: (i) to evaluate the influence of different core materials, panel architecture and passive fire protection systems on the fire response of sandwich panels; and to (ii) provide a better understanding about the evolution of the stress fields in the panels (not possible to measure in tests) with the time/temperature increase. The information reported in this chapter and the numerical models developed herein can be used as supporting tools to the fire design of sandwich panels for building applications, allowing the optimisation of the panel's geometry and the development of passive fire protection systems. It is worth mentioning that the results obtained with the models are validated from the comparison with experimental data presented in Chapter 6.

7.2 DESCRIPTION OF THE NUMERICAL MODELS

7.2.1 FE model labelling, geometry and type of elements

The mechanical and thermal response of six sandwich panels subjected to fire was simulated using the commercial package *ABAQUS*. Each specimen is labelled according to the following nomenclature: (i) core material (PET or PUR); (ii) cross-section (U – unreinforced/homogeneous-core; LW – reinforced with lateral webs), and (iii) fire protection (U – unprotected; CS – adherent CS boards; AC – suspended CS boards). The labelling of the FE models is reported in Table 29

(coincident with the nomenclature of tested specimens adopted in chapter 6 – *cf.* Table 24), which also includes the geometry, the duration of the fire exposure (coincident with the time to "experimental failure"), the applied load and the consideration of damage in the constituent materials (foam and GFRP – more details about the material models are provided in the next section).

Table 29 – Labelling of the FE models

Specimen ID	Geometry	Duration [min]	Load level [kN]	Foam damage	GFRP damage
PET-U-U	2D	8	18	Yes	No
PET-U-CS	2D	48	18	Yes	No
PUR-U-U*	2D	5	-	-	-
PUR-U-CS*	2D	46	-	-	-
PET-LW-U	3D	29	38	No	No
PET-LW-AC	3D	96	38	No	No

*Only thermal models were developed

As reported in Table 27, 2D FE models of the sandwich panels with homogeneous-PET core were developed aiming at simulating the thermal and mechanical response under fire of the tested specimens. Concerning the numerical simulations of the homogeneous-PUR sandwich panels, as detailed ahead in section 7.2.2, only the thermal response was modelled.

For both thermal and mechanical models, taking advantage of symmetry simplifications, only half of the panel's length was modelled to reduce the computational effort. The unprotected panels as well as the panels protected with CS boards were discretized using 4-node isoparametric plane quadrilateral elements: DC2D4 elements were used for the thermal analysis, whereas CPS4 elements were considered for the mechanical analysis. After performing a preliminary mesh sensitivity study, a mesh size of about 10 × 10 mm^2 was selected for the foam, while the GFRP material and CS boards were discretized using elements with an approximate size of 2 × 10 mm^2 (*cf.* Figure 121). For the unprotected panels, these mesh sizes involved 1370 elements and 1640 nodes; while for the protected panels, the number of elements and nodes considered was 1515 and 1820, respectively.

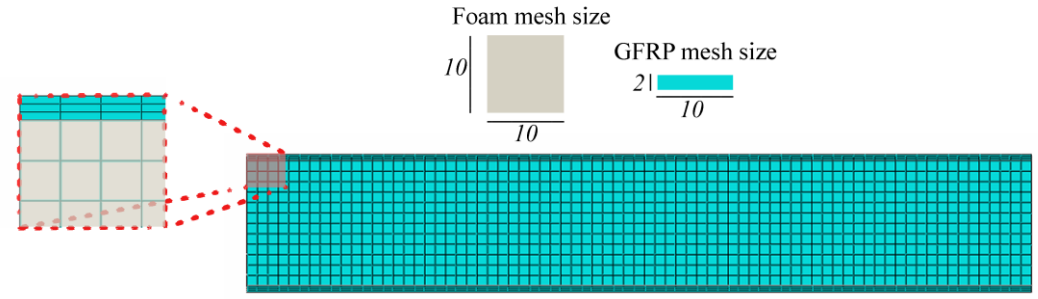

Figure 121 - Mesh of 2D FE model (dimensions in mm).

Three-dimensional (3D) models were developed to simulate the thermal and mechanical response of the web-core sandwich panels (only with lateral webs) subjected to fire. The geometry of the models was the same as the tested sandwich panels (*cf.* chapter 6); however, to reduce the computational

effort, only a quarter of the specimens' dimension was modelled. The core materials were discretized with a mesh size of 10 × 10 × 10 mm^3, whereas the face sheets and the webs were discretized with a mesh size of 2 × 10 × 10 mm^3. The entire model involved a total of 77116 nodes and 57360 elements. As for the 2D models, the mesh sizes were selected after an initial mesh sensitivity analysis. In the mechanical models, all the elements were developed with eight-node solid elements with reduced integration, DC3D8 for the thermal model and C3D8R for the mechanical model.

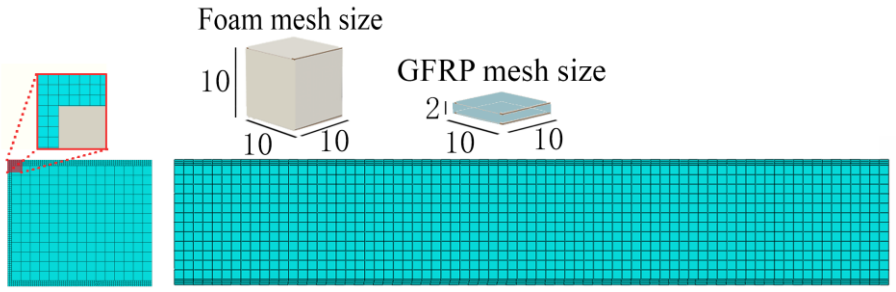

Figure 122 - Mesh of 3D FE model (dimensions in mm).

The contact between the face sheets and the core was modelled using the tie constraints option for the interaction properties in *ABAQUS*. This assumption, together with the non-consideration of any failure criteria (material damage initiation and progression), is a limitation of the current FE model, which is not able to reproduce the failure mechanisms observed in the experiments (*cf.* chapter 6) and, consequently it is not able to predict the time to failure. This is due to the lack of experimental data about the temperature-dependent constitutive behaviour of such bonded interface.

Note that the contribution of the CS boards to the mechanical response of the panel was considered negligible; for this reason, only the GFRP and foam materials were modelled in the mechanical analysis.

7.2.2 Temperature-dependent material properties

With the objective of predicting with good accuracy the thermal and mechanical response of the sandwich panels when exposed to fire, the FE models comprised the incorporation of the thermophysical properties and constitutive relations as a function of temperature of all materials.

For both GFRP and foam materials, the variation with temperature of the density was determined from TGA tests (*cf.* chapter 2 and chapter 3), while for the CS boards this property was defined in accordance with the TGA results provided by Morgado [96], as the experiments were made in the same type of CS material – Figure 123 shows the variation of density with temperature considered as input in the numerical models.

Due to (i) the lack of information available in the literature and (ii) difficulties in performing reliable direct measurements of specific heat and thermal conductivity at elevated temperatures, the variation

of those thermophysical properties with temperature for both GFRP and foam cores was obtained by inverse analyses, as described in chapter 4. The specific heat and thermal conductivity as a function of temperature considered in the numerical models are reported in Figure 124.

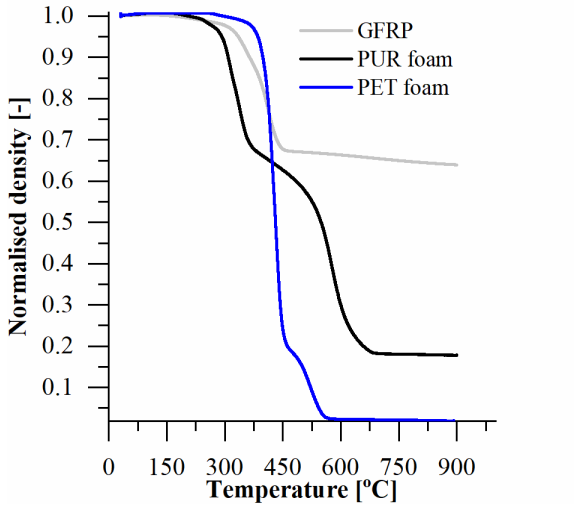

Figure 123 - Normalised density vs. temperature curves considered as input data in the FE models.

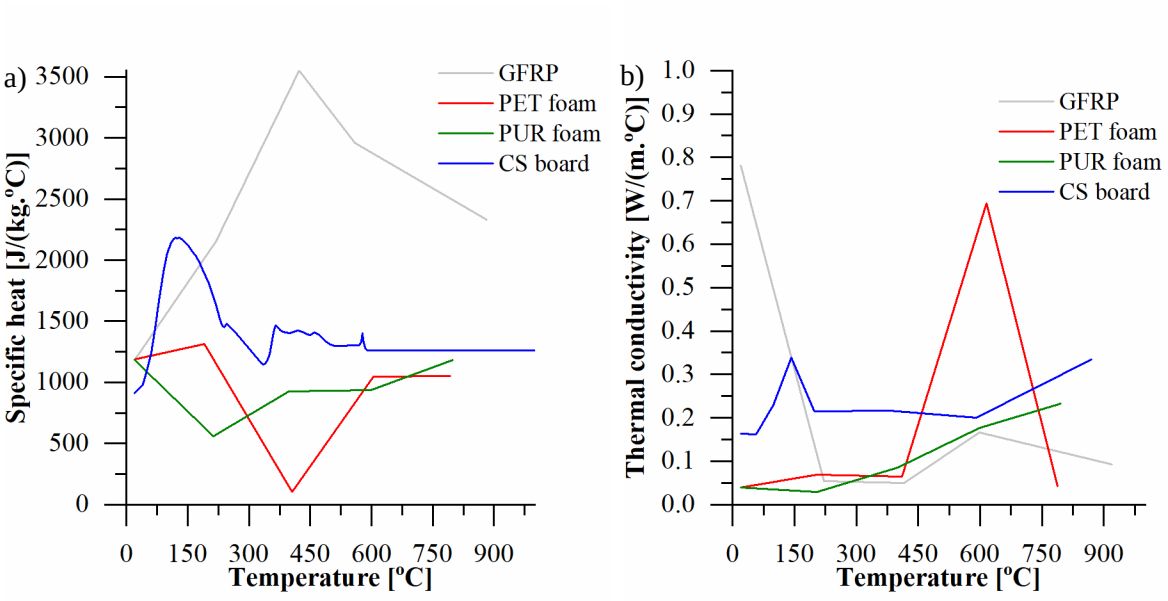

Figure 124 - Thermophysical properties considered in the FE model: (a) specific heat and (b) thermal conductivity.

In what concern the CS board, the variation with temperature of its thermal conductivity (λ_{cs}) and specific heat ($C_{p,cs}$) up to 600 ºC was defined according to the datasheet provided by the manufacturer [106]; for temperatures above 600 ºC, the results obtained through the numerical-inverse analysis mentioned above were used (*cf.* Figure 124).

Concerning the mechanical properties, the GFRP material was modelled as a linear elastic orthotropic material, using the "engineering constants" option available in *ABAQUS*, whereas the PET foam was simulated assuming a plastic orthotropic behaviour defined by using the Hill-criterion. Nonetheless, it should be highlighted that the Hill model was not applicable to the PUR foam tested

in this study (as detailed ahead); for this reason, only the mechanical response of the homogeneous-PET core panels was studied herein.

For both GFRP and foam materials, temperature-dependent material properties were assumed based on the results obtained from the small-scale material characterisation tests (*cf.* chapters 2 and 3), which were complemented with data available in the literature and empirical degradation models. It is worth mentioning that different elastic moduli of the GFRP material were considered in the FE model: the compressive modulus was assigned to the elements in compression (*i.e.* top half of the web and top face sheet), whereas the tensile modulus was considered for the elements in tension (*i.e.* lower half of the web and bottom face sheet). The effects of changes in the neutral axis position during fire exposure in material assignment were not considered. This is a limitation of the present FE models.

The longitudinal tensile and compressive properties as well as the in-plane shear properties as a function of temperature considered in the FE models are presented in Figure 125.

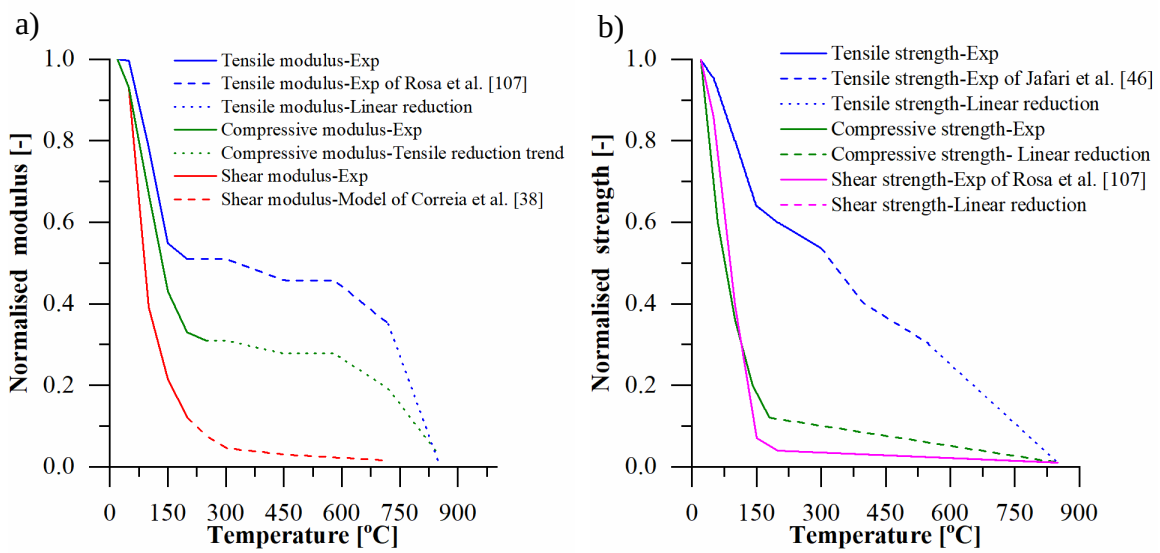

Figure 125 - GFRP temperature-dependent normalised mechanical properties considered in the FE models: (a) modulus and (b) strength.

In the experiments carried out in this thesis (*cf.* Chapter 3), it was only possible to determine the degradation with temperature of the longitudinal tensile and compressive moduli up to 200 ºC and 250 ºC, respectively - for higher temperatures, the reduction of both compressive and tensile modulus was assumed similar to that obtained by Rosa *et al*. [107], who performed tensile tests on pultruded GFRP rebars up to 715 ºC. This assumption stems from the fact that both tensile and compressive modulus are mostly dependent on the thermomechanical response of the fibres rather than the matrix. For temperature above 715 ºC, a linear reduction until reaching a null value at 850 ºC (fibres softening) was applied (*cf.* Figure 125). It is worth mentioning that, for temperatures higher than 200 ºC, the reduction of the shear modulus was defined according to the analytical model proposed by Correia *et al*. [38].

In this study, the reduction of the tensile strength of the GFRP used on the face sheets was experimentally assessed up to 300 ºC (*cf.* chapter 3); for temperature ranging from 300 and 550 ºC, the variation with temperature of the tensile strength reported by Jafari *et al.* [46] for comparable GFRP laminates was assumed herein. For higher temperatures, a linear reduction was considered until 850 ºC (null strength retention) - the same procedure was also adopted for the compressive and shear strengths.

Concerning the variation with temperature of the mechanical properties of the GFRP material in the transverse direction, since no specific tests were performed in the present study and the information in the literature is very limited (regarding the reduction with temperature of the mechanical properties throughout the different directions), the same reduction trend observed in the longitudinal direction was assumed.

With respect to the Poisson' ratios of the GFRP material, typical values of υ_{lt}=0.30 and υ_{tl}=0.11 were defined according to Morgado *et al*. [96], who performed experimental tests on comparable GFRP materials - note that this property was assumed constant with temperature due to the lack of information in the literature.

As reported by Morgado *et al*. [103], the coefficient of thermal expansion (α) in the longitudinal direction plays an important role in the mechanical response of the GFRP material when subjected the temperature variations. In this study, the coefficient of thermal expansion in the longitudinal direction (α=2.42 × 10^{-5}) was computed from the analytical relationship proposed by Holloway and Teng [108],

$$\alpha_{long} = \frac{\alpha_{matrix}(1 - V_{fibre})E_{matrix} + \alpha_{matrix}V_{fibre}E_{fibre}}{(1 - V_{fibre})E_{matrix} + V_{fibre}E_{fibre}} \quad (23)$$

where E is the elastic modulus, V_{fibre} is the fibre volume fraction and α is the coefficient of thermal expansion. The elastic properties of both fibres and matrix were provided by the manufacturers [109,110], while the volume fibre fraction was determined from burn-off tests and taken as 0.45. Note that the value obtained from equation 23 is in line with experimental data reported in the literature [111]; again, due to the lack of information available in the literature, this parameter was considered temperature-independent - a similar approach was also adopted by Morgado *et al*. [103].

In accordance with Eaves [84], the coefficients of thermal expansion of polymeric foams are very similar to those of the corresponding solid polymer; for this reason, a reference value of α=4.20 × 10^{-4} (constant with temperature) was considered herein.

Poisson's ratios of υ=0.3 (temperature-independent) were defined in each direction in accordance with the values reported by Gibson *et al*. [31] for polymeric foams comparable to those used in this study.

As mentioned above, the orthotropic plastic behaviour of the foam was modelled using the Hill-criterion, which is an extension of the Von Mises criterion. The use of this criterion was prompted by the limitations found in the hyper-foam model available in Abaqus (typically used to simulate the foams), which does not take into account the (i) foam's anisotropy and (ii) temperature-dependency of the mechanical properties [112]. The Hill's potential function can be expressed as follows,

$$f(\sigma) = \sqrt{F(\sigma_{22} - \sigma_{33})^2 + G(\sigma_{33} - \sigma_{11})^2 + H(\sigma_{11} - \sigma_{22})^2 + 2L\sigma_{23}^2 + 2M\sigma_{31}^2 + 2N\sigma_{12}^2} \quad (24)$$

where *F*, *G*, *H*, *L*, *M* and *N* are constant values, which can be defined using the following equations:

$$F = \frac{1}{2}\left(\frac{1}{R_{22}^2} + \frac{1}{R_{33}^2} - \frac{1}{R_{11}^2}\right) \quad (25)$$

$$G = \frac{1}{2}\left(\frac{1}{R_{33}^2} + \frac{1}{R_{11}^2} - \frac{1}{R_{22}^2}\right) \quad (26)$$

$$H = \frac{1}{2}\left(\frac{1}{R_{11}^2} + \frac{1}{R_{22}^2} - \frac{1}{R_{33}^2}\right) \quad (27)$$

$$L = \frac{3}{2R_{23}^2} \quad (28)$$

$$M = \frac{3}{2R_{13}^2} \quad (29)$$

$$L = \frac{3}{2R_{12}^2} \quad (30)$$

where R_{ij} are the normal yield stress ratios that are defined with respect to a user-defined reference yield stress (σ_o). In this study, the reference yield stress at a given temperature was assumed equal to the out of plane compressive strength of the foam determined in the experimental campaign (*cf.* Chapter 2). The yield stress ratios are computed using the following equations:

$$R_{11} = \frac{\sigma_{11}}{\sigma^0} \quad (31)$$

$$R_{22} = \frac{\sigma_{22}}{\sigma^0} \quad (32)$$

$$R_{33} = \frac{\sigma_{33}}{\sigma^0} \quad (33)$$

$$R_{12} = \frac{\sigma_{12}}{\tau^0} \quad (34)$$

$$R_{13} = \frac{\sigma_{13}}{\tau^0} \quad (35)$$

$$R_{23} = \frac{\sigma_{23}}{\tau^0} \quad (36)$$

where σ_{11}, σ_{22} and σ_{33} are the compressive strengths in each direction at a given temperature, and σ_{12}, σ_{13} and σ_{23} are the shear strengths of the material in the different directions at that temperature. Note that the yield shear stress τ^0 was defined as,

$$\tau^0 = \frac{\sigma^0}{\sqrt{3}} \tag{37}$$

According to the Hill-criterion, a ratio between the axial stress and shear stress of the material (*cf.* equation 37) needs to be considered; however, because this ratio was not valid for the PUR foam tested in this study (*cf.* chapter 2), the mechanical response of homogeneous-PUR core sandwich panels under fire was not numerically modelled in this work.

It is worth mentioning that due to the absence of specific data in the literature about the tensile properties of PET foam, the same mechanical behaviour in tension and compression was assumed in the model. However, this is a simplifying assumption, as the mechanical behaviour of polymeric foams in tension is expected to be brittle, while the compressive behaviour is characterised by yielding and plastic deformations. Concerning the reductions of the compressive properties (strength and modulus) at temperatures above 190 ºC and of the shear modulus above 100 ºC, they were defined using the empirical equation proposed by Correia *et al*. [38]. In what concern the shear strength, because no experimental data was available for this specific foam, the variation with temperature of the shear strength for temperature above 60 ºC was assumed to be similar to that of the compressive strength. The normalised variation with temperature of the out-of-plane compressive and tensile modulus and shear modulus considered in the FE models is reported in Figure 126, while the normalised shear and compressive strengths reductions with temperature are presented in Figure 127.

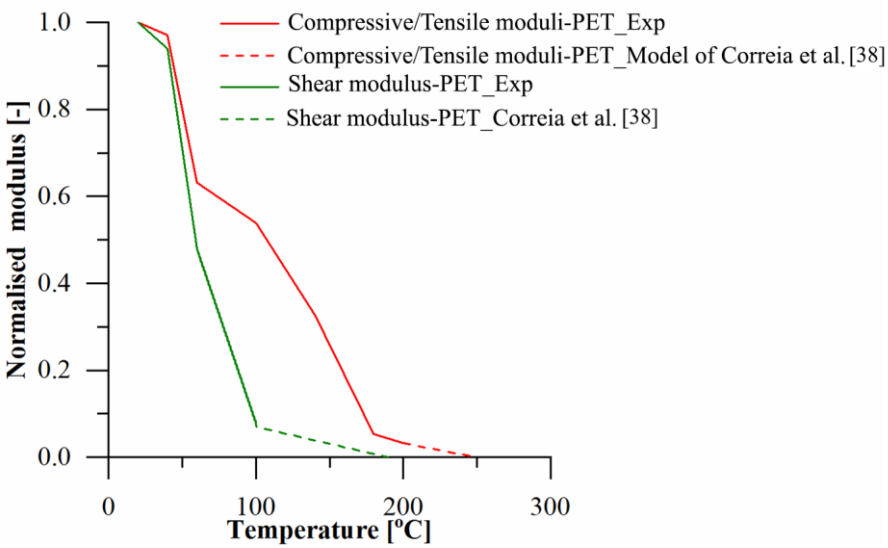

Figure 126 - PET foam temperature-dependant compressive and shear moduli considered in the FE model.

With respect to the variation with temperature of the compressive properties (strength and modulus) in the in-plane directions, they were assumed to follow that of the out-of-plane direction measured

in the compressive tests described in chapter 2. Regarding the compressive strength at ambient temperature in the two in-plane directions (σ_{22} and σ_{33}), the results obtained by Fathi [34] were assumed in this work; such data was obtained from compressive tests on the same PET foam studied herein. It is worth noting that the author found that the compressive strength in both in-plane directions is very similar; for this reason, these properties were considered coincident in this study (*i.e.* σ_{22}=σ_{33}).

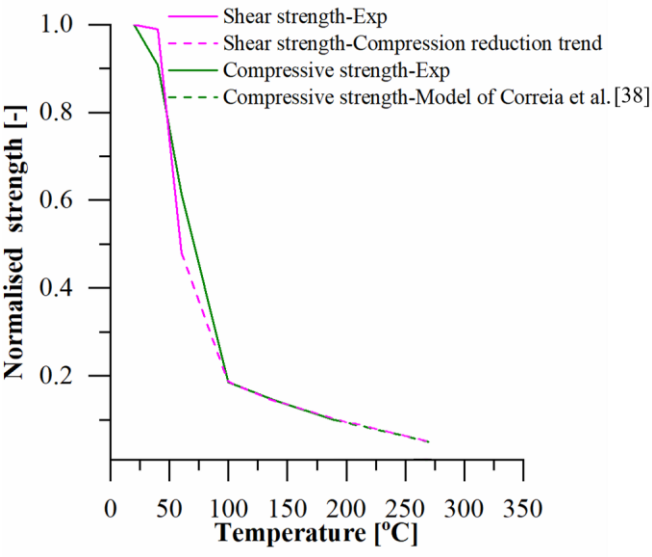

Figure 127 - Temperature-dependant compressive and shear strengths of the PET foam considered in the FE model.

Based on input data reported above, the yield stress ratios as a function of temperature considered in the Hill-criterion (given by equations 31 to 37) that were adopted to model the PET foam material are listed in Table 30.

Table 30 - Variation of the yield stress ratios with temperature considered in Hill-criterion.

PET						
T [°C]	R_{11} [-]	R_{22} [-]	R_{33} [-]	R_{12} [-]	R_{13} [-]	R_{23} [-]
20	1.0	0.4	0.4	1.1	1.1	1.1
40	1.0	0.4	0.4	1.2	1.2	1.2
60	1.0	0.4	0.4	1.2	1.2	1.2
100	1.0	0.4	0.4	1.2	1.2	1.2
140	1.0	0.4	0.4	1.2	1.2	1.2
190	1.0	0.4	0.4	1.1	1.1	1.1
220	1.0	0.4	0.4	1.1	1.1	1.1
270	1.0	0.4	0.4	1.2	1.2	1.2

7.2.3 Boundary conditions, thermal and structural loadings

As explained in chapter 6, the length of the sandwich panels directly exposed to fire was 1.1 m; in addition, ceramic wool blankets were also positioned along the panel's length in order to minimize the heat transfer through the lateral sides. In this context, the following boundary conditions were defined in the numerical model (*cf.* Figure 128): (i) the heat transfer through the top and bottom face

sheets was considered to occur by radiation and convection, while (ii) the heat transfer through the lateral sides of the panel was considered null (*i.e.* adiabatic surfaces were assumed).

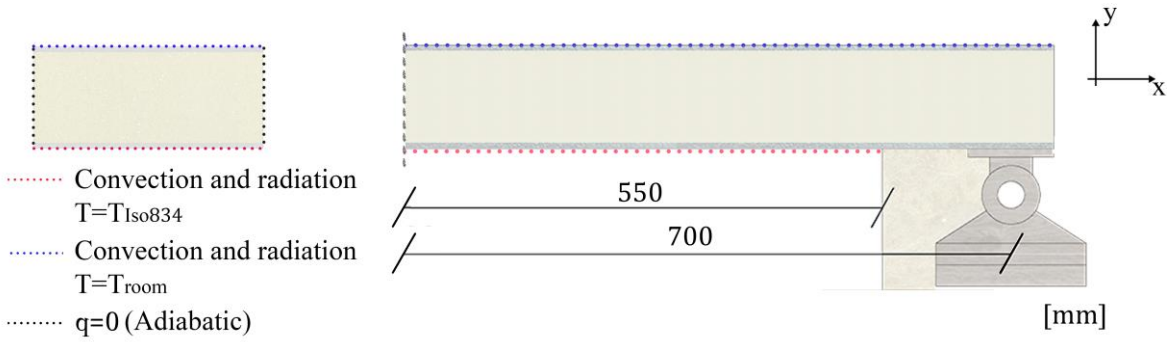

Figure 128 - Boundary conditions defined in the thermal models.

For the bottom face sheet (directly exposed to the ISO 834 curve), the emissivity coefficients of the GFRP material (ε_{GFRP}) and CS board (ε_{cs}) were set equal to 0.75 and 0.70, respectively [72,113], while the convection coefficient (h) was set as h=25 W/m^2K [79]. In what concern the "cold" face sheet (the top face sheet was not directly exposed to fire), a convection coefficient h=10 W/m^2K and an emissivity coefficient ε_{GFRP}=0.75 were considered.

Aiming at simulating with good accuracy the thermal conditions adopted in the experiments, the bottom part of the panel (either the bottom face sheet or the CS board) was exposed to the furnace temperature variation (ISO 834 fire curve), considering both convection and radiation boundary conditions. Such procedure was adopted for all models with the exception of specimen PET-LW-AC, in which the bottom face sheet was exposed to the temperature *vs*. time curves measured by the thermocouple placed in the air cavity (*cf.* Figure 97). It is worth referring that the initial temperature set in the numerical model was defined in accordance with the temperature measured in each of the experimental tests (ranging from 18 ºC to 25 ºC).

In order to accurately simulate the mechanical response of the panel, the following boundary conditions were set in the models: the vertical displacement (δ_y) of the support was restricted, as well as the (ii) horizontal displacement (δ_x) across the height of panel at the mid-span section. For the 3D model, the symmetry was also assumed with respect to the y-z plane, thus the displacement in the z axis (δ_z) was restrained.

Concerning the mechanical load, it was applied through a concentrated load for the 2D model and pressure for the 3D model distributed in the loading steel plate. The load was defined in order to cause a mid-span deflection of 5.6 mm, corresponding to a deflection limit of L/250 (L is the span). It is worth mentioning that the load level was defined based on the results obtained from the flexural static tests described in chapter 5.

7.2.4 Type of analysis

Regarding the modelling of the fire resistance behaviour, an uncoupled approach was followed to determine the thermomechanical response of the sandwich panels under a fire scenario. The thermal model aimed at determining the temperature distribution in the panel (maximum allowable temperature change per increment of 10 ºC and time step of 1 sec), while the mechanical model aimed at evaluating the displacement and stress fields. In this context, the numerical simulation was performed in two steps: (i) first, the fire load was applied and kept constant during the whole duration of the simulation; then (ii) the thermal action was imposed by considering the temperature *vs.* time curve through convection and radiation boundary conditions. It is worth referring that both thermal and mechanical models were simulated using the same FE mesh.

7.3 SUMMARY OF MODELING ASSUMPTIONS

In summary, the following assumptions were considered in the numerical simulations of the fire behaviour of GFRP sandwich panels:

- The thermal conductivity and specific heat of both GFRP and foam materials were obtained from numerical inverse analysis (chapter 4);
- The temperature-dependent constitutive relationship of the materials set in the model were taken from experimental results (available only up to a given temperature), and complemented with experimental data available in the literature and analytical laws;
- The GFRP was modelled as a linear-elastic material (with no failure criteria), while the plastic behaviour of the foam was modelled using the Hill-criterion;
- The contribution of the CS boards to the mechanical response of the sandwich panel was considered negligible;
- A perfect connection between the GFRP and the core material was assumed (this was modelled using tie constraints in Abaqus); *i.e.*, the models did not take into account any failure criteria at the interface between the materials;
- The coefficient of thermal expansion and the Poisson's ratios were considered constant with temperature;
- The thermal degradation of the elastic moduli of the GFRP material in the transverse direction was assumed similar to that of the longitudinal elastic moduli;
- The tensile behaviour of the PET foam was assumed similar to the compressive one;
- The variation with temperature of the in-plane properties of the PET foam was considered equal to those of the out-of-plane properties.

7.4 HOMOGENEOUS -CORE SANDWICH PANELS: RESULTS AND DISCUSSION

7.4.1 Thermal response

As discussed in chapter 6, the thermal response of the sandwich panels was measured by placing thermocouples across the height of the panels at different locations, namely at the mid-span, intersection and support sections.

Figure 129 shows the numerical temperature field calculated for a reference unprotected panel (specimen PET-U-U) at the end of the fire exposure (after 8 min, corresponding to the "experimental failure time" – *cf.* chapter 6). As expected, the temperature distribution obtained in the FE model confirms the non-uniform temperature evolution across the depth of the panel, with the exposed length of the bottom face sheet presenting the highest values, and most of the volume of the core, as well as the top face sheet, presenting very limited/negligible increase of temperature.

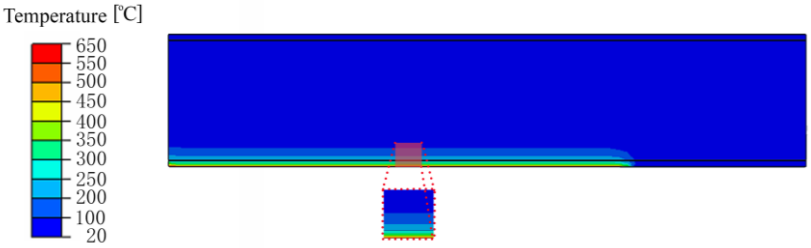

Figure 129 - Temperature distribution in specimen PET-U-U at the end of the fire exposure (8 min).

Figure 130 shows the comparison between the experimental and numerical temperature profiles measured at the mid-span section of specimens PET-U-U and PUR-U-U.

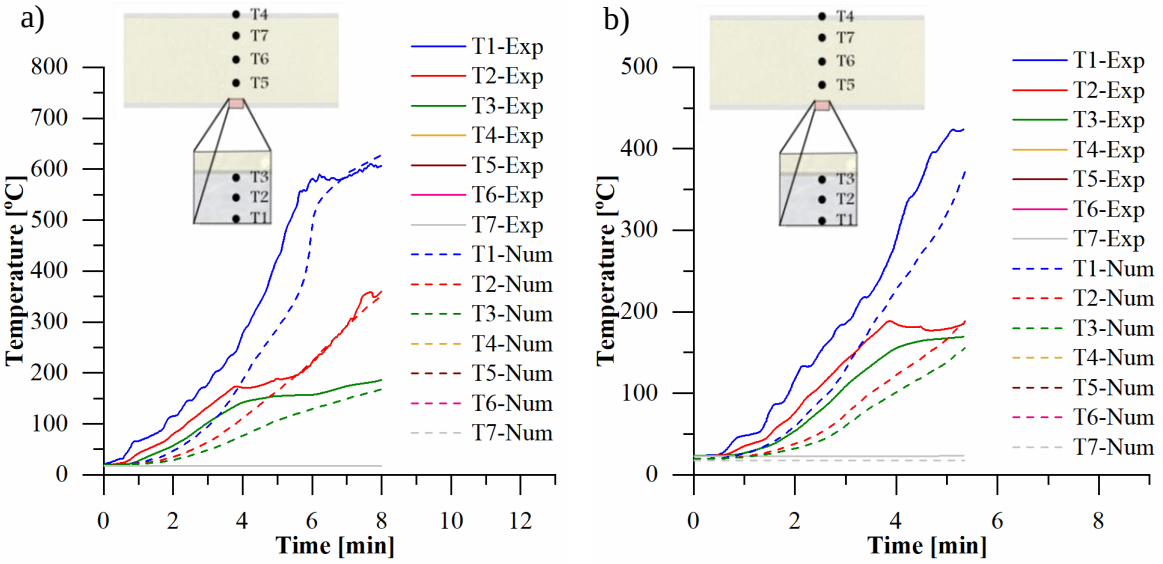

Figure 130 - Experimental (Exp) and numerical (Num) temperatures at the mid-span section: (a) specimen PET-U-U and (b) specimen PUR-U-U.

Despite the very short time of fire exposure (ranging from 5 to 8 minutes), the numerical curves are in relatively good agreement with the experimental ones, although in the former the temperatures

increased at a slower rate (especially during the very initial stage of the test). These deviations may stem from the differences between the actual thermophysical properties of the constituent materials (mostly the GFRP ones) and those obtained by means of the numerical procedure described in chapter 4 and, possibly, the differences between the nominal ISO 834 temperature *vs*. time curve and those measured in the furnace (which had some early deviations). Similarly to what was observed in the experimental tests, the numerical temperature profiles measured at the bottom face sheet, directly exposed to fire (T1 to T3), showed a steady increase, with some nonlinearities at around 600 ºC (*cf.* Figure 130a), when the organic fraction of the material becomes null. Concerning the thermal response of the core material, no significant variations of temperature were observed in both numerical and experimental results - this is mainly due to the very good thermal insulation of the core material, together with the very short duration of fire exposure. It is worth noting that owing to the excellent thermal insulation provided by the core, almost null variations of temperatures were measured at the top face sheet (T5).

As expected, the numerical temperatures at the intersection section (T8 to T10) were much lower than those at mid-span (T1 to T3), which is consistent with the boundary conditions considered in the simulation - this result agrees with the experimental measurements (*cf.* Figure 131).

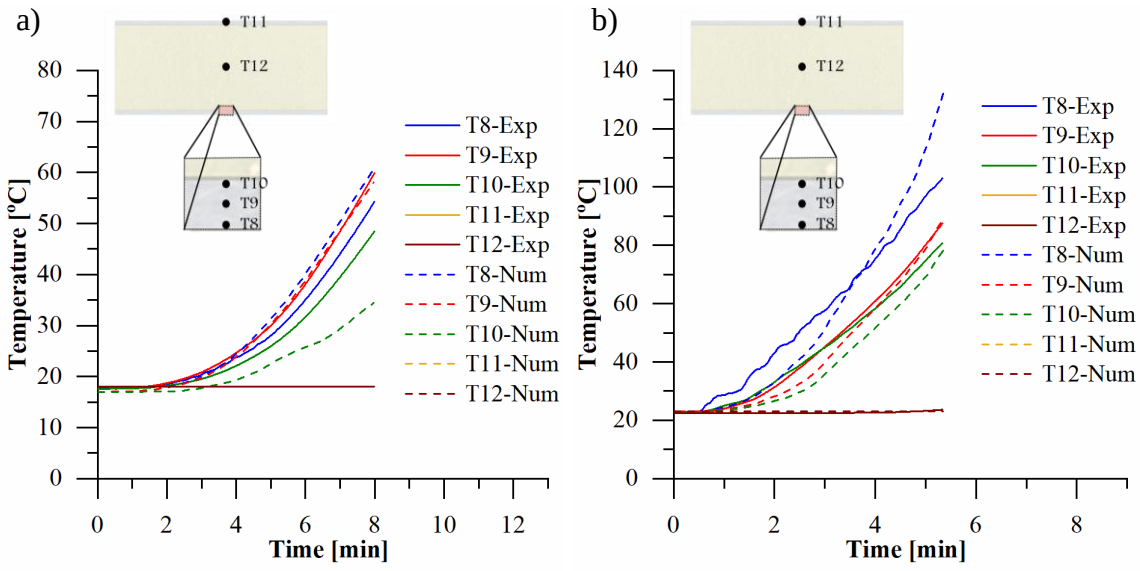

Figure 131 - Experimental (Exp) and numerical (Num) temperatures at the intersection section: (a) specimen PET-U-U and (b) specimen PUR-U-U.

Figure 132 shows the temperature field of specimen PET-U-CS at the end of the fire exposure (after 46 min – corresponding to the "experimental failure time" – *cf.* chapter 6). Taking specimens PET-U-U and PUR-U-U as references, major reductions of temperature were observed when using CS boards as screen protection.

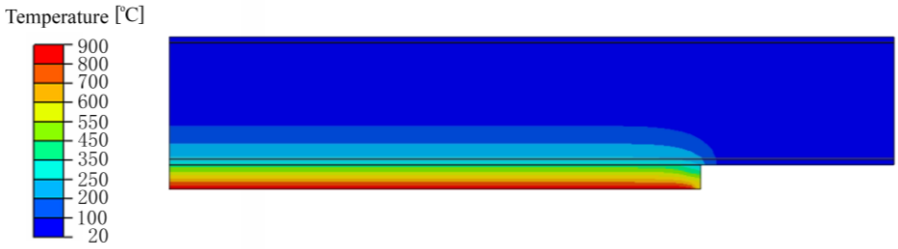

Figure 132 - Temperature distribution in specimen PET-U-CS at the end of the fire exposure (after 46 min).

Overall, the temperature profiles at the mid-span section of specimens PET-U-CS and PUR-U-CS obtained in the FE models were similar to those obtained in the experimental tests (*cf.* Figure 133). Concerning the measured temperatures at the bottom face sheet (T1 to T3), unlike the FE models, the measured temperature profiles presented a plateau at around 100 ºC, which was due to the evaporation of moisture from the CS boards. This different behaviour between the experimental and numerical curves might be due to differences between the actual and the simulated thermophysical properties of the CS boards; further work is needed to determine and/or measure more accurately the thermophysical properties of the CS boards for temperatures close to the evaporation point of water.

In what concerns the thermal response of the core at the mid-span section (T5 to T7), the models provided relatively good estimates of the temperature evolution in the foam compared to the experiments. Regarding the temperature at a distance to the hot face of 35.6 mm (T5), both experimental and numerical temperature *vs*. time curves presented the following behaviour: (i) a relatively slow temperature increase rate at the initial stage of the test (up to 10 min) followed by (ii) a steady increase until the end of the fire exposure. As observed in the experiments, in the numerical model, the decomposition temperature of both foams was never attained (425 ºC and 300 ºC for PET and PUR, respectively).

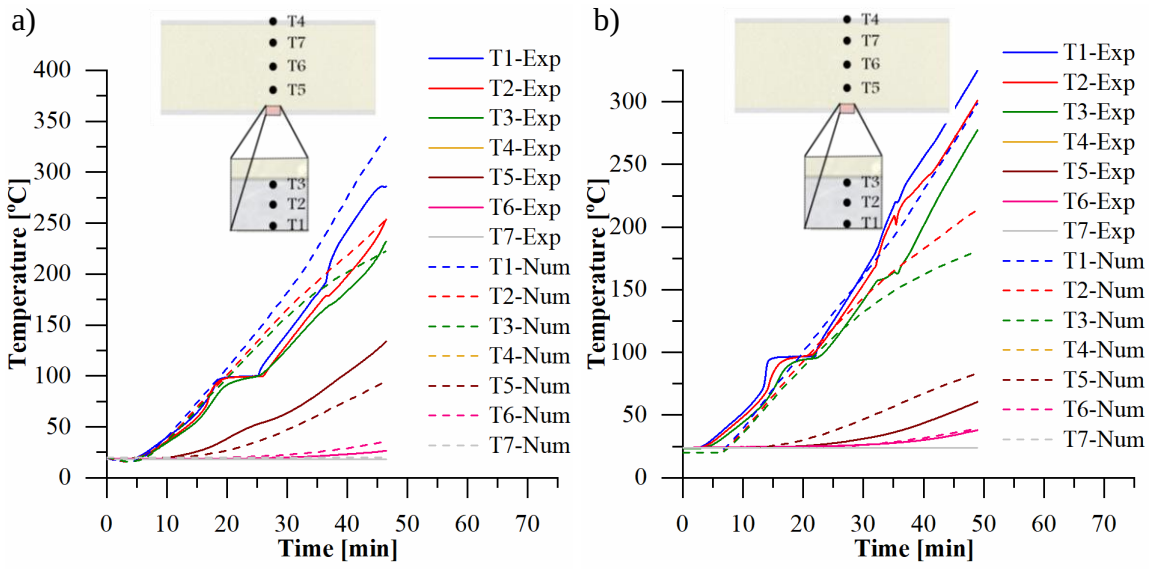

Figure 133 - Experimental (Exp) and numerical (Num) temperatures at the mid-span section: (a) specimen PET-U-CS and (b) specimen PUR-U-CS.

A similar temperature evolution, but with a time delay, can also be observed at the intersection section (T8 to T12). It can be seen that despite the relatively good agreement at the initial stage of the simulation (up to 30 minutes), for a longer duration of fire exposure, the numerical models were not able to accurately predict the temperature evolution in the panel, overestimating the experimental temperatures. As mentioned above, this difference should be related to the effects of water content (*i.e.* water vaporization) in the CS boards, which were not well captured by the thermophysical properties considered in the model. Further investigations should assess the variation with temperature of the thermophysical properties (*i.e.* specific heat and thermal conductivity) of the CS board in a range of temperature that includes the water vaporization in the material.

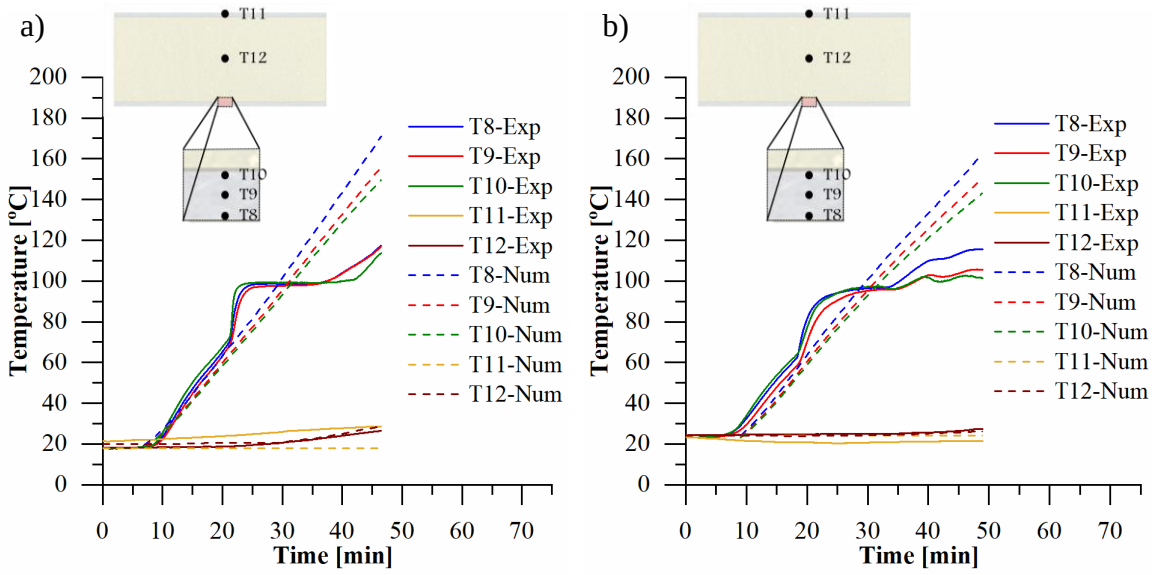

Figure 134 - Experimental (Exp) and numerical (Num) temperatures measured at the intersection section: (a) specimen PET-U-CS and (b) specimen PUR-U-CS.

Similarly to what was observed in the numerical simulations of the unprotected panels, the predicted temperatures across the support section were constant with time.

7.4.2 Mechanical response

Figure 135a shows the comparison between the experimental and numerical mid-span deflection increase *vs*. time curves of specimen PET-U-U.

The numerical results, similarly to the experimental data, indicate a mid-span displacement increase with time, which is due to the following two main reasons: (i) the thermal bowing related to the temperature gradient in the cross-sections exposed to fire, and (ii) the significant reductions of the moduli of the constituent materials of the sandwich panels with the increase of time/temperature. In general, a relatively good agreement was obtained between numerical and experimental curves, with the highest relative differences being observed in the brink of collapse; this was expected and it is explained by the fact the models do not consider any failure criteria in the GFRP material nor on the GFRP-foam interface (*e.g.* damage initiation and progression evolution). Additionally, these relative

differences could also be related to (i) uncertainties related to some temperature-dependent material properties (some mechanical properties were defined according to the literature and analytical equations), and to (ii) some simplifying assumptions made in the definition of the thermal boundary conditions (*e.g.* lateral sides considered as adiabatic surfaces).

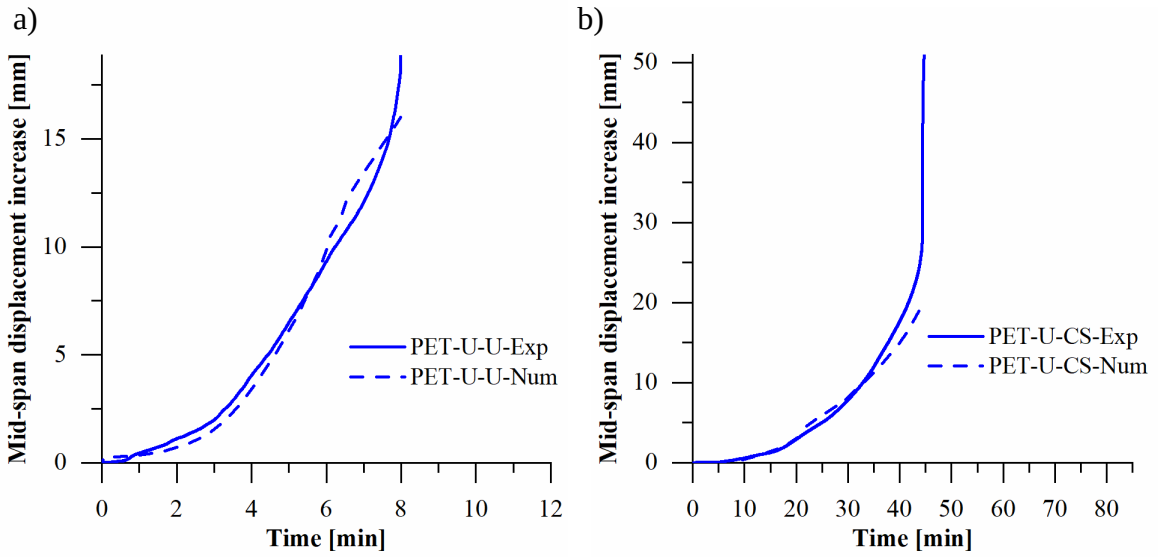

Figure 135 - Experimental (Exp) and numerical (Num) mid-span displacement increase vs. time curves for the: (a) unprotected and (b) protected homogeneous-PET sandwich panels.

Figure 135b shows the comparison between numerical and experimental mid-span displacement increase of PET-U-CS specimen. As expected, the (numerical) deformation increase rate of the protected specimens is much lower compared to that observed in the corresponding unprotected specimen; this is naturally due to the reduction of temperatures in the panel afforded by the thermal protection conferred by the passive fire protection system. As shown in Figure 135, the numerical models were able to simulate with relatively good accuracy the mechanical response of the protected panel. However, similarly to what was observed in the simulation of the unprotected specimen, more significant differences were observed at the final stage of the fire resistance tests, again attributed to the non-consideration of failure criteria in the models.

The numerical models were also used to obtain a better understanding about the stress distribution in the sandwich panels during the fire resistance tests. The longitudinal stresses in the face sheets were evaluated in 6 finite elements located in the top (P1 to P3) and bottom (P4 to P6) face sheets at the mid-span section, where maximum bending moments develop. The evolution of the shear stresses with fire exposure time along the path defined in Figure 136 was also evaluated. It is worth referring that path 1 corresponds to the section where maximum shear force was observed.

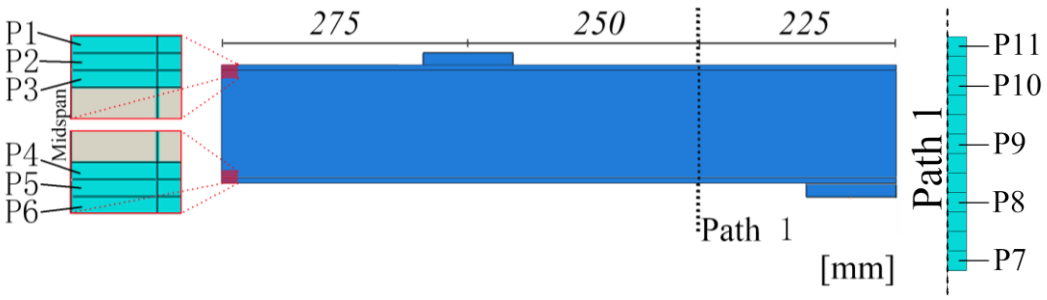

Figure 136 - Finite elements in the bottom (P1 to P3) and top (P4 to P6) face sheet at the mid-span section for longitudinal stress analysis and finite elements (P7 to P11) along path 1 considered for shear stress analysis.

The evolution with time of fire exposure of the longitudinal stresses in the top and bottom face sheets at the mid-span section of specimens PET-U-U and PET-U-CS are plotted in Figure 137. In the unprotected panel (Figure 137a), the longitudinal stresses in the external layer of the bottom face sheet (in tension, P6) exhibited significant reductions due to the decrease of the tensile modulus with temperature, as well as the non-uniform through-the-thickness thermal expansion of the bottom face sheet (as a result of the high thermal gradient); as a consequence, longitudinal stresses in the internal layers of the bottom face sheet (P4 and P5) increased to guarantee the maintenance of the equilibrium – in other words, the high thermal expansion of the bottom layer of the bottom face sheet (P6) was restricted by its internal layer (P4 – where lower temperatures were attained), resulting in an increase of longitudinal tensile stresses at the level of P4 and a reduction at P6 (where after 7 min compression stresses developed).

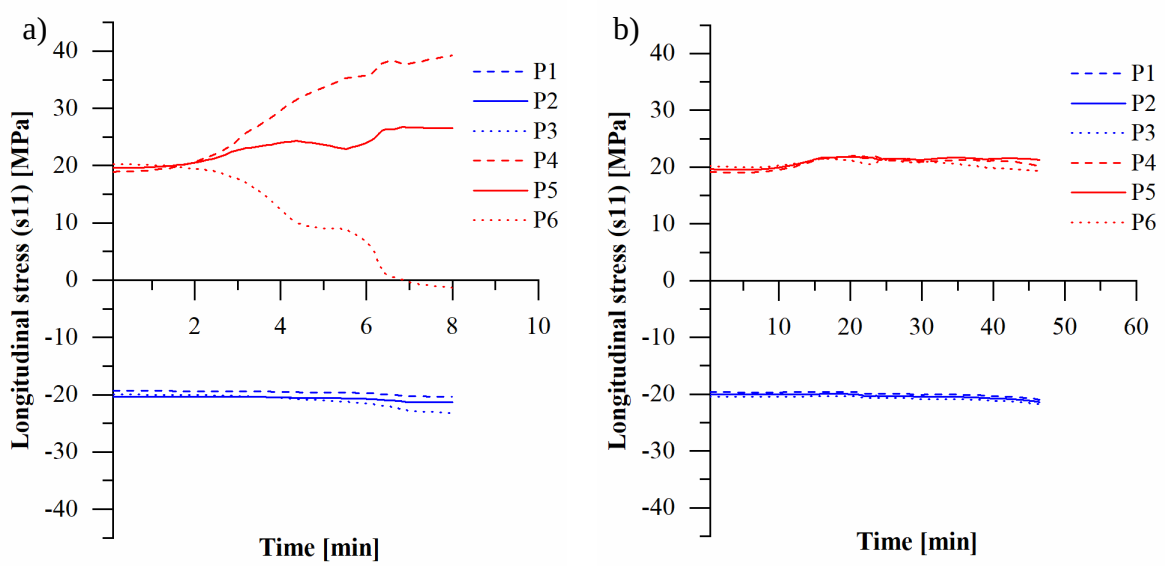

Figure 137 - Evolution with time of fire exposure of longitudinal stresses at the mid span section in different finite elements of top (P1 to P3) and bottom (P4 to P6) face sheet of specimens (a) PET-U-U and (b) PET-U-CS.

It is worth noting that a slight increase of compressive stresses was observed in the top face sheet (P1 to P3) most likely due to the loss of stiffness of the bottom face sheet, which caused a stress transfer across the height of the panel. Despite these small variations, the compressive stresses in the top face sheet did not present significant changes, since it remained approximately at room temperature for the entire duration of the fire exposure (only 8 min).

Regarding the variation, with time of fire exposure, of the longitudinal stresses in specimen PET-U-CS (Figure 137b), it can be observed that the overall magnitude of the changes in longitudinal stresses was much lower compared to those measured in the unprotected panel. Unlike the unprotected panel, the tensile stresses in the bottom face sheet of specimen PET-U-CS remained almost constant during fire exposure. Such results can be related to (i) the moderate temperature increase underwent by this panel and (ii) the fact that the thermal gradient through-the-thickness of the bottom face sheet was less significant (when compared to that of PET-U-U, *cf.* Figure 133a) for the entire duration of fire exposure. Similarly to what was observed in the unprotected specimen, the compressive stresses at the top face sheet remained almost constant with time.

Figure 138 shows the evolution with time of the normalised longitudinal stresses (with respect to the tensile or compressive strength at a given temperature) at the centre of the top (P2) and bottom (P5) face sheets (*cf.* Figure 136). It is interesting to note that, in spite of the very high temperatures attained at the bottom face sheet, the normalized tensile stresses were always very low; such fact confirms why the bottom face sheet did not fail in tension during the fire resistance tests.

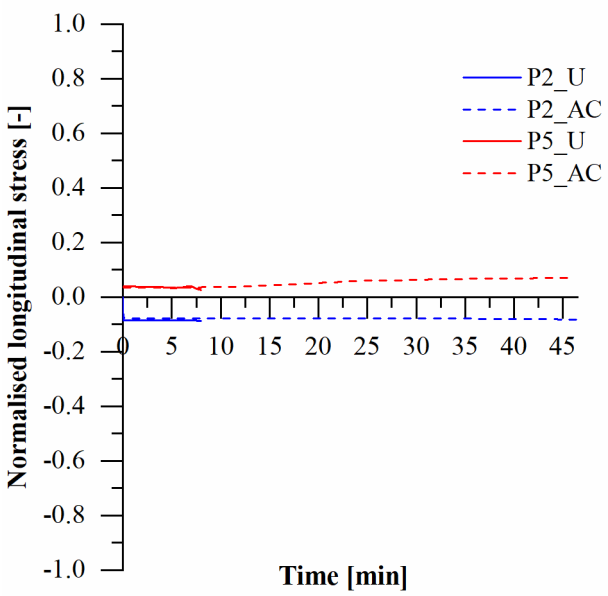

Figure 138 - Evolution with time of fire exposure of normalised longitudinal stresses at the top (P2) and bottom (P5) face sheets at the mid-span section.

The variation of the shear stresses across the depth of the core along the path defined in Figure 136 is reported in Figure 139. In what concerns the unprotected panel (Figure 139a), during the first 3 min of fire exposure, the shear stresses were almost constant across the depth of the core, which is logical since the temperature in the core was almost uniform (room temperature). After this initial stage, the temperature in the bottom part of the core increased and, as a consequence, a stress transfer from the bottom part of the core (degraded) to the upper part (non-degraded) was observed – at the final stage of the test, shear stresses at the upper part of the core had increased by almost 1.4 times (from 0.25 to 0.35 MPa). Such stress transfer can be associated to the thermal degradation of the PET foam

through the depth of the panel, namely the reduction of its shear modulus with temperature. A similar behaviour had been reported earlier by Morgado *et al*. [104] in pultruded GFRP tubular beams exposed to fire and using a similar test setup (where only the bottom surface was exposed to fire).

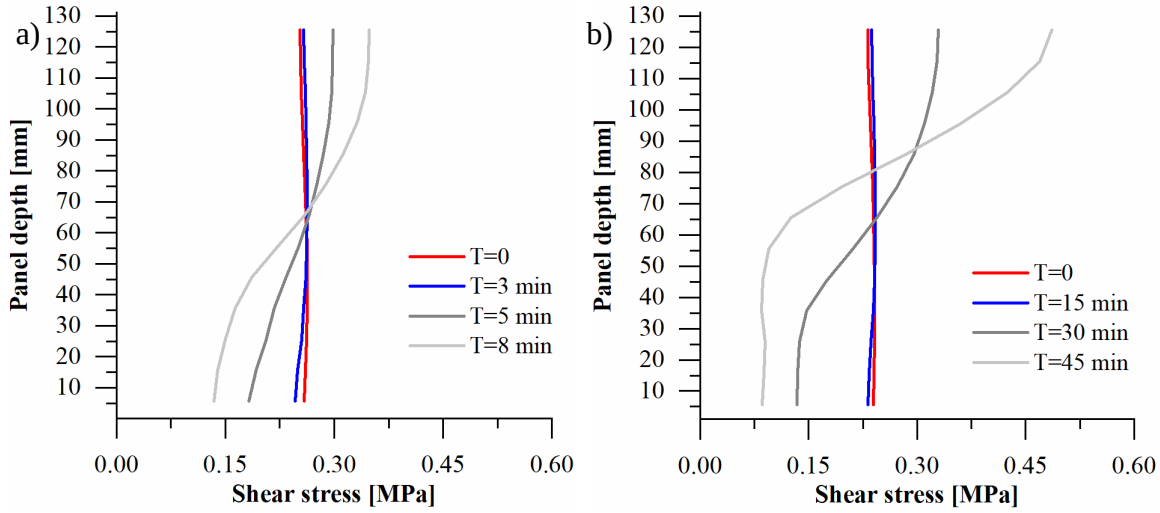

Figure 139 - Evolution of shear stresses along path 1 for different durations of fire exposure: (a) specimen PET-U-U and (b) specimen PET-U-CS.

In specimen PET-U-CS, the magnitude of the shear stress changes was higher compared to those observed in panel PET-U-U, which is consistent with the higher temperatures attained by the bottom part of the foam core in the former panel. At the end of the test, the upper part of the core attained a maximum shear stress of 0.48 MPa, which is 54% of the shear strength of the foam at that temperature (20 ºC).

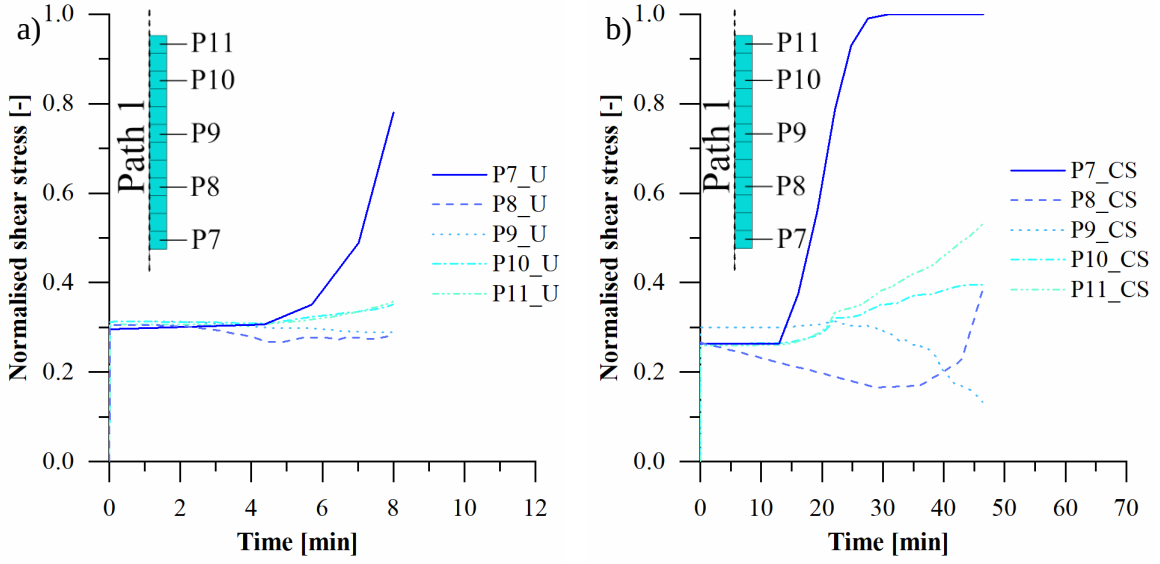

Figure 140 - Evolution with time of fire exposure of normalised shear stresses at the core (P7 to P11) along path 1: (a) unprotected (U) and (b) protected (CS) panels.

Figure 140 shows the evolution with time of fire exposure of the normalised shear stresses (ratio between the shear stress and the shear strength at a given temperature) in different elements of the core (P7 to P11) along path 1. In the unprotected panel (Figure 140a), after ~8 minutes of fire

exposure (*i.e.* when the "experimental failure" occurred), a normalized shear stress of ~0.8 was computed in the bottom part of the core at failure (P7). To further understand the correlation between the shear stresses and strengths in the core throughtout the test, Figure 141 shows the shear plastic strains in the core of the unprotected sandwich panel for different times of fire exposure. As shown in Figure 141, the plastic shear strains at the interface between the PET foam and the bottom GFRP face sheet started to be non-negligible after 6 minutes of fire exposure; this indicates that the shear stresses in that part of the panel exceeded the shear yield stress defined by the Hill-criterion.

In this context, the reduction of the shear interaction at the interface together with the reduction of the shear modulus of the material may have led to a change of the structural response from beam-type to arch-type, in which the top and bottom face sheets behaved as a strut and a tie, with the non-degraded part of the core transmitting the load to the supports. Nonetheless, it should be noted that, although compressive (flexural) failure of the top face sheet was observed in experiments, the normalised compressive stresses at the mid-span section (*cf.* Figure 138) were very low, indicating that the model was not able to accurately reproduce the stress fields of the panel at failure, due to limitations of the material model implemented in the FEM analysis.

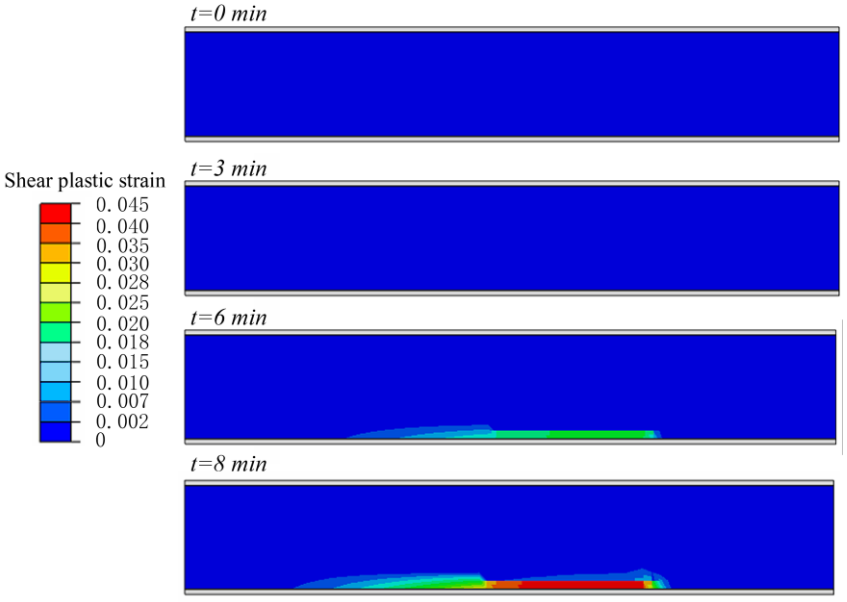

Figure 141 - Shear plastic strains in the core of specimen PET-U-U-1 for different times of fire exposure.

Figure 142 presents the plastic shear strains in specimen PET-U-CS computed at different times of the fire exposure. In the protected specimen, no plastic strains were computed up to 15 min of fire exposure; this is consistent with the relatively low deflection increase observed from the mid-span displacement *vs.* time curve. After 30 minutes of fire exposure, relatively high plastic shear strains developed at the bottom face sheet-core interface (with a much higher magnitude than those developed in the PET-U-U, *e.g.* 0.045 *vs.* 0.406 at the end of each test/simulation). As observed in Figure 140b, the normalised shear stress computed in the bottom element of the core at the position of path 1 (P7) attained values close to 1.0 after ~30 minutes of fire exposure, indicating a section

where failure would be expected to occur. However, this result does not find correlation with the experiments, in which the collapse of specimen PET-U-CS was trigerred by the foam crushing under the loading point, where stress concentrations develop - further investigations (either experimental and numerical) are needed in order to fully understand this "premature" failure mechanism that was observed in the fire resistance tests of protected homogeneous-PET sandwich panels.

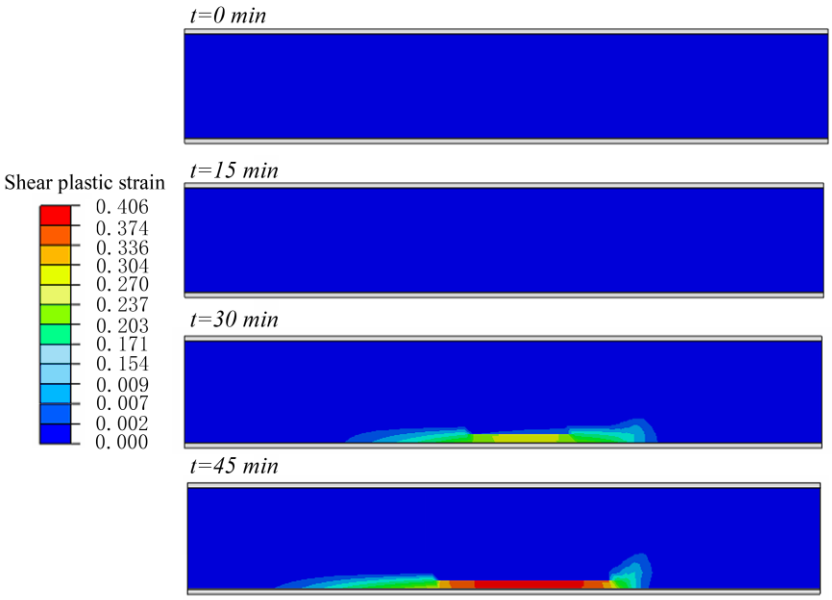

Figure 142 - Shear plastic strains in the core of specimen PET-U-CS-1 for different time of fire exposure.

7.5 WEB-CORE SANDWICH PANELS: RESULTS AND DISCUSSION

7.5.1 Thermal response

Figure 143 shows the numerical temperature distribution at the end of the fire exposure (after 29 min) of specimen PET-LW-U, illustrating a longitudinal view (right) and the transversal view at the mid-span section (left). Figure 144 presents the numerical and experimental temperature *vs*. time curves measured at different depths of specimen PET-LW-U at the mid-span section.

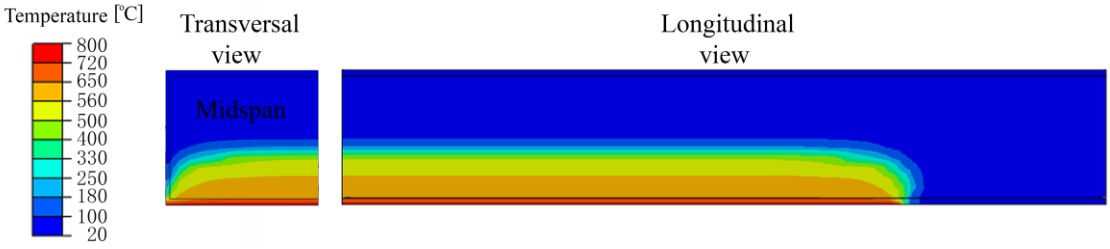

Figure 143 - Temperature distribution of specimen PET-WL-U at the end of the fire exposure (after 29 min).

In general, the experimental and numerical temperatures measured at the bottom face sheet are in relatively good agreement, although at a distance to the hot face of 5.6 mm (T3) the numerical model significantly overestimated the experimental temperature after approximately 15 to 20 minutes of fire exposure. This relatively high difference observed at thermocouple T3 may stem from the

possible variation of the actual position of the thermocouple during the test; indeed, the mid-span displacement increase together with the degradation (thermal decomposition) of the bottom face sheet (and later of the bottom part of the foam core) may have changed the position of the thermocouple, moving it towards the core material; in that case, after 15-20 minutes of fire exposure, the temperature *vs*. time curve of that thermocouple would no longer be accurate. Figure 144 also highlights that the numerical and experimental temperatures developed in the core (T5-T6-T7) followed a similar pattern, although exhibiting some relative differences in the temperature values. As mentioned, these relative differences between experimental and numerical temperatures are probably related to uncertainties about the thermophysical properties of the materials considered in the FE model. Concerning the temperatures across the depth of the web (T8-T12), the numerical model provided lower values compared to the experimental temperatures, suggesting that the cover sets used as lateral insulation (described in section 6.2.2) were not fully effective in preventing the heat transfer through the panel sides. This result points out that the assumption of adiabatic lateral faces, for this case, is not completely accurate.

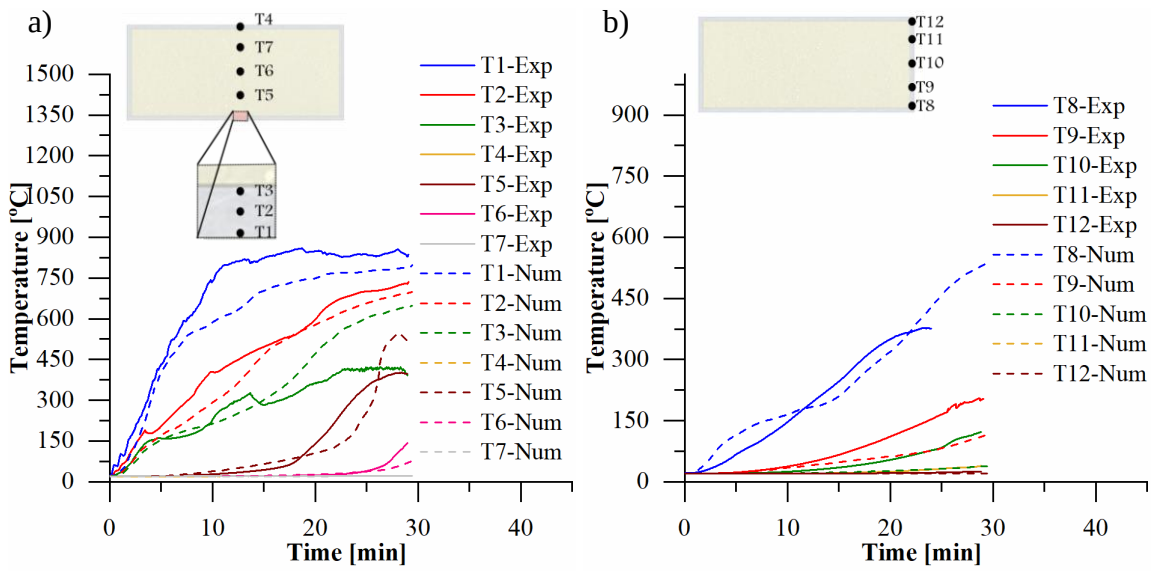

Figure 144 - Experimental (Exp) and numerical (Num) temperature vs. time curves at the mid-span section of specimen PET-LW-U: (a) mid-width and (b) web.

Figure 145 shows the comparison between numerical and experimental temperature *vs*. time curves at the intersection section. Despite showing a relatively good agreement at the initial stage of the test (up to ~8 minutes), the temperatures obtained from the FE model are significantly lower than those measured in the tests beyond ~8 minutes of fire exposure. These relative differences may be explained by experimental issues (already mentioned in section 5.4.2) concerning the loss of effectiveness of the insulation system placed next to the support after 7 minutes of fire exposure – this is consistent with the (much) higher experimental values measured after that instant.

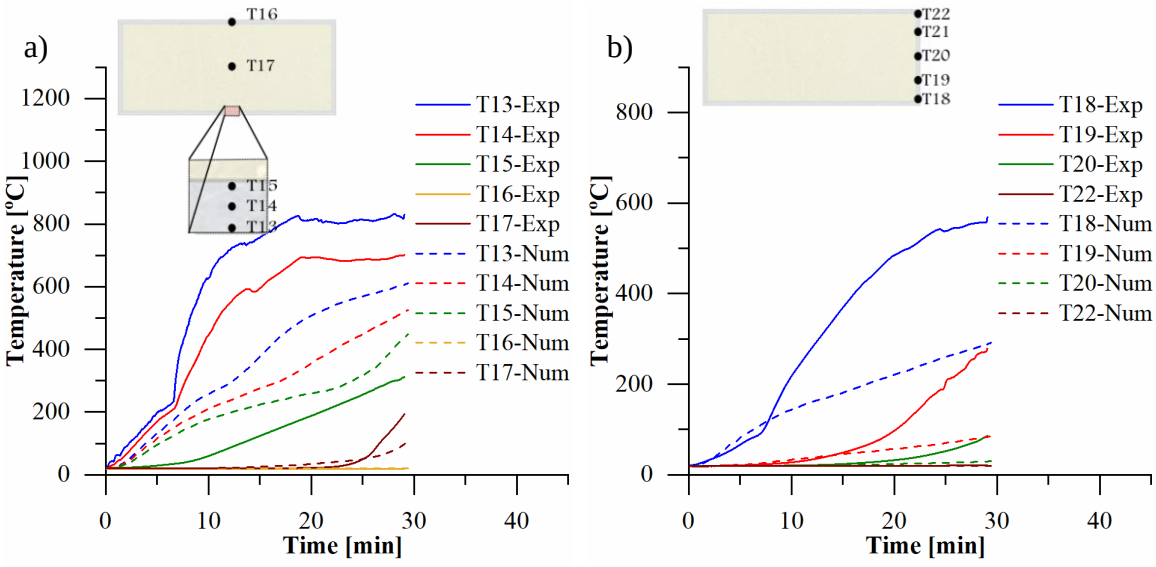

Figure 145 - Experimental (Exp) and numerical (Num) temperature vs. time curves at the intersection section of specimen PET-LW-U: (a) mid-width and (b) web.

Figure 146 shows the numerical temperature distribution at the end of the fire exposure (after 96 min) for specimen PET-LW-AC, illustrating a longitudinal view (right) and the transversal view at the mid-span section (left). Taking as a reference the temperature distribution shown in Figure 143 for the unprotected panel, the numerical model confirms the effectiveness of the AC system in lowering the temperature in the panel.

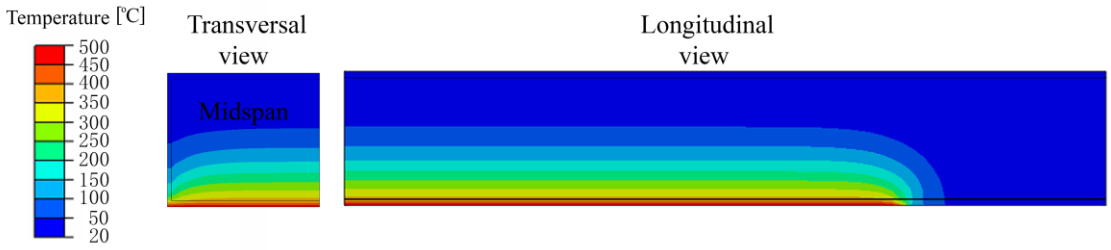

Figure 146 - Temperature distribution of specimen PET-LW-AC at the end of the fire exposure (after 96 min).

Figure 147 presents the numerical and experimental temperature *vs*. time curves at the mid-span section of specimen PET-LW-AC. As shown in Figure 147, a good agreement between numerical and experimental temperatures was obtained. Concerning the temperature evolution across the GFRP web (*cf.* Figure 147b), taking as a reference the results obtained for specimen PET-LW-U, a better agreement was obtained. Indeed, the FE model predicted more accurately the evolution of the temperatures across the depth of the GFRP web of specimen PET-LW-AC, suggesting that for this specific case the thermal insulation applied in the outer surfaces of the webs was effective (as well as the fact overall lower temperatures had been measured/computed).

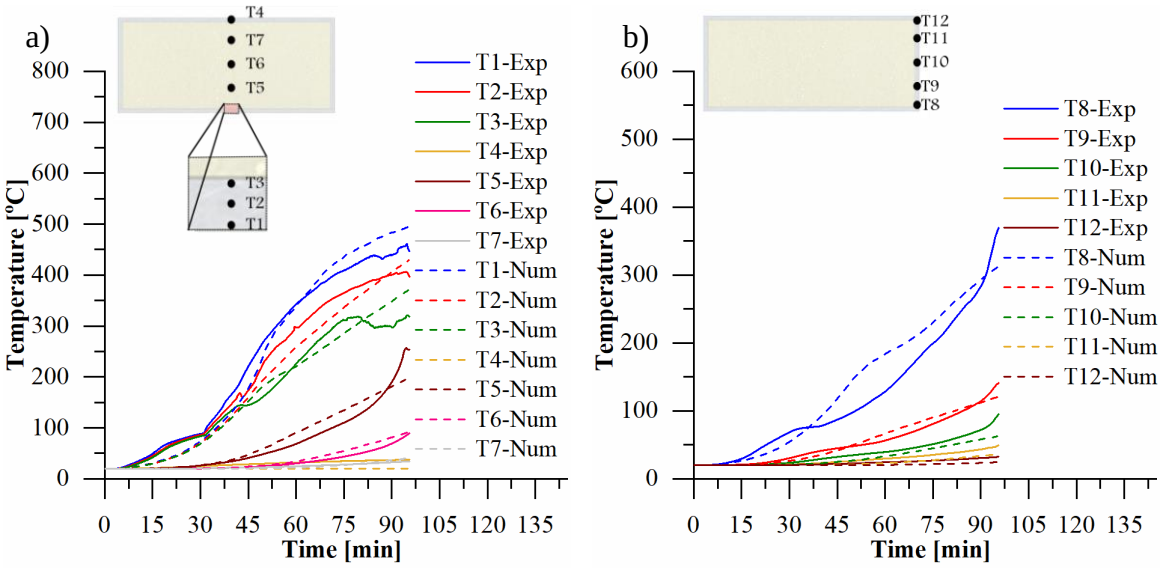

Figure 147 - Experimental (Exp) and numerical (Num) temperature vs. time curves at the mid-span section of specimen PET-LW-AC: (a) mid-width and (b) web.

Figure 148 shows the experimental and numerical temperature *vs*. time curves at different depths of the panel PET-LW-AC, at the intersection section. As for the protected homogeneous-core sandwich panels, the numerical temperatures follow a more regular pattern than the experimental ones, which present a plateau for temperatures of about 100 ºC. This result results from the aforementioned inability of the FE model in capturing the water vaporization phenomenon that seems to have occurred in the CS boards. In what concerns specifically the web, despite some differences between numerical and experimental temperatures at its bottom part, namely at a distance to the hot face of ~5.6 cm (T18), the results obtained from the FE model are qualitatively similar to the experimental measurements.

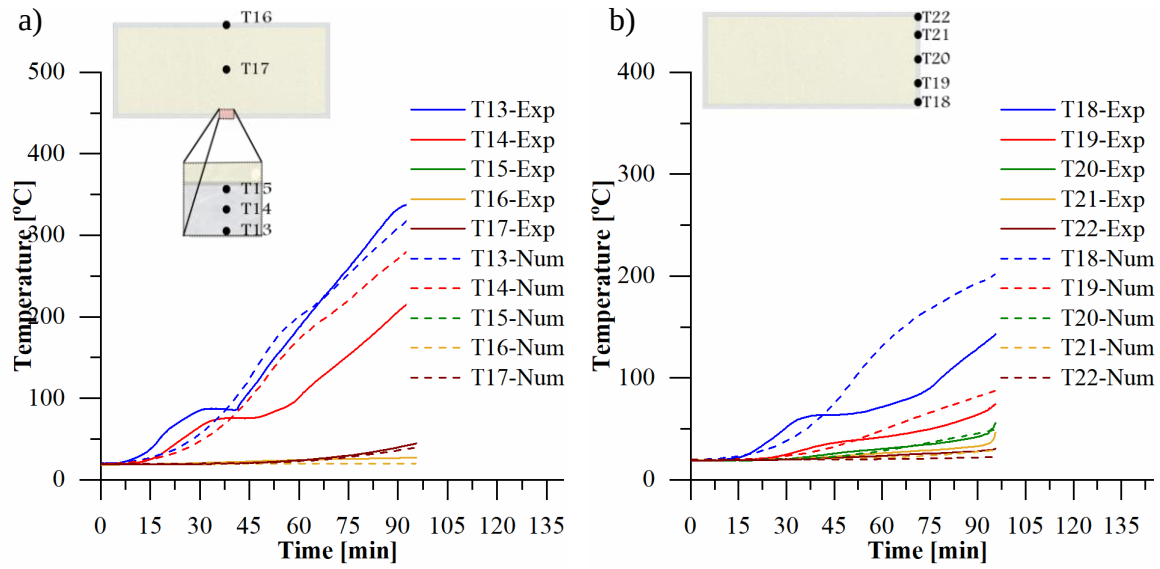

Figure 148 - Experimental (Exp) and numerical (Num) temperature vs. time curves at the intersection section of specimen PET-LW-AC-1: (a) mid-width and (b) web.

7.5.2 Mechanical response

Figure 149 plots the numerical mid-span displacement increase *vs*. time curves of specimen PET-LW-U and PET-LW-AC, together with the experimental results. Similarly to what was observed in the tests, the numerical mid-span displacement increase rate of the web-core sandwich panel protected with a passive fire protection system (*i.e*. with an air cavity) is significantly lower compared to that of the unprotected panel. Indeed, as shown in chapter 6, the AC system was able to significantly reduce the temperature in the panel; and, as a consequence, the thermal gradient across the section depth and the degradation of the material properties was also reduced.

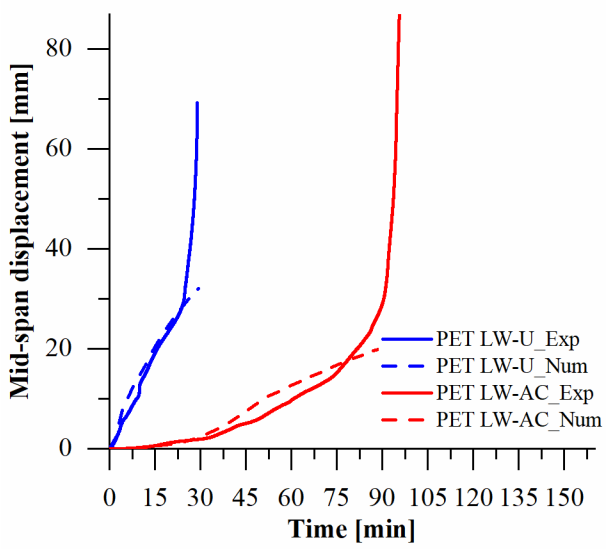

Figure 149 - Experimental (Exp) and numerical (Num) mid-span displacement increase vs. time curves for the unprotected homogeneous-core sandwich panels.

Overall, the variation of the mid-span displacement of specimen PET-LW-U obtained numerically is in very good agreement with the experimental result. However, as expected, the model was not able to capture the final steep increase of displacement; indeed, as for the 2D model, no GFRP or face sheet-core interface failure criterion was implemented in the FE simulation (due to lack of data). In what concerns the protected specimen, during the first 35 minutes, the predicted mid-span deflection increased at a relatively slow rate, confirming what was observed in the experimental tests. Subsequently, in the FE model, the mid-span deflection presented a higher increase rate compared to experimental measurements; again, such difference is probably related to uncertainties related to some temperature-dependent material properties and assumptions considered in the FE model.

As for the homogenous-core sandwich panel, the numerical models were also used to obtain a better understanding about the stress distribution in web-core sandwich panels exposed to fire. To this end, the evolution of the longitudinal stresses with fire exposure in different finite elements of the top (P1 to P3) and bottom (P4 to P6) face sheets at the mid-span section was evaluated. In addition, the variation of the longitudinal and shear stresses across the web in two heated sections (S_A and S_B, *cf.* Figure 150) are presented and discussed next.

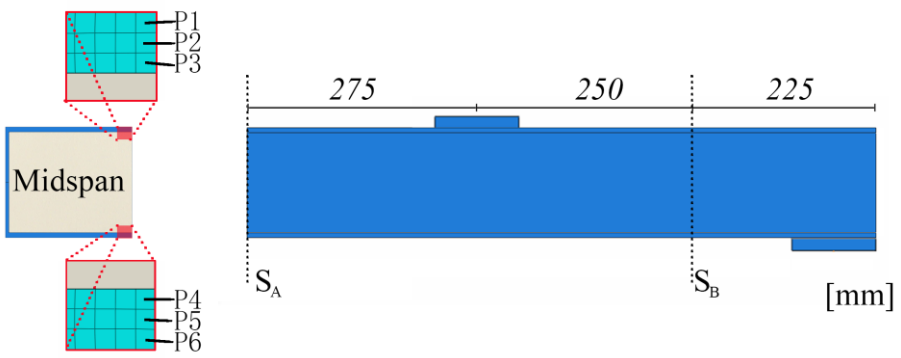

Figure 150 - Finite elements in the top (P1 to P3) and top (P4 to P6) face sheet and paths 2 and 3 across the web's depth considered in the FE analysis of panels PET-LW-U and PET-LW-AC.

Figure 151 shows the evolution of the axial stresses in the longitudinal direction of mid-span section of specimen PET-LW-U and PET-LW-AC in the top and bottom face sheets.

Figure 151a shows that the longitudinal stresses vary significantly with time: the temperature increase across the bottom face sheet leads to the reduction of the tensile modulus and, consequently, cause the increase of longitudinal (compression) stresses in the top face sheet (P1 to P3). As shown in Figure 151a, the compressive stresses present an almost steady increase, which is logical since the top face sheet remains approximately at room temperature for the entire duration of the test, and hence, almost null reductions of its mechanical properties occur.

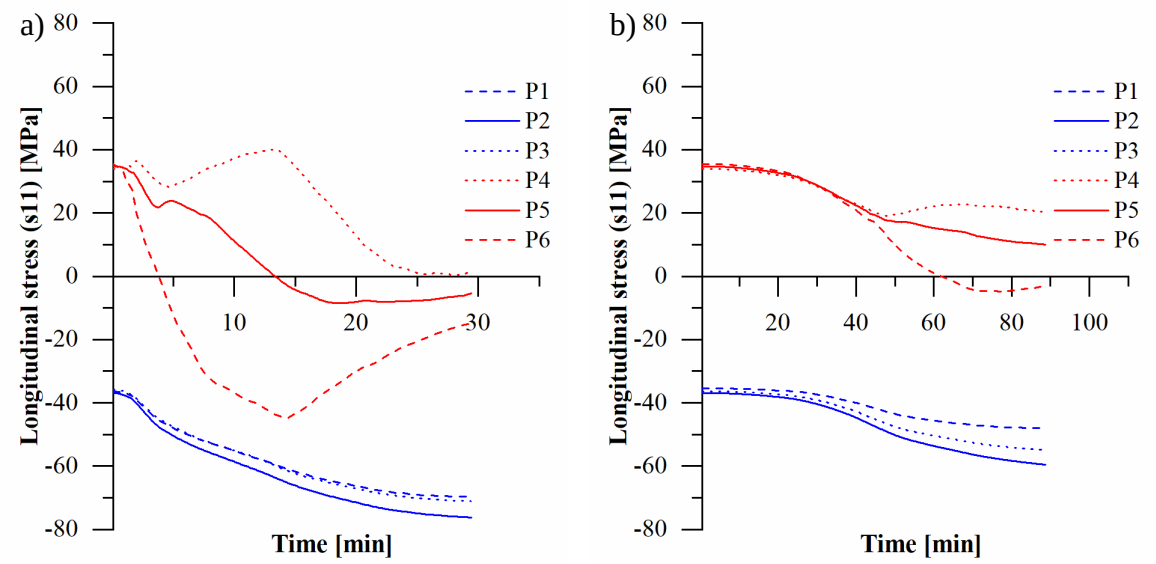

Figure 151 - Longitudinal stresses in the top and bottom face sheets (P1 to P6): (a) specimen PET-LW-U and (b) specimen PET-LW-AC.

Regarding the variation of the longitudinal stresses in the bottom face sheet (P4 to P6 in Figure 151), a rapid drop of the tensile stresses was observed due to the reduction of the tensile modulus; in addition, after ~4 min of fire exposure, compressive stresses arose at the external layer at the position of P6. A similar behaviour was observed at the position of P5, but with a time delay. This result (unexpected a priori) probably stemmed from the through-the-thickness thermal gradient of the bottom face sheet; indeed, the thermal expansion of the external layer (directly exposed to fire) was

retrained by the internal layers (which were maintained "colder"/"stiffer"); consequently, axial thrust forces developed, causing a (local) negative bending moment in opposition to the downward deflection induced by the applied load. This phenomenon was also observed in specimen PET-LW-AC (*cf.* Figure 151b) but presenting a much lower magnitude, as the thermal gradient across the depth of the bottom face sheet was less significant. As shown in Figure 151b, the tensile stresses in the bottom face sheet of specimen PET-LW-AC decreased as a result of the loss of stiffness associated to the temperature increase and, as a consequence, an increase of compressive stresses was observed at the top face sheet, reflecting a stress transfer across the section depth. From the results obtained, it can be also observed that the magnitude of the stress changes in the protected panel was much lower compared to the unprotected one; this also reflects the effectiveness of the passive fire protection system in delaying the temperature increase, as well as the thermal degradation of the material properties in the panel.

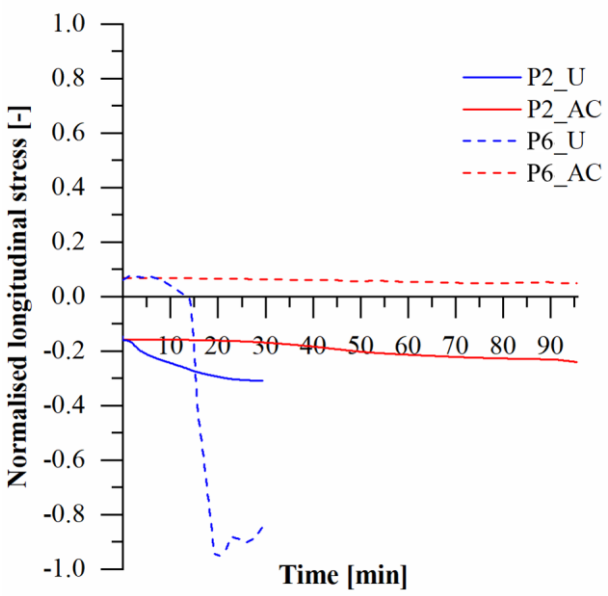

Figure 152 - Evolution with time of fire exposure of normalised longitudinal stresses at the top (P2) and bottom (P6) face sheet at the mid-span section: (a) unprotected (U) and (b) protected (AC) panels.

As shown in Figure 152, after 15 minutes of fire exposure the normalised tensile stresses at the position of P6 at the mid-span section were very low. After that initial period, compressive stresses arose in the external layer of the bottom face sheet mainly due to thermal expansion effects; and, consequently, the normalised longitudinal stresses significantly increased until almost exceeding the compressive strength of the material after 20 minutes. In this context, it is worth mentioning that the strength of GFRP materials in compression is far more sensitive to temperature than that in tension, since the compressive strength is a matrix-dominated property.

Figure 153 presents the variation of axial stresses across the web of both protected and unprotected panels for different durations of fire exposure measured in section S_A (*cf.* Figure 150).

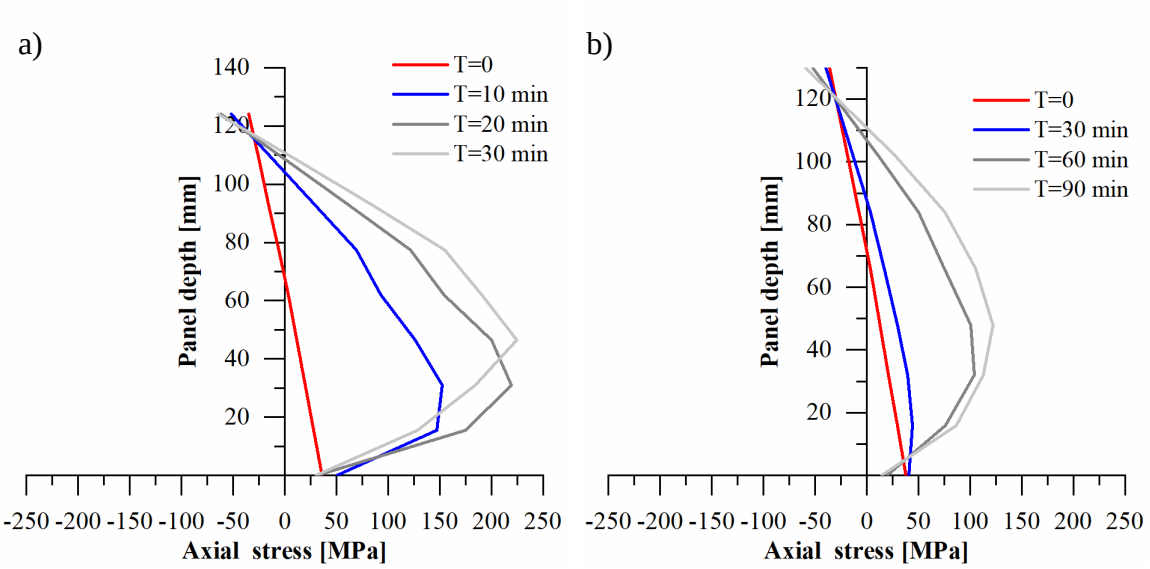

Figure 153 - Evolution of the axial stresses across the web at S_A section (cf. Figure 150) for different durations of fire exposure: (a) specimen PET-LW-U and (b) specimen PET-LW-AC.

Figure 154 shows the evolution of shear stresses across the web of specimens PET-LW-U and PET-LW-AC in S_B section (*cf.* Figure 150) for different durations of fire exposure.

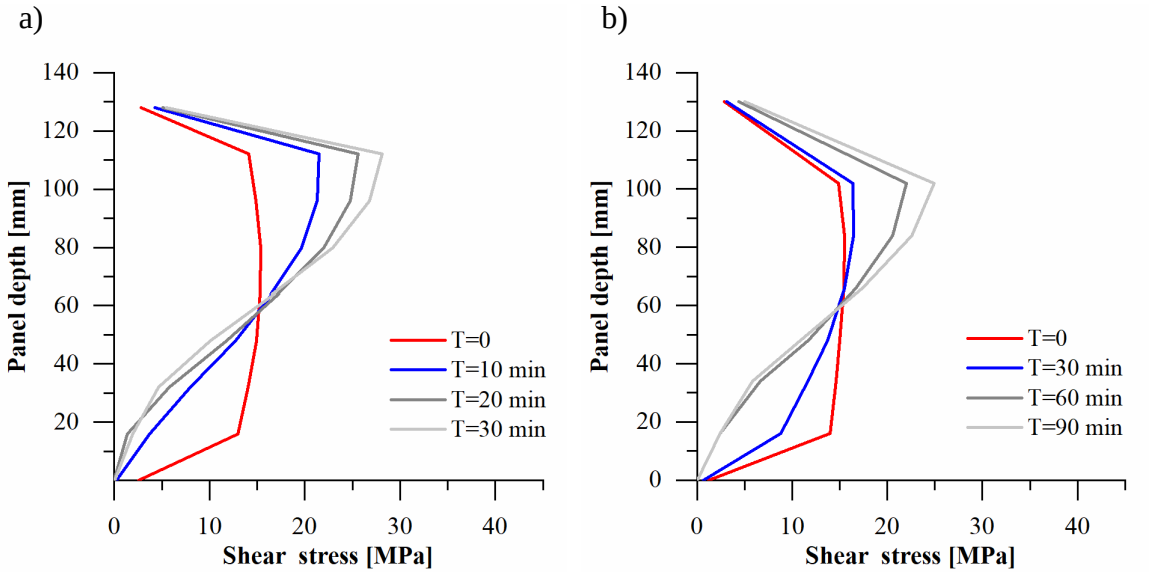

Figure 154 - Evolution of the shear stresses across the web at S_A section (cf. Figure 150) for different durations of fire exposure: (a) specimen PET-LW-U and (b) specimen PET-LW-AC.

Before fire exposure (T=0 min), the axial and shear stresses diagrams were symmetric, as expected, presenting the typical stress distributions of panels with this type of cross-section and loading configuration. After this initial period, both diagrams became markedly asymmetric over the time of fire exposure. This result is explained by the fact that the increase of temperature caused a progressive reduction of the shear and axial moduli in the bottom part of the web (which experienced higher temperatures) and, consequently, a progressive increase of those stress components in the non-degraded height of the section occurred. As expected, the stress increase in specimen PET-LW-AC was lower than that observed in the unprotected specimen, most likely due to the thermal protection

conferred by the passive fire protection system, which significantly delayed the degradation of mechanical properties.

Figure 153a also highlights the significant increase of axial stresses in the web at a distance to the exposed face of ~50 mm; in fact, the maximum tensile stress attained after 29 min (230 MPa) is 6.2 times higher than that observed at the initial stage of the test. Unfortunately, tensile tests were not performed on the GFRP web used in the sandwich panel, which would allow for a more accurate and comprehensive correlation between the numerical stresses and experimental tensile strength of the material. However, this result highlights the importance of duly considering the tensile behaviour of the web in the fire design of composite sandwich panels.

As shown in Figure 154, at the end of the fire exposure, the upper part of the webs of specimens PET-LW-U and PET-LW-AC reached maximum shear stresses of 30 MPa and 26 MPa, respectively; these values are significantly lower than the shear strength of the GFRP material of the web (161.2±2.4 MPa, at ambient temperature) obtained in the Iosipescu tests presented in chapter 3.

Aiming at providing a better understanding about the shear stress distribution in the web, Figure 156 plots the evolution of the normalised shear stress as a function of time of fire exposure of 5 elements selected across the height of the web (*cf.* Figure 155) at section S_B (*cf.* Figure 150).

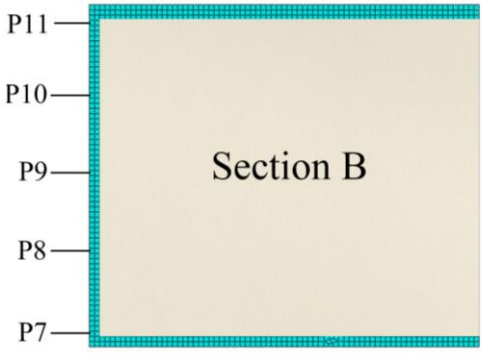

Figure 155 - Transverse cross-section of the panel at section S_B cf. (Figure 150) and finite elements (P7 to P11) across the web depth.

From the results obtained, it can be seen that all elements, with the exception of P7 (distance to the hot face of 5.6 mm) in specimen PET-LW-U, exhibited a progressive increase of the normalised shear stresses with increasing time; moreover, this ratio remained always well below 1, indicating that shear failure of the webs was not likely to occur during the entire duration of the fire exposure. However, it is worth mentioning that further analysis involving the combination of the different stress components throughout the web's depth would be needed to provide a better understanding of their mechanical contribution/effectiveness for the overall panel behaviour during fire exposure.

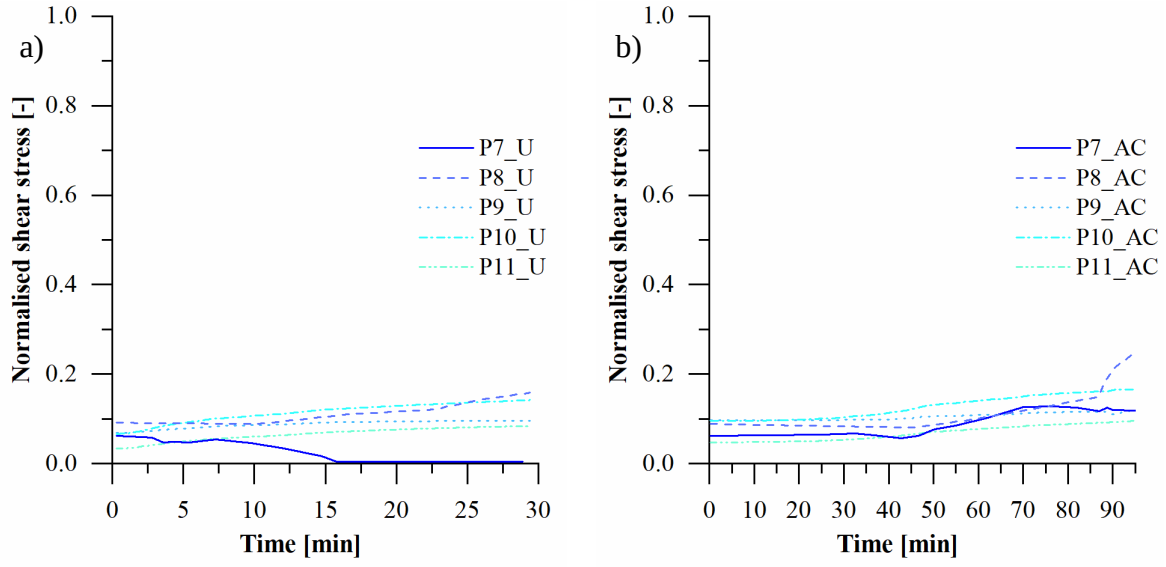

Figure 156 - Evolution with time of fire exposure of normalised shear stresses at the web (P7 to P11) along path 1: (a) unprotected (U) and (b) protected (AC) panels.

7.6 CONCLUDING REMARKS

This chapter presented a numerical study about the fire behaviour of GFRP composite sandwich panels. The influence of using different longitudinal webs and passive fire protection was studied. The FE models were developed using an uncoupled approach: in a first step, the thermal response was modelled, and then the structural response was simulated using the thermal distribution as input data. For all the materials involved (*i.e.* GFRP, foam core and CS boards), temperature-dependent thermophysical and mechanical properties were considered.

- Despite all the complexities involved, the simulated temperatures were in relatively good agreement with the experimental ones; the differences between experimental and numerical temperatures might be associated (at least partially) to some uncertainties regarding the thermophysical properties of the materials, as well as the thermal boundary conditions considered.

- The numerical models were able to simulate with good accuracy the mechanical response of the sandwich panels (except for failure, as discussed below). The models confirmed the ability of passive fire protection in reducing the thermal-induced degradation of the material and, as a consequence, in reducing the deformation increase rate. Overall, the most relevant differences between the experimental and numerical curves were observed in the brink of collapse, due to the fact that no failure criterion was considered in the models for the GFRP material and the GFRP-foam interface.

- In the unprotected homogeneous-core sandwich panel, the external layers of the bottom face sheet exhibited an initial reduction of the tensile stresses, mainly due to the reduction of the tensile modulus. Consequently, the axial stresses in the internal layer of the bottom face sheet

and the top face sheet increased, indicating a stress transfer across the height of the panels. As expected, the magnitude of the axial stresses changes in the protected panel was much lower compared to the unprotected one.

- In the unprotected web-core sandwich panels, compressive stresses developed at the bottom face sheet due to the relatively high thermal gradient between the different layers, causing a non-uniform thermal expansion through-the-thickness of this GFRP sheet. In the protected specimen, the thermal gradient was considerably lower due to the thermal protection conferred by the AC system, and thus the development of compressive stresses at the bottom face sheet was less significant.

- The variation of the shear stresses across the heigh of the core was qualitatively similar for both protected and unprotected homogeneous-core panels. The results obtained show that the shear stresses changes at the initial stage of the tests are negligible. With increasing time, the shear stresses decreased in the bottom part of the core due to the thermal degradation of the material. In the bottom part of the core of specimen PET-U-CS, the maximum shear stress in some elements attained the shear strength of the material. As a consequence, the shear stresses significantly increased in the top part of the core (still non-degraded). It can also be seen that the magnitude of the above-mentioned stress changes was higher in the protected specimen, as the temperatures in the core were much higher compared to the unprotected specimen. The Hill-criterion considered in the models confirmed a significant degradation of the foam next to the interface between the bottom face sheet and the core, as observed in the experiments performed on specimens PET-U-U; this result suggests a change of structural behaviour with time/temperature, from beam-type to arch-type. Unfortunately, the model was not able to reproduce the local crushing or shear distortion that probably caused the failure of specimens PET-U-CS.

- In the web-core sandwich panels, either unprotected or protected with an AC system, both axial and shear stress distributions were symmetric before fire exposure. With increasing time/temperatures, both diagrams became markedly asymmetric; such results can be associated with the increase of stresses in the top part of the web, caused by the axial and shear modulus reductions in the degraded lower part of the web. In both panels, the longitudinal stress in the GFRP face sheets and the shear stress across the web (at predefined sections) remained well below the corresponding strengths (at the given temperatures) during the entire duration of the fire exposure. Further studies involving the combination of the different stress components in the materials throughout the panels are needed to provide a better understanding of their mechanical response during fire exposure, as well as the development of appropriate failure criterion in order accurately predict the structural collapse of the panels, and, therefore, their fire resistance.

Part IV. Conclusions and future developments

CHAPTER 8

CONCLUSIONS AND RECOMMENDATIONS FOR FUTURE RESEARCH

8.1 CONCLUSIONS

GFRP sandwich panels are finding increasing interest for a wide range of civil engineering structural applications because of their improved thermal insulation and good strength-to-weight ratio, especially when compared to traditional solutions (*e.g.* made of concrete and/or steel). However, there is a major gap in the knowledge that is hindering their widespread use: the lack of information about their thermal and mechanical response at elevated temperature or under fire. In this context, it is worth mentioning that building structural elements are expected to present sufficient fire resistance (usually from 60 to 90 min); the use of GFRP sandwich panels in the rehabilitation of building floors is, therefore, a matter of concern, as their mechanical properties are significantly reduced when exposed to moderately high temperatures (100-200ºC).

The present thesis comprised an extensive experimental programme, ranging from small-scale material testing on the constituent materials of GFRP sandwich panels - GFRP laminates and two types of polymeric foams, PET and PUR- to intermediate-scale fire resistance tests on loaded panels, unprotected and protected with CS boards, either adherent or suspended from their bottom face sheet. In parallel, numerical models were developed to simulate their thermal and mechanical responses when subjected to fire.

The results obtained from the material characterisation tests confirmed that the mechanical properties of the GFRP laminates and both polymeric foams undergo significant reductions even at moderately elevated temperatures; moreover, it was possible to quantify such degradation. With respect to the GFRP material, the compressive and shear strength presented a greater sensitivity to temperature than the tensile properties and compressive modulus. Regarding the core materials, the results obtained show that the compressive and shear properties of both PET and PUR foams suffer drastic reductions with temperature, especially when their T_g is approached and exceeded; such reductions occur for lower temperatures in the PET foam, mainly due to its lower T_g.

Similarly to the mechanical properties, the results obtained from an inverse heat transfer analysis highlighted that the thermophysical properties (especially the specific heat and thermal conductivity)

of the GFRP and polymeric foams materials undergo significant changes with temperature – the calibration of those properties up to very high temperatures (absent in the literature up to the present study) provided essential input data to be used in the numerical models developed to simulate the thermal response of the panels under fire exposure (chapter 7).

The flexural tests at ambient temperature confirmed the significant influence of the core material on the mechanical response of homogeneous sandwich panels; in addition, the experimental results also confirmed that the introduction of longitudinal GFRP webs remarkably improve the flexural strength and stiffness, with web-core sandwich panels presenting significantly higher ultimate loads when compared to homogeneous-core panels. Regarding the fire resistance tests, the use of passive fire protection systems had a remarkable effect in extending the fire endurance of the sandwich panels, as they delayed the thermal degradation of their constituent materials. As expected, the web-core sandwich panels presented longer fire resistances compared to the homogenous-core ones, essentially due to the higher shear stiffness provided by the webs and the fact that their fire resistance behaviour is less dependent on the mechanical response of polymeric foam core, which, as mentioned above, is significantly degraded at high temperatures.

The numerical models developed using the commercial FE package *Abaqus* to simulate the behaviour of sandwich panels during fire exposure provided reasonably accurate results in terms of thermal and mechanical responses compared to the experimental data. The results obtained showed the importance of using precise input data (*e.g.* temperature-dependent material properties) in the numerical models. The mid-span displacement curves of the sandwich panels were also predicted with good accuracy; as expected, the major differences were observed in the brink of collapse due to the non-implementation of failure criteria in the GFRP face sheets and in the PET foam. Furthermore, the FE models confirmed the effectiveness of passive fire protection systems in reducing the temperatures across the depth of the panels, thus allowing to improve their fire endurance.

More detailed conclusions about the two main topics investigated in this thesis are described in the following subsections.

8.1.1 Characterisation of materials at elevated temperatures

In the first research domain of the thesis, comprehensive experimental studies about the mechanical and thermophysical characterisation of both polymeric foams and GFRP materials were performed.

In what concerns the effect of elevated temperature on the mechanical properties of PUR and PET foams, compressive and shear tests were performed up to 200 ºC. The study provided a better understanding about the effects of elevated temperature on the mechanical behaviour of these polymeric foams, providing a wealth of experimental data that were very scarce or not available in the literature. The results obtained show that the shear and flatwise compressive properties (both

strength and stiffness) of PUR and PET foams suffer very significant reductions with increasing temperature, namely for temperatures approaching and exceeding the T_g of the material (ranging from 65 to 90 °C). This is naturally ascribed to the foam softening due to the glass transition process underwent by the polymeric material. When temperatures approach the T_g, the shear and compressive behaviour of the foam materials changes from quasi-linear to non-linear, and the degree of non-linearity increases with temperature. The foam materials tested in this study present roughly similar shear and compressive modulus reductions with temperature; thus, it seems that these properties are more dependent on the thermophysical changes undergone when the polymeric material is heated (*e.g.* softening and viscosity increase) than on the possible changes in the deformation mechanism of their close-cell microstructure. However, different trends were obtained in terms of strength properties - in fact, the shear strength was significantly less affected by temperature than the compressive one. This result may be associated to the different failure modes occurring within the cells in the two loading scenarios – for the strength properties, the different deformation mechanisms developing within the foams seem to be more dominant than the thermophysical changes caused by increasing temperatures. The results obtained also show that the reduction of mechanical properties – strength and modulus - with temperature of the PET foam occurs for lower temperature when compared to PUR foam, which is consistent with the lower T_g of the former foam.

Regarding the mechanical properties at elevated temperature of the GFRP material, most previous studies have focused on the mechanical characterisation of quasi-unidirectional GFRP composites, namely pultruded profiles, rebars and strips; much less data was available about GFRP materials with more balanced fibre architectures. This study aimed at contributing to fulfil this knowledge gap by presenting experimental investigations about the effects of elevated temperatures on the mechanical properties of GFRP laminates produced by vacuum infusion with a balanced fibre architecture. The experimental programme included (i) tensile tests up to 300 ºC, (ii) compressive tests up to 250 ºC, and (iii) shear tests up to 200 ºC. Complementary, dynamic mechanical analysis (DMA) and thermogravimetric analysis (TGA) were also performed. A T_g of 103 ºC was set based on the onset of the storage modulus decay obtained from DMA tests, while the T_d, determined based on the middle temperature of the drop in the remaining mass curve, was set as 400 °C (for air atmosphere). The results obtained from the mechanical characterisation tests confirm that the mechanical properties of the GFRP laminate are severely affected by the temperature increase, especially those that are matrix-dependent: compared to room temperature, at 200 ºC the shear modulus and the compressive strength were reduced by 85%. The tensile properties and the compressive modulus (fibre-dominated) were much less affected - at 200 ºC the residual compressive modulus was 33%, whereas the tensile strength and modulus were reduced by 40% and 48%, respectively. The results obtained in the present study were then compared with those reported in the literature for GFRP materials produced by pultrusion and vacuum infusion. Overall, it can be observed that despite presenting different fibre

architectures, all the materials tested followed qualitatively a similar reduction trend. However, in the present study, the tensile modulus reductions were higher than those reported by several authors in the literature on quasi-unidirectional materials, which may be explained by the reduction of the load transfer capacity between fibres (associated to the resin softening), which severely reduced the contribution of the 45º oriented plies to the longitudinal tensile modulus at elevated temperature.

Regarding the determination of the thermophysical properties of the materials, an inverse numerical analysis, based on a 1D heat transfer model together with experimental temperature distributions, was performed with the objective of calibrating (and providing a better understanding of) the variation with temperature of the thermal conductivity and specific heat of both GFRP and polymeric foam materials. The numerical procedure was validated by comparing the temperature distribution predictions obtained against numerical results from a commercial FE package and experimental results on unloaded GFRP laminates and foam-filled sandwich panels (with steel face sheets) exposed to the temperature *vs.* time curved defined in the ISO 834 standard. The results obtained from the numerical model confirmed that assuming temperature-independent thermophysical properties affects considerably the evolution of temperatures and provides a poor agreement with the experimental temperatures. On the other hand, the temperature distributions obtained using the calibrated temperature-dependent thermophysical properties presented a significantly better agreement with the experimental data. These temperature-dependent thermophysical properties, that were not available in the literature, are key input data for the thermomechanical simulation of GFRP foam-filled sandwich panels under fire, allowing to optimize the geometry of sandwich panels and fire protection schemes, as well as to develop fire design rules.

8.1.2 Fire behaviour of GFRP sandwich panels

At a structural level, the following experiments were conducted on intermediate-scale GFRP sandwich panels: (i) reference flexural tests at ambient temperature conditions and (ii) fire resistance tests on loaded panels to assess the influence of different parameters (detailed below) on their fire behaviour.

Regarding the reference flexural tests at ambient temperature conditions, the main objectives were to assess the influence of using different core materials (PUR *vs.* PET foams) and panel configurations (homogeneous-core *vs.* web-core panels) and to define the fire load to be used in the fire resistance tests. Apart from the panel with central web (PET-CW-1), which exhibited a slight stiffness reduction prior to collapse, all specimens presented a linear response until failure, regardless of the type of core materials and panel architectures. Concerning the web-core sandwich panels, the position of the longitudinal web did not have any influence on the stiffness of the load *vs.* mid-span displacement response, as expected. In terms of load-bearing capacity, the homogeneous PET sandwich panels exhibited higher ultimate loads compared to the PUR panel (about 1.5 times); this

naturally stems from the higher shear strength of the PET foam compared to the PUR foam. As expected, the longitudinal web reinforcement significantly increased the load-bearing capacity of the web-core sandwich panels compared to the homogeneous-core specimens (up to 9.3 times), as the GFRP webs were able to significantly increase the shear strength of the panels, thus providing a relevant contribution to their load-bearing capacity.

Then, the experimental study moved to the main topic of this thesis – the fire behaviour of GFRP sandwich panels. To this end, 11 fire resistance tests were performed on intermediate-scale panels simultaneously subjected to a service load and the ISO 834 standard fire on their bottom face sheet; the influence of the following parameters on their thermomechanical response was assessed: (i) panel configurations (homogeneous-core *vs.* web-core panels), (ii) core materials (PUR *vs.* PET) and passive fire protection systems (adherent CS boards *vs.* suspended ones, forming an air cavity - typically used in building's ceilings). The tests provided temperature profiles, evolution of deflections, failure modes, fire resistance and the effects of fire protection systems on those responses.

Concerning the thermal response, as expected, the temperature increased at a different rate across the height of the panels; for all the tested specimens, the GFRP bottom face sheet attained very high temperatures, whereas significantly lower temperatures were registered in the top face sheet. This result confirmed the effectiveness of polymeric foams in providing significant thermal insulation before their decomposition. In this context, it is worth referring that for all the tested panels, both insulation and integrity criteria were fulfilled before their structural collapse. The temperatures measured at the centre of the bottom face sheet of the unprotected homogeneous-core sandwich panels attained the T_g of the GFRP after only 3 min. In addition, the temperature measured in the bottom part of the PET and PUR foam cores (distance to the exposed face of 3.5 cm) was lower than 20 ºC, remaining well below the T_g of those foams. From the results obtained it can also be observed that in the sandwich panels protected with passive fire protection systems, the maximum temperatures attained were significantly lower compared to those observed in the unprotected specimens, due to the thermal protection conferred by the CS boards. In general, the temperatures measured in the bottom face sheet of specimens PET-U-CS-1 and PUR-U-CS-1 presented a very similar qualitative pattern, exceeding the T_g of the GFRP after 25 min, whereas the T_d was never attained. Concerning the thermal behaviour of the PET and PUR foams, the temperature measured at a distance to the exposed face of 3.5 cm exceeded the T_g of the PET foam (65 ºC) after 30 min (maximum temperature ~140 ºC), whereas the T_g of the PUR foam was never attained (maximum temperature ~65 ºC). As for the unprotected homogeneous panels, the bottom face sheet of specimen PET-LW-U-1 presented very high temperatures, attaining the T_g of the GFRP after only 3 min. In addition, the bottom part of the core (distance to the exposed face of 3.5 cm) also presented relatively high temperature, reaching a maximum temperature of about 400 ºC at the end of the tests (slightly

below the T_d of the foam – 425 °C). From the results obtained, it is also relevant to note that the temperatures measured in the lower half of the webs (distances to the exposed face of 0.5, 3.5 and 6.5 cm) exceeded the T_g of the GFRP after ~30 min. As for the protected homogeneous-core sandwich panels, the use of calcium silicate boards significantly reduced the temperature evolution in the web-core sandwich panels (compared to the unprotected specimen): indeed, the maximum temperatures attained in the lower half of the webs were very similar to those observed in specimen PET-LW-U-1, but for a much longer duration of fire exposure (70 *vs.* 28 min).

In terms of mechanical response, the results obtained from the experiments confirmed that the fire resistance performance is mostly dependent on (i) the cross-sectional configuration (*i.e.* homogeneous-core *vs.* web-core) and (ii) the type of fire protection. In general, the unprotected homogeneous-core sandwich panels presented a similar mechanical behaviour, exhibiting a relatively fast initial displacement increase, due to the reduction of the bottom face sheet stiffness and thermal bowing effects. As expected, the homogeneous-core sandwich panels protected with CS boards (used as a screen protection) presented very limited increase in mid-span displacement for a longer time of fire exposure, when compared to the unprotected homogeneous-core specimens. Both protected specimens presented a very similar mechanical response up to 20 min of fire exposure; after this instant, the mid-span displacement increase rate of specimen PET-U-CS-1 became higher than that observed in specimen PUR-U-CS-1, probably due to the significant thermal degradation underwent by the PET foam, which, as mentioned, has lower T_g. Finally, specimens PUR-U-CS-1 and PET-U-CS-1 presented a sudden increase in deflection after 35 and 45 min of fire exposure, respectively. The homogeneous-core sandwich panels tested in this study collapsed in a brittle manner due to one or more of the following mechanisms: (i) shear failure of the core; (ii) bending failure of the core, (iii) compressive failure of the top face sheet; and (iv) delamination between the core and the bottom face sheet. The experiments also showed that, for some cases, the thermal degradation of the materials led to changes in the structural response, from beam-type to arch-type, with the top and bottom face sheets behaving as a strut and a tie, respectively, and the non-degraded volume of foam transmitting the load through the supports. The homogeneous-core sandwich panels collapsed after less than 10 minutes, thus not achieving the lowest fire resistance class REI 15. By applying CS boards to the bottom face sheet, a significant improvement of the fire resistance behaviour was observed, with specimens PUR-U-CS-1 and PET-U-CS-1 achieving fire resistance classes REI 30 and REI 45, respectively.

As expected, the addition of webs either at the panel edges or within the core significantly improved the fire endurance of the sandwich panels, when compared to the homogeneous-core panels. In the web-core sandwich panels, the deformation increase occurred at a slower rate compared to that observed in the unreinforced specimens. Again, this progressive increase of mid-span displacement was due to the loss of stiffness, which first occurred in the bottom face sheet and then progressed

along the height of the webs. As for the homogeneous-core sandwich panels, the use of CS boards (either suspended or directly applied to the bottom surface of the panels) proved to be very effective in extending the fire endurance of the GFRP sandwich panels. In general, all the web-core sandwich panels exhibited a sudden increase of mid-span displacement at the end of the fire exposure, which was caused mostly by the progressive loss of stiffness experienced by the web at elevated temperature, which at a certain point was no longer able to sustain the applied load, causing the failure of the panels. In the web-core sandwich panels (either unprotected or protected), failure seems to have been triggered by the crushing of the top face sheet (under the loading point) together with transverse compressive failure of the upper part of the webs. Depending on the type of passive fire protection used, the fire resistance classes of the web-core sandwich panels varied from REI 60 (specimen PET-LW-CS) to REI 90 (specimen PET-LW-AC).

The results reported above confirm the potential of GFRP sandwich panels to be used in building applications; however, passive fire protection systems, such as the ones used in this study, are necessary to comply with the fire requirements set in building codes.

The experimental studies were complemented with the development of numerical modelling tools that aimed at providing a better understanding of the thermomechanical response of GFRP sandwich panels, by means of both thermal and mechanical simulations. The main objectives were two-fold: (i) to evaluate the influence of different panel architectures and passive fire protection systems on the fire response of sandwich panels; and (ii) to provide a better understanding about the evolution of the stress fields in the panels (not possible to measure in the tests) with time/temperature increase. To this end, FE thermal models were first developed, considering the variation with temperature of the thermophysical properties of the materials (*e.g.* density, thermal conductivity and specific heat capacity), in order to simulate the evolution of the temperature field. Next, FE mechanical models were developed to simulate the mechanical response of the panels, considering as input data (i) the temperature distributions obtained from the thermal models, and (ii) the temperature-dependent mechanical properties determined in the small-scale material characterisation tests.

Concerning the thermal response of the panels, the FE models presented a reasonably good approximation to the experimental results, confirming the effectiveness of the CS boards in reducing the temperature evolution in the panels. Concerning the mechanical response, the predicted mid-span displacement *vs.* time curves exhibited a reasonably good agreement with the experimental ones; however, significant differences were observed in the brink of collapse since no failure criterion was considered in the models for the GFRP material and the GFRP-foam interface.

The FE models were also used to obtain further insights about the stress distribution in the panel with increasing time/temperatures. With respect to the unprotected homogeneous-core sandwich panels, the longitudinal stresses developed in the external layer of the bottom face sheet were reduced over

the time of fire exposure, as a result of the thermal degradation of the tensile modulus of the GFRP material. In opposition, longitudinal stresses increased in the internal layer of the bottom face sheet and in the top face sheet to maintain the equilibrium of the member. Concerning the variation of the shear stress in the core of specimen PET-U-U, the magnitude was almost negligible at the beginning of the fire exposure (after 3 min); this is mainly due to the very limited temperature increase in the core. After 3 min of fire exposure, the temperature in the bottom part of the core started to increase and, consequently, a stress transfer from the bottom part of the core (degraded) to the upper part (non-degraded) was observed. At the end of the tests, the maximum shear stress developed in the upper part of the core (temperature attained of about 20 ℃) was 0.4 times the shear strength of the material, thus explaining why the PET foam did not fail in shear during the fire test. As expected, the magnitude of the shear stress changes was much higher in the protected homogeneous-core panel, mainly due to the higher temperatures attained by the core compared to the unprotected specimen: after 30 minutes of fire exposure, the shear stresses in the bottom part of the core attained the shear strength of the material, indicating that the shear failure of the core is likely to have occurred during the test. In addition, the results obtained showed that the Hill-criterion used to simulate the behaviour of the PET foam was able to predict with success the degradation of the interface between the bottom face sheet and the core. Concerning the variation of the longitudinal stresses in specimen PET-R-U, it can be observed that compressive stresses arose in the external layer of the bottom face sheet; this unexpected result probably stemmed from the high thermal gradient developed between the layers of the bottom face sheet. In this context, the restrained external layer (directly exposed to fire) developed a compressive force, as it expanded against the stiffer (and colder) internal layers. Consequently, the thermally induced axial thrust caused a negative bending moment in opposition to the downward deflection induced by the applied load. A similar behaviour was also observed in specimen PET-R-AC; however, the magnitude of such axial thrust force was much lower, as the through-the-thickness thermal gradient of the bottom face sheet was less significant. With respect to the variation of the axial and shear stresses across the web of specimens PET-R-U and PET-R-AC, the FE models highlighted that the symmetric axial and shear stress diagrams initially observed become markedly nonlinear with increasing temperature/time. These stress changes were mostly caused by the significant loss of tensile and shear modulus experienced by the GFRP web at elevated temperature, which consequently led to a considerable stress increase in the non-degraded part of the material. Finally, for both web-core panels, the normalised axial stresses at the GFRP face sheet and the normalised shear stresses at the web over the time of fire exposure remained well below 1.0, suggesting that neither the axial failure of the GFRP face sheet nor the shear failure of the web were likely to occur during the fire resistance tests.

8.2 RECOMMENDATIONS FOR FUTURE RESEARCH

The experimental and numerical investigations presented in this thesis allowed for a better understanding of the fire behaviour of GFRP composite sandwich panels. In spite of the various scientific contributions of the present study, several topics remain to be investigated. Recommendations for further research are listed below:

- Investigation of the mechanical behaviour (in tension, compression and shear, in different directions) of polymeric foams, for temperatures above the glass transition temperature of the solid polymer.
- Additional experimental tests at elevated temperature on polymeric foams (with different densities and made from different solid polymers) to correlate the "micro" deformation mechanisms of the cell's structure with the "macro" mechanical properties of the materials.
- Study of the short-term creep behaviour (in tension, compression and shear) of GFRP and polymeric foam materials at elevated temperature, which may be relevant to model more accurately the response under fire exposure of composite sandwich panels.
- Characterisation of the mechanical properties at elevated temperatures of GFRP materials with different resins (*e.g.* phenolic, with improved fire behaviour), fibre architectures, correlating the properties of GFRP with those of the fibres, matrix and fibre-matrix interface at elevated temperatures;
- Additional experimental tests at temperatures above the decomposition temperature of the GFRP material, to assess the full degradation with temperature of both tensile properties and compressive modulus (fibre-dominated properties).
- Characterisation of the thermal expansion coefficient (in different directions) at elevated temperature.
- Additional flexural static tests on homogeneous-PET foam sandwich panels to have a better understating about the size effects (or premature interfacial debonding) that may affect the mechanical properties of the foam material (and the structural behaviour of the panels).
- Experimental evaluation of the fire reaction properties of different GFRP sandwich panels, both unprotected and protected with different fire protection materials.
- Additional fire resistance tests on GFRP sandwich panels with different core materials and web configurations, protected with different passive fire protection systems (*e.g.* gypsum plasterboard, calcium silicate boards, intumescent coatings).
- Development of user-defined material models to simulate the orthotropic mechanical behaviour of the polymeric foams at elevated temperature.

- Development of thermomechanical models of sandwich panels exposed to fire considering (i) the above referred thermomechanical properties, (iii) the variation of thermal expansion coefficient with temperature, (iii) the (short-term) creep behaviour at elevated temperature, and (iv) appropriate failure criteria.
- Development of numerical models to simulate the thermochemical and thermomechanical response to fire of GFRP panels with arbitrary cross-section and different fire protection systems, thus enabling to create structural design supporting tools.

BIBLIOGRAPHY

[1] D. Zenkert, The Handbook Of Sandwich Construction, in: Engineering Materials Advisory Services (EMAS), Worcestershire, UK, 1997: pp. 23–43.

[2] J. Davies, Lightweight sandwich construction, in: Blackwell Science, Oxford, 2001: pp. 26–36.

[3] J.R. Correia, GFRP pultruded profiles in civil engineering: hybrid solutions, bonded connections and fire behaviour, PhD Thesis in Civil Engineering, IST, Technical University of Lisbon, 2008.

[4] T. Morgado, J.R. Correia, N. Silvestre, F.A. Branco, Experimental study on the fire resistance of GFRP pultruded tubular beams, Compos. Part B. 139 (2018) 106–116.

[5] T. Keller, C. Tracy, E. Hugi, Fire endurance of loaded and liquid-cooled GFRP slabs for construction, Compos. Part A Appl. Sci. Manuf. 37 (2006) 1055–1067.

[6] J.R. Correia, F.A. Branco, J.G. Ferreira, Y. Bai, T. Keller, Composites : Part B Fire protection systems for building floors made of pultruded GFRP profiles Part 1 : Experimental investigations, 41 (2010) 617–629.

[7] Y. Bai, T. Keller, Pultruded GFRP tubes with liquid-cooling system under combined temperature and compressive loading, Compos. Struct. 90 (2009) 115–121.

[8] A. Hörold, B. Schartel, V. Trappe, M. Korzen, J. Bünker, Fire stability of glass-fibre sandwich panels: The influence of core materials and flame retardants, Compos. Struct. 160 (2017) 1310–1318.

[9] C. Luo, J. Lua, P.E. Desjardin, Thermo-mechanical damage modeling of polymer matrix sandwich composites in fire, Compos. Part A Appl. Sci. Manuf. 43 (2012) 814–821.

[10] S. Feih, Z. Mathys, A.G. Gibson, A.P. Mouritz, Modeling compressive skin failure of sandwich composites in fire, J. Sandw. Struct. Mater. 10 (2008) 217–245.

[11] M. Proença, M. Garrido, J.R. Correia, M.G. Gomes, Fire resistance behaviour of GFRP-polyurethane composite sandwich panels for building floors, Compos. Part B Eng. 224 (2021) 109171.

[12] CEN/TC 250, prEN 19101: 2020- Design of fibre-polymer composite structures, (2020).

[13] T. Morgado, N. Silvestre, J.R. Correia, F.A. Branco, T. Keller, Numerical modelling of the thermal response of pultruded GFRP tubular profiles subjected to fire, Compos. Part B Eng.

137 (2018) 202–216. https://doi.org/10.1016/j.compositesb.2017.11.009.

[14] Z. Yu, A. Zhou, Fiber reinforced polymer composite structures in fire: Modeling and validation, Mech. Adv. Mater. Struct. 20 (2013) 361–372.

[15] T. Keller, C. Tracy, A. Zhou, Structural response of liquid-cooled GFRP slabs subjected to fire – Part II : Thermo-chemical and thermo-mechanical modeling, 37 (2006) 1296–1308.

[16] M. Garrido, J.R. Correia, T. Keller, Effects of elevated temperature on the shear response of PET and PUR foams used in composite sandwich panels, Constr. Build. Mater. 76 (2015) 150–157.

[17] M. Rezaei, V. Karatzas, C. Berggreen, L.A. Carlsson, The effect of elevated temperature on the mechanical properties and failure modes of GFRP face sheets and PET foam cored sandwich beams, J. Sandw. Struct. Mater. (2018) 1–21.

[18] D. Benderly, S. Putter, Characterization of the shear/compression failure envelope of Rohacell foam, Polym. Test. 23 (2004) 51–57.

[19] S. Zhang, J.M. Dulieu-Barton, R.K. Fruehmann, O.T. Thomsen, A Methodology for Obtaining Material Properties of Polymeric Foam at Elevated Temperatures, Exp. Mech. 52 (2012) 3–15.

[20] ASTM D5379/D 5379M - 05, Standard Test Method for Shear Properties of Composite Materials by the V-Notched Beam Method, West Conshohocken (PA,USA); ASTM international, 2005.

[21] ASTM C393/C 393 M - 06, Standard Test Method for Core Shear Properties of Sandwich Constructions by Beam, West Conshohocken (PA,USA); ASTM international, 2009.

[22] Saenz E, Fatigue and Fracture of Foam Cores Used in Sandiwch Composites, MSc Dissertation, Florida Atlantic University, Boca Raton, Florida, USA, 2012.

[23] T. Thomas, H. Mahfuz, L.A. Carlsson, K. Kanny, S. Jeelani, Dynamic compression of cellular cores: Temperature and strain rate effects, Compos. Struct. 58 (2002) 505–512.

[24] S. Zhang, J.M. Dulieu-barton, O.T. Thomsen, The effect of elevated temperatures on the bending behaviour of foam cored sandwich structures, J. Compos. Mater. (2015) 1–14.

[25] S. Arezoo, V.L. Tagarielli, C.R. Siviour, N. Petrinic, Compressive deformation of Rohacell foams: Effects of strain rate and temperature, Int. J. Impact Eng. 51 (2013) 50–57.

[26] J.T. Siivola, S. Minakuchi, N. Takeda, Effect of temperature and humidity conditions on polymethacrylimide (PMI) foam core material and indentation response of its sandwich structures, J. Sandw. Struct. Mater. 17 (2015) 335–358.

[27] M. Garrido, J.R. Correia, Elastic and viscoelastic behaviour of sandwich panels with glass-fibre reinforced polymer faces and polyethylene terephthalate foam core, J. Sandw. Struct. Mater. 20 (2018) 399–424.

[28] ISO 11357-2, Differential scanning calorimetry (DSC) determination of glass transition temperature, International Organization for Standardization, Geneve, Switzerland, 1999.

[29] ASTM E 519 – 02, Standard Test Method for Diagonal Tension (Shear) in Masonry Assemblages, West Conshohocken (PA,USA); ASTM international, 2002.

[30] ASTM C365/365, Standard Test Method for Flatwise Compressive Properties of Sandwich Cores, West Conshohocken (PA,USA); ASTM international, 2003.

[31] L.J. Gibson, M.F. Ashby, Cellular Solids: Structure & properties, in: Pergamon Press, Oxford, 1997: pp. 236–257.

[32] A. Fathi, J. Keller, V. Altstaedt, Composites : Part B Full-field shear analyses of sandwich core materials using Digital Image Correlation (DIC), Compos. Part B. 70 (2015) 156–166.

[33] J.P. Firmo, M.G. Roquette, J.R. Correia, A.S. Azevedo, Influence of elevated temperatures on epoxy adhesive used in CFRP strengthening systems for civil engineering applications, Int. J. Adhes. Adhes. 93 (2019) 8–18.

[34] A. Fathi, Mechanical Properties of Strand PET Foams at Different Length Scales, Phd Thesis in polymer engineering, University of Bayreuth, Bayreuth, Germany, 2018.

[35] AIREX, T92 Foam datasheets, (2020).

[36] A.G. Gibson, Y.S. Wu, J.T. Evans, A.P. Mouritz, Laminate Theory Analysis of Composites under Load in Fire, J. Compos. Mater. 40 (2005) 639–658.

[37] K. Wang, B. Young, S.T. Smith, Mechanical properties of pultruded carbon fibre-reinforced polymer (CFRP) plates at elevated temperatures, Eng. Struct. 33 (2011) 2154–2161.

[38] J.R. Correia, M.M. Gomes, J.M. Pires, F.A. Branco, Mechanical behaviour of pultruded glass fibre reinforced polymer composites at elevated temperature: Experiments and model assessment, Compos. Struct. 98 (2013) 303–313.

[39] C.A. Mahieux, K.L. Reifsnider, S.W. Case, Property modeling across transition temperatures in PMC's: Part I. Tensile properties, Appl. Compos. Mater. 8 (2001) 217–234.

[40] I. Grace, V. Pilipchuk, R. Ibrahim, E. Ayorinde, Temperature effect on non-stationary compressive loading response of polymethacrylimide solid foam, Compos. Struct. 94 (2012) 3052–3063.

[41] ASTM C273/C273 M, Standard Test Method for Shear Properties of Sandwich Core

Materials, West Conshohocken (PA,USA); ASTM international, 2012.

[42] L.C. Bank, Composites for construction : structural design with FRP materials, John Wiley & Sons, Hoboken, New Jersey, 2006.

[43] J.R. Correia, Fibre-Reinforced (FRP) Composites, in: Mater. Constr. Civ. Eng. Sci. Process. Des., Springer Netherlands, Dordrecht, 2015: pp. 501–543.

[44] A.P. Mouritz, S. Feih, E. Kandare, Z. Mathys, A.G. Gibson, P.E. Des Jardin, S.W. Case, B.Y. Lattimer, Composites : Part A Review of fire structural modelling of polymer composites, Compos. Part A. 40 (2009) 1800–1814.

[45] Y. Bai, T. Keller, Modeling of Strength Degradation for Fiber-reinforced Polymer Composites in Fire, J. Compos. Mater. 43 (2009) 2371.

[46] A. Jafari, M. Bazli, H. Ashrafi, A. Vatani, S. Azhari, X. Zhao, Effect of fibers configuration and thickness on tensile behavior of GFRP laminates subjected to elevated temperatures, Constr. Build. Mater. 202 (2019) 189–207.

[47] E.U. Chowdhury, R. Eedson, M.F. Green, L.A. Bisby, N. Benichou, Mechanical Characterization of Fibre Reinforced Polymers Materials at High, (2011) 1063–1080.

[48] I.C. Rosa, T. Morgado, J.R. Correia, J.P. Firmo, N. Silvestre, Shear Behavior of GFRP Composite Materials at Elevated Temperature, J. Compos. Constr. 22 (2018) 1–10.

[49] P. Feng, J. Wang, Y. Tian, D. Loughery, Y. Wang, Mechanical Behavior and Design of FRP Structural Members at High and Low Service Temperatures, J. Compos. Constr. 20 (2016).

[50] P.M.H. Wong, J.M. Davies, Y.C. Wang, An experimental and numerical study of the behaviour of glass fibre reinforced plastics (GRP) short columns at elevated temperatures, Compos. Struct. 63 (2004) 33–43.

[51] ASTM D3410/D3410 M, Compressive properties of polymer matrix composite materials with unsupported gage section by shear loading, West Conshohocken (PA,USA); ASTM international, 2012.

[52] ASTM E1640, Assignment of the Glass Transition Temperature By Dynamic Mechanical Analysis, West Conshohocken (PA,USA); ASTM international, 2011.

[53] ASTM D3039/D3039M-08, Standard Test Method for Tensile Properties of Polymer Matrix Composite Materials, West Conshohocken (PA,USA); ASTM international, 2010.

[54] ASTM D6641/D6641M-09, Standard Test Method for Compressive Properties of Polymer Matrix Composite Materials Using a Combined Loading Compression (CLC), West Conshohocken (PA,USA); ASTM international, 2012.

[55] I.C. Rosa, J.P. Firmo, J.R. Correia, J.A.O. Barros, Bond behaviour of sand coated GFRP bars to concrete at elevated temperature – Definition of bond vs. slip relations, Compos. Part B Eng. 160 (2019) 329–340.

[56] J.R. Correia, T. Keller, M. Garrido, M. Sà, J.P. Firmo, M.D. Shahid, M. Machado, Mechanical properties of FRP materials at elevated temperature - definition of a temperature conversion factor for design in service conditions, Constr. Build. Mater. (2022).

[57] Y. Frostig, O.T. Thomsen, Non-linear thermal response of sandwich panels with a flexible core and temperature dependent mechanical properties, Compos. Part B Eng. 39 (2008) 165–184.

[58] F. Klaus, U. Breuer, Multifunctionality of Polymer Composites Multifunctionality of Polymer Composites Challenges and New Solutions, in: Elsevier, Oxford, 2015: pp. 262–296.

[59] D.S.W. Pau, C.M. Fleischmann, M.J. Spearpoint, K.Y. Li, Thermophysical properties of polyurethane foams and their melts, Fire Mater. 38 (2014) 433–450.

[60] P. Mazzuca, J.P. Firmo, J.R. Correia, E. Castilho, Mechanical behaviour in shear and compression at elevated temperature of polyethylene terephthalate (PET) foam, J. Build. Eng. 42 (2021) 102526.

[61] P. Mazzuca, J.P. Firmo, J.R. Correia, M. Garrido, Mechanical behaviour in shear and compression of polyurethane foam at elevated temperature, J. Sandw. Struct. Mater. 0 (2021) 1–21.

[62] M. Proença, J.R. Correia, M. Garrido, Fire behaviour of GFRP composite sandwich panels, Report 4.7, Easyfloor Project, (2020).

[63] L. Valencia, Experimental and numerical investigation of the thermal decomposition of materials at three scales: application to polyether polyurethane foam used in upholstered furniture, University of Edinburgh, Edinburgh, 2009.

[64] H. Zhang, W. Fang, Y. Li, W. Tao, Experimental study of the thermal conductivity of polyurethane foams, Appl. Therm. Eng. 115 (2017) 528–538.

[65] U. Jarfelt, O. Ramnäs, Thermal conductivity of polyurethane foam - best performance Thermal conductivity of polyurethane foam Best performance, 10th Int. Symp. Dist. Heat. Cool. (2006) 12.

[66] S. Dias, A. Tadeu, A. Ramalho, M. Brett, F. Pedro, Thermal and Mechanical Characterisation of Sandwich Core Materials for Climatic Chamber Shells Subjected to High Temperatures, Energies. (2022).

[67] L.R. Glicksman, Heat transfer in foams, Low Density Cell. Plast. (1994) 104–152.

[68] Y.C. Wang, A. Foster, Experimental and numerical study of temperature developments in PIR core sandwich panels with joint, Fire Saf. J. 90 (2017) 1–14.

[69] N. Vahedi, C. Tiago, A.P. Vassilopoulos, J.R. Correia, T. Keller, Thermophysical properties of balsa wood used as core of sandwich composite bridge decks exposed to external fire, Constr. Build. Mater. 329 (2022) 127164.

[70] Y.I. Dimitrienko, Thermomechanical behaviour of composite materials and structures under high temperatures : 1. Materials, Compos. Part A Appl. Sci. Manuf. 461 (1997) 453–461.

[71] Y.I. Dimitrienko, Thermal stresses and heat-mass transfer in ablating composite materials, Int. J. Heat Mass Transf. 38 (1995) 139–146.

[72] Y. Bai, T. Vallée, T. Keller, Modeling of thermo-physical properties for FRP composites under elevated and high temperature, Compos. Sci. Technol. 67 (2007) 3098–3109.

[73] J.R. Correia, Y. Bai, T. Keller, A review of the fire behaviour of pultruded GFRP structural profiles for civil engineering applications, Compos. Struct. 127 (2015) 267–287.

[74] A. Samanta, M.R.E. Looyeh, S. Jihan, J. McConnachie, Thermo-mechanical Assessment of Polymer Composites Subjected to Fire, Engineering and Physical Science Research Council & The Robert Gordon University, Aberdeen, UK., 2004.

[75] C. Tracy, Fire endurance of multicellular panels in an FRP building system, Ph.D. thesis, ´Ecole Polytechnique Federale de Lausanne, Lausanne, Switzerland., 2005.

[76] ASTM-D-5344, Standard test method for determination of thermal conductivity of soil and soft rock by thermal needle probe procedure., West Conshohocken (PA,USA); ASTM international, 2014.

[77] ASTM D- 5930- 17, Standard test method for thermal conductivity of plastics by means of a transient line-source technique., West Conshohocken (PA,USA); ASTM international, n.d.

[78] ISO 834, Fire resistance tests. Elements of building construction., Geneve, Switzerland, 2018.

[79] CEN, Eurocode 1: General actions—Actions on structures exposed to fire, 2002.

[80] J. D'Errico, https://www.mathworks.com/matlabcentral/fileexchange/8277-fminsearchbnd-fminsearchcon, (2022).

[81] A. Duarte, P. Mazzuca, C. Tiago, J.P. Firmo, J.R. Correia, Determination of temperature-dependent thermophysical properties of polymeric foams using numerical inverse engineering (IN PREPARATION), (2022).

[82] CEN, Eurocode 3: Design of Steel Structures, 2010.

[83] EN 1363-1, Fire resistance tests. Part 1: General requirements., Brussels, 2012.

[84] D. Eaves, Handbook of Polymer Foams, Rapra Technology Limited, Shropshire, United Kingdom, 2004.

[85] P.K. Latha, Y. Darshana, V. Venugopal, Role of building material in thermal comfort in tropical climates – A review, J. Build. Eng. 3 (2015) 104–113.

[86] M. Moradibistouni, B. Vale, N. Isaacs, Evaluating the use of polymers in residential buildings: Case study of a single storey detached house in New Zealand, J. Build. Eng. 32 (2020) 101517.

[87] A. Manalo, T. Aravinthan, A. Fam, M. Asce, B. Benmokrane, State-of-the-Art Review on FRP Sandwich Systems for Lightweight Civil Infrastructure, J. Compos. Constr. 21 (2016) 1–16.

[88] T. Keller, C. Haas, T. Vallée, Structural Concept, Design, and Experimental Verification of a Glass Fiber-Reinforced Polymer Sandwich Roof Structure, J. Compos. Constr. 12 (2008) 454–468.

[89] A. Fam, T. Sharaf, Flexural performance of sandwich panels comprising polyurethane core and GFRP skins and ribs of various configurations, Compos. Struct. 92 (2010) 2927–2935.

[90] S. Reeze, New FRP pedestrian bridge deck improves safety and provides critical connecting link., JEC Compos. Mag. (2013) 85, 44.

[91] F. Nunes, Development of a web app for the assessment of general stack FRP laminates subjected to different loading conditions, (2020).

[92] F. Zhang, W. Liu, H. Fang, Z. Jia, Flexural behavior of composite sandwich beams with di ff erent kinds of GFRP ribs in fl atwise and edgewise positions, Compos. Part B. 156 (2019) 229–239.

[93] J.R. Correia, M. Garrido, J.A. Gonilha, F.A. Branco, L.G. Reis, GFRP sandwich panels with PU foam and PP honeycomb cores for civil engineering structural applications: Effects of introducing strengthening ribs, Int. J. Struct. Integr. 3 (2012) 127–147.

[94] M. Garrido, Composite sandwich panel floors for building rehabilitation Civil Engineering, PhD Thesis in Civil Engineering, IST, Technical University of Lisbon, 2016.

[95] S. Feih, E. Boiocchi, E. Kandare, Z. Mathys, A.G. Gibson, A.P. Mouritz, Strength degradation of glass and carbon fibres at high temperature, J. Mater. Sci. 44 (2009) 392–400.

[96] T. Miguel, R. Morgado, Thermal and structural response of pultruded GFRP profiles under fire exposure, PhD Thesis in Civil Engineering, IST, Technical University of Lisbon, 2018.

[97] Decree-law 220/2008, Legal regime for fire safety in buildings, 2008.

[98] Decree-law 3/2015, Fire prevention code, 2015.

[99] Y. Bai, T. Keller, J.R. Correia, F.A. Branco, J.G. Ferreira, Composites : Part B Fire protection systems for building floors made of pultruded GFRP profiles – Part 2 : Modeling of thermomechanical responses, Compos. Part B. 41 (2010) 630–636.

[100] T. Morgado, N. Silvestre, J.R. Correia, F.A. Branco, T. Keller, Numerical modelling of the thermal response of pultruded GFRP tubular profiles subjected to fire, Compos. Part B Eng. 137 (2018) 202–216.

[101] L. Zhang, W. Liu, G. Sun, L. Wang, L. Li, Two-Dimensional Modeling of Thermomechanical Responses of Rectangular GFRP Profiles Exposed to Fire, Adv. Mater. Sci. Eng. (2017).

[102] T. Keller, C. Tracy, A. Zhou, Structural response of liquid-cooled GFRP slabs subjected to fire – Part I : Material and post-fire modeling, 37 (2006) 1286–1295.

[103] T. Morgado, N. Silvestre, J.R. Correia, Simulation of fire resistance behaviour of pultruded GFRP beams – Part I: Models description and kinematic issues, Compos. Struct. 187 (2018) 269–280. https://doi.org/10.1016/j.compstruct.2017.12.063.

[104] T. Morgado, N. Silvestre, J.R. Correia, Simulation of fire resistance behaviour of pultruded GFRP beams – Part II: Stress analysis and failure criteria, Compos. Struct. 188 (2018) 519–530. https://doi.org/10.1016/j.compstruct.2017.12.064.

[105] J.B. Henderson, J.A. Wiebelt, M.R. Tant, Journal of Composite Materials, (1985).

[106] Promat, Promatect-H technical data sheet., 2012.

[107] I.C. Rosa, P. Firmo, R. Correia, P. Mazzuca, Influence of elevated temperatures on the bond behaviour of ribbed GFRP bars in concrete, 122 (2021).

[108] L.C. Hollaway, J.-G. Teng, Strengthening and rehabilitation of civil infrastructures using fibre-reinforced polymer (FRP) composites, 2008.

[109] Scott Bader, Crestapol 1261, (2020).

[110] METYX Composite Reinforcements, UNIE500, (2020).

[111] C. Lopez Sanchez, Numerical modelling of the thermomechanical behaviour of GFRP pultruded profiles subjected to fire, PhD Thesis in Civil Engineering, IST, Technical University of Lisbon, 2017.

[112] L. Marsavina, D.M. Constantinescu, E. Linul, T. Voiconi, D.A. Apostol, Shear and mode II fracture of PUR foams, Eng. Fail. Anal. 58 (2015) 465–476.

[113] J. Mimoso, Theoretical bases for building applications - technical information for buildings, Lisbon, 1987.